UNIVERSITÀ DEGLI STUDI DI MILANO
FACOLTÀ DI SCIENZE E TECNOLOGIE

Ph.D course in Industrial Chemistry

XXXV Cycle

GREEN STRATEGIES FOR THE SYNTHESIS OF BIOBASED BUILDING-BLOCKS

Ph.D candidate: **Denise Cavuoto**

R12557

Supervisor: Prof. Antonella Gervasini

Co-Supervisor: Dr. Federica Zaccheria

Academic Year 2021/2022

ABSTRACT

Green chemistry is an important tool in the roadmap towards a sustainable economy system. Biomass-waste valorization, in particular ligno-cellulosic wastes, and the use of sustainable processes are pillars of the green chemistry approach. Notably, biobased lactones can be valorized into new valuable molecules such as diols and amines that are ubiquitous chemicals in today's chemical industry. The use of simple and cheap heterogeneous copper catalysts supported on various materials, prepared with the Chemisorption-Hydrolysis method, will avoid toxic and expensive noble metal catalysts. These materials are easy to prepare, resistant and provide reliable results. Depending on the nature of the support they can have different acidic/basic or wettability properties making them very versatile in organic synthesis. Deep characterization was performed on the catalytic system to enlighten the relationship between physicochemical properties of the catalysts with their performances. Particularly, a focus was given on the study of copper phase morphology, wettability and acidity of the surfaces.

The first part of the Ph.D project was devoted to study the hydrogenation of γ-valerolactone (GVL) to 1,4-pentanediol (1,4-PDO) (scheme A1), using silica supported copper catalysts under the green solvent cyclopentylmethylether (CPME).
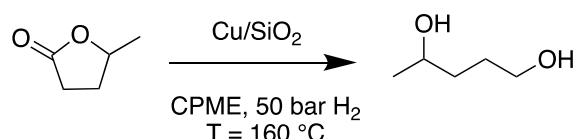
Scheme A1. Hydrogenation of GVL to give 1,4-PDO.

Notably, two different methods have been implemented to obtain low hydrophilic catalysts namely the right choice of the support and the post-metal deposition hydrophobization through silane grafting. In the first case, two different SiO_2 materials, namely one less hydrophilic pyrogenic and one hydrophilic gel, were chosen to prepare two copper catalysts CuO/SiO_2 A and CuO/SiO_2 B respectively. The wettability properties of the two supports were confirmed through static contact angle measurements and with hydroxyl density determination using TGA. The catalysts were tested in the hydrogenation of GVL to give 1,4-PDO (T=160 °C, P(H_2) = 50 bar, t = 22h) after catalysts pre-reduction under CPME. The best performances were obtained using Cu/SiO_2 A achieving 78% in the diol while 47% was achieved by Cu/SiO_2 B. The catalysts performances were ascribed to the SiO_2 support wettability: a low hydrophilicity allows the diol product a better desorption, preventing

methyltetrahydrofuran formation by dehydration side reaction. Moreover, as confirmed by XPS analysis, a low -OH surface density allows to achieve a higher Cu dispersion, thus a higher hydrogenation activity compared to the catalyst CuO/SiO_2 B prepared with the more hydrophilic silica. Furthermore, the activity was found to be dependent on the nature and on the effective number of the acid sites on the surface measured in CPME through FT-IR after pyridine adsorption and through liquid-solid titration using phenylethylamine (PEA) as a probe molecule respectively. In fact, the presence of a lower quantity and density (1 $\mu mol_{PEA}/m^2$ vs 5 $\mu mol_{PEA}/m^2$ for CuO/SiO_2 A and CuO/SiO_2 B respectively) of strong acid sites observed with CuO/SiO_2 A in CPME could therefore be the main reason for its much higher selectivity (98% vs 82% for CuO/SiO_2 A and CuO/SiO_2 B respectively). This has a more pronounced masking effect on the case of CuO/SiO_2 A Lewis acid sites.

Successively, an uncomplicated procedure of surface functionalization of the more hydrophilic CuO/SiO_2 B catalyst using trietoxyoctylsilane (TEOCS), was set up to explore the possibility to obtain low hydrophilic systems with a post metal deposition method. Four samples with different silane loading were obtained (namely 1, 5, 10 and 15% wt/wt) and the catalysts properties were investigated by several characterization techniques. The effective silane grafting was confirmed by IR and XPS while the stability at the reaction temperature (T=160 °C) was assessed using TGA. The progressive reduction of hydrophilicity was confirmed by SCA measurements and water adsorption isotherms. The results obtained showed that the functionalization significantly lowers the hydrophilicity of the surface with a decrease of SCA of 20% from the bare CuO/SiO_2 to the CuO/SiO_2 B - 15% TEOCS. The materials were tested in the hydrogenation reaction under the same conditions and an increase in the diol yield from 47% in the case of the unfunctionalized one to 80% in the case of the 10% wt/wt TEOCS was observed. However, a further organosilane loading, as in the case of 15%, gives rise to a decrease in activity due to the scarce accessibility of GVL to the copper sites. This behavior was corroborated by ^{29}Si CP MAS solid state NMR measurements that is able to distinguish the silicon of the bulk silica and the organosilicon. The spectra showed a dense surface silane layer on the 15% loaded sample with a T^3 configuration, namely in a reticulated-type structure, if compared to the 10% one. From the results it was possible to deduce that the capability to easily tune the wettability properties of the metal supported catalysts paves the way to a wide range of applications in which both the metallic phase activity and the polarity of the surface play a pivotal role in affecting the catalytic reaction.

The second part of the Ph.D thesis was focused on the synthesis of N-heterocycles once again starting from GVL. N-alkyl-5-methyl-2-pyrrolidinones and pyrrolidines are an important class of chemicals that can be used as benign alternative solvent or as the starting material for the synthesis of agrochemicals and pharmaceuticals. GVL has been coupled with butylamine to obtain N-butyl-5-methyl-2-pyrrolidone (NBPO) and N-butyl-5-methyl-2-pyrrolidine (NBPE) (Scheme A2) utilizing similar copper catalysts supported on different materials.
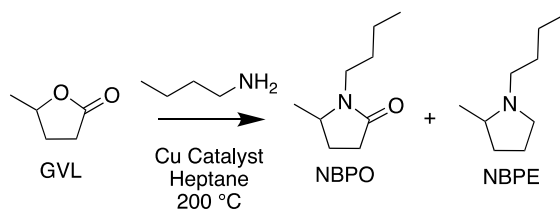
Scheme A2. Reaction of amination of GVL to give NBPO and NBPE.

Initially, copper was deposited on three different supports widely used in catalysts preparation: one amphoteric, namely hydroxyapatite (HAP), one acidic, namely SiO_2-Al_2O_3 and one moderately acidic, namely SiO_2 and the acidity of the readily made catalysts was deeply characterized through FT-IR after pyridine adsorption and solid-liquid acid-base titration using PEA as basic probe molecule. Copper phase morphology was investigated through TEM, UV-DRS and TPR analysis. Subsequently the catalysts were tested in the lactamization of GVL with butylamine. (T=200 °C, P(H_2) = 10 bar and GVL:BuNH$_2$ = 1:1) The reaction conditions and the set up were improved to lower the impact avoiding catalyst pre-treatment and high hydrogen pressure. The best results were achieved by CuO/HAP with the highest conversion and selectivity towards the green solvent product NMPO (77% and 61% respectively) while the most selective toward NBPE was CuO/SiO$_2$. This behavior was ascribed to the high density while low strength Lewis acidity of the CuO/HAP if compared to the other samples. Once again, this moderate Lewis acidity allows to coordinate the C=O group and activate the GVL to the amine nucleophilic attack. On the other hand, the higher reducibility of CuO/SiO$_2$ gives account for its higher activity in the deoxygenation of NBPO to NBPE, due to the *in situ* easier formation of reduced copper phase. Considering these results, other supports, namely Al$_2$O$_3$ A, Al$_2$O$_3$ B, ZrO$_2$ and TiO$_2$, were chosen to prepare the corresponding copper catalysts that were also tested in the lactamization reaction. The best performances were observed with the CuO/Al$_2$O$_3$ B achieving 75% conversion of GVL with a selectivity towards NMPO of 75% while the worst results were obtained using CuO/Al$_2$O$_3$ A (30% conversion and 70% selectivity). The reasons were found in the higher copper dispersion and in the lower particle size of Cu on the CuO/Al$_2$O$_3$ B catalyst

investigated by TEM and XRD. The system also showed its efficacy for the lactamization of other biobased lactones.

Also in this case, the characterization of the morphology of the copper phase and of the acidity of the systems was of great importance to understand the catalytic behavior of the samples. Moreover, the activity and selectivity can be easily tuned by varying the hydrogen pressure in the reaction environment and the acidic properties of the support. In particular, modulating the acidity properties of the catalysts is an important tool to drive the reaction selectivity towards each product.

LIST OF ABBREVIATION

1,4-PDO	1,4-pentanediol
CH	Chemisorption Hydrolysis
CP-MAS	Cross Polarization Magic Angle Spinning
CPME	Cyclopentylmethylether
GVL	γ-valerolactone
STEM	Scanning Transmission Electron Microscopy
HMF	Hydroxymethylfurfural
ICP	Inductively Coupled Plasma
IW	Incipient Wetness
LA	Levulinic Acid
NAMP	N-alkyl-5-methylpyrrolidinone
NBP	N-butyl-pyrrolidinone
NBPE	N-butyl-5-methylpyrrolidinine
NBPO	N-butyl-5-methylpyrrolidinone
NMP	N-methylpyrrolidinone
PEA	Phenylethylamine
PV	Pore Volume
SCA	Static Contact Angle
SSA	Specific Surface Area
TEM	Transmission Electron Microscopy
TGA	Thermogravimetric Analysis
TPR	Temperature Programmed Reduction
UV DRS	Ultra Violet Diffuse Reflectance Spectroscopy
wt/wt	Weight on Weight
XRD	X-Ray Diffraction
XPS	X-Ray Spectroscopy

1 GENERAL CONSIDERATION

1.1 Introduction

1.1.1 Green Chemistry

Facing the pressing need for climate change mitigation, one of the most important challenges in chemistry is to devise green and sustainable technologies for the conversion of waste biomass to biofuels, commodity chemicals and new bio-based materials such as bioplastics. Green or sustainable chemistry is an area of chemistry aimed to reduce or eliminate, in chemical processes, harmful substances for humans and the environment merging chemical competences to an ecological approach. Notably, green chemistry has not to be mented as a single scientific discipline, but as a universal approach to science, based on chemical, ecological and social responsibility [1]. Moreover, it is an innovative, non regulatory and economically driven approach to sustainability that can be defined as "meeting the needs of the present generation without compromising the needs of future generations to meet their own needs" [2]. Pursuing these goals, green chemistry is focused on innovative process design with the aim to protect human health and environment rather than limiting the pollution generation through regulation: stimulating creativity and scientifical innovations [3].

Paul Anastas and John Warner of EPA developed the twelve principles of green chemistry (Table 1.1) in their Green Chemistry Theory and Practice book, 1998. These principles are the product of environmental and social consideration of the authors summing up the green chemistry approach.

Table 1.1. The twelve principles of green chemistry

Prevention	The prevention principle is referred to waste generation. It is better to prevent waste rather than treat them after.
Atom economy	Waste generation can be prevented also planning synthetic methods in a way that the final product includes as much as possible the starting reagents.
Safer chemical synthesis	Processes and synthetic pathways should be designed in order to use and generate non toxic substances both for humans and the environment.

Safer chemicals design	The new chemicals should be designed to be the lowest toxic possible.
Use of safer solvents and auxiliaries	It is better to avoid the use of solvents and other supplementary reagents, if this is not possible they should be non toxic.
Design for energy	Chemical processes should be designed to require the less amount of energy as possible. They should be carried out, if possible, at ambient temperature and pressure.
Use of renewable raw materials	The use of renewable material should be preferred to non renewable ones when it is possible from the economic and technical point of view.
Reduction of derivatives	The derivatization processes that are not necessary should be avoided or minimized.
Catalysis	The use of selective catalyst is preferred rather than stoichiometric reagents.
Degradation products design	The chemicals involved in a process should be designed in a way that when they decompose they produce harmless, not polluting byproduct.
Real-time analysis for pollution prevention	The chemical processes should be monitored with proper analytical methods in order to avoid the formation of harmful substances.
Accidents prevention	The substances and the type of chemical process involved should be chosen keeping in mind the minimization of potential accidents in order to obtain a safer situation both for workers and the environment[3].

It can be derived that one of the main focuses of green chemistry is the general prevention of wastes reducing the number of feedstocks needed for a process. A useful tool used to estimate the efficiency of a process is the calculation of Atom Economy that is defined as the ratio of the relative molecular masses of the desired products and all reactants expressed in percentage [3].

An even more efficient way to quantify the wastes produced is the *E* factor that is defined as everything but the desired product: the ideal *E* factor is zero. *E* factor not only includes reagents and the chemical yield of the products but also solvents and auxiliaries.

Water is generally not included in the calculation because it would increase exceptionally the factors making comparisons among processes very difficult to perform [4].

A great challenge

A green chemistry approach to industry could be fundamental to reach social, economic and environmental sustainability and chemists have a great role in reaching these common objectives. In fact, chemical industry is one of the widest industrial sectors considering the moles of production and invested money [5]. Pursuing green chemistry principles surely provides a demanding challenge for the entire scientific community, especially in the industry field. The final objective is to transform present technologies in more innovative and environmentally friendly ones and, as a consequence, to radically transform most of the current industrial processes. These huge changes require, of course, a lot of money, time and intellectual and material resources making opportunities of profit for company difficult to grasp. As a consequence, newer greener processes are implemented only if there is a reasonable probability of payback [6]. Moreover, generally the green chemistry approach is perceived only as a cost without economic benefits. This is not true for several reasons: the green technologies transformation surely requires initial high investments cost but in the long term will provide an advantageous economic return due to reduced cost of wastes, energy and the use of less feedstocks [5].

The great industrial research challenges provided by green chemistry is oriented broadly into three categories: the research of alternative feedstock, alternative solvents and alternative synthetic pathways.

The most intuitive approach to alternative feedstock is the substitution of the petroleum deriving feedstocks with biobased, renewable resources [5]. Cellulose and hemicellulose represent an important and versatile source of biomass because they can be obtained from agriculture wastes. In this way, hydrocarbons, fuels and primary chemicals can be obtained easily [6].

Organic solvents represent one of the major problems because at the end of their lifecycle they constitute a great toxic and polluting waste source. The most convenient way to prevent this is to avoid their use. Since this strategy can not be suitable for every industrial
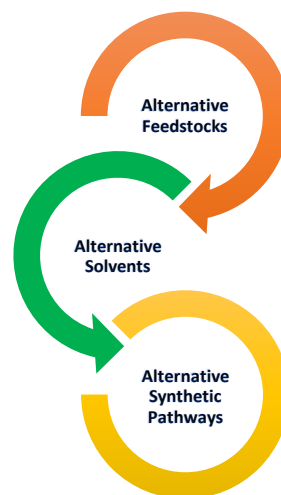
process, non-toxic, easy to recover and greener solvents combined with recycle strategies could be a great alternative [5].

The most convenient synthetic pathways usually include the use of a catalyst. Heterogeneous catalysts are advantageous because they are used not in a stoichiometric amount but only in catalytic. They can provide alternative synthetic routes that avoid the use of many supplementary reagents or a big energy consumption [5]. Moreover, their easy separation strongly limits purification steps that are usually time and cost consuming.

1.1.2 Biomass Valorization

As mentioned in the previous paragraph, the best way to conduct a chemical process is to use raw materials deriving from renewable sources. Thus, to find alternative feedstock to substitute non-renewable fossil materials is of a crucial importance [6,7]. Excluding fossils, biomass is the only source of carbon available, and so represents one possible alternative raw material for the production of energy and chemicals. In fact, the term biorefinery can be associated with the coproduction of biofuels and chemicals from renewable biomass feedstock, in a parallel way to the classic petroleum refinery [8].

There are several reasons to apply biorefinery processes to chemicals and energy production. First of all, it would afford an environmentally beneficial reduction of carbon emission of chemicals and liquid fuels, contributing also to provide a positive common perception of the chemical industry. Then, the coproduction of biofuels combined to platform chemicals in an integrated production chain will provide a higher return of investment [8]. Biobased chemicals also furnish a new portfolio of products that are diverse in terms of structure and functional groups with the ones deriving from oil refinery [9]. Eventually, they could meet legislative requirements for human toxicity and environmental pollution more easily.

Dedicated crops vs Lignocellulosic wastes

The first generation of biomass feedstocks were grown for the biofuel production. In North America it consisted especially in crops of maize and edible oil seeds, such as soybean, while sugarcane was a relevant cultivation in Brazil. Corn was cultivated for this scope in Asia while palm oil in Germany and Malaysia. Other investigated oilseed crops were canola, sunflower and cotton flower. As already mentioned, the main problem is that

this type of dedicated crops ultimately competes with food production for land, water and other resources use. This enters in conflict with the concept of sustainability; the use of food cultivation resources to produce biofuels can not be considered ethical, bearing in mind that a large part of the human population still remains malnourished. Unfortunately, due to biofuels economy, food commodities have encountered inflation in prices causing a consisting number of people to fall into poverty [10,11]. Furthermore, dedicated crops for the production of biofuels often use lands converted from rainforest, savannas and grasslands causing a high amount of released that is several times more CO_2 than the quantity saved for the production of biofuel [10].

To avoid this situation, instead of cultivating dedicated crops, renewable resources can be obtained from agro-food industrial wastes, not competing with the global food supply chain [4]. The main waste resources used as biomass are lignocellulose waste (figure 1.1), such as corn stover, rice husks and inedible oil seeds, which are estimated to surpass 2×10^{11} t/year worldwide. These residues can be divided into two categories: residues left in the field directly after harvest of crops and residues separated from the product as it is processed [12]. Such feedstocks could provide the basis of bio-renewable chemical production without the need to allocate land for specific dedicated crops and it is in harmony with the green chemistry concept of waste reduction considering that in the agricultural sector this kind of waste is unavoidable [4].
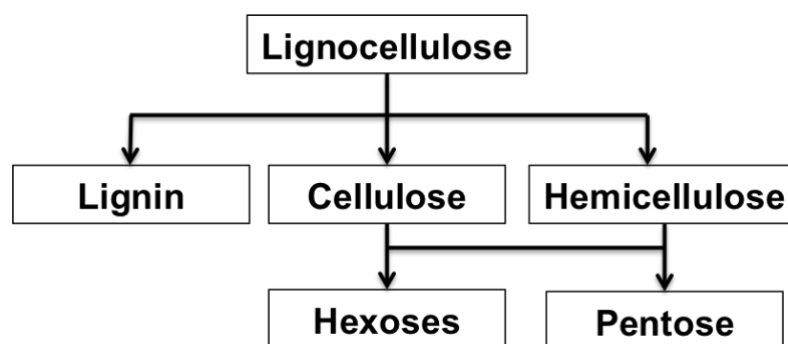
Figure 1.1. Lignocellulose deriving biomasses.

Lignocellulose is a complex biopolymer with an intricate structure that is primarily composed of cellulose (34–54 wt %), hemicellulose (19–34 wt %) and lignin (11-30 wt %) [13]. Depending on the source, the percentege of this constitutive elements could differ. Lignin is a cross-linked polymer with covalent linkages with cellulose and hemicellulose, increasing its complexity [9,13]. It connects cellulose and hemicellulose fibers in lignocellulosic biomass by filling the spaces between them, thus displaying a 3D

cross-linked, stable molecular structure that consists of monomers of coniferyl, coumaroyl, and sinapyl alcohols. Hemicellulose is a branched amorphous polysaccharide with a lower polymerization degree. This feature makes it more prone to degradation than cellulose. Its structure consists of random C_5 or C_6 sugars, being xylan the main structural unit. This gives the possibility to produce from it xylitol, furfural, and furfural derivatives [14]. Cellulose is the main component of lignocellulosic materials. It is a biopolymer constituted of glucosyl residues and its valorization often entails depolymerization into glucose. Nevertheless, due to its complex structure characterized by a dense H-bonds network, cellulose is almost chemically inert and insoluble under usual conditions of solvent and temperature [15]. On the other hand, it can be a valuable source for the production of ethanol, platform chemicals, such as levulinic acid (LA) and 5-hydroxymethylfurfural (HMF), and liquid fuels [16].

Currently, four main classes of conversion processes are involved in biorefinery system. These are the biochemical (fermentation), the thermochemical (pyrolysis, gasification and aqueous phase reforming), the chemical (esterification) and the mechanical (size reduction) ones [8] (figure 1.2).
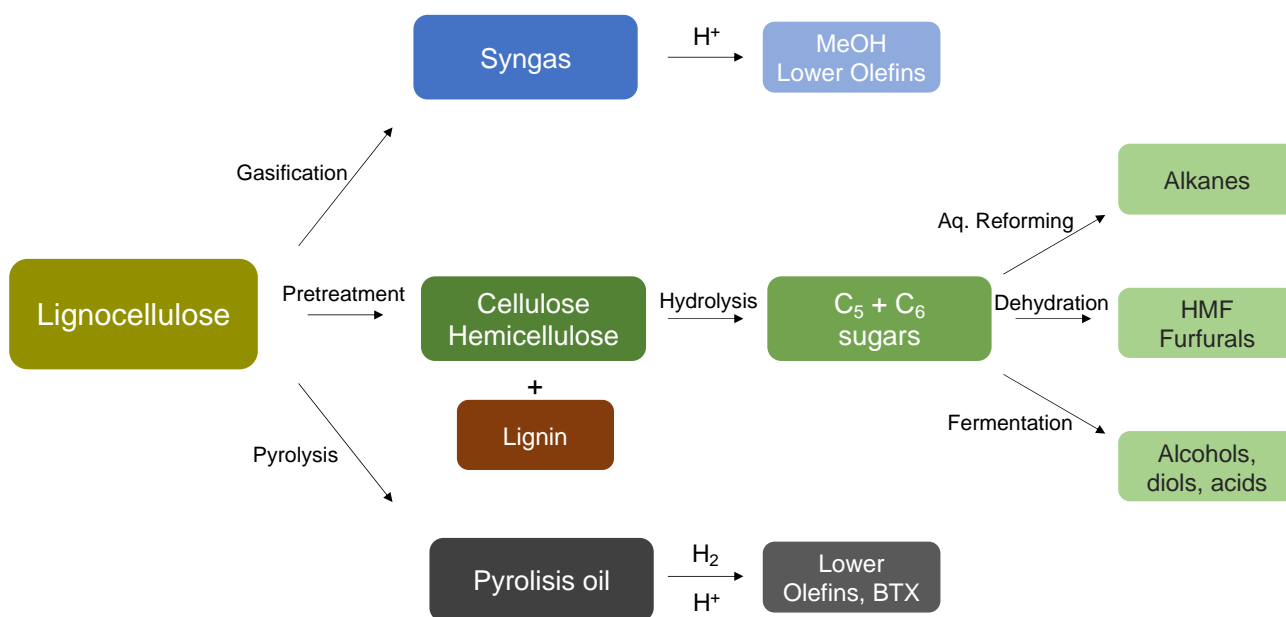
Figure 1.2. Methods for lignocellulosic conversion.

One of the greatest challenges is converting lignocellulosic biomass to chemicals achieving high selectivity and yields at economical costs. One-step methods, like pyro- lysis, depend on high temperatures, but can deconstruct the polymeric matrix and lead to lower costs due to the lack of pretreatment steps, excluding drying and size reduction. However, downstream separations are required increasing the costs. In fact, the so-called bio-oil produced is a mixture of hundreds of compounds, making separations of the targeted

chemicals really challenging [9]. To improve selectivity controlling the reactivity, two-step processing methods are often employed. Using this strategy, it is possible to fractionate the lignocellulosic biomass into its main components, that are, as already mentioned, hemicellulose, cellulose and lignin. Subsequently, each fraction can therefore be processed under different conditions to achieve high yields of target products [9,16,17].

The obtained C_6 and C_5 sugars can be processed under mild conditions to produce intermediate molecules that have enough reactivity to be used as building blocks to synthetize a variety of chemicals and fuels depending on the necessities of the market (Figure 1.3) [8,18].
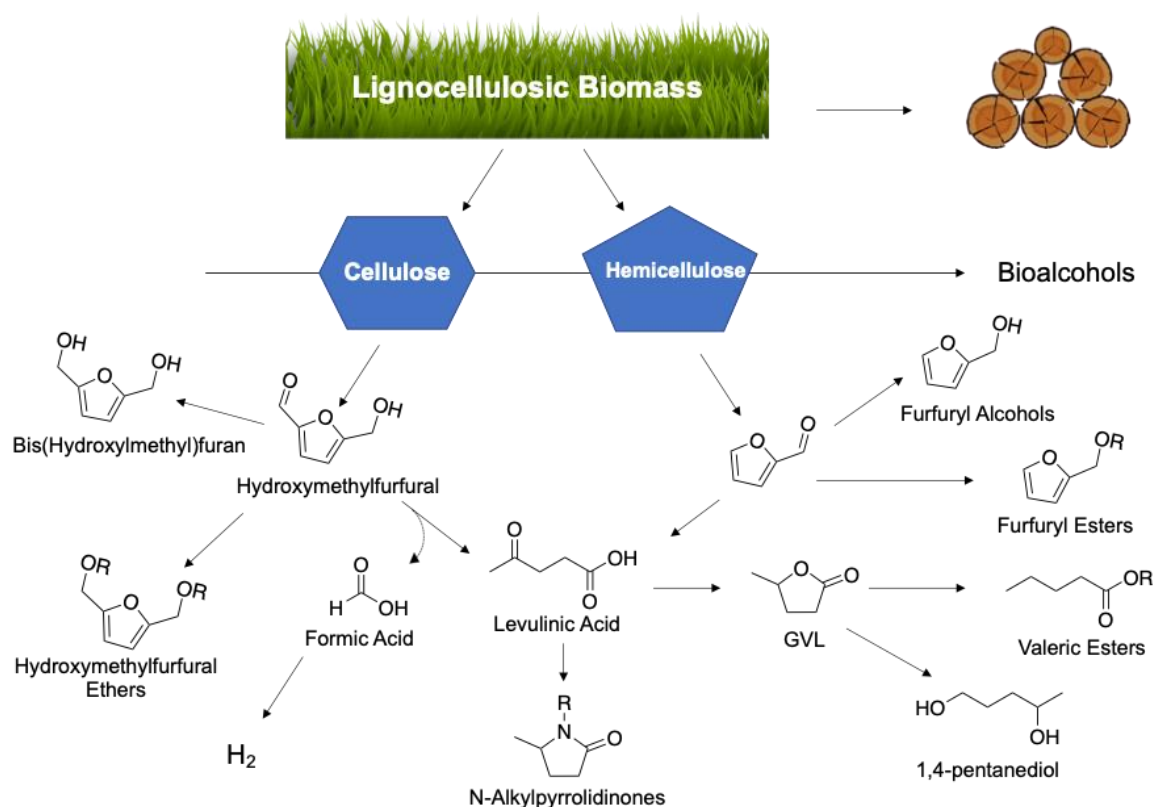
Figure 1.3. Cellulose and hemicellulose derived molecules valorization.

One of the most promising building blocks is Levulinic Acid (LA) that can be obtained from cellulose, starch or C_6 sugars by acid dehydration passing through HMF as an intermediate. In alternative, LA can be synthetized from hemicellulose in a three steps process through furfural and furfuryl alcohol as intermediates [19]. LA has a wide application scope: its derivatives constitute an important class of five carbon molecules with several different applications (figure 1.3). Levulinic esters can be obtained through esterification of LA and they are useful as oxygenated fuels. Hydrogenation of LA gives

methyltetrahydrofuran which is an additive in gasoline and also finds a great application as electrolyte for lithium rechargeable batteries [19,20].

LA and levulinates can also be hydrogenated to give γ-valerolactone (GVL) [21–23] that has excellent properties as solvent [24,25], food and perfume ingredient [26] as well as fuel additive [27]. In this thesis the importance of GVL as substrates will be underlined: its valorization produces important building block chemicals such as 1,4-Pentanediol (1,4-PDO) [28,29]. See section 1.15 for a brief review for the production of GVL starting from LA using copper heterogeneous catalysts.

As already mentioned, several methods can be employed for the valorization of lignocellulosic biomass to upgraded chemicals, from the depolymerization of the starting materials to the transformation of intermediates. The application of heterogeneous solid catalysts, alternative to homogeneous liquid ones, has great importance because of their versatile physicochemical properties, high hydrothermal stability, and efficient catalyst recovery/reusability [30,31].

1.1.3 Heterogeneous Catalysis in Biomass Valorization, Criticity and Issues

Heterogeneous catalysis is one of the cornerstones of the chemical and energy industries and will be a key tool towards sustainability and bioeconomy objectives. Heterogeneous catalysts are solid materials that allow reactions at the solid interface. Moreover, they can be easily separated from the reactants and product phase and recycled. Generally, they are easier to handle, safer and prevent waste formation with respect to their homogeneous counterpart [32]. The manageability, low harmfulness and high waste prevention of heterogeneous catalysis perfectly meet the green chemistry principles, making it one of the twelve [33].

The three key factors that describe the performances of a catalyst are activity, selectivity and stability. The activity is generally related to the reaction rate, selectivity is the percentage of the consumed reagent that forms the desired product while stability is referred to the rate of catalyst activity decay, thus, it determines a catalysts frequency of replacement [34].

The rational design of a catalyst is of fundamental importance to ensure high activity, selectivity and stability and it is conducted by understanding the key descriptors that determine the surface activation of reactants and intermediates for the synthesis of products.

A heterogeneously catalyzed reaction is a combination of physical and chemical reaction phenomena. These are associated to the mass transport of the substrates to the solid surface, the reaction and the product desorption. Particularly, the steps involved are i) diffusion of the reaction media through the boundary layer on the catalyst surface ii) pore diffusion iii) adsorption of the reactants on the inner surface of the pores iv) chemical reaction on the catalyst surface v) desorption of the products from the catalyst surface vi) diffusion of the products out of the pores vii) diffusion of the products away from the catalyst through the boundary layer [34]. It can be deduced that a catalytic reaction does not include only a single interaction with the active site but a complex mechanism of adsorption and desorption to the surface. In this respect, it is of paramount importance to understand, when possible, the physicochemical properties of a catalytic material to establish structure-activity relationship to carefully tailor its activity.

Valorization of oxygenated feedstock

Heterogeneous catalysts are used on large scale in the production of organic and inorganic chemicals, particularly, in crude oil refining and petrochemistry [32]. However, due to its versatility, it could be applied also for sustainable production of chemicals from renewable biomass waste. Notably, the oxygen-rich and multifunctional nature of biobased feedstocks imply that more cost-effective, direct synthetic route should be developed to manufacture O-containing chemicals, *i.e.* alcohols, ketones, acids and esters.

The typical reactions involved in biomass valorization are hydrolysis, dehydration, isomerization, aldol condensation, hydrogenation, hydrogenolysis, hydrodeoxygenation, ring-opening, decarboxylation and oxygenation [35]. It is noticeable that the majority of the reactions related to biomass require an acid (hydrolysis, dehydration, isomerization, aldol condensation and ring opening) or a redox metal center (hydrogenation, hydrogenolysis, hydrodeoxygenation and oxygenation). However, there are several issues related to these procedures.

The catalytic processes requirements for biomass conversion are really distant from the petroleum industry ones. In fact, as already mentioned, oil-deriving feedstocks are poor in oxygenated compound in contrast to biomass ones [31]. Moreover, biomass supplies are quite varied and complex as they can derived from many different resources [36]. The variety and high density of functionalized molecules makes mass transport phenomena even more complicated especially at the pores. In addition, biomass feedstock presents a high

concentration of diverse impurities or chelating functional groups that can cause catalyst poisoning or active phase leaching [37].

Stability of catalyst issue in biomass valorization processess

In a heterogeneous catalytic process, a catalyst may suffer of activity and or selectivity loss as the reaction proceeds. This phenomenon is called catalyst deactivation and it is defined as loss of activity/selectivity on reaction time. Deactivation can occur in different ways that can be classified into three categories: mechanical, chemical or thermal deactivation. The first is related to fouling events or attrition that cause crushing or erosion. Chemical deactivation considers the poisoning and leaching of the active phase while the thermally-induced deactivation is related to catalyst sintering that result in loss of surface area [38].

Moreover, due to the high polarity of the bioderived feedstock, valorization processes often rely to water as solvent. As a consequence, catalysts must be chosen or designed to resist water or polar solvents. Low hydrothermal stability of the materials could cause dissolution or leaching in the aqueous media especially under different pH conditions. Water can be present in the reaction environment not only as solvent medium but also as byproduct of dehydration or condensation reaction. Hence, development of water-tolerant catalyst, in particular acid catalysts, could have a major impact on industrial applications involving biomass transformation. Water can adsorb on hydrophilic solid acid surface resulting in a partial deactivation of acidic sites and or, sometime, even the hydrolysis of the inorganic frameworks. Most Brønsted and Lewis acids sites can be permanently poisoned by water adsorption creating a highly stable water adduct that can block their original Lewis acidity. Moreover, in some cases Lewis acids are unstable into the water environment tend to decompose into the corresponding metal hydroxides. It was also reported that Lewis acid (M^+) could react with water molecules acting as Lewis Base, saturating the coordinative unsaturation and forming surface hydroxyl groups that generate a Brønsted acid site [39,40]. On the other hand, if two Brønsted acid sites dehydrates could convert into one Lewis site and one base site. This can be observed for many different materials such as silica aluminas metal oxides and zeolites with several techniques such as IR measurements after probe adsorption like pyridine or CO [40–42].

In this respect the effect of water must be properly studied to design a water tolerant solid acid catalyst [43]. For instance, in the case of γ-Al_2O_3 the Lewis acidity decreases due to water and no Brønsted acid sites are produced [44,45]. However, many examples of water-resistant catalysts are reported in literature. In particular, the behaviors of niobium oxide and H-ZSM-5 zeolites in presence of water vapor was studied using FT-IR spectroscopy after pyridine adsorption. While H-ZSM-5 showed no changes in acidity, niobium oxide exhibited the presence of new reversible Brønsted acid sites caused by water addition to Lewis centers [44]. Niobium oxide materials acidic centers had showed a typical water resistance: in the case of $Nb_2O_5 \bullet n\,H_2O$, in the presence of water, readily forms NbO_4-H_2O adducts that preserve the Lewis acid functionality and still catalyze the conversion of glucose into 5-(hydroxy- methyl)furfural in water [46]. Zeolites acidic sites can also show water tolerance: Sushkevich and coworkers [39] demonstrated that the Lewis and Brønsted acid properties of Sn-BEA zeolite before and after the adsorption of water on Lewis sites change in a significant manner. In fact, it causes the formation of bridged OH groups that act as new Brønsted sites. Conversely, in the case of just Sn supported Si-BEA zeolites, water causes the hydrolysis of Si-O-Sn bonds without the formation of new acidic sites due to a different coordinative environment of the Sn respect to the one of Sn incorporated zeolite [39]. The water resistance of a solid material is strictly related to its surface wettability [43]. Its modulation could be also an effective tool to impart water resistance and protect acidic active sites [43]. In the following section, the importance of the catalysts surface wettability will be discussed.

Wettability of solid catalysts

Surface phenomena are related to surface free energy that regulates the adsorption and desorption of different chemical species. This is connected to the wettability properties of a solid surface that can be defined as the ability to be covered by a liquid, therefore describing the affinity between a solid and liquid interface [47–49]. Understanding the wettability properties of a surface is fundamental in heterogeneous catalysis studies. A surface can be hydrophobic or hydrophilic depending on the affinity that it has with water. This property is generally described by the contact angle, which is the result of the balance between interfacial free energies. In fact, the water contact angle value is the most straightforward way to evaluate wettability measuring the angle formed by a drop of water with a solid surface. If the angle θ is smaller than 90°, the surface is hydrophilic, if $\theta > 90°$ the surface is hydrophobic [50] (figure 1.4).
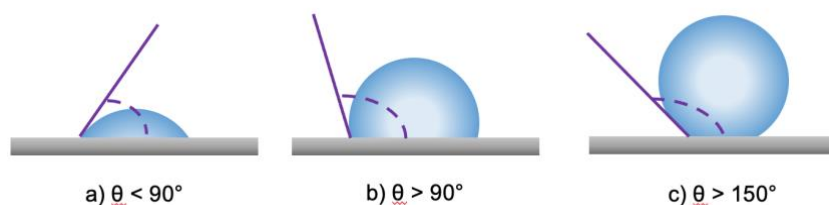
Figure 1.4. Water contact angles for hydrophilic (a), hydrophobic (b) and superhydrophobic (c) surfaces.

According to this, surface hydrophobicity and hydrophilicity regulates its catalytic applications range since key catalytic steps are related to adsorption and desorption of the substrates.

Surface polarity or wettability of a catalyst is affected by several surface groups such as hydroxyl (-OH), carboxyl and esters (-COOH, -COOR), carbonyl (-C=O), ethers (R-O-R) and ionic species (H$^+$, Na$^+$, Cl$^-$, CO$_3^{2-}$ etc.) that are highly polar or alkylic groups, siloxanes, etc. that have low polarity. Biomass transformation involves hydrophilic and hydrophobic molecules or substrates that possess different functional groups with opposite polarity. Hence, once again, it is necessary to tune the wettability properties of a catalysts surface to optimize the adsorption and desorption of the substrates and products towards the catalytic active site. Therefore, catalytic materials with suitable hydrophobic properties may enhance adsorption of more lipophilic reactants and desorption of hydrophilic reactants or products, thus boosting the catalytic activity and preventing poisoning of the active sites caused by strong molecules adsorption. For instance, in a work of 2020, copper catalyst with a low hydrophilic character was found to be more effective in the selective hydrogenation of the α,β double bond of natural enones compared to a more hydrophilic material. The results were in agreement with the easier interaction of the hydrophobic C=C bond with a less polar surface [51].

The water scavenging during condensation reactions is very well known to improve the catalytic activity therefore pushing the conversion. Otomo *et al.* tested a series of zeolites with different Si/Al ratio in the dehydration of sorbitol to give isosorbide. Materials with a low Al content exhibited a higher catalytic activity if compared to the one with high Al content, despite the small number of acid sites. The reason was ascribed to the higher hydrophobicity of the beta Si/Al=75 catalyst surface that allowed a better desorption of the water produced during the dehydration step and a higher hydrothermal stability of the material [52].

As already mentioned, another important aspect of surface studies is the presence of water in the reaction medium both as solvent or as byproduct of dehydration and

condensation reactions that can cause the poisoning of the active sites and the hydrolysis of the inorganic frameworks of the catalytic materials [53]. Moreover, water environment can cause the leaching of many active sites especially metal-based Lewis acid ones [53].

Hydrophobization of a solid surface through functionalization can drastically improve the hydrothermal stability of a catalyst protecting frameworks and active sites from water. In a work of Resasco's research group [54] it was demonstrated that hydrophobization of H-USY zeolite with octadecyltrichlorosilane drastically enhances the stability of the material in the alkylation of m-cresol with cyclopentanol in a water/oil emulsion system. The organosilane grafting onto -OH groups of the zeolite prevents a direct contact between the zeolite with the condensed water, thus stabilizing it from structural degradation and poisoning and also making it more active if compared to the bare zeolite [54]. Similarly, SBA-15 mesoporous silica can be functionalized with hydrophobic phenyl sulfonic groups in three steps. These modified materials had greater stability towards water if compared to the simply sulfonated SBA-15. It was demonstrated that phenyl residues imparted a suitable hydrophobicity to drive out water formed during the synthesis of 2H-indazolo[2,1-b]phthalazine-triones and triazolo[1,2-a]indazole-triones [55].

Bifunctional supported metal catalyst for biomass valorization

In the previous sections it has been underlined that multifunctional catalysts could be effective in biomass valorization processes. Notably, solid catalysts offer the possibility to integrate different types of active sites that is not possible to obtain with homogeneous catalysis. In fact, solid materials can have on their surface the co-existence of acidic, basic and redox active sites. This opens a wide spectrum of possibilities to implement complex transformations in one-pot processes. In this case catalyst design becomes even more crucial: actually, multistep synthesis performed in one pot can often result in the formation of several byproducts [56]. In particular, bifunctional catalysts consisting in supported acid-basic functions and metals are fundamental in promoting organic reaction such as hydrolysis and condensation and reactions involving hydrogen such as hydrogenation and oxidation, that are crucial in the valorization of the high content of oxygenated molecules present in the biomass feedstocks. Moreover, acid sites could have a role in the activation of C-O bonds making them more prone to hydrogenation. It can be derived that combining two different active sites and finely tuning their properties could be a fundamental tool in biomass valorization.

Metallic phases can be supported on a variety of materials such as metal oxides, mixed oxides, carbons or organic polymeric frameworks [32]. Supports have different properties in terms of acidity, basicity, wettability or inertness.

For instance, in a work of Zhu's group several 1% Pt/HBeta Zeolite with different Brønsted acid sites to Pt ratio were prepared changing only the acid sites density combining the hydrogenation power of the platinum phase with the acidity of the support. This series of catalyst was tested in the hydrodeoxygenation of the lignin derived monomer *m*-cresol. The fine tuning of acidity was pivotal in diverting the reaction conversion and selectivity. In fact, varying the acid sites/Pt ratio affects the product distribution and the reaction turnover frequency due to the different transportation of the reactant/intermediates through the micropore of the zeolite crystallite [57].

Another example demonstrating the significant effect of the proper choice of the support and, as consequence, of the combination of the various functionality of a catalyst in diverting conversion and selectivity of a process was shown by a work from Ravasio's group. A one step synthesis of butyl butyrate starting from butanol was set up using a Cu/ZrO_2 catalyst. They manage to demonstrate that ZrO_2 was fundamental in the first activation of the alcohol to alkoxide if compared to SiO_2, but not enough as itself to promote the dehydrogenation step. For this a metallic phase such as the supported copper one was necessary. Thus, the synergistic effect of ZrO_2 and Cu was found to be crucial in the successful reaction proceeding [58].

Bifunctionality can be also imparted by a single element of a catalytic material. In a work of the same group copper was supported on a quite inert SiO_2 material. Thanks to the preparation method, the very low particle size of Cu not only showed a remarked hydrogenation power but also a sharp Lewis acidic character. The combination of both features was the key in achieving good yields of pentyl valerate starting from GVL and 1-pentanol. The moderate copper Lewis acidity activates the carbonyl group of the lactone to the 1-pentanol attack and to the consequent hydrogenation step [57], while limiting the by-product formation otherwise formed in higher amounts when using an acidic support.

1.1.4 Deposition of dispersed metal oxides phases on supports

In the previous section, the advantages, the criticality and issues of heterogeneous catalysis in sustainable chemistry processes has been discussed, in particular concerning

supported metal catalyst. In the literature, there are several developed methods for the preparation of supported metal catalysts, but only few examples exist relying on robust and active materials for industrial applications [34,59].

The most widespread methods to prepare supported metal catalysts are the coprecipitation and impregnation techniques, that consist in effortless preparation procedures that utilize cheap and simple precursors. Nevertheless, materials prepared with these strategies present some drawbacks such as low metal phase dispersion and lack in particle size control and uniformity, especially for high metal loadings. For instance, supported, mixed and single component catalysts can be produced with the coprecipitation method but the synthesis could be difficult to be controlled, in particular, the final features of the solid could not be easily tuned. Similarly, impregnation methods consist in facile preparation steps but low dispersion of the metal phase, low homogeneity, different size and shape of the active particles and support interaction are the main drawbacks [34,59].

In the work of this thesis, catalysts were prepared using an unconventional method called Chemisorption-Hydrolysis (CH), which allowed us to prepare supported copper catalysts that have hydrogenation and acidic catalytic properties with an easy and reproducible protocol. This method has been demonstrated to combine the easiness of impregnation techniques while ensuring high metal dispersion and low particle size [60]. Furthermore, the versatility of this method offers the possibility to obtain highly dispersed copper catalyst on a variety of different inorganic matrices on which the final catalyst properties will depend [61]. The peculiar feature of the copper phase deposited with CH method confers outstanding hydrogenation activity to the copper oxide nanoparticles and an unexpected Lewis acidic character that is due to the Cu phase morphology. This method offers the possibility to exploit non-noble Cu catalysts that have hydrogenation activity comparable to the most used noble metal catalysts, such as Ru, Pt and Pd, and of Ni using a cheap, non-noble and non-toxic Cu catalysts. Catalysts prepared with this method demonstrated to be highly stable and suitable for many industrial applications. For instance, Cu/ZrO$_2$ system was stable up to 90 hours of reaction during the production of a mixture of butanol/butyl butyrate via a dehydrogenative coupling reaction under no solvent conditions at 250-350 °C of temperature [62]. In another case Cu/SiO$_2$ was stable up to 250 °C and 100 bar of H$_2$ pressure during dimethyl adipate hydrogenolysis [63].

A detailed explanation of the synthetic procedure and overlook of the characteristic features of the Cu catalysts prepared with CH method is shown in appendix section 6.3.

1.1.5 γ-Valerolactone: an important bioderived platform chemical

In the work of the present thesis GVL was used as the main substrate for the production of value-added chemicals. GVL is a C_5 membered lactone that has natural occurrence *i.e.,* in fruits and vegetables. It is a renewable, non-toxic and biodegradable substance that can be easily and safely stored and transported due to its low melting point (-31 °C) and high boiling one (207 °C). For these reasons, GVL is widely employed in the industrial and manufacture field as food and fuel additive, solvent and as renewable and sustainable precursor for other important chemicals such as 2-methyltetrahydrofurane, alkanes and 1,4-pentanediol [16,64].

As already mentioned, GVL can be obtain by hydrogenation of LA that can be derived from cellulosic biomass (see section 1.2). Actually, there are different ways to produce GVL from LA following two main mechanism pathways (Scheme 1.1). One route starts from hydrogenation of LA to give γ-hydroxyvaleric acid followed by a dehydration step to the desired GVL. The second way proceeds *via* dehydration of LA to give angelica lactone that is subsequently hydrogenated to GVL. In both cases, there is a dehydration step that relies on an acidic active site and a hydrogenation step that requires a metal active center [19,65].
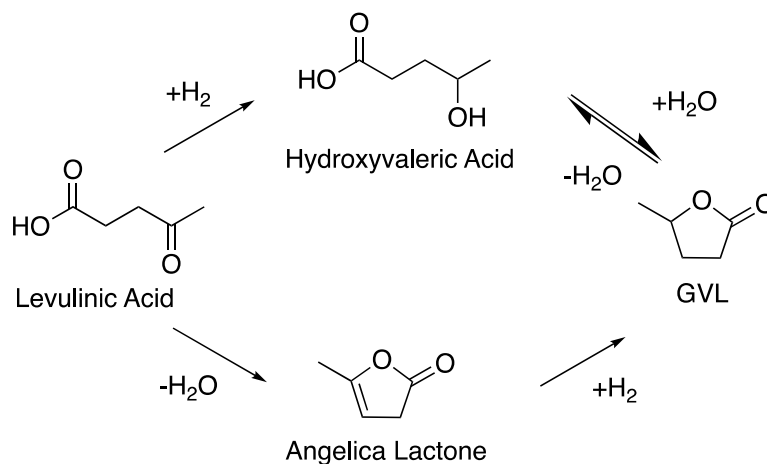
Scheme 1.1. LA hydrogenations pathway to give GVL.

Several hydrogenation strategies can be utilized in the hydrogenation of LA to give GVL. Hydrogenation of LA to give GVL can be achieved using indirect source of hydrogen, such as formic acid or alcohols, with a mechanism called catalytic transfer hydrogenation (CTH) that is surely one of the most interesting approaches for a safe, environmentally friendly and cost-effective GVL production.

However, typically hydrogenation is carried out by using exogenous hydrogen gas that is the most straightforward way to hydrogenate different compounds [66]. Non-noble metal catalysts, in particular supported copper catalysts, has demonstrated to be efficient system for the hydrogenation of LA with molecular hydrogen. In agreement with the scope of this thesis work, some structure-activity-relationship examples of heterogeneous copper catalysis used to perform hydrogenation of LA to GVL will be briefly discussed.

As already mentioned, in this case, a highly performing catalyst must possess a great hydrogenation activity combined with a marked acidity to activate the carbonyl group to hydrogen attack and to enhance dehydration. Hydrogenation power can be enhanced by well-dispersed, low size metal nanoparticles: In a work of Obrégon's research group [67] different bimetallic Ni-Cu materials prepared with wet impregnation and sol gel methods were tested in the hydrogenation of LA to GVL. Similar conversions and yields profiles (up to 96% yield after six hours) in GVL were achieved with the catalysts prepared with wet impregnation and sol gel method. However, the materials prepared with the latter method possessed around half of the metal content (14% against 34% wt/wt respectively). The better performances were ascribed to the higher dispersion obtained with the sol gel method in contrast to the wet impregnation technique together with a balanced amount of acidic and metallic sites. The authors stated that a higher dispersion allowed a more intimate contact between the acidic and hydrogenating sites, therefore boosting the reaction rate, and preventing coke deposition [67]. Similarly, the dispersion of the metal phase in Cu/ZrO_2 catalysts prepared with coprecipitation was again critical in the hydrogenation of LA to give GVL. In this case, activity was not proportional with copper content because it could be incorporated into the zirconia lattice or present as large bulk aggregates. A proper Cu/Zr (ratio =1) with high dispersion was the key to achieve the highest yields in GVL (80%) with a total conversion of LA [68].

A well-fitting example of tailoring hydrogenation activity and acidity is proposed by a work of Chary's group [23]: Cu/Al_2O_3 systems were prepared with different Cu loading. The conversion of LA reached a maximum at 5-10% copper loading (98%), then it decreased to 41% at 20% Cu loading wt/wt. The drop of catalyst activity was ascribed to the lacking of availability of acidic sites at high Cu loading that enables the dehydration step from LA to angelicalactone. Selectivity towards GVL followed the same trend and the authors suggested that selectivity was related to the copper dispersion too [23]. The same catalytic behavior was observed when using Cu/ZrO_2 materials by the same group [69].

1.1.6 Aims of the thesis

The work of this Ph.D thesis project was dedicated to the valorization of platform molecules derived from biomass cellulosic waste, in particular, biobased lactones such as GVL using heterogeneous copper catalysts. These can be valorized into new valuable molecules such as diols and amines that are ubiquitous chemicals in today's chemical industry. The use of simple and cheap heterogeneous copper catalysts supported on various materials, prepared with the Chemisorption-Hydrolysis method [70], will avoid toxic and expensive noble metal catalysts. These materials are easy to prepare, resistant and provide reliable results. Depending on the nature of the support they can have different acidic or wettability properties making them very versatile in organic synthesis. Deep characterization was performed on the catalytic system to enlighten the relationship between physicochemical properties of the catalysts with their performances. Particularly, a focus was given on the study of copper phase morphology, wettability and acidity of the surfaces.

The work will follow two main research lines:

1. Study on GVL hydrogenation to give 1,4-PDO
2. Synthesis of N-containing chemicals starting from bioderived molecules.

1.2 References

1. Ivanković, A. Review of 12 Principles of Green Chemistry in Practice. *Int. J. Sustain. Green Energy* **2017**, *6*, 39.

2. Brundtland, G.G. *Our Common Future, The World Commis- sion on Environmental Development,*; 1987;

3. de Marco, B.A.; Rechelo, B.S.; Tótoli, E.G.; Kogawa, A.C.; Salgado, H.R.N. Evolution of green chemistry and its multidimensional impacts: A review. *Saudi Pharm. J.* **2018**.

4. Sheldon, R.A. Green and sustainable manufacture of chemicals from biomass: State of the art. *Green Chem.* 2014.

5. Clark, J.H. Green chemistry : challenges and opportunities. *Green Chemestry* **1999**, *1*, 1–8.

6. Poliakoff, M.; Fitzpatrick, J.M.; Farren, T.R.; Anastas, P.T. Green chemistry: Science and politics of change. *Science (80-.).* **2002**, *297*, 807–810.

7. Kubička, D.; Aubrecht, J.; Pospelova, V.; Tomášek, J.; Šimáček, P.; Kikhtyanin, O. On the importance of transesterification by-products during hydrogenolysis of dimethyl adipate to hexanediol. *Catal. Commun.* **2018**, *111*, 16–20.

8. Gallezot, P. Conversion of biomass to selected chemical products. *Chem. Soc. Rev.* 2012.

9. Velvizhi, G.; Goswami, C.; Shetti, N.P.; Ahmad, E.; Kishore Pant, K.; Aminabhavi, T.M. Valorisation of lignocellulosic biomass to value-added products: Paving the pathway towards low-carbon footprint. *Fuel* **2022**, *313*, 122678.

10. Ghatak, H.R. Biorefineries from the perspective of sustainability: Feedstocks, products, and processes. *Renew. Sustain. Energy Rev.* **2011**, *15*, 4042–4052.

11. Horta Nogueira, L.A.; Moreira, J.R.; Schuchardt, U.; Goldemberg, J. The rationality of biofuels. *Energy Policy* **2013**, *61*, 595–598.

12. Tuck, C.O.; Pérez, E.; Horváth, I.T.; Sheldon, R.A.; Poliakoff, M. Valorization of biomass: Deriving more value from waste. *Science (80-.).* **2012**, *338*, 604.

13. Kohli, K.; Prajapati, R.; Sharma, B.K. Bio-based chemicals from renewable biomass for integrated biorefineries. *Energies* **2019**, *12*.

14. Haq, I.U.; Qaisar, K.; Nawaz, A.; Akram, F.; Mukhtar, H.; Zohu, X.; Xu, Y.; Mumtaz, M.W.; Rashid, U.; Ghani, W.A.W.A.K.; et al. Advances in valorization of lignocellulosic biomass towards energy generation. *Catalysts* **2021**, *11*, 1–26.

15. Djakovitch, L.; Essayem, N.; Eternot, M.; Rataboul, F. A landscape of lignocellulosic biopolymer transformations into valuable molecules by heterogeneous catalysis in c'durable team at ircelyon. *Molecules* **2021**, *26*.

16. Alonso, D.M.; Wettstein, S.G.; Dumesic, J.A. Gamma-valerolactone, a sustainable platform molecule derived from lignocellulosic biomass. *Green Chem.* **2013**, *15*, 584–595.

17. Alonso, D.M.; Wettstein, S.G.; Mellmer, M.A.; Gurbuz, E.I.; Dumesic, J.A. Integrated conversion of hemicellulose and cellulose from lignocellulosic biomass. *Energy Environ. Sci.* **2013**, *6*, 76–80.

18. Sheldon, R.A. Green and sustainable manufacture of chemicals from biomass: State of the art. *Green Chem.* **2014**, *16*, 950–963.

19. Pileidis, F.D.; Titirici, M.M. Levulinic Acid Biorefineries: New Challenges for Efficient Utilization of Biomass. *ChemSusChem* **2016**, *9*, 562–582.

20. Adeleye, A.T.; Louis, H.; Akakuru, O.U.; Joseph, I.; Enudi, O.C.; Michael, D.P. A Review on the conversion of levulinic acid and its esters to various useful chemicals. *AIMS Energy* **2019**, *7*, 165–185.

21. Son, P.A.; Nishimura, S.; Ebitani, K. Production of γ-valerolactone from biomass-derived compounds using formic acid as a hydrogen source over supported metal catalysts in water solvent. *RSC Adv.* **2014**, *4*, 10525–10530.

22. Kleist, W.; Grunwaldt, J.-D.; Schubert, M.; Carvalho, H.W.P.; Hengst, K.; Lu, C. Synthesis of γ-valerolactone by hydrogenation of levulinic acid over supported nickel catalysts. *Appl. Catal. A Gen.* **2015**, *502*, 18–26.

23. Balla, P.; Perupogu, V.; Vanama, P.K.; Komandur, V.R.C. *Hydrogenation of biomass-derived levulinic acid to γ-valerolactone over copper catalysts supported on ZrO2*; 2016; Vol. 91; ISBN 9140271609.

24. Germán, L.; Cuevas, J.M.; Cobos, R.; Pérez-Alvarez, L.; Vilas-Vilela, J.L. Green alternative cosolvents toN-methyl-2-pyrrolidone in water polyurethane dispersions. *RSC Adv.* **2021**, *11*, 19070–19075.

25. Strappaveccia, G.; Ismalaj, E.; Petrucci, C.; Lanari, D.; Marrocchi, A.; Drees, M.; Facchetti, A.; Vaccaro, L. A biomass-derived safe medium to replace toxic dipolar solvents and access cleaner Heck coupling reactions. *Green Chem.* **2015**, *17*, 365–372.

26. Oser, B.L.; Carson, S.; M. Oser Toxicological tests on flavouring matters. *Food Cosmet. Toxicol.* **1965**, *3*, 563–569.

27. Horváth, I.T.; Mehdi, H.; Fábos, V.; Boda, L.; Mika, L.T. γ-Valerolactone-a sustainable liquid for energy and carbon-based chemicals. *Green Chem.* **2008**, *10*, 238–242.

28. Bababrik, R.M.; Wang, B.; Resasco, D.E. Reaction Mechanism for the Conversion of γ-Valerolactone (GVL) over a Ru Catalyst: A First-Principles Study. *Ind. Eng. Chem. Res.* **2017**, *56*, 3217–3222.

29. Simakova, I.; Demidova, Y.; Simonov, M.; Prikhod'ko, S.; Niphadkar, P.; Bokade, V.; Dhepe, P.; Murzin, D.Y. Heterogeneously Catalyzed γ-Valerolactone Hydrogenation into 1,4-Pentanediol in Milder Reaction Conditions. *Reactions* **2020**, *1*, 54–71.

30. Zaccheria, F.; Ravasio, N. *Solid Catalysts for the Upgrading of Renewable Sources*; 2019; Vol. 9; ISBN 9783038975724.

31. Conversion, B. *Catalysis for Clean Energy and Environmental Sustainability*; 2021; Vol. 1; ISBN 9783030650162.

32. Védrine, J.C. Heterogeneous catalysis on metal oxides. *Catalysts* **2017**, *7*.

33. Anastas, P.; Eghbali, N. Green Chemistry: Principles and Practice. *Chem. Soc. Rev.* **2010**, *39*, 301–312.

34. Hagen, J. *Industrial catalysis: A practical approach*; 2015; ISBN 9783527331659.

35. Lin, L.; Han, X.; Han, B.; Yang, S. Emerging heterogeneous catalysts for biomass conversion: Studies of the reaction mechanism. *Chem. Soc. Rev.* **2021**, *50*, 11270–11292.

36. Dada, T.K.; Sheehan, M.; Murugavelh, S.; Antunes, E. A review on catalytic pyrolysis for high-quality bio-oil production from biomass. *Biomass Convers. Biorefinery* **2021**.

37. Gao, X.; Wang, Z.; Ashok, J.; Kawi, S. A comprehensive review of anti-coking, anti-poisoning and anti-sintering catalysts for biomass tar reforming reaction. *Chem. Eng. Sci. X* **2020**, *7*, 100065.

38. Kim, S.; Tsang, Y.F.; Kwon, E.E.; Lin, K.Y.A.; Lee, J. Recently developed methods to enhance stability of heterogeneous catalysts for conversion of biomass-derived feedstocks. *Korean J. Chem. Eng.* **2019**, *36*, 1–11.

39. Sushkevich, V.L.; Kots, P.A.; Kolyagin, Y.G.; Yakimov, A. V.; Marikutsa, A. V.; Ivanova, I.I. Origin of Water-Induced Brønsted Acid Sites in Sn-BEA Zeolites. *J. Phys. Chem. C* **2019**, *123*, 5540–5548.

40. Busca, G. Spectroscopic characterization of the acid properties of metal oxide catalysts. *Catal. Today* **1998**, *41*, 191–206.

41. Busca, G. The surface acidity of solid oxides and its characterization by IR spectroscopic methods. An attempt at systematization. *Phys. Chem. Chem. Phys.* **1999**, *1*, 723–736.

42. Basila, M.R.; Kantner, T.R.; Rhee, K.H. The Nature of the Acidic Sites on a Silica-Alumina. Characterization by Infrared Spectroscopic Studies of Trimethylamine and Pyridine Chemisorption1. *J. Phys. Chem.* **1964**, *68*, 3197–3207.

43. Okuhara, T. Water-tolerant solid acid catalysts. *Chem. Rev.* **2002**, *102*, 3641–3666.

44. Omata, K.; Nambu, T. Catalysis of water molecules acting as Brönsted acids at Lewis acid sites on niobium oxide. *Appl. Catal. A Gen.* **2020**, *607*, 117812.

45. Roy, S.; Mpourmpakis, G.; Hong, D.-Y.; Vlachos, D.G.; Bhan, A.; Gorte, R.J. Mechanistic Study of Alcohol Dehydration on γ-Al2O3. *ACS Catal.* **2012**, *2*, 1846–1853.

46. Nakajima, K.; Baba, Y.; Noma, R.; Kitano, M.; N. Kondo, J.; Hayashi, S.; Hara, M. Nb2O5•nH2O as a heterogeneous catalyst with water-tolerant lewis acid sites. *J. Am. Chem. Soc.* **2011**, *133*, 4224–4227.

47. Erbil, H.Y. *Surface Chemistry: Of Solid and Liquid Interfaces*; 2009; ISBN 1405119683.

48. Gläser, R.; Weitkamp, J. Surface Hydrophobicity or Hydrophilicity of Porous Solids. In *Handbook of Porous Solids*; WILEY-VCH, Germany, 2008 ISBN 9783527302468.

49. Myers, D. *Surfaces, Interfaces, and Colloids: Principles and Applications, Second Edition*; John Wiley & Sons, Inc.: New York, 1999; ISBN 9780471234999.

50. Stubenrauch, C. *Emulsions, Foams and Suspensions . Fundamentals and Applications. By Laurier L. Schramm.*; 2006; Vol. 7; ISBN 9783527307432.

51. Cavuoto, D.; Zaccheria, F.; Marelli, M.; Evangelisti, C.; Piccolo, O.; Ravasio, N. The Role of Support Hydrophobicity in the Selective Hydrogenation of Enones and Unsaturated Sulfones over Cu/SiO2 Catalysts. *Catalysts* **2020**, 515.

52. Otomo, R.; Yokoi, T.; Tatsumi, T. Synthesis of isosorbide from sorbitol in water over high-silica aluminosilicate zeolites. *Appl. Catal. A Gen.* **2015**, *505*, 28–35.

53. Xiong, H.; Pham, H.N.; Datye, A.K. Hydrothermally stable heterogeneous catalysts for conversion of biorenewables. *Green Chem.* **2014**, *16*, 4627–4643.

54. Pino, N.; Bui, T.; Hincapié, G.; López, D.; Resasco, D.E. Hydrophobic zeolites for the upgrading of biomass-derived short oxygenated compounds in water/oil emulsions. *Appl. Catal. A Gen.* **2018**, *559*, 94–101.

55. Veisi, H.; Sedrpoushan, A.; Faraji, A.R.; Heydari, M.; Hemmati, S.; Fatahi, B. A

mesoporous SBA-15 silica catalyst functionalized with phenylsulfonic acid groups (SBA-15-Ph-SO3H) as a novel hydrophobic nanoreactor solid acid catalyst for a one-pot three-component synthesis of 2H-indazolo[2,1-b]phthalazine-triones and triazolo[1,2-a]. *RSC Adv.* **2015**, *5*, 68523–68530.

56. Rinaldi, R.; Schüth, F. Design of solid catalysts for the conversion of biomass. *Energy Environ. Sci.* **2009**, *2*, 610–626.

57. Scotti, N.; Dangate, M.; Gervasini, A.; Evangelisti, C.; Ravasio, N.; Zaccheria, F. Unraveling the role of low coordination sites in a cu metal nanoparticle: A step toward the selective synthesis of second generation biofuels. *ACS Catal.* **2014**, *4*, 2818–2826.

58. Scotti, N.; Zaccheria, F.; Evangelisti, C.; Psaro, R.; Ravasio, N. Dehydrogenative coupling promoted by copper catalysts: A way to optimise and upgrade bio-alcohols. *Catal. Sci. Technol.* **2017**, *7*, 1386–1393.

59. Santen, R.A. van *Modern Heterogeneous Catalysis*; WILEY-VCH, Germany, 2017; ISBN 9783527339617.

60. Boccuzzi, F.; Chiorino, A.; Martra, G.; Gargano, M.; Ravasio, N.; Carrozzini, B. Preparation, characterization, and activity of Cu/TiO2 catalysts: I. Influence of the preparation method on the dispersion of copper in Cu/TiO2. *J. Catal.* **1997**, *165*, 129–139.

61. Gervasini, A.; Manzoli, M.; Martra, G.; Ponti, A.; Ravasio, N.; Sordelli, L.; Zaccheria, F. Dependence of copper species on the nature of the support for dispersed CuO catalysts. *J. Phys. Chem. B* **2006**, *110*, 7851–7861.

62. Scotti, N.; Ravasio, N.; Zaccheria, F.; Irimescu, A.; Merola, S.S. Green pathway to a new fuel extender: Continuous flow catalytic synthesis of butanol/butyl butyrate mixtures. *RSC Adv.* **2020**, *10*, 3130–3136.

63. Aubrecht, J.; Kikhtyanin, O.; Pospelova, V.; Paterová, I.; Kubička, D.; Zaccheria, F.; Scotti, N.; Ravasio, N. Enhanced activity of Cu/SiO2 and Cu/ZrO2 catalysts in dimethyl adipate hydrogenolysis. *Catal. Today* **2022**.

64. Dutta, S.; Yu, I.K.M.; Tsang, D.C.W.; Ng, Y.H.; Ok, Y.S.; Sherwood, J.; Clark, J.H. Green synthesis of gamma-valerolactone (GVL) through hydrogenation of biomass-derived levulinic acid using non-noble metal catalysts: A critical review. *Chem. Eng. J.* **2019**, *372*, 992–1006.

65. Wright, W.R.H.; Palkovits, R. Development of heterogeneous catalysts for the conversion of levulinic acid to γ-valerolactone. *ChemSusChem* **2012**, *5*, 1657–1667.

66. Nishimura, S. *Handbook of heterogeneous catalytic hydrogenation for organic synthesis*; John Wiley & Sons, Inc.: New York, 2001; ISBN 0-471-39698-2.

67. Obregón, I.; Corro, E.; Izquierdo, U.; Requies, J.; Arias, P.L. Levulinic acid hydrogenolysis on Al2O3-based Ni-Cu bimetallic catalysts. *Cuihua Xuebao/Chinese J. Catal.* **2014**, *35*, 656–662.

68. Jones, D.R.; Iqbal, S.; Ishikawa, S.; Reece, C.; Thomas, L.M.; Miedziak, P.J.; Morgan, D.J.; Edwards, J.K.; Bartley, J.K.; Willock, D.J.; et al. The conversion of levulinic acid into γ-valerolactone using Cu-ZrO2 catalysts. *Catal. Sci. Technol.* **2016**, *6*, 6022–6030.

69. Balla, P.; Perupogu, V.; Vanama, P.K.; Komandur, V.R.C. Hydrogenation of biomass-derived levulinic acid to γ-valerolactone over copper catalysts supported on ZrO2. *J. Chem. Technol. Biotechnol.* **2016**, *91*, 769–776.

70. Zaccheria, F.; Scotti, N.; Marelli, M.; Psaro, R.; Ravasio, N. Unravelling the properties of supported copper oxide: Can the particle size induce acidic behaviour? *Dalt. Trans.* **2013**, *42*, 1319–1328.

2 HYDROGENATION OF γ-VALEROLACTONE TO 1,4-PENTANEDIOL WITH Cu/SiO$_2$ CATALYSTS

2.1 Introduction

In this introduction section, an overview on the recent literature concerning heterogeneous catalytic processes aimed to obtain 1,4-Pentandiol (1,4-PDO) starting from Levulinic acid (LA) and γ-valerolactone (GVL) is proposed.

1,4-PDO is an interesting and useful biomass deriving diol that could be utilized not only as bio-monomers to synthetize bioderived polyesters [1,2] and polyurethanes [3,4] but also as solvent [5,6]. As already showed in the previous chapter, LA can be converted in GVL through hydrogenation and dehydration reactions but also can be furtherly hydrogenated to give the 1,4-PDO. The reaction pathways of LA hydrogenation to give GVL and 1,4-PDO can divert depending on dehydration or hydrogenation sequences involving the formation of 4-hydroxypentanoic acid (4-HPA) intermediate if the hydrogenation occurs at first, or angelicalactone (AL) intermediate if the dehydration takes place before. GVL can be subsequently hydrogenated to 1,4-PDO that can be further dehydrated to give 2-Methyltetrahydrofuran (2-Me-THF) [7]. As observable, the fine tune of the dehydration acid/base properties and the hydrogenation power of the catalysts could modulate the reaction mechanism pathways and subsequently the obtained products.
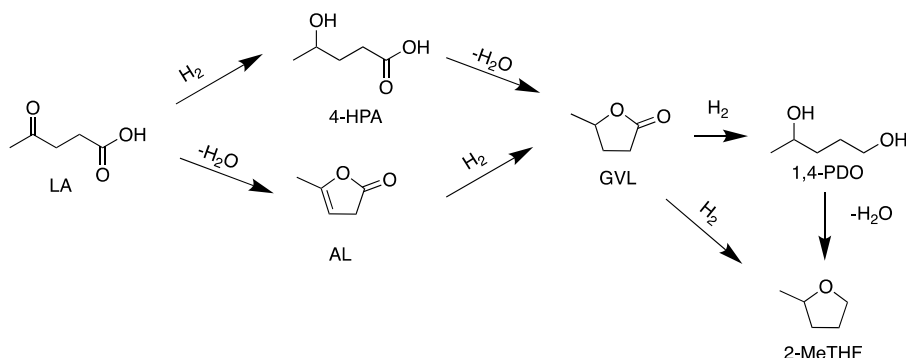
Figure 2.1. LA hydrogenation pathways to give GVL and or 1,4-PDO. Adapted from ref. [7].

2.1.1 Levulinic acid hydrogenation to 1,4-pentandiol

Noble metal catalysts

LA hydrogenation to 1,4-PDO is a non-trivial reaction that in the literature is reported to be mainly achieved by using noble metal catalyst. Supported noble metal catalysts can be utilized such as Mo-modified Rh/SiO_2 catalyst in aqueous media at 80 °C and 6 MPa of hydrogen [8]. The modification of the catalyst with small amount of Mo was effective in switching the selectivity from the product GVL to the 1,4-PDO reaching 70% yield using the

optimized 0.13 Mo/Rh ratio. Exceeding ratio of 0.25 shifts the selectivity back to GVL. After some tests with model carboxylic acid, it was found that the Mo modification may promote the adsorption of the acid group and subsequently its hydrogenation. This could be the reason for the high selectivity towards the diol [8]. Similarly, Mo can be used to prepare Pt-Mo system supported on hydroxyapatite using a co-impregnation method [9]. This catalyst was effective in the hydrogenation of LA reaching 93% of 1,4-PDO yield at 130 °C and 6 MPa of H_2. Similarly, to the previous example, the Pt/Mo ratio affected the selectivity towards the 1,4-PDO with a volcano-type dependency with the maximum at Pt/Mo=4 [9].

LA hydrogenation to 1,4-PDO can be achieved with 100% yield using a commercial catalyst 1 wt% Au/TiO$_2$ by AUROlite^{TM} with microwave irradiation at 200 °C and 5 MPa of H_2 for 4 h under no solvent conditions [10]. The presence of water strongly inhibited the reaction influencing the reversibility as it proceeds through a hydration/dehydration step. The choice of the support was of pivotal importance for the selectivity towards the diol as in the case of 2.5 wt% Au/ZrO$_2$ 100% conversion of LA was reached but with only 9% selectivity in the diol. In fact, it was found that in the case of TiO$_2$, the presence of oxygen vacancies generated by the loss of structural oxygen, alters reactant adsorption/activation and therefore affects the catalytic performance. Moreover, at the surface of the titania, dissociated H atoms are ionized to H^+ that in turns react with activated LA and GVL improving the dehydration and hydrogenation process [10].

Non-noble metal catalysts

There are few examples of non-noble metal supported catalysts used in the LA hydrogenation to give 1,4-PDO: supported Cu catalysts with tunable distribution of acidic and basic sites could switch the production of GVL or of 1,4-PDO from levulinic acid/ester. Brønsted acid sites over CuAl catalyst suppress the opening of the ring of GVL, thus, inhibiting 1,4-PDO formation. On the contrary, the introduction of basic Mg species boosted the selective conversion of GVL to 1,4-PDO *via* opening of the ring structure of GVL [11]. Similarly, in a work of the same group, the hydrogenation of ethyl levulinate to give 1,4-PDO was favored on CuMg catalyst with abundant basic sites that were essential in the GVL ring-opening process [12]. Moreover, a proper amount of Brønsted acid sites could promote the GVL ring-opening in the case of Co-based catalyst. Also in this case, an excessive amount of Brønsted sites suppresses the formation of 1,4-PDO facilitating the formation of byproducts [13].

2.1.2 Γ-valerolactone hydrogenation to 1,4-pentandiol

Due to the complexity of the LA hydrogenation mechanism, the separation of the LA hydrogenation step to give GVL from the further GVL hydrogenation to give 1,4-PDO could be efficient in the achievement of high diol yields. Moreover, GVL hydrogenation to 1,4-PDO is easier to achieve using non-noble metal catalysts. However, some consideration about the reaction mechanism has to be done also in this case.

The group of Resasco has proposed a possible reaction pathway and intermediates formation thanks to a combination of experimental and theoretical studies, considering in particular the hydrogenation in aqueous phase over a 5% Ru/C catalyst [14]. The reaction may start with a ring opening step between the carbonylic carbon and oxygen that forms a surface intermediate, $CH_3CH(O*)-(CH_2)_2 -CO*$. This intermediate can undergo three reversible parallel pathways: i) decarbonylation that leads to 2-butanol, ii) hydrogenation that leads to 1,4-PDO and iii) C-O hydrogenolysis that leads to 2-pentanol [14]. Successively, the same research group has further investigated the reaction profile to shed light on the rate limiting step. In particular, DFT studies suggested that the rate limiting step for the formation of the 1,4-PDO is the hydrogenation one underlining the need to design hydrogenation-promoting catalysts [15]. Actually, in a work on hydrogenation of GVL, Zhang et al. observed also the formation of valeric acid (VA) caused by the cleavage of the C-O bond between the -O- oxygen ester and the $-CH_2-$ [16]. Utilizing MoO_x decorated Ni/Al_2O_3 catalyst, it is possible to switch the selectivity form VA to 1,4-PDO. In particular, when the reduction temperature is increased from 400° to 600 °C, the 1,4-PDO yield increases from 25% to 66%. This could be due to the fact that the catalyst reduced at 600 °C possesses more exposed surface catalytically active Ni^0 with a high hydrogenating power. Moreover, the MoO_x decoration was crucial in tuning the selectivity towards the diol: the surface oxygen vacancies allow a stronger adsorption of GVL, that interacts with the lone electron pair of the oxygen of carbonyl group. In this way, the C-O ester bond can be weakened and finally hydrogenated to 1,4-PDO [16].

Copper catalyst for GVL hydrogenation to 1,4-PDO

Recently, supported copper-based catalysts had showed to be effective in the selective hydrogenation of GVL to give 1,4-PDO. Copper can be supported on a wide variety of metal oxide supports with different properties. A summary of the main results that can be found in the literature is shown in table 2.1.

Table 2.1 Hydrogenation of GVL to give 1,4-PDO by using copper catalysts.

Catalyst	GVL conversion (%)	1,4-PDO selectivity (%)	Reference
Cu/MgO	91	94	[17]
Cu/ZnO (flow)	82	99	[18]
Cu/SiO$_2$ (flow)	32	67	[19]
Cu$_{1.5}$/Mg$_{1.5}$AlO	93	99	[20]
ZnCu/Al$_2$O$_3$	91	98	[21]

A 18% Cu/MgO prepared with metal-organic chemical vapor deposition method allowed to achieve 91% of γ-GVL conversion and 94% selectivity to 1,4-PDO at 10 MPa for 10 h [17]. The copper loading was found to be crucial in the catalytic activity and selectivity towards 1,4-PDO. Passing from 6% Cu/MgO catalysts to the 18% loaded one, the conversion of GVL increased from 71.4% to 80.0% respectively, reaching the maximum selectivity of 1,4-PDO observed of 86%. If the copper loading is further increased an increase in selectivity for 2-MTHF and *n*-pentanol was observed [17]. Cu can be supported on ZnO with a co-precipitation method with a different copper loading and calcination temperature. These catalysts, were used in the hydrogenation of GVL to give 1,4-PDO in a continuous flow reactor. The 40% Cu/ZnO calcined at 500 °C was the best and gave the GVL conversion and the PDO selectivity of 82.3 and 99.2%, respectively at a GVL feed rate of 0.4 g h^{-1}, 140 °C, H$_2$ pressure of 1.5 MPa and H$_2$ flow rate of 90 cm^3 min^{-1} [18]. Also in this case, the selectivity towards the 1,4-PDO increased with the H$_2$ pressure, while the increase in temperature enhances the formation of the dehydration product such as 2-Me-THF [18]. These dependances were observed also in a work of Simakova et al. where Cu/SiO$_2$ were used to achieve 1,4-PDO from GVL [19] with a 32% GVL conversion in a continuous flow reactor using *n*-butanol as the solvent and reaching a selectivity of 1,4-PDO of 67% (GVL = 6.9 mmol, *n*-butanol = 15 mL, m$_{cat}$ = 0.455 g, T = 130 °C, P$_{H2}$ = 1.3 MPa, time = 4 h). The lower selectivity towards 1,4-PDO compared to the one achieved with Cu/ZnO was ascribed to the acidity of the silanol groups that promotes the dehydration of the diol to 2-Me-THF [19]. As already cited, it is important to underline the major role of acid/basic sites when considering this hydrogenation reaction. The basic Cu$_{1.5}$/Mg$_{1.5}$AlO catalyst derived from layered double hydroxides precursors was found particularly efficient achieving a conversion of GVL of 93% and a selectivity to 1,4-PDO >99% [20]. These results were mainly attributed to the cooperative effect of its well-dispersed active Cu nanoparticles

and the appropriate surface base sites nearby. Notably, when the acidic Cu/HZSM-5 is utilized, larger amount of 2-Me-THF were obtained due to the acidic-assisted dehydration of the diol. This was observed also when 1,4-PDO was used as the substrate: a conversion of 69% for 1,4-PDO to 2-Me-THF was found over the Cu/HZSM-5 catalyst when, in contrast, no conversion of 1,4- PDO was observed using the basic $Cu_{1.5}/Mg_{1.5}AlO$ catalyst [20]. The addition of Zn on Cu/Al_2O_3 catalyst improved significantly the selectivity towards the diol passing from 46% of the bare Cu/Al_2O_3 to 98% reported in the case of $ZnCu/Al_2O_3$ catalyst with a Zn/Cu molar ratio =1 [21]. It was observed that 1,4-PDO selectivity increases while selectivity of 2-Me-THF decreases when the amount of Lewis acid sites is decreased by the addition of Zn. In fact, Zn decreases the quantity of surface Lewis acid sites and then promotes the preferential formation of 1,4-PDO than 2-Me-THF [21]. However, high yields in 1,4-PDO from GVL hydrogenation can be obtained using mild acidic supports such as SiO_2 not only under flow conditions [19] but also in batch.

2.1.3 Hydrophobization of heterogeneous catalysts

A reaction catalyzed by heterogeneous catalyst involves a combination of physical and chemical phenomena. Notably, they include the transport of the reactants to the solid surface, the reaction and the removal of the products. Thus, it is clear that a heterogeneously catalyzed reaction does not only include a single interaction with a distinct active site but a complex scenario of adsorption and desorption pathways on and from the catalyst surface.

This becomes of fundamental importance in the rational catalyst design process especially when the reaction takes place in a liquid medium. In particular, if it is true that the reactant chemisorption to the catalyst active site is crucial during a catalytic reaction, it could not be considered independently from its physisorption. In this respect, the study of the wettability properties of a surface could be critical: a solid surface presents a surface free energy that have a role in the adsorption and desorption of different chemicals. In fact, it can be described as the affinity between a solid and a fluid interface [22,23].

As widely explained in the 1.1.3 section, heterogeneous catalysis has been employed in biomass valorization processes being versatile and in agreement with the Green Chemistry principles [24,25]. Nevertheless, biomass is a really diverse and complex resource that requires the development of new chemical processes compared to the traditional oil refinery-based ones. In fact, compared to the fossil resources, biobased molecules can contain up to 50% wt/wt of oxygenated groups imparting a certain polarity to

the feedstock [26,27]. Bearing this in mind, it is deducible that working with highly polar molecules make a catalyst surface property such as wettability a key problem to be faced in order to improve the performances of a catalytic material, in particular, to modulate the stability and the preferential adsorption or desorption of organic molecules [28,29].

In the literature, several examples are reported describing the ability of a more hydrophobic surface to increase the solid resistance towards water, in particular, avoiding the poisoning of the active sites, especially acidic ones, hence allowing long-life and good recyclability of the system [30–33]. Moreover, a low hydrophilic surface is excellent in improving the catalytic dehydration of bio-based molecules [34,35], but also the condensation reactions like esterification of fatty acids [36–38] or biobased acids [39,40] and etherification [41,42].

Despite this, there are still few studies in the literature about the hydrophobization of metal catalysts that are able to promote hydrogenation or oxidation reactions too. An interesting strategy is represented by the deposition or incorporation of metal particles onto a hydrophobic support matrix. Pd can be incorporated in hierarchically porous zeolites, with different hydrophobic/hydrophilic character, imparting water resistance and demonstrating that modulating the wettability properties of the support affects the activity of the Pd active phase [43]. Differently, Pd can be deposited on carbonaceous material for furfural and 5-(hydroxymethyl)-furfural hydrogenation in water. Again, finely tuning of the support wettability was crucial to modulate the selectivity of the reaction obtaining up to 99% selectivity towards tetrahydrofurfuryl alcohol [44].

Another strategy to tune the wettability properties of metal catalysts is the post-synthesis modification of the surface [45]. A high water tolerance and stability can be achieved by grafting phenyltriethoxysilane onto Ru/TiCeOx catalysts surface for o-dichlorobenzene catalytic combustion obtaining a superhydrophobic water repellant and self-cleaning material [46]. Many works had showed how surface modification of supported metal catalyst can drive the reaction pathway, boosting the selectivity towards a desired product. A series of organophosphonic acids can be used to tune the surface hydrophobicity of Pd/Al$_2$O$_3$ catalyst therefore allowing to control the selectivity in vanillin hydrodeoxygenation reaction pathways [47]. Stearic acid functionalized Cu/ZnO exhibited a strong inhibitory effect on the unfavorable water−gas shift reaction in one-step synthesis of dimethyl ether from syngas [48]. Trietoxyoctylsilane was utilized as a coupling agent for Cu catalyst in the hydrogenation of levulinic acid to give GVL. The obtained higher water

repellency of the grafted materials not only boosted catalyst resistance but also GVL yield preventing the stabilization of the 4-hydroxyvaleric acid intermediate through intermolecular hydrogen bonds with water molecules [49].

2.1.4 Aim of the work

The aim of the work presented in this chapter is to obtain 1,4-PDO through GVL hydrogenation (Scheme 2.1) by using silica supported copper catalyst. In the literature, there are no evidence of effective Cu/SiO_2 catalysts due to the low activity and selectivity of silica-based systems in this type of reaction. The chosen strategy is to modulate the surface properties of the catalysts in different way to tune the morphology of the copper phase, the wettability and the acidity to boost the catalytic performances and selectivity towards the diol product.
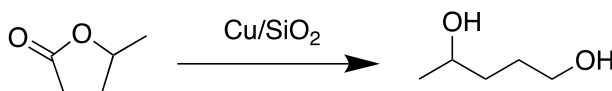
Scheme 2.1. Hydrogenation of GVL to give 1,4-PDO using silica supported copper catalysts

To modulate the wettability two different strategic pathways were pursued, namely the choiche of the appropriate silica support to drive the final physico-chemical properties and the post copper deposition organosilane grafting.

2.2 Choosing the appropriate SiO_2 support

Silica materials comprise a large variety of material with the general formula SiO_2 that could, however, present different textural properties. Generally, the silica materials used with chemical application are from synthetic origins. There are several methods to synthetize amorphous silica materials. In this thesis, two classes of silica were utilized for the catalyst preparation: silica gel and pyrogenic silica. The former is prepared solubilizing a soluble silicate, *i. e.* alkoxysilane, in water and then acid is added. In this way, stable particles of colloidal size are formed by condensation. As condensation proceeds, a gel is formed that is successively dried and washed. Silica gels result in a coherent, rigid, 3D network of contiguous particles of colloidal silica [50]. Silica could be also synthetized using high temperature processes burning $SiCl_4$ with oxygen or hydrogen. In this way, pyrogenic silicas

are formed in which primary particles are connected into linear chains and a non-porous structure is formed [50].

In this work, four commercial silicas, namely two pyrogenic (SiO_2 A and SiO_2 C) and two silica gel (SiO_2 B and SiO_2 D) were used as the support in the preparation of four CuO/SiO_2 catalysts with the aim to obtain copper catalysts with different textural, wettability and acidity properties. In fact, the adsorption-desorption mechanism of reactants and products on the catalyst surface is crucial in affecting the activity and selectivity of a catalytic system in a reaction, in particular considering the different polarities of the substrate GVL and product 1,4-PDO. The acidity of the surface has also a major role: acid sites can activate the carbonyl functionality of the GVL to the hydrogenation reaction thus, boosting the conversion [51]. However, it could limit the selectivity favoring the formation of dehydration byproduct such as 2-Me-THF and valerates. The textural properties of the four silicas are shown in table 2.1.

Table 2.1 . Specific Surface Area (SSA) and Pore Volume (PV) of the selected silica supports.

	$SSA / m^2 g^{-1}$	$PV / cm^3 g^{-1}$
SiO_2 A	251	1.74
SiO_2 B	486	0.79
SiO_2 C	30	/
SiO_2 D	681	0.66

In truth, surface wettability and acidity are related to each other [30], and their fine tuning is of great importance to drive the reaction pathway. Thus, the supports surface properties were deeply studied focusing in particular on their wettability properties and surface acidity. This had the scope to enlighten their role in the catalyst performances.

2.2.1 Characterization of the SiO₂ support

Several characterization techniques aimed to investigate the wettability feature of a solid material are reported in the literature [28]. In this work, Static Contact Angle (SCA) measurements and TG analysis were performed with this aim (figure 2.2). SCA were evaluated depositing a drop of 1,3-propandiol, as a model, onto pressed disk of the silica samples (see experimental section 5.4.1) and the angle was obtained with extrapolation with a fitting function. On the other hand, TGA was used to measure the weight loss of the sample

between 200° and 900 °C. The loss values were elaborated with equation (4) showed in experimental section 5.4.4 to obtain the hydroxyl density of each sample. The SCA values and the surface hydroxyl density determined with TGA are reported in table 2.2. The relevant SCA standard deviation of the SiO_2 B is due to the inhomogeneity surface texture. Notwithstanding slight differences are appreciable due to the typical hydrophilic character of silica, observing the SCA values and the hydroxyl density values of the samples, it is clear that the two pyrogenic silicas present a less hydrophilic surface. In particular, in the case of SiO_2 C, the hydroxyl density was under the detection limit using this method.
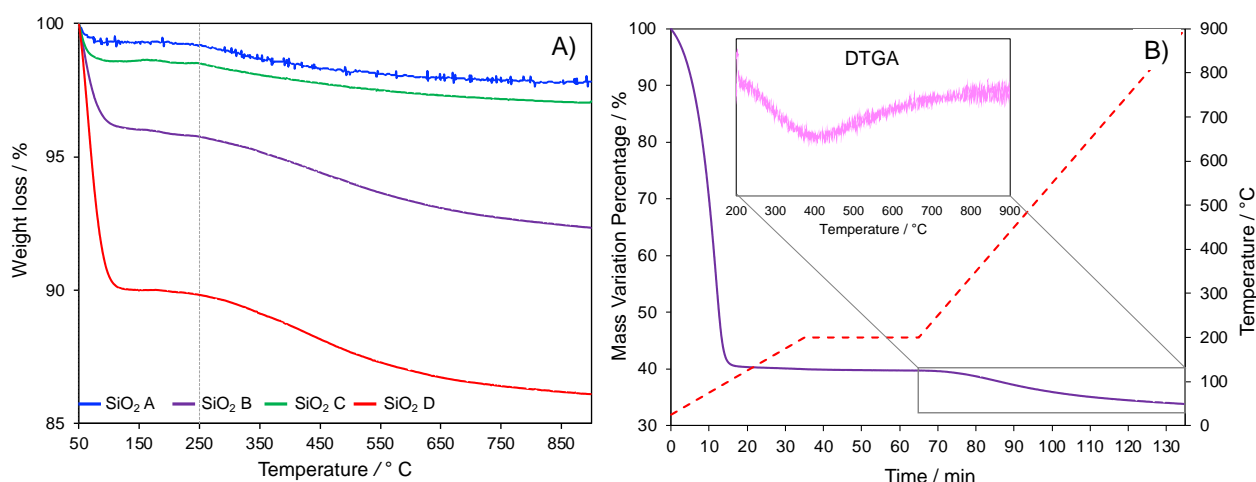

Figure 2.2. TGA thermograms (A) of the SiO_2 supports and an example of DTGA of SiO_2 B (B). Adapted from ref. [52].

Moreover, it also presented the highest contact angle among the analyzed samples. On the contrary, SiO_2 D emerged to be the most hydrophilic sample among the silicas with the highest value of hydroxyl density and the lowest contact angle value. Porous fumed SiO_2 A and silica gel SiO_2 B were then selected as models.

Table 2.2 . Hydroxy density and 1,3-propandiol contact angle of the silica supports

	Hydroxyl density ($mmol_{OH} g^{-1}$)	*θ (°)[a]*
SiO_2 A	3.1	25 ± 3
SiO_2 B	6.6	19 ± 6
SiO_2 C	n.d.	31 ± 3
SiO_2 D	7.9	17 ± 4

[a]1,3-propandiol was used for the measurement

To quantify and identify the strenght of the surface acidic sites of the support materials is of outstanding importance due to the nature of the surface adsorption phenomena that take place during metal deposition and catalytic processes. With this aim, liquid-phase acid−base titrations of the two model silicas by a strong basic probe, such as 2-phenylethylamine (PEA) were performed to investigate the acidic properties of the chosen silica support before copper deposition. The titrations were carried out using a closed HPLC line as apparatus (see paragraph 2.5.4 in the experimental section) choosing a non-polar, aprotic solvent such as cyclohexane that mimics gas-solid titration conditions. The amount of the acidic sites determined with this method corresponds to the intrinsic acidity of the sample as result of the characteristics of the cyclohexane [53,54]. The adsorption isotherms are shown in figure 2.3. Data were collected and elaborated as explained in the materials and methods section. The first run quantifies the total amount of acid sites resulting in the surface saturation of the solid with the probe PEA. After the desorption of the physisorbed and weakly adsorbed PEA with fresh solvent, the second run evaluates the remaining weak acid sites. The difference in the adsorbed PEA between the two runs therefore corresponds therefore to the number of strong acid sites. It is observable from the isotherms that the SiO_2 B sample surface presents a higher number of acidic sites if compared to the SiO_2 A sample that is coherent with the more hydrophilic behavior showed by the wettability characterization [30].
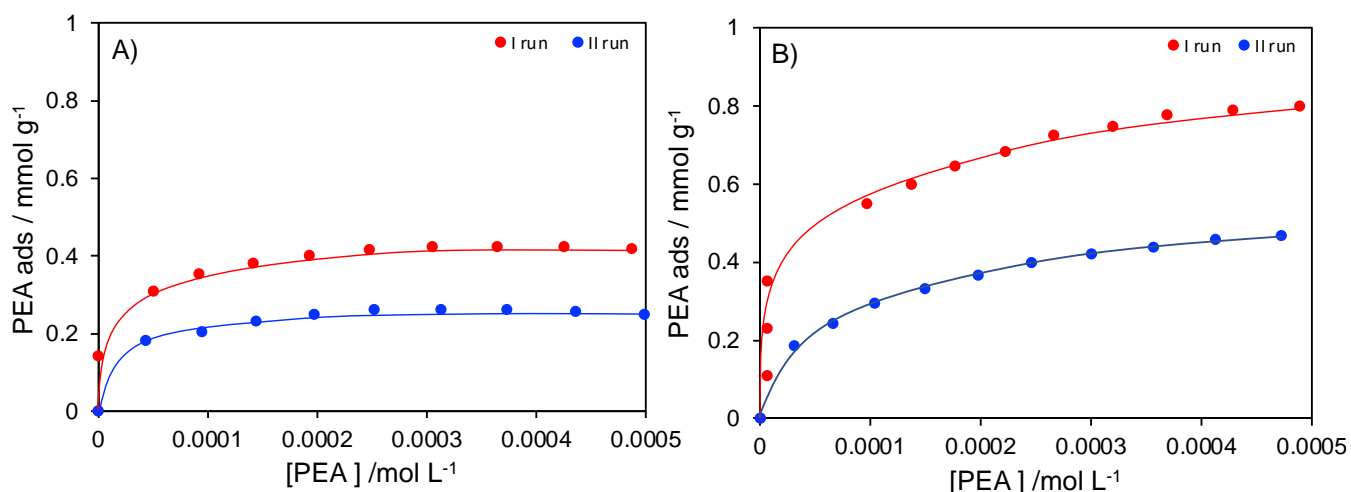

Figure 2.3 . Liquid-solid acid-base adsorption isotherms (T = 30.0 ± 0.1 ∘C) of PEA on A) SiO_2 A e B) SiO_2 B in cyclohexane. Adapted from ref. [52].

2.2.2 Synthesis and Characterization of the copper catalysts

The copper catalysts were synthetized utilizing Chemisorption-Hydrolysis (CH) as deposition method. This technique allows to obtain a high dispersion of the metal phase and lower particle size with respect to the traditional impregnation methods [55] (see section 1.1.2). The catalysts were prepared with a nominal copper loading of 16% wt/wt. The procedure was optimized to achieve the 16% of Cu confirmed by ICP analysis several times in previous works [56]. The morphological properties such as SSA and porosity are showed in the appendix section 6.4. Notably, the TEM analysis of CuO/SiO_2 A sample displayed a similar nanoparticle morphology and the particle size distribution was centered around a mean value of 2.8 nm. On the other hand, the distribution of CuO/SiO_2 B nanoparticles was reported to be centered around 2.3 nm (figure 2.4 A2 and B2) and in both cases more than 90% of the nanoparticles were under 3.5 nm. Besides, the nanoparticles are dispersed on the SiO_2 support very homogeneously and without aggregation. Moreover, in previous works, no significant copper phase reflection was detected by XRD analysis suggesting that the particle size is under the detection limit [55].
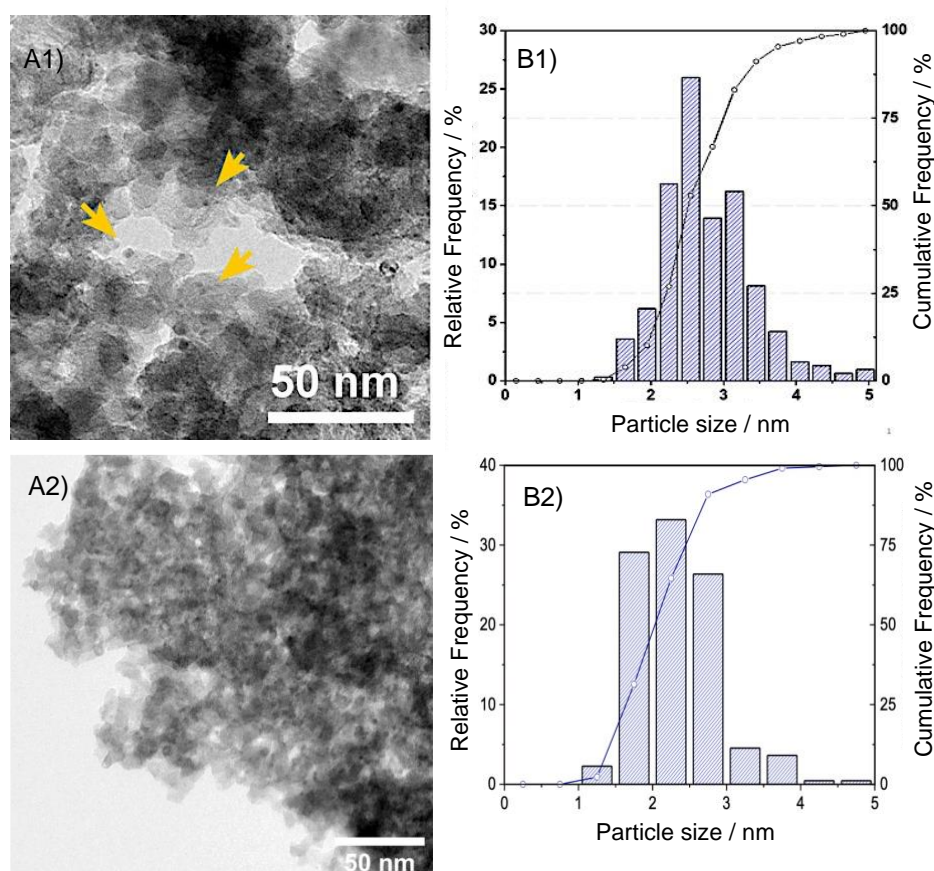

Figure 2.4. TEM micrograph of CuO/SiO_2 A sample (A1) and CuO/SiO_2 B (A2) and related size distribution (B1 and B2 respectively). Yellow arrows highlighted small Cu nanoparticles. Adapted from ref. [52]. Copyright Elsevier.

X-ray Photoelectron Spectroscopy (XPS) analysis were performed with the scope to further investigate the copper phase dispersion and the surface elemental composition of the two catalyst CuO/SiO_2 A and CuO/SiO_2 B both before, and after the reducing pre-treatment (obtaining Cu/SiO_2 A and Cu/SiO_2 B). The surface atomic composition expressed in percentage are showed in table 2.3. Si, O and C were presents as elements on the surface at the expected binding energy coherently. The presence of moderate quantities of carbon even after the subtraction of the adventitious one is probably due to residues of the precursors in the synthesis of silica. The Cu/Si ratio was calculated for both the calcined and reduced sample as a measure of the copper surface dispersion. In particular, considering the CuO/SiO_2 A sample the Cu/Si ratio is halved passing from the calcined to the reduced form (table 2.3). This could be caused by a rearrangement phenomenon of the support that may occur during the reduction pre-treatment in presence of hydrogen. Despite this, CuO/SiO_2 A possesses a higher Cu/Si ratio if compared to CuO/SiO_2 B, even after reduction. Considering that the CH preparation method exploits the electrostatic interaction between the silica surface and the copper precursor, a lower hydroxyl density, as in the case of SiO_2 A, permits a better distribution of the non-vicinal copper centers, thus preventing clusters aggregation during the calcination step.

Besides, the photoelectron spectra of the Cu 2p region was deconvoluted (figure 2.5). With this method it is possible to investigate the copper oxidation state before and after reduction and some possible interactions between the metallic phase and the silica. The values of the Cu $2p^{1/2}$ and Cu $2p^{3/2}$ binding energies can be found in table S3 in the appendix section. Split spin-orbit components can be noticed with the typical splitting (Δ ca. 19 eV) [57]. Cu(II) species can be recognized in the sample CuO/SiO_2 B at the characteristic binding energies of Cu $2p^{3/2}$ peak at about 933 eV and of Cu $2p^{1/2}$ peak at about 953 eV. Moreover, they can be also identified by the typical shake up peaks near the main $2p^{1/2}$ and $2p^{3/2}$ [58]. However, two different Cu(II) species are present, recognizable by two contributions [59]. Analogously, Cu(II) can be acknowledged also in the case of CuO/SiO_2 A but the main $2p^{1/2}$ and $2p^{3/2}$ photopeaks present only one main contribution. Furthermore, it is noticeable that the binding energies for all the contributions are shifted at slightly higher values if compared to the sample CuO/SiO_2 B and the typical value of CuO systems. In the literature, it can be found some evidences of copper species binding energy shift for a Cu/SiO_2 system, ascribing it to the decrease of electron density of the copper caused by the electron scavenging properties of the SiO_2 [60]. This phenomenon could indicate a strong interaction between the metal phase and the support. This was observed also in the case

of CuO supported on SiO_2-Al_2O_3 systems [61]. The XP spectra of the reduced Cu/SiO_2 A and Cu/SiO_2 B presented a different peak profile with the absence of any shake ups. It is known that Cu(I) and Cu(0) species are hardly distinguishable considering the binding energies of the relevant peaks, however, it could be assumed that almost all the Cu (II) species was reduced to Cu(0). In fact, the highest contribution peaks are now at 933.1 eV (Cu 2p$^{3/2}$) and 952.9 eV (Cu 2p$^{1/2}$) in the case of Cu/SiO_2 A and 932.7 eV (Cu 2p$^{3/2}$) and 952.3 eV (Cu 2p$^{1/2}$) in the case of Cu/SiO_2 B. These values are in agreement with the binding energies of various Cu(0) standard [62,63]. Moreover, a minor contribution peak could be still observed in the Cu 2p$^{3/2}$ and Cu 2p$^{1/2}$ main peak for both the reduced samples. This could be due to partial oxidation of the Cu(0) to Cu(I) caused by a brief contact with air previous the analysis.

Table 2.3. Atomic percentages of surface elements present on CuO/SiO_2 A and CuO/SiO_2 B before and after reduction determined by XPS analysis.

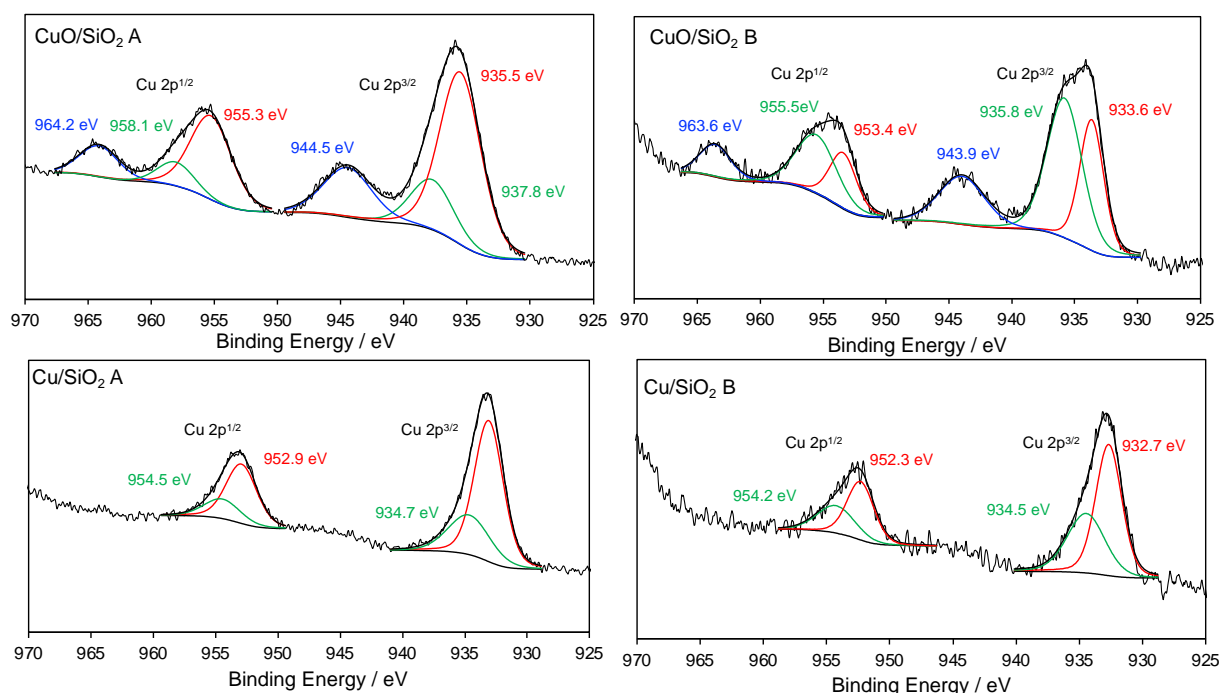| Sample	Si Atomic %	O Atomic %	C Atomic %	Cu Atomic %	Cu/Si
CuO/SiO_2 A	25	55	15	5	0.2
Cu/SiO_2 A	29	60	8	3	0.1
CuO/SiO_2 B	30	63	6	1	0.03
Cu/SiO_2 B	32	61	6	1	0.03

Figure 2.5 . Cu 2p High resolution XP spectra of CuO/SiO_2 A and CuO/SiO_2 B catalysts before (up) and after reduction (bottom). Adapted from ref. [52]. Copyright Elsevier.

Considering the results obtained with the performed surface characterizations, it is deducible that the fumed silica favors the formation of very small copper nanoparticles together with a high dispersion. Besides, the presence of unsaturated coordination sites on the Cu nanoparticle, specifically when reduced, provides a Lewis acidity character [56]. Thus, the nature and quantity of the acidic sites present onto the surface of the reduced catalysts was studied using a spectroscopic approach. In particular, IR spectroscopy using pyridine as probe molecule is able to distinguish between Lewis and Brønsted acid sites and to quantify them through integration of the typical absorption bands. The one at 1450 cm^{-1} and 1610 cm^{-1} can be ascribed to the pyridine-Lewis acid sites bond, while the bands at 1550 cm^{-1}, 1620 cm^{-1} and 1640 cm^{-1} are related to the Brønsted acid sites [64]. The FT-IR spectra of the pre-reduced Cu/SiO$_2$ A and Cu/SiO$_2$ B in comparison with the corresponding support after pyridine adsorption are showed in figure 2.6. It is noticeable that the catalysts present only a Lewis type of acidity, identified through the distinctive bands. According to the quantification calculations (table 2.5), Cu/SiO$_2$ A displays a higher number of sites compared to the Cu/SiO$_2$ B. This evidence confirms furtherly that a highly dispersed copper phase confers the material Lewis acidity that is absent on the bare silica.
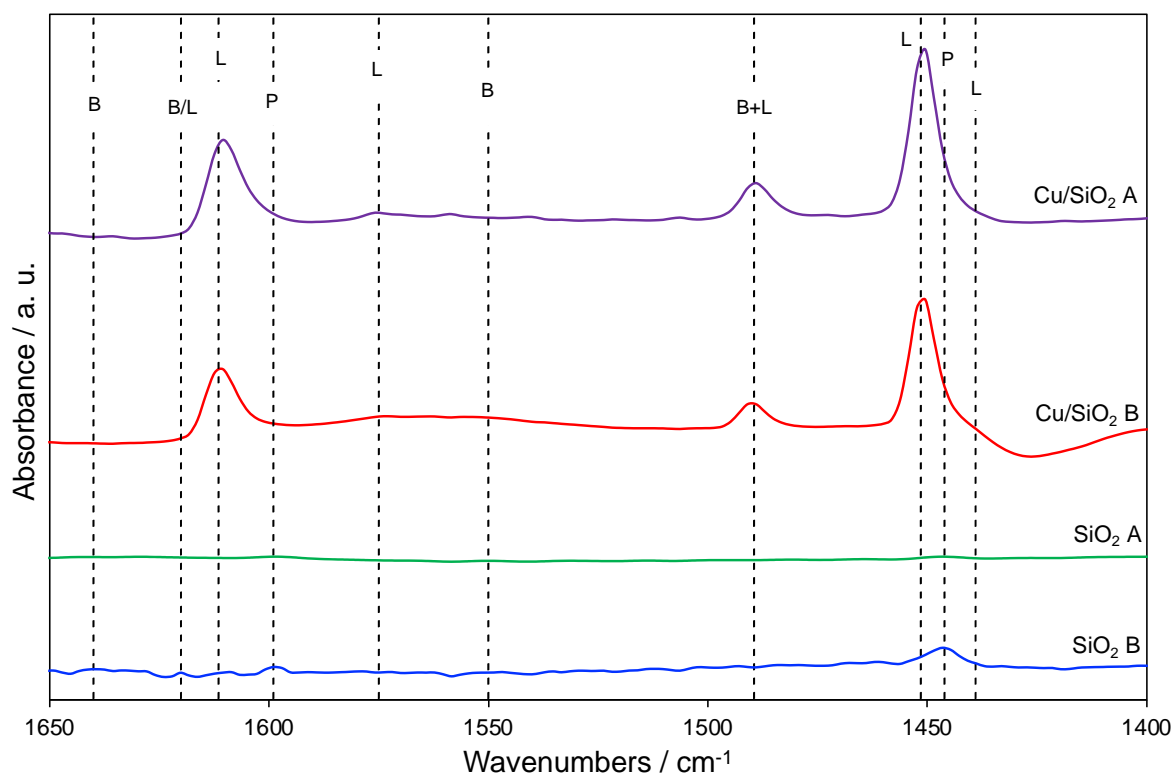
Figure 2.6. FT-IR spectra of absorbed pyridine onto the Cu/SiO$_2$ catalysts. Spectra were taken after pyridine desorption at 150 °C (see Experimental section). Adapted from ref. [52]. Copyright Elsevier.

Table 2.5. Lewis acid sites quantification at 100 °C and 150 °C by FT-IR of pyridine desorption.

	Adsorbed pyridine (mmol$_{py}$ g$_{cat}$$^{-1}$)	
Desorption T (°C)	Cu/SiO$_2$ A	Cu/SiO$_2$ B
100	0.18	0.15
150	0.13	0.08

Liquid-solid titrations with PEA were performed also for of the two catalysts, in cyclohexane to determine the intrinsic acidity and into the two chosen reaction solvents, namely dioxane and CPME, for the effective acidity [53]. The quantification of the acidic sites is displayed in figure 2.7 while experimental isotherms in figure S20 in the Appendix section. As presented, the CuO deposition impacts differently on the acidity of the two silica supports. In particular, the number of total sites of SiO$_2$ B after the deposition of copper (from 0.813 to 0.512 mmol$_{PEA}$ g$_{cat}$$^{-1}$ SiO$_2$ B and CuO/SiO$_2$ B, respectively), while the strong sites increase slightly from 0.336 to 0.392 mmol$_{PEA}$ g$_{cat}$$^{-1}$ and significantly in percent

On the other hand, if the CuO/SiO$_2$ A is compared to SiO$_2$ A the total number of acidic sites increases from 0.427 to 0.483 mmol$_{PEA}$ g$_{cat}$$^{-1}$ after copper deposition, whereas the strong sites almost double passing from 0.180 to 0.316 mmol$_{PEA}$ g$_{cat}$$^{-1}$ and in percentage from 42% to 65%. Interestingly, none of the two silica supports were able to adsorb the PEA probe in the reaction solvents, namely dioxane and cyclopentyl methyl ether (CPME). This indicates that the support acidity is not involved in the reaction.
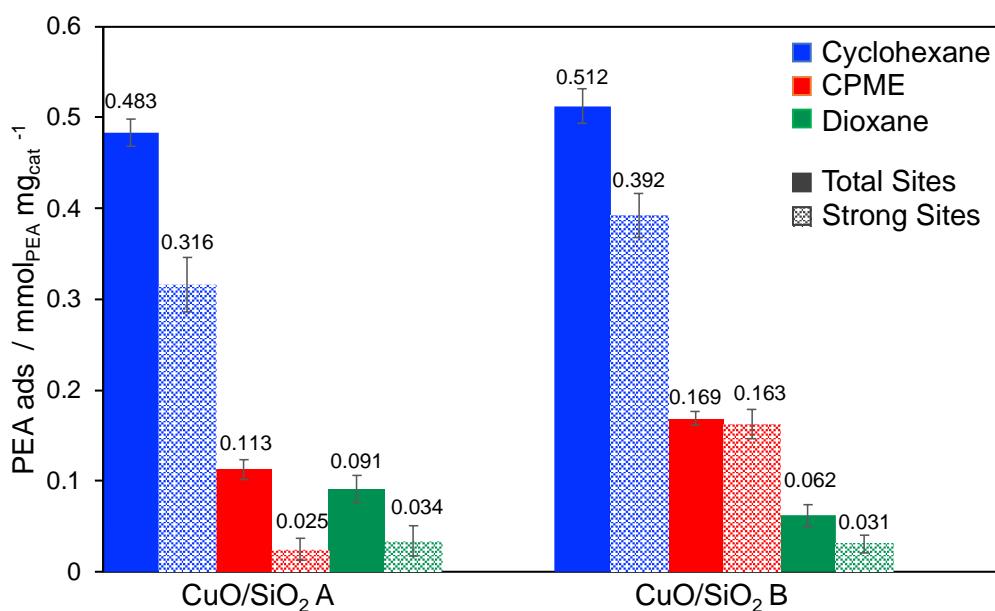
Figure 2.7 . Intrinsic acidity of CuO/SiO2 A and CuO/SiO2 B in cyclohexane and Effective acidity of CuO/SiO2 A and CuO/SiO2 B in CPME and in dioxane. Adapted from ref. [52]. Copyright Elsevier.

With this results in mind, it is likeable that the copper deposition involves a decrease in the silica surface silanols that mainly affects the total acidity as measured with PEA titration. Moreover, the copper phase imparts also a further Lewis type acidity proportional to the copper dispersion. In fact, XPS results display a higher copper dispersion for the CuO/SiO$_2$ A. In particular, the coverage of the surface silanols by copper is balanced by the addition of the metal that causes an increase in the total acidity. On the contrary, a lower copper dispersion, as in the case of CuO/SiO$_2$ B is not enough to raise the total acidity if compared to the bare SiO$_2$ B support. Furthermore, as already enlightened, the intrinsic acidity of SiO$_2$, in particular the number of strong acidic sites, is almost twice than the one of SiO$_2$ A. Nonetheless, after the formation of the CuO phase the total and strong acidic sites number are comparable between the two materials. This is due to a strong decrease in the total sites, particularly on the silica gel.

2.2.3 Catalytic test and discussion

The aforementioned acidity and dispersion properties of the CuO/SiO$_2$ catalysts make them suitable candidates for GVL hydrogenation into 1,4-PDO. The catalytic test results are

shown in table 2.6. The reaction conditions were the same reported for a CuMgAl system, namely dioxane as solvent, P(H_2) = 50 bar and T = 160 °C (table 2.6, entries 1 and 2) [65].

To improve the sustainability of the reaction the green solvent CPME was chosen as alternative to the toxic dioxane. Under the conditions, the differences between the two catalysts started to show. The Cu/SiO_2 A allowed to obtain a 78% yield of 1,4-PDO with no formation of 2-Me-THF (table 2.6, entry 3) while no differences were noticed for the Cu/SiO_2 B catalyst. The result achieved with Cu/SiO_2 A was quite outstanding if compared to a 37% Cu/SiO_2 system that, under the same conditions, was able to achieve only 5% conversion [65]. Similarly, as showed in another paperwork [66], various 30% Cu catalysts at 200 °C and under 50 bar of H_2 gave unsatisfactory results. In particular, Cu/TiO_2 allowed to obtain 84% selectivity to 1,4-PDO at 45% of conversion whereas Cu/SiO_2 gave 58% of conversion with no selectivity to 1,4-PDO [66]. It is worth to note that when the hydrogenation is carried out in a continuous flow reactor using a 27% Cu/SiO_2 catalyst poor results in terms of activity and selectivity were obtained. On the contrary, a 44% Cu/ZnO catalyst allowed to achieve 98% selectivity to the diol at 16% conversion.

In a work of Simakova et al. [19,] a deep study was performed on the influence reaction conditions such as temperature, pressure, solvent and substrate/catalyst on Cu/SiO_2 achieving 32% conversion of GVL and 67% selectivity of 1,4-PDO.

Table 2.6. Catalytic tests for hydrogenation of GVL. Reaction conditions were T=160 °C, pH_2= 50 bar, Substrate/Catalyst = 5/1 for 22 h. Catalysts are pre-reduced at 270 °C.

Entry	Catalyst	Solvent	Conversion (%)	Selectivity to 1,4-PDO (%)
1	Cu/SiO_2 A	dioxane	49	81
2	Cu/SiO_2 B	dioxane	57	80
3	Cu/SiO_2 A	CPME	80	98
4	Cu/SiO_2 B	CPME	57	82
5	Cu/SiO_2 A[a]	CPME	58	81
6	Cu/SiO_2 A[b]	CPME	30	82
7	Cu/SiO_2 A[c]	CPME	90	74
8	Cu/SiO_2 A[d]	CPME	49	90
9	Cu/SiO_2 A[e]	CPME	67	93

[a]pH_2= 30 bar, [b]T=140 °C, [c]T=180 °C, [d]Substrate/Catalyst = 10/1 (wt/wt), [e]t=12 h.

Bearing this in mind, the effect of the variation of the reaction conditions was also studied for Cu/SiO$_2$ A and Cu/SiO$_2$ B. An increase in the temperature to 180 °C enhances the conversion but significantly compromise the selectivity, leading to a yield of 63% (table 2.6, entry 7), while a decreasing in both the temperature and H$_2$ pressure has a negative effect on the conversion (table 2.6, entry 4, 5 and 6). In contrast, the increase in Substrate/Catalyst ratio or the decrease of reaction time negatively impacted on the conversion despite keeping a good selectivity.

The moderate increase in both conversion and selectivity when using CPME as the solvent was primarily observed for the catalyst prepared with the less hydrophilic silica. On the contrary, the activity and selectivity of the one prepared with the silica gel did not show remarkable differences. The substantial effect of the solvent on the catalyst acidity was underlined by the titration with PEA. As shown in figures 2.7, the total acid sites density and the strong ones over CuO/SiO$_2$ A remarkably decreases when titrations are performed under dioxane and CPME. Comparing the effective acidity measurements in the two solvents it is noticeable that, in dioxane, the number of strong acid sites is comparable while in CPME both the number of total and strong sites are truly higher on CuO/SiO$_2$ B (0.163 vs 0.025 mmol$_{PEA}$ g$_{cat}^{-1}$). According to this, the higher selectivity of CuO/SiO$_2$ A in CPME could be ascribable to the lower strong acidic site density. As a consequence, acidity could be finely tuned through the reaction solvent, preserving the lactone activation capacity and, at the same time, limiting the side reactions. In fact, moving from dioxane to CPME a mitigation of strong acid sites occurred, improving thus the selectivity, despite the preservation of a moderate total sites density.

The choice of CPME was the pivotal point in achieving these results. Moreover, it was demonstrated that using Cu catalyst under dioxane mitigates the copper hydrogenation activity [67,68]. The physicochemical properties such as low toxicity, high boiling and low melting point and mostly low peroxide formation rate, make CPME a suitable green solvent that can be employed in a variety of chemical reactions [69–71]. Nevertheless, its usage in platform molecules valorization is not common. Moreover, alcoholic solvents are not suitable for this kind of reaction, in fact, as already reported, alcohols can add to the carbonyl group with a nucleophilic attack resulting in the formation of esters. In particular, the use of Cu/SiO$_2$ D under the reaction conditions of 250 °C and 10 bar of H$_2$ gives high yield in the ester [56].

The activity of the catalysts in the hydrogenation of GVL is related to the Lewis acidity, in this case expressed by the metal nanoparticles. The CPME solvent allows to exploit the

higher dispersion of Cu/SiO$_2$ A demonstrated by XPS results. Moreover, the less hydrophilic nature of the silica support has a role in promoting the product desorption, preventing side reactions. Recently, the fine tuning of the wettability has been considered as a new tool for the improvement of a catalytic process. HMF can be obtained as the only dehydration of product using a superhydrophobic mesoporous acid that prevents HMF rehydration [72]. Naturally hydrophobic carbon supports were utilized to improve the catalytic efficiency of palladium nanoparticles in the dehydrogenative coupling of organosilanes [73]. An outstanding catalytic turnover frequency in hydrolysis of acetate esters was reached using sulfonic group by a highly hydrophobic environment [74]. It is worth to mention that the tune of wettability properties of a catalysts has a primary role in three-phase gas-liquid-solid reactions, such as catalytic hydrogenations [75,76]. In fact, the solubility of hydrogen in liquid media is quite low deriving in a low H$_2$ availability on the surface of the catalyst. However, lowering its hydrophilicity, that is related to an increase aerophilicity, can improve the hydrogen availability on the surface, thus allowing the use of lower hydrogen pressure. Indeed, by lowering the H$_2$ pressure over the more hydrophobic catalyst Cu/SiO$_2$ A we have the same result obtained at higher P over the less hydrophobic Cu/SiO$_2$ B (entries 5 vs 4). This could be related to the higher catalytic performance of Cu/SiO$_2$ A observed in the catalytic hydrogenation of α,β-unsaturated ketones and sulphones compared to the Cu/SiO$_2$ B (prepared with 8% wt/wt Cu loading) [77].

In the present case, the lower hydrophilcity of SiO$_2$ allows the highest conversion. This is in full agreement with the contact angle trend, in fact, the higer the θ the lower is the affinity of the surface with the diol. As a consequence, a lower hydrophilicity seems to facilitate the desorption of the diol molecules, justifying the optimal conversion as shown in figure 2.9.
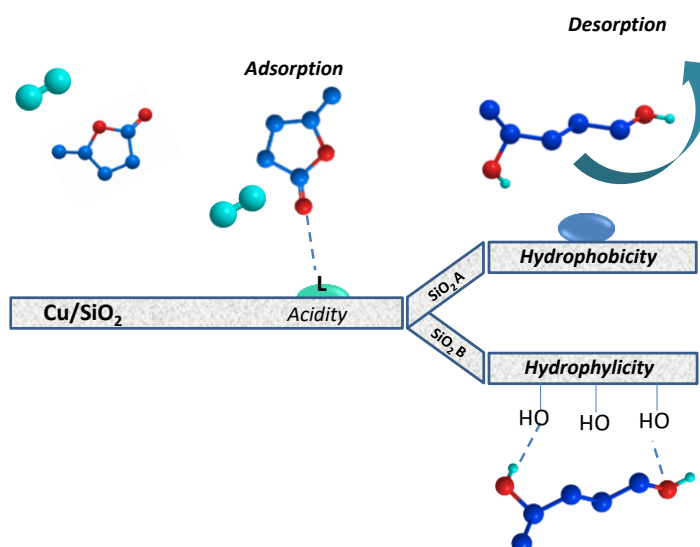
Figure 2.9. Supposed adsorption and desorption mechanism on the Cu/SiO$_2$ A and B catalysts. Adapted from ref. [52]. Copyright Elsevier.

2.2.4 Conclusion

The large abundance of biobased lactones deriving from renewable sources gives the opportunity to synthetize diols using hydrogenation processes. In this paragraph, it was shown that the finely tune of the GVL hydrogenation processes that includes catalyst preparation method, choice of the support and solvent, allowed to reach 78% yield of 1,4-PDO. In particular, it has been demonstrated that the wettability feature of the catalyst surface drives the dispersion of the copper phase: XPS analysis results showed that a Cu/SiO$_2$ A presents an higher Cu/Si ratio. Moreover, a lower hydrophilicity increases H$_2$ availability on the surface and promotes the product desorption.

The presence of acidic sites is fundamental in activate the carbonyl group of lactone which opening requires harsh conditions therefore often resulting in the formation of byproducts. Indeed, the proper choice of the reaction solvent had shown to be a very effective tool to tune the catalysts surface acidity. Using liquid-solid acid-base titration with PEA, it was demonstrated that moving from dioxane to CPME the number of acidic sites on CuO/SiO$_2$ A increased by 24%, enhancing the activity while the strong ones decrease by almost one third enabling to reach 98% of selectivity.

2.3 Modification Cu/SiO$_2$ catalyst with organosilane compounds

On the basis of the results shown in the previous paragraph, the aim of the work presented this section was use an uncomplicated procedure of functionalization of the surface of a supported copper catalyst using trietoxyoctylsilane (TEOCS) to improve the catalytic performance of an hydrophilic catalyst, namely Cu/SiO$_2$ B, in the hydrogenation of GVL to give 1,4-PDO in order to reduce the overall hydrophilicity. Silanization has revealed to be effective for the hydrophobization of silica based materials [78–80].

2.3.1 *Functionalization and characterization of the CuO/SiO$_2$ B catalyst*

CuO/SiO$_2$ B was prepared as explained in the previous paragraph, through the Chemisorption-Hydrolysis method [55]. To modify the wettability properties of the surface, TEOCS molecules were grafted to the surface hydroxyl groups using diverse silane percentage loadings, namely 1, 5, 10 and 15% wt/wt (see the experimental section for the procedure). In this section, a deep characterization of the physico-chemical surface properties of the catalysts was realized with the aim of enlight their relationship with the catalytic activity.

The effective grafting of octylsilane functional groups on the catalyst surface was investigated by IR spectroscopy (figure 2.10). In the IR spectra are visible the characteristic bands of alkanes. Specifically, at 2926 cm^{-1} and 2853 cm^{-1} the signals ascribable respectively to the asymmetric and symmetric stretching of C-H bond and -CH$_2$- groups of the organosilane residues can be detected. Furthermore, the signal at 2962 cm^{-1} are diagnostic of the asymetric stretching of C-H bond in the -CH$_3$ residues [46,81]. Moreover, the intensity of the alkane bands proportionally grows to the silane loading coherently.
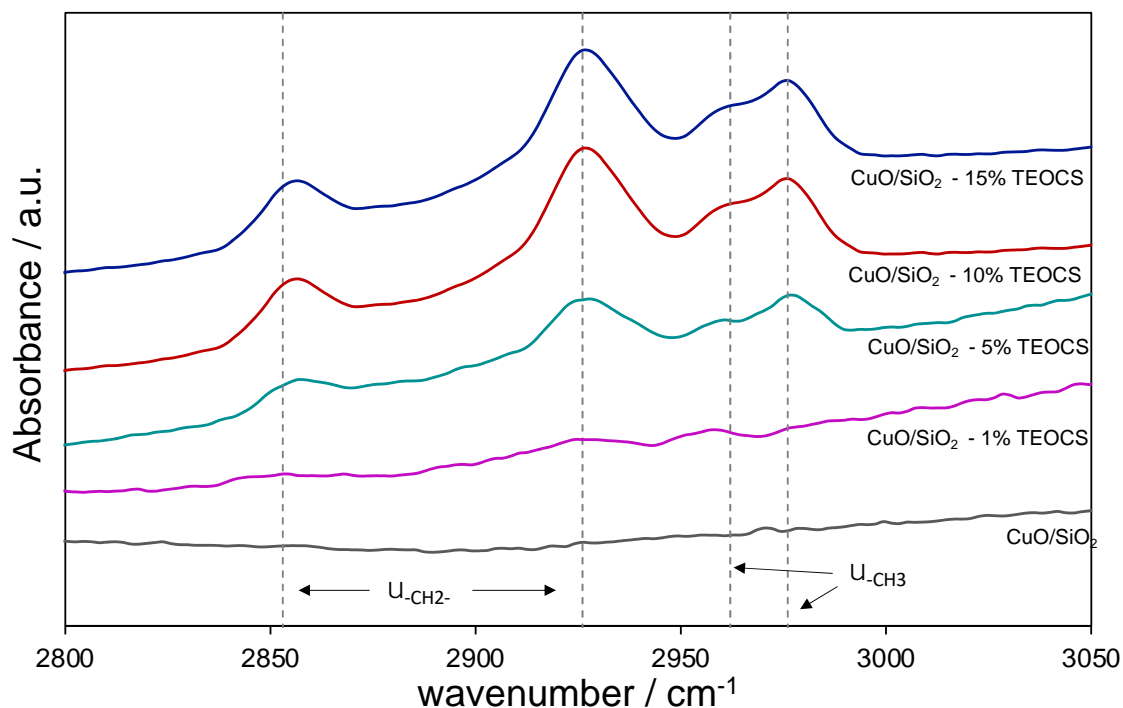
Figure 2.10. IR spectra of the catalysts. Adapted from ref. [82] Copyright Elsevier.

XPS was also utilized as a tool to investigate the enrichment of silane groups on the catalyst chains, particularly, to clear the effect of the grafting on the copper reducibility (figure 2.11). Samples were therefore analyzed before and after reduction (see the experimental section for the reduction procedure). Although the high complexity of the Si 2p and O 1s peaks does not enable an exhaustive fitting, the main species can be still acknowledged (figure 2.11 A and B). From the spectra, it is noticeable a moderate enlargement of the Si and O bands. This could be ascribed to the contributions related to the oxidated surface species, namely the siloxane bonds [83].

The reducibility of the copper phase was investigated performing XPS on a fresh calcined and reduced selected sample (namely CuO/SiO_2 – 10% TEOCS). As it can be noticed in figure 2.11, Cu(II) can be identified by Cu $2p^{3/2}$ peak at about 933 eV and of by Cu $2p^{1/2}$ peak at about 953 eV and by recognizing the presence of the shake up peaks near the main ones. The copper phase reduction was corroborated by the changing of the contribution peak areas [52] and from the disappearance of the shake-up peaks [58].
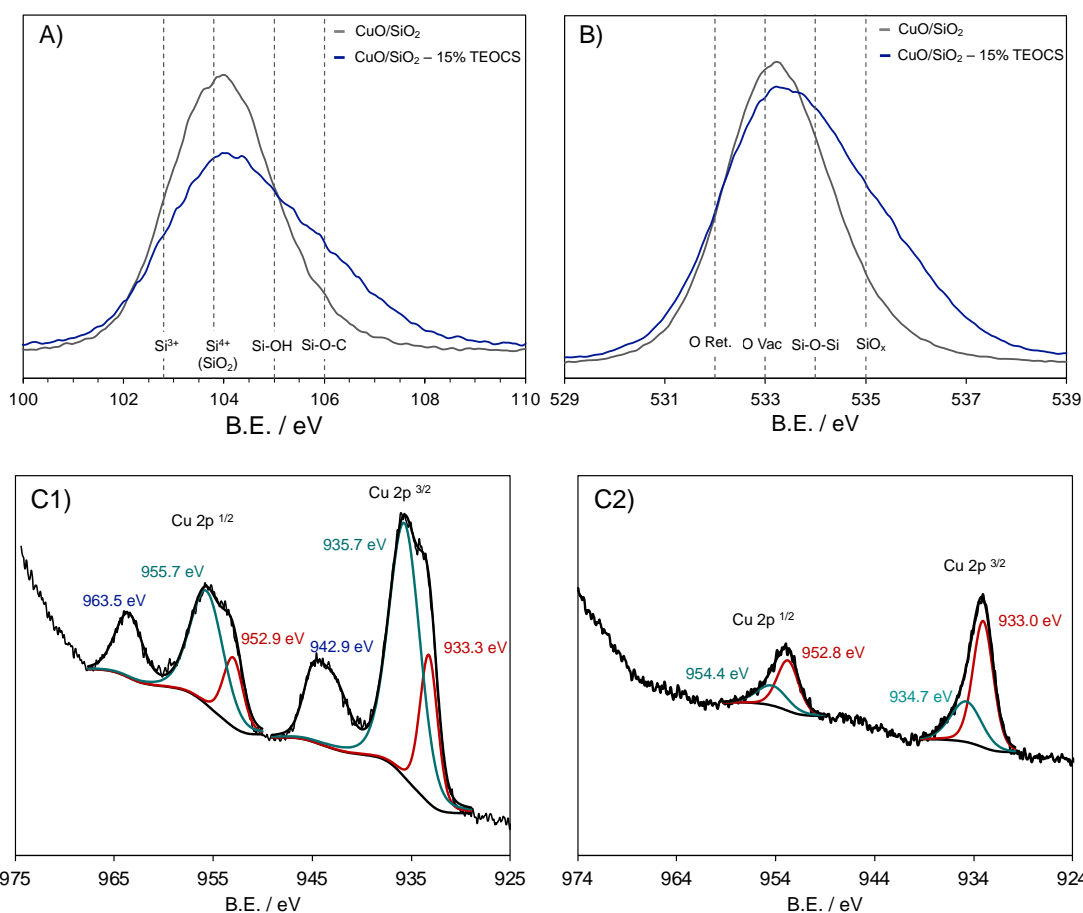
Figure 2.11. XPS spectra A) Si 2p$^{3/2}$ band of bare sample CuO/SiO$_2$ and CuO/SiO$_2$ – 15% TEOCS. The typical bands of defective (Si^{3+}) [84,85], Si^{4+}(SiO$_2$) [86,87], Si-OH [88], Si-O$_3$-C$_3$ [89] are reported. B) O 1s High resolution spectra of the bare and functionalized CuO/SiO$_2$ – 15% TEOCS catalysts The typical band of SiO$_2$ reticular oxygen [90,91], CuO oxygen [58], Si-O-Si [88] bond of silane, SiO$_x$ [92,93] are showed. C1) Cu 2p spectra of the calcined CuO/SiO$_2$ – 15% TEOCS and (C2) Cu 2p spectra of the reduced CuO/SiO$_2$ – 15% TEOCS catalyst (right). Adapted from ref. [82]. Copyright Elsevier.

Nitrogen adsorption isotherms were performed to determine the specific surface area (SSA) and the total pore volume (PV) of the samples (table 2.7, column 2 and 3). The SSA and PV values of the silane grafted catalysts were slightly lower if compared to the non-functionalized CuO/SiO$_2$. This could be ascribed to the progressive loss of accessibility of the pores caused by the interaction of the silane chains [94]. On the other hand, the small increase in SSA and PV of CuO/SiO$_2$ – 15% TEOCS could be due to a rougher surface caused by the organosilane grafting [95].

Table 2.7. Specific surface area (SSA), total pore volume (PV) and diol static contact angle (SCA) values

Sample	SSA / $m^2\,g^{-1}$	Pore Volume / $cm^3\,g^{-1}$	SCA (θ_{diol}) / °
SiO_2	410	0.63	50 ± 1
CuO/SiO_2	365	0.54	62 ± 1
CuO/SiO_2 – 1% TEOCS	358	0.52	65 ± 1
CuO/SiO_2 – 5% TEOCS	331	0.41	72 ± 1
CuO/SiO_2 – 10% TEOCS	245	0.37	75 ± 3
CuO/SiO_2– 15% TEOCS	263	0.50	75 ± 4

TG analysis was chosen to the stability of the silane bond under the reaction temperature. Thus, the analyses were carried out on the bare and modified samples and the TG profiles are shown in figure 2.12 while the temperature values of the onset and end of the major weight loss steps with the associated weight loss percentage are reported in table S4. As deducible, the great mass loss evaluated at 550 °C was reconducible to the CuO/SiO_2 -15% TEOCS sample followed by, in decresing order of mass loss, CuO/SiO_2 -10% TEOCS, CuO/SiO_2 -5% TEOCS, CuO/SiO_2 -1% TEOCS and CuO/SiO_2. Generally, the loss of the physisorbed water ends at around 200 °C where a plateau is noticed. Then, the mass loss related to the decomposition of the grafted silane is observed at around 320-330 °C [96]. From the TGA datas it is deducible that the silane grafting bond is stable onto the surface of the catalysts up to 320 °C, fairly higher compared to the reaction temperature of 160 °C.
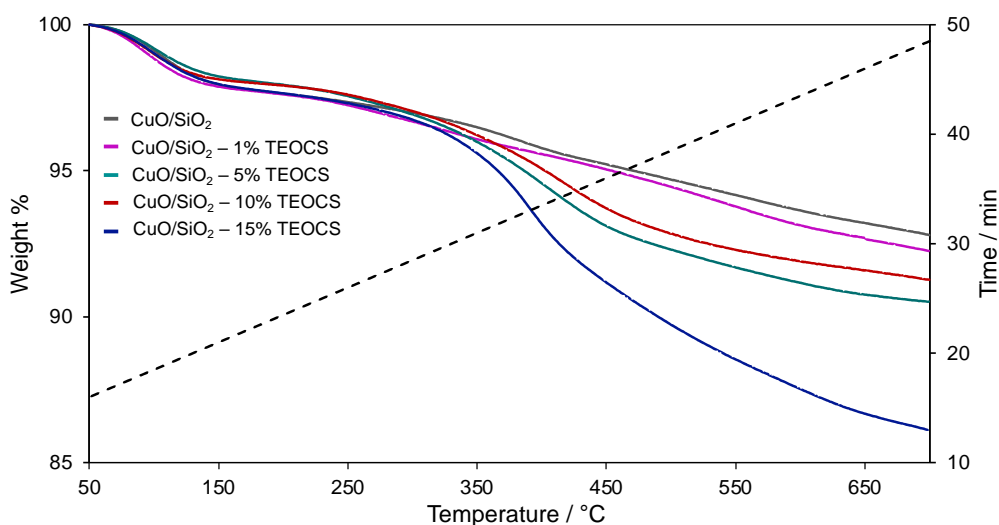

Figure 2.12. TGA profiles of all the CuO/SiO_2 samples. Adapted from ref. [82] Copyright Elsevier.

After this, TEM analyses were performed on the bare and silanized samples to understand the possible influence of the organic moieties on the metallic phase morphology and the micrograph are shown in figure 2.13. From the analysis results it is clear that all the samples have a similar copper nanoparticles morphology: the mean value of the particle diameter was around 2.3 nm and they appeared well dispersed onto the support. No copper nanoclusters bigger than 5 nm nor aggregation were detected (see figure 2.13 size distribution graph). A different case was observed on the 15% functionalized sample surface. In fact, the copper nanoparticles are less detectable in TEM but are visible in STEM analysis (figure 2.14). HAADF-STEM contrast is less sensitive to the particle morphology and proportional to the atomic number Z, thus, it allows a detection of particles buried in thin depth. However, the particle size and morphology are comparable to those of the other samples.

To have a clue onto the variation wettability properties of the catalysts surfaces according to the silane loading, the static contact angle (SCA) among 1,3-propandiol and the sample surface was measured (table 2.7, column 3). The 1,3-propandiol is a poorly viscous diol that can efficiently mimic the reaction product 1,4-PDO, giving an overall indication of the alcoholphilicity of the surface. From the SCA data it is noticeable that copper deposition limits the polarity of the surface and, as a consequence, increases the SCA probably due to a partial coverage of the surface hydroxyl groups of silica. Moreover, after the silanization the affinity with the 1,3-propandiol decreases, from a value of 62° of CuO/SiO_2 to a one of 75° of CuO/SiO_2 -15% TEOCS.
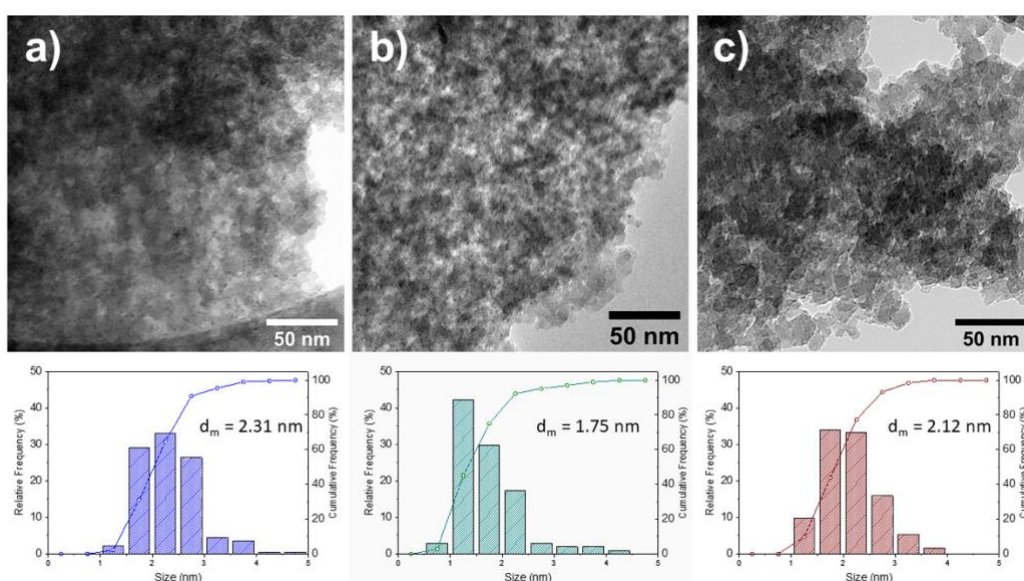

Figure 2.13. Representative TEM micrographs of selected samples a) CuO/SiO_2, b) CuO/SiO_2 - 5% TEOCS, c) CuO/SiO_2 - 10 % TEOCS, top, and associated size distributions of copper NPs, down. Adapted from ref. [82] Copyright Elsevier.
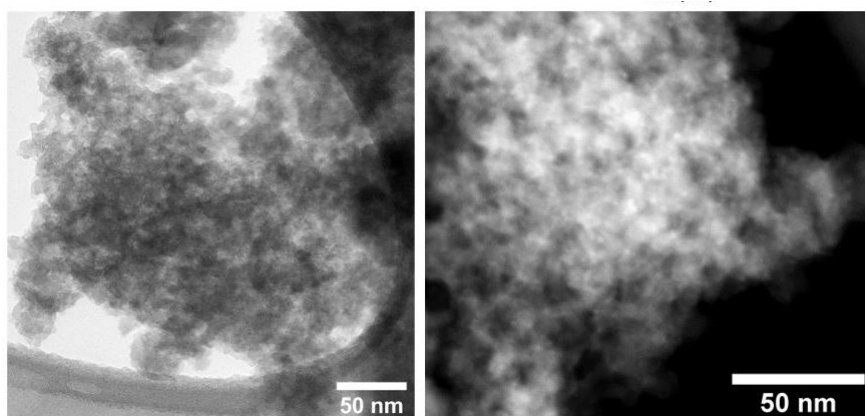
Figure 2.14. Representative micrographs for sample CuO/SiO_2 - 15 % TEOCS. On the left bright field TEM image and on the right side HAADF-STEM image (copper particles are the brighter roundish spots). Adapted from ref. [82] Copyright Elsevier.

Due to its intrinsic nature, SCA measurements on porous solids present some limitations caused by the roughness and irregularity of the sample surfaces. To overcome these constraints, water adsorption isotherms could be effective into assess the hydrophilicity of a porous solid, measuring the water affinity. The water adsorption isotherms of the support and of the catalyst samples are shown in figure 2.15. A decreasing trend similar to the one observed for the N_2 adsorption experiments can be found: the affinity with water drops as the density of the silane increases on the CuO/SiO_2 catalyst surface. Particularly, the computed monolayer volume, V_m, decreases from a value of 42 cm^3/g to a value of 22 cm^3/g in the case of CuO/SiO_2 and CuO/SiO_2 respectively. This was analogue to the decrease of the V_m calculated for the N_2 adsorption experiments, which drops from 84 to 29 cm^3/g for the same samples respectively. Consequently, there are appreciable differences in the SSA_{water} of the samples that goes from 128 m^2/g in the case of CuO/SiO_2 to 68 m^2/g for the CuO/SiO_2 −10 % TEOCS. This could be ascribed to the hydrophobic interactions among the organosilane chains that decrease the affinity of the surface towards water. The differences in the adsorbed volume of water are more significant moving towards higher relative pressures (p/p° = 0.5). In fact, passing from the bare SiO_2 support to CuO/SiO_2, the adsorbed volume of water decreases from 107 cm^3/g STP to 88 cm^3/g STP respectively. Moreover, it decreases proportionally with the increase of silane loading (from 88 cm^3/g STP for the bare catalyst to 23 cm^3/g STP for the 10% functionalized one).
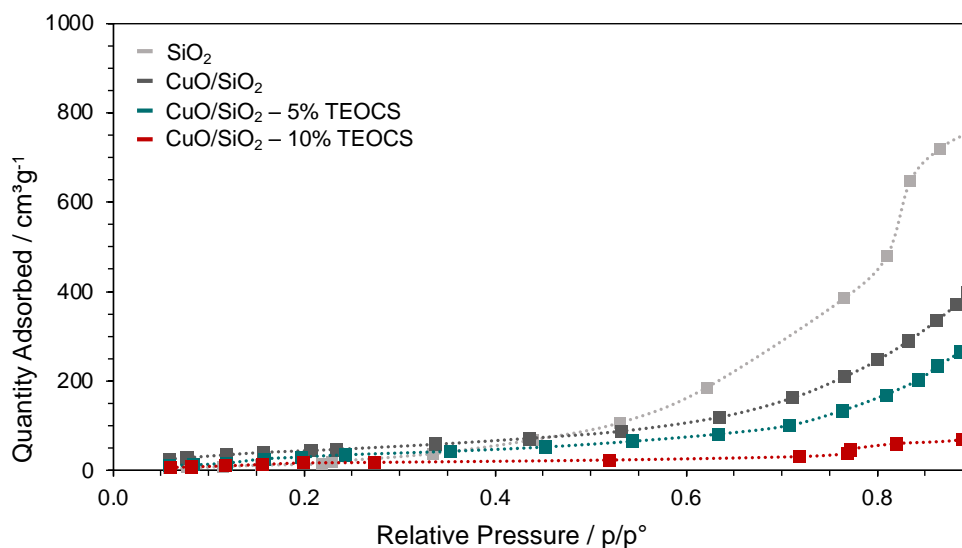
Figure 2.15. Water adsorption isotherms at temperature of 40 °C on SiO_2, CuO/SiO_2, CuO/SiO_2 – 5% TEOCS and CuO/SiO_2 – 10 % TEOCS. Adapted from ref. [82] Copyright Elsevier.

2.3.2   Catalytic test and discussion

The fresh prepared silane-functionalized CuO/SiO_2 catalysts were tested in the hydrogenation of GVL to give 1,4-PDO (scheme 2.1) to determine the effect of the silane hydrophobization on the catalytic performances under the same conditions used in the paragraph 2.2.2 catalytic tests. The results of the experiments are shown in figure 2.16.

It is evident that even after low silane anchoring degree (1% of loading) on Cu/SiO_2 the selectivity to 1,4-PDO readily increases reaching 99% with the 5%, or superior, loading. The overall activity improved too: there was an increase in the yield of diol from 47% obtained with the bare Cu/SiO_2 catalyst reaching 80% of yield using the Cu/SiO_2 – 10% TEOCS. Surprisingly, a considerable decrease of the yield is appreciable when the silane loading is increased from 10% to 15%, despite keeping an excellent selectivity towards the 1,4-PDO. This is in agreement with the fact that a more efficient desorption of the 1,4-PDO, occurring on a less hydrophilic surface, strongly limits the formation of dehydration byproducts such as 2-Me-THF [52]. Surprisingly, if the spent catalyst is analyzed with the same procedure the presence of the same alkane bands can be still clearly visible, therefore indicating the stability of the grafted organosilane chains (figure 2.17).
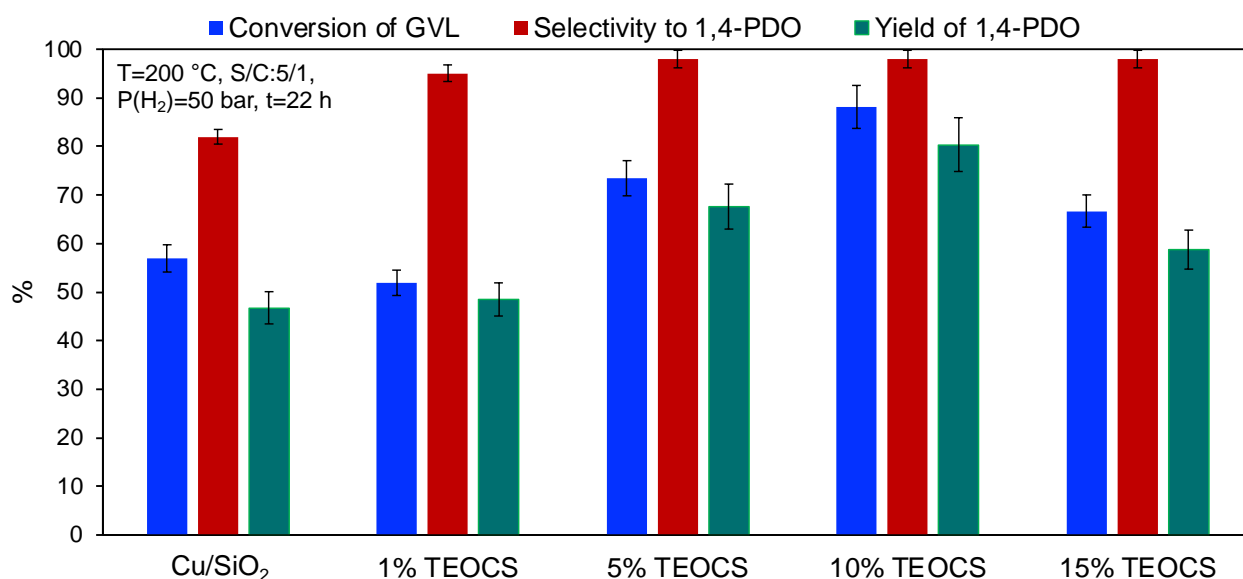
Figure 2.16. Catalytic test results of the organosilane grafted catalysts in the GVL hydrogenation. Reaction conditions: T = 160°C, P(H$_2$) = 50 bar, t = 22 h, substrate/catalyst = 5/1 (500 mg of GVL/100 mg of catalyst) and solvent: CPME. Conversion was normalized by the copper content percentage of the samples. Adapted from ref. [82]. Copyright Elsevier.
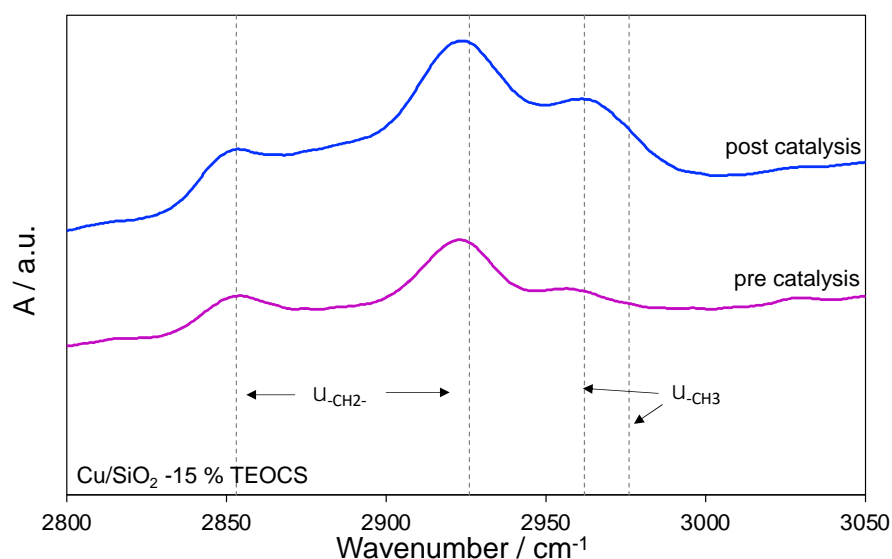

Figure 2.17. IR spectra of the spent CuO/SiO$_2$ – 15% TEOCS catalyst. Adapted from ref. [82]. Copyright Elsevier.

The characterization results of SCA and water adsorption measurements underline the reduction of the surface polarity deriving from the silane functionalization in a proportional manner with the silane loading. The overall decrease in hydrophilicity/polarity of the catalysts surface significantly boosts the selectivity to the 1,4-PDO having a role in preventing the side reactions as demonstrated also in the previous section. However, it can

be observed that the activity of the catalytic system conspicuously decreases, surprisingly, when the silane loading is increased from 10 to 15% despite the decrease in alcolphilicity. The reasons could be searched in the different bonding configuration of the silane moieties bonded to the catalyst surface (figure 2.18) that could hinder the Cu active sites. Particularly, TEOCS molecules could be bounded to the surface mainly into three different configurations: with a single bond (T^1), two bonds (T^2) and bonding with adjacent silane chain (T^3) [94,97]. Considering this, the prevalence of a T^3 type structure configuration could lead to a decrease of the copper active site accessibility, hampering the GVL substrate to approach the hydrogenation site. To validate this hypothesis, CP-MAS NMR was chosen as characterization technique: ^{29}Si CP-MAS NMR spectra of our samples were recorded and compared to the ^{29}Si NMR of the pure triethylethoxysilane as standard. As shown in figure 2.18 inset, the ^{29}Si NMR of pure TEOCS presents a singlet at -45 ppm. Conversely, ^{29}Si CP-MAS NMR of bare CuO/SiO_2 presents the two contributions attributable to the bulk of the SiO_2 support, namely the tetra-coordinate siloxane $Si-(OSi)_4$ (Q^4 at -110 ppm) and the siloxane bonded to a single silanol $Si-(OSi)_3-(OH)$ (Q^3 at -101 ppm) [98]. On the other hand, if the functionalized catalysts are taken into consideration, a further group of signals can be detected at higher ppm. If the spectra are deconvoluted, four distinguished contributions can be identified between -80 and 30 ppm. Notably, T^1 configuration can be identified at -49 ppm, at -58 ppm the T^2 and finally T^3 configuration can be assigned to the signal at -68 ppm [49,94,98]. Besides, a small amount of the silane precursor (T^0 configuration) can be still found at -40 ppm [99]. If the CuO/SiO_2 – 5% TEOCS is considered, no fitting analysis procedure was performed due to the fact that the signal intensities were comparable to the background noise. Conversely, CuO/SiO_2 – 10 % TEOCS and CuO/SiO_2 – 15 % TEOCS spectra revealed that the silane molecules are bounded in a different configuration depending on the silane surface loading. In particular, the signal ascribable to T^1 and T^2 structures decreases, while the T^3 contribution enhances, passing from the 10% to the 15% TEOCS loaded catalyst. Area percentage of the deconvolution peaks are reported in table 2.8. This demonstrates that, at higher concentration, the silane is prone to reticulate [94], hindering the copper active site.
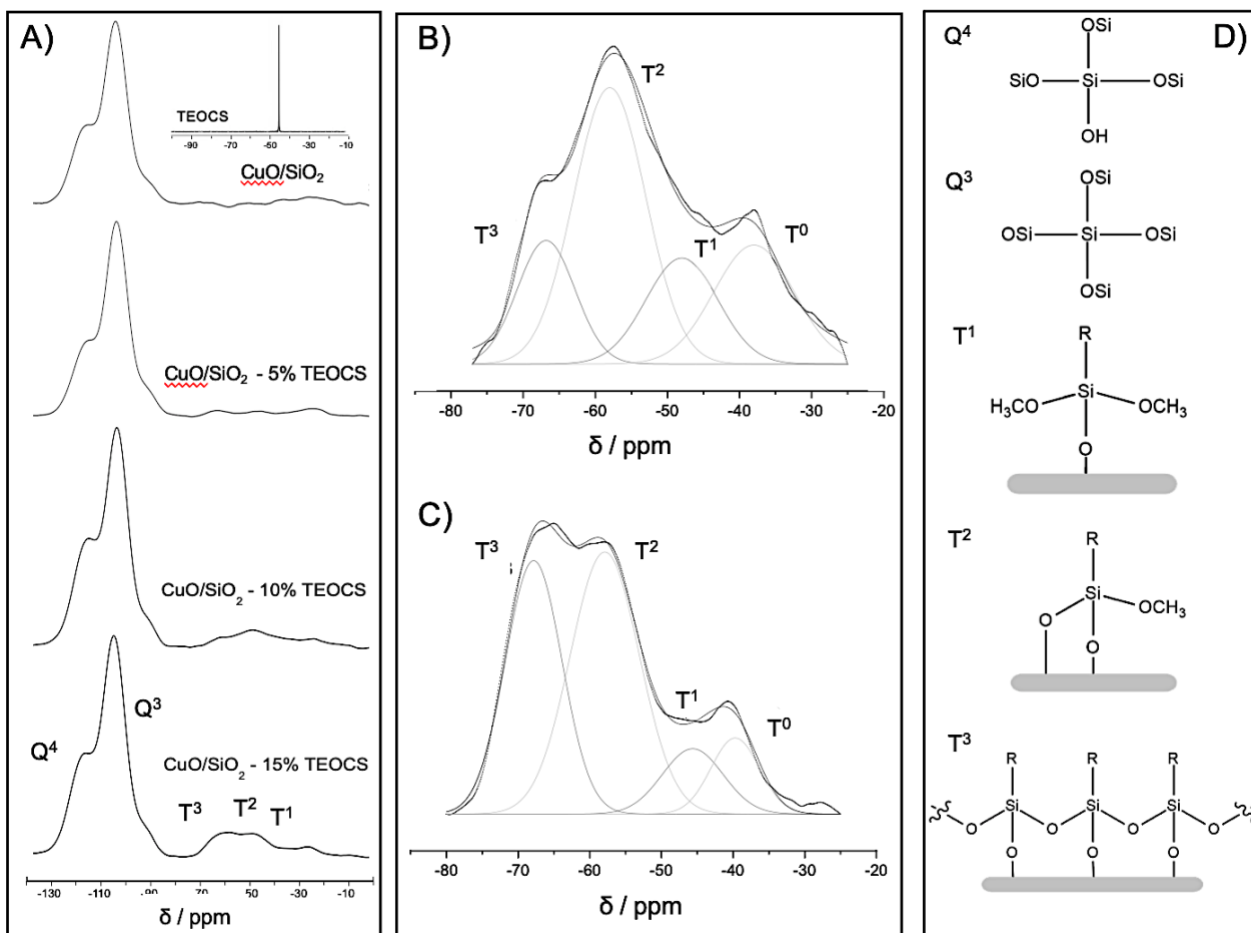
Figure 2.18. A) ^{29}Si NMR of pure triethylethoxysilane and ^{29}Si CP-MAS NMR of the sample catalysts; fitting procedures of B) CuO/SiO_2 – 10 % TEOCS and C) CuO/SiO_2 – 15 % TEOCS. D) sketches of the possible silane/SiO_2 configurations. Adapted from ref. [82].

Table 2.8. 29Si CP-MAS NMR chemical shifts and relative percentages for the three proposed structure

	Adj. R²	*T¹*		*T²*		*T³*	
		δ (ppm)	*%*	*δ (ppm)*	*%*	*δ (ppm)*	*%*
10% TEOCS	0.99	-49	24	-58	64	-67	12
15% TEOCS	0.98	-48	13	-58	46	-67	41

In the previous section, it has been already demonstrated that the fine tune of the surface acidity properties is functional to achieve high selectivity and yield in 1,4-PDO starting from GVL [52]. Again, FT-IR characterization after pyridine adsorption can enlighten

the nature and quantity of acidic sites and the possible influence of the silane moieties on the copper Lewis acidic sites. Moreover, the use of a moderately hindered probe molecule could give another clue on copper accessibility. The FT-IR spectra after pyridine adsorption on the bare and functionalized catalysts are shown in figure 2.19 and the quantification of the acidic sites is shown in table 2.9, first column. From the data, it is deducible that the catalysts preserve the typical acidity of those prepared with the CH method. Besides, the band at 1575 cm^{-1} was more enhanced in the case of silanized samples. This could be ascribable to the in-plane atomic displacements for the pyridine 8b vibrational modes of adsorbed pyridine corresponding to the vibrational modes of its benzenic ring [100,101] (figure S25). If quantitative analysis is considered, the concentration of Lewis acid sites was higher for the silane grafted samples with the only exception represented by the 15% loaded one. This suggests that the TEOCS grafting plays a role in promoting the acidity of the surface, particularly, the mild electron withdrawing ability of Si involved in -Cu-O-Si-R bonds could further lower the electron density of copper nanoclusters, promoting their acidity. In the literature, this phenomenon was observed by Tsou and co-workers: the silane grafted on copper phyllosilicates catalysts induced the formation of new acidic sites [49]. Interestingly, in the case of CuO/SiO_2 – 15% TEOCS, the values of acidic sites drop to a number even lower to the bare sample one. This could be explained by the fact that the higher density of silane chains of the 15% sample encourages the reticulation of the structure on the surface as already explained before in the case of CP-MAS NMR experiments. Again, this could hamper the pyridine probe to approach the copper active sites, coherently with the hypothesis regarding the GVL interaction with the copper site. Thus, the masking effect of the silane chain could cause the apparent reduction of acidity.
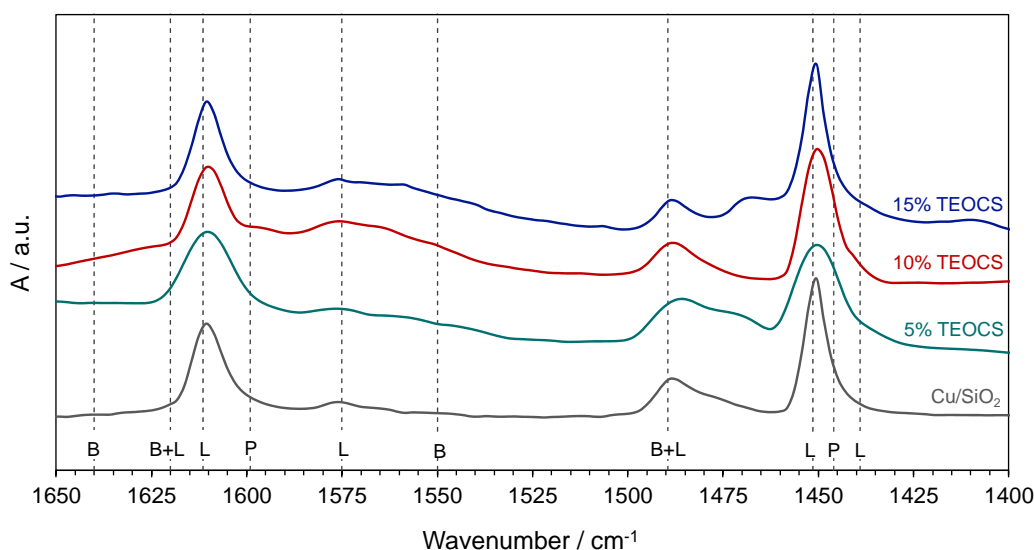
Figure 2.19. FT-IR spectra after pyridine adsorption of the catalysts. The spectra are obtained after pyridine desorption at 150 °C (L = Lewis, B = Brønsted). Adapted from ref. [82]. Copyright Elsevier.

Total surface acidity of the samples can be measured also through gas-solid titration with ammonia (table 2.9, second column). In this case, all the samples have a similar acidity quantification value (0.31-0.35 mmol(NH3) gcat-1), suggesting that the silanization doesn't compromise the acidic features of the copper phase. The steric hindrance of the two different molecules could be the reason of the different observed results: ammonia has a smaller kinetic diameter compared to pyridine; thus, it could be less influenced by the steric hindering effect of the organosilane chains and could be able to titrate all the accessible Cu sites on the surfaces independently on the silane loading degree. The use of different sized probes to evaluate the acidic site accessibility is a common method that could be found in literature [101–103].

Table 2.9. Adsorbed pyridine and ammonia quantification

Sample	Adsorbed pyridine at 150 °C $(mmol(py)\ g_{cat}^{-1})$	Adsorbed ammonia[a] / $(mmol(NH_3)\ g_{cat}^{-1})$
Cu/SiO$_2$	0.24	0.35
Cu/SiO$_2$ – 5% TEOCS	0.25	0.31
Cu/SiO$_2$ – 10% TEOCS	0.34	0.33
Cu/SiO$_2$ – 15% TEOCS	0.22	0.36

[a] the measure were affected by 8% error

The information obtained by the characterization of the surface properties such as morphology, wettability and acidity help to visualize a feasible explanation for the increased selectivity to the 1,4-PDO in the hydrogenation of GVL. The wettability properties of the catalyst surface are a key factor in promoting the desorption of the diol product from the active sites thus preventing side reactions. Those properties are finely tuned introducing on the catalyst surface alkyl silane chains that lower the hydrophilicity/alcoholphilicity of the materials. In particular, the selectivity to the diol increases up to 99% when silane loading reaches the 5% wt/wt. Nevertheless, acidity has a major role in the reaction conversion, activating the carbonyl group of GVL. In fact, the conversion trend of the GVL is coherent with the acidic sites density one, that in both cases reaches both a maximum for the Cu/SiO$_2$ – 10% TEOCS catalysts and then decrease when using the 15% TEOCS loaded catalyst. (0.34 against 0.22 mmol$_{py}$ g$_{cat}^{-1}$ respectively). Nonetheless, the activation of GVL is

connected to Cu accessibility that is hampered by a too high TEOCS concentration (figure 2.20). Considering these results, it is clear that the proper choice of the TEOCS grafting degree allows to opportunely modulate the surface properties and the copper activity finding in Cu/SiO$_2$ – 10% TEOCS the best compromise for catalyst performances.

The opportunity to modulate the surface wettability through organic molecules grafting is already known in the literature: the affinity of a catalyst surface for a reaction substrate is an important parameter to be considered when designing materials. The hydrophobicity increasement of Pd/SiO$_2$ catalyst was beneficial in decreasing the hydrogenation of styrene to ethylbenzene activation energy improving the affinity of the catalyst surface with the phenyl substrate [104]. Furthermore, the grafting of trietoxyoctylsilane grafting onto CuPS catalysts increases the hydrophobicity, thus raising the yield in GVL in the hydrogenation of LA and preventing the stabilization of the 4-hydroxyvaleric acid intermediate [49]. Another example reported is the hydrophobization of Cu/ZnO catalysts that showed a great inhibitory effect on the water gas-shift occurring in the one step synthesis of dimethyl ether from syngas, preserving also the catalytic activity. Also in this case, an excessive degree of stearic acid loading negatively influenced the conversion causing a partial coverage of the active sites [48].

2.4 Conclusions

The design of the heterogeneous catalytic systems becomes crucial in the biomass-derived platform molecules transformation. Particularly, the high oxygen content and polarity of bioderived molecules requires a fine tune of the surface wettability. In this section, it was demonstrated that a simple and reliable protocol can be exploited for the surface modification of CuO/SiO$_2$ catalyst. The effective functionalization was confirmed by several characterization techniques, namely IR and XP spectroscopy, that enlighten the presence of C-C, Si-O and O-C bonds. SCA and water adsorption measurements demonstrated the efficacy of the organosilane grafting in lowering the hydrophilicity of the surface. The silane-modified catalysts were tested in the hydrogenation of GVL to give 1,4-PDO and the results confirmed that as soon the silane is introduced on the surface the selectivity to 1,4-PDO boosted up to 99% due to easier desorption of the produced diol, therefore preventing side reactions. Notably, a silanization degree corresponding to the 10% wt/wt was optimal to increase the diol yield of about 40% while a further organosilane loading affects negatively the activity causing scarce accessibility of the GVL to the copper active site. This

phenomenon was confirmed by CP MAS analysis that showed a denser surface silane reticulation (Figure 2.20).
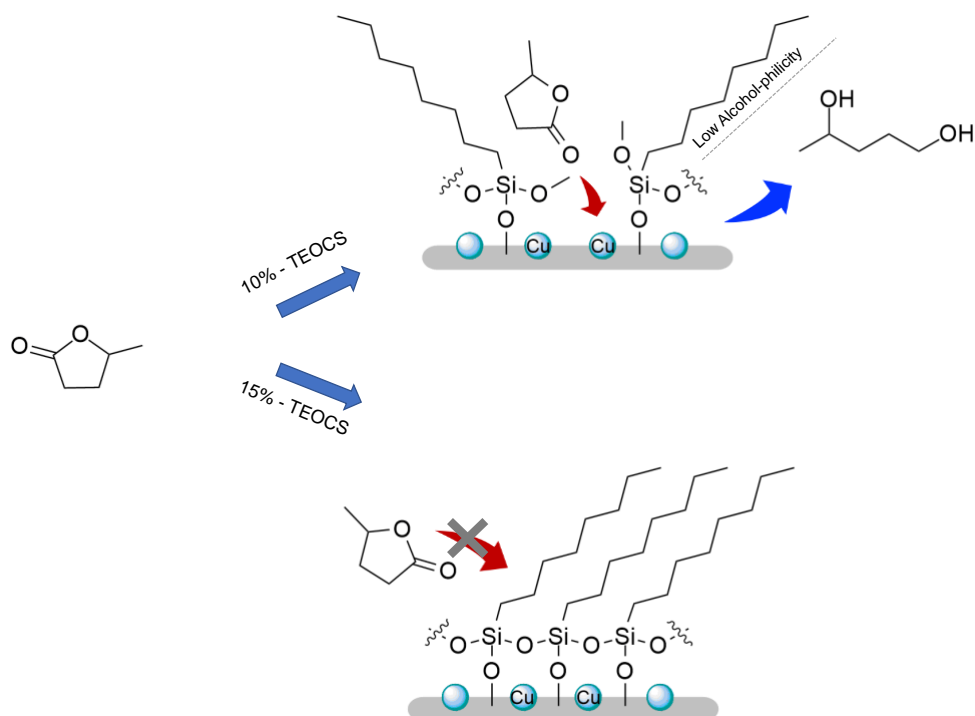

Figure 2.20. Possible mechanism for the hydrogenation of GVL on CuO/SiO$_2$ silane-grafted catalysts. Adapted from ref. [82]. Copyright Elsevier.

2.5 References

1. Arnaud, S.P.; Wu, L.; Wong Chang, M.A.; Comerford, J.W.; Farmer, T.J.; Schmid, M.; Chang, F.; Li, Z.; Mascal, M. New bio-based monomers: Tuneable polyester properties using branched diols from biomass. *Faraday Discuss.* **2017**, *202*, 61–77.

2. Stadler, B.M.; Brandt, A.; Kux, A.; Beck, H.; de Vries, J.G. Properties of Novel Polyesters Made from Renewable 1,4-Pentanediol. *ChemSusChem* **2020**, *13*, 556–563.

3. Tang, D.; Macosko, C.W.; Hillmyer, M.A. Thermoplastic polyurethane elastomers from bio-based poly(δ- decalactone) diols. *Polym. Chem.* **2014**, *5*, 3231–3237.

4. Shen, R.; Long, M.; Lei, C.; Dong, L.; Yu, G.; Tang, J. Anticorrosive waterborne polyurethane coatings derived from castor oil and renewable diols. *Chem. Eng. J.* **2022**, *433*, 134470.

5. Zhang, Y.; Liu, Z.; Hui, L.; Wang, H. Diols as solvent media for liquefaction of corn stalk at ambient pressure. *BioResources* **2019**, *13*, 6818–6836.

6. Samoilov, V.; Ni, D.; Goncharova, A.; Zarezin, D.; Kniazeva, M.; Ladesov, A.; Kosyakov, D.; Bermeshev, M.; Maximov, A. Bio-based solvents and gasoline components from renewable 2,3-butanediol and 1,2-propanediol: Synthesis and characterization. *Molecules* **2020**, *25*, 1–26.

7. Piskun, A.S.; van de Bovenkamp, H.H.; Rasrendra, C.B.; Winkelman, J.G.M.; Heeres, H.J. Kinetic modeling of levulinic acid hydrogenation to γ-valerolactone in water using a carbon supported Ru catalyst. *Appl. Catal. A Gen.* **2016**, *525*, 158–167.

8. Li, M.; Li, G.; Li, N.; Wang, A.; Dong, W.; Wang, X.; Cong, Y. Aqueous phase hydrogenation of levulinic acid to 1,4-pentanediol. *Chem. Commun.* **2014**, *50*, 1414–1416.

9. Mizugaki, T.; Nagatsu, Y.; Togo, K.; Maeno, Z.; Mitsudome, T.; Jitsukawa, K.; Kaneda, K. Selective hydrogenation of levulinic acid to 1,4-pentanediol in water using a hydroxyapatite-supported Pt-Mo bimetallic catalyst. *Green Chem.* **2015**, *17*, 5136–5139.

10. Bucciol, F.; Tabasso, S.; Grillo, G.; Menegazzo, F.; Signoretto, M.; Manzoli, M.; Cravotto, G. Boosting levulinic acid hydrogenation to value-added 1,4-pentanediol using microwave-assisted gold catalysis. *J. Catal.* **2019**.

11. Shao, Y.; Sun, K.; Li, Q.; Liu, Q.; Zhang, S.; Liu, Q.; Hu, G.; Hu, X. Copper-based catalysts with tunable acidic and basic sites for the selective conversion of levulinic acid/ester to γ-valerolactone or 1,4-pentanediol. *Green Chem.* **2019**, *21*, 4499–4511.

12. Fan, M.; Shao, Y.; Sun, K.; Li, Q.; Zhang, S.; Wang, Y.; Xiang, J.; Hu, S.; Wang, S.; Hu, X. Switching production of γ-valerolactone and 1,4-pentanediol from ethyl levulinate via tailoring alkaline sites of CuMg catalyst and hydrogen solubility in reaction medium. *Mol. Catal.* **2021**, *510*, 111680.

13. Shao, Y.; Ba, S.; Sun, K.; Gao, G.; Fan, M.; Wang, J.; Fan, H.; Zhang, L.; Hu, X. Selective production of γ-valerolactone or 1,4-pentanediol from levulinic acid/esters over Co-based catalyst: Importance of the synergy of hydrogenation sites and acidic sites. *Chem. Eng. J.* **2022**, *429*, 132433.

14. Rozenblit, A.; Avoian, A.J.; Tan, Q.; Sooknoi, T.; Resasco, D.E. Reaction mechanism of aqueous-phase conversion of γ-valerolactone (GVL) over a Ru/C catalyst. *J. Energy Chem.* **2016**, *25*, 1008–1014.

15. Bababrik, R.M.; Wang, B.; Resasco, D.E. Reaction Mechanism for the Conversion of γ-Valerolactone (GVL) over a Ru Catalyst: A First-Principles Study. *Ind. Eng. Chem. Res.* **2017**, *56*, 3217–3222.

16. Zhang, G.; Li, W.; Fan, G.; Yang, L.; Li, F. Controlling product selectivity by surface defects over MoOx-decorated Ni-based nanocatalysts for γ-valerolactone hydrogenolysis. *J. Catal.* **2019**.

17. Zhai, X.J.; Li, C.; Di, X.; Yin, D.D.; Liang, C.H. Preparation of Cu/MgO catalysts for γ-valerolactone hydrogenation to 1, 4-pentanediol by MOCVD. *Ranliao Huaxue Xuebao/Journal Fuel Chem. Technol.* **2017**, *45*, 537–546.

18. Sun, D.; Saito, T.; Yamada, Y.; Chen, X.; Sato, S. Hydrogenation of Γ-valerolactone to 1,4-pentanediol in a continuous flow reactor. *Appl. Catal. A Gen.* **2017**, *542*, 289–295.

19. Simakova, I.; Demidova, Y.; Simonov, M.; Prikhod'ko, S.; Niphadkar, P.; Bokade, V.; Dhepe, P.; Murzin, D.Y. Heterogeneously Catalyzed γ-Valerolactone Hydrogenation into 1,4-Pentanediol in Milder Reaction Conditions. *Reactions* **2020**, *1*, 54–71.

20. Wu, J.; Gao, G.; Li, Y.; Sun, P.; Wang, J.; Li, F. Highly chemoselective hydrogenation of lactone to diol over efficient copper-based bifunctional nanocatalysts. *Appl. Catal. B Environ.* **2019**, *245*, 251–261.

21. Liu, Q.; Zhao, Z.; Arai, M.; Zhang, C.; Liu, K.; Shi, R.; Wu, P.; Wang, Z.; Lin, W.; Cheng, H.; et al. Transformation of γ-valerolactone into 1,4-pentanediol and 2-

methyltetrahydrofuran over Zn-promoted Cu/Al2O3catalysts. *Catal. Sci. Technol.* **2020**, *10*, 4412–4423.

22. Sievers, C.; Scott, S.L.; Noda, Y.; Qi, L.; Albuquerque, E.M.; Rioux, R.M. Phenomena affecting catalytic reactions at solid−Liquid interfaces. *ACS Catal.* **2016**, *6*, 8286−8307.

23. Erbil, H.Y. *Surface Chemistry: Of Solid and Liquid Interfaces*; 2009; ISBN 1405119683.

24. Sheldon, R.A. Green and sustainable manufacture of chemicals from biomass: State of the art. *Green Chem.* **2014**, *16*, 950–963.

25. Gallezot, P. Catalytic conversion of biomass: Challenges and issues. *ChemSusChem* **2008**, *1*, 734–737.

26. Covinich, L.G.; Clauser, N.M.; Felissia, F.E.; Vallejos, M.E.; Area, M.C. The challenge of converting biomass polysaccharides into levulinic acid through heterogeneous catalytic processes. *Biofuels, Bioprod. Biorefining* **2020**, *14*, 417–445.

27. Gayubo, A.G.; Aguayo, A.T.; Atutxa, A.; Aguado, R.; Bilbao, J. Transformation of oxygenate components of biomass pyrolysis oil on a HZSM-5 zeolite. I. Alcohols and phenols. *Ind. Eng. Chem. Res.* **2004**, *43*, 2610–2618.

28. Cavuoto, D.; Zaccheria, F.; Ravasio, N. Some critical insights into the synthesis and applications of hydrophobic solid catalysts. *Catalysts* **2020**, *10*, 1–26.

29. Li, T.; Wang, J.; Wang, F.; Zhang, L.; Jiang, Y.; Arandiyan, H.; Li, H. The Effect of Surface Wettability and Coalescence Dynamics in Catalytic Performance and Catalyst Preparation: A Review. *ChemCatChem* **2019**, *11*, 1576–1586.

30. Liu, F.; Huang, K.; Zheng, A.; Xiao, F.S.; Dai, S. Hydrophobic Solid Acids and Their Catalytic Applications in Green and Sustainable Chemistry. *ACS Catal.* **2018**, *8*, 372–391.

31. Okuhara, T. Water-tolerant solid acid catalysts. *Chem. Rev.* **2002**, *102*, 3641–3666.

32. Sánchez-Vázquez, R.; Pirez, C.; Iglesias, J.; Wilson, K.; Lee, A.F.; Melero, J.A. Zr-Containing Hybrid Organic-Inorganic Mesoporous Materials: Hydrophobic Acid Catalysts for Biodiesel Production. *ChemCatChem* **2013**, *5*, 994–1001.

33. Manayil, J.C.; Lee, A.F.; Wilson, K. Functionalized periodic mesoporous organosilicas: Tunable hydrophobic solid acids for biomass conversion. *Molecules* **2019**, *24*.

34. Zhang, J.; Wang, L.; Liu, F.; Meng, X.; Mao, J.; Xiao, F.S. Enhanced catalytic performance in dehydration of sorbitol to isosorbide over a superhydrophobic

mesoporous acid catalyst. *Catal. Today* **2015**, *242*, 249–254.

35. Cubo, A.; Iglesias, J.; Morales, G.; Melero, J.A.; Moreno, J.; Sánchez-Vázquez, R. Dehydration of sorbitol to isosorbide in melted phase with propyl-sulfonic functionalized SBA-15: Influence of catalyst hydrophobization. *Appl. Catal. A Gen.* **2017**, *531*, 151–160.

36. Kong, P.S.; Pérès, Y.; Wan Daud, W.M.A.; Cognet, P.; Aroua, M.K. Esterification of glycerol with oleic acid over hydrophobic zirconia-silica acid catalyst and commercial acid catalyst: Optimization and influence of catalyst acidity. *Front. Chem.* **2019**, *7*, 1–11.

37. Kong, P.S.; Pérès, Y.; Cognet, P.; Senocq, F.; Daud, W.M.A.W.; Aroua, M.K.; Ahmad, H.; Sankaran, R.; Show, P.L. Structure–selectivity relationship of a zirconia-based heterogeneous acid catalyst in the production of green mono- and dioleate product. *Clean Technol. Environ. Policy* **2021**, *23*, 19–29.

38. Kong, P.S.; Cognet, P.; Pérès, Y.; Esvan, J.; Daud, W.M.A.W.; Aroua, M.K. Development of a Novel Hydrophobic ZrO2-SiO2 Based Acid Catalyst for Catalytic Esterification of Glycerol with Oleic Acid. *Ind. Eng. Chem. Res.* **2018**, *57*, 9386–9399.

39. Nguyen, V.C.; Bui, N.Q.; Mascunan, P.; Vu, T.T.H.; Fongarland, P.; Essayem, N. Esterification of aqueous lactic acid solutions with ethanol using carbon solid acid catalysts: Amberlyst 15, sulfonated pyrolyzed wood and graphene oxide. *Appl. Catal. A Gen.* **2018**, *552*, 184–191.

40. Sreeprasanth, P.S.; Srivastava, R.; Srinivas, D.; Ratnasamy, P. Hydrophobic, solid acid catalysts for production of biofuels and lubricants. *Appl. Catal. A Gen.* **2006**, *314*, 148–159.

41. Veiga, P.M.; Gomes, A.C.L.; Veloso, C. de O.; Henriques, C.A. Etherification of different glycols with ethanol or 1-octanol catalyzed by acid zeolites. *Mol. Catal.* **2018**, *458*, 261–271.

42. Veiga, P.M.; Gomes, A.C.L.; Veloso, C.O.; Henriques, C.A. Acid zeolites for glycerol etherification with ethyl alcohol: Catalytic activity and catalyst properties. *Appl. Catal. A Gen.* **2017**, *548*, 2–15.

43. Losch, P.; Huang, W.; Vozniuk, O.; Goodman, E.D.; Schmidt, W.; Cargnello, M. Modular Pd/Zeolite Composites Demonstrating the Key Role of Support Hydrophobic/Hydrophilic Character in Methane Catalytic Combustion. *ACS Catal.* **2019**, *9*, 4742–4753.

44. Silva, W.R.; Matsubara, E.Y.; Rosolen, J.M.; Donate, P.M.; Gunnella, R. Pd catalysts

supported on different hydrophilic or hydrophobic carbonaceous substrate for furfural and 5-(hydroxymethyl)-furfural hydrogenation in water. *Mol. Catal.* **2021**, *504*.

45. Mu, S.; Li, L.; Zhao, R.; Lu, H.; Dong, H.; Cui, C. Molecular-Scale Insights into Electrochemical Reduction of CO2on Hydrophobically Modified Cu Surfaces. *ACS Appl. Mater. Interfaces* **2021**, *13*, 47619–47628.

46. Wu, S.; Zhao, H.; Dong, F.; Ling, W.; Tang, Z.; Zhang, J. Construction of superhydrophobic Ru/TiCeO xcatalysts for the enhanced water resistance of o-dichlorobenzene catalytic combustion. *ACS Appl. Mater. Interfaces* **2021**, *13*, 2610–2621.

47. Hao, P.; Schwartz, D.K.; Medlin, J.W. Effect of Surface Hydrophobicity of Pd/Al2O3 on Vanillin Hydrodeoxygenation in a Water/Oil System. *ACS Catal.* **2018**, *8*, 11165–11173.

48. Tan, M.; Tian, S.; Zhang, T.; Wang, K.; Xiao, L.; Liang, J.; Ma, Q.; Yang, G.; Tsubaki, N.; Tan, Y. Probing Hydrophobization of a Cu/ZnO Catalyst for Suppression of Water-Gas Shift Reaction in Syngas Conversion. *ACS Catal.* **2021**, *11*, 4633–4643.

49. Tsou, Y.J.; To, T.D.; Chiang, Y.C.; Lee, J.F.; Kumar, R.; Chung, P.W.; Lin, Y.C. Hydrophobic Copper Catalysts Derived from Copper Phyllosilicates in the Hydrogenation of Levulinic Acid to γ-Valerolactone. *ACS Appl. Mater. Interfaces* **2020**, *12*, 54851–54861.

50. Vansant, E.E.; Van Der Voort, P.; Vrancken, K.C. *Characterization and Chemical Modification of the Silica Surface*; 1995; ISBN 0-444-81928-2.

51. Wu, J.; Gao, G.; Sun, P.; Long, X.; Li, F. Synergetic Catalysis of Bimetallic CuCo Nanocomposites for Selective Hydrogenation of Bioderived Esters. *ACS Catal.* **2017**, *7*, 7890–7901.

52. Cavuoto, D.; Ravasio, N.; Scotti, N.; Gervasini, A.; Campisi, S.; Marelli, M.; Cappelletti, G.; Zaccheria, F. A green solvent diverts the hydrogenation of γ – valerolactone to 1 , 4 - pentanediol over Cu / SiO 2. *Mol. Catal.* **2021**, *516*, 111936.

53. Carniti, P.; Gervasini, A.; Marzo, M. Silica-niobia oxides as viable acid catalysts in water: Effective vs. intrinsic acidity. *Catal. Today* **2010**, *152*, 42–47.

54. Gervasini, A.; Bennici, S.; Auroux, A.; Guimon, C. Surface acidic properties of supported binary oxides containing CuO coupled with Ga2O3 and SnO2 studied by complementary techniques. *Appl. Catal. A Gen.* **2007**.

55. Zaccheria, F.; Scotti, N.; Marelli, M.; Psaro, R.; Ravasio, N. Unravelling the properties of supported copper oxide: Can the particle size induce acidic behaviour? *Dalt. Trans.*

2013, *42*, 1319–1328.

56. Scotti, N.; Dangate, M.; Gervasini, A.; Evangelisti, C.; Ravasio, N.; Zaccheria, F. Unraveling the role of low coordination sites in a cu metal nanoparticle: A step toward the selective synthesis of second generation biofuels. *ACS Catal.* **2014**, *4*, 2818–2826.

57. Moulder, J.F.; Stickle, W.F.; Sobol, P.E.; Bomben, K.D. Handbook of X-ray Photoelectron Spectroscopy Edited by. **1993**, 1–261.

58. Biesinger, M.C. Advanced analysis of copper X-ray photoelectron spectra. *Surf. Interface Anal.* **2017**, *49*, 1325–1334.

59. Gervasini, A.; Manzoli, M.; Martra, G.; Ponti, A.; Ravasio, N.; Sordelli, L.; Zaccheria, F. Dependence of copper species on the nature of the support for dispersed CuO catalysts. *J. Phys. Chem. B* **2006**, *110*, 7851–7861.

60. Zhu, S.; Gao, X.; Zhu, Y.; Fan, W.; Wang, J.; Li, Y. A highly efficient and robust Cu/SiO2 catalyst prepared by the ammonia evaporation hydrothermal method for glycerol hydrogenolysis to 1,2-propanediol. *Catal. Sci. Technol.* **2015**, *5*, 1169–1180.

61. Auroux, A.; Gervasini, A.; Guimon, C. Acidic character of metal-loaded amorphous and crystalline silica-aluminas determined by XPS and adsorption calorimetry. *J. Phys. Chem. B* **1999**, *103*, 7195–7205.

62. Dong, G.; Ai, Z.; Zhang, L. Total aerobic destruction of azo contaminants with nanoscale zero-valent copper at neutral pH: Promotion effect of in-situ generated carbon center radicals. *Water Res.* **2014**, *66*, 22–30.

63. Monte, M.; Munuera, G.; Costa, D.; Conesa, J.C.; Martínez-Arias, A. Near-ambient XPS characterization of interfacial copper species in ceria-supported copper catalysts. *Phys. Chem. Chem. Phys.* **2015**, *17*, 29995–30004.

64. Emeis, C.A. Determination of integrated molar extinction coefficients for infrared absorption bands of pyridine adsorbed on solid acid catalysts. *J. Catal.* 1993, *141*, 347–354.

65. Du, X.L.; Bi, Q.Y.; Liu, Y.M.; Cao, Y.; He, H.Y.; Fan, K.N. Tunable copper-catalyzed chemoselective hydrogenolysis of biomass-derived γ-valerolactone into 1,4-pentanediol or 2-methyltetrahydrofuran. *Green Chem.* **2012**, *14*, 935–939.

66. Xu, Q.; Li, X.; Pan, T.; Yu, C.; Deng, J.; Guo, Q.; Fu, Y. Supported copper catalysts for highly efficient hydrogenation of biomass-derived levulinic acid and γ-valerolactone. *Green Chem.* **2016**, *18*, 1287–1294.

67. Ravasio, N.; Antenori, M.; Gargano, M. The Role of the Support in Selective

Hydrogenations promoted by Cu/Al2O3. *Stud. Surf. Sci. Catal.* **1993**, *78*, 75–82.

68. Zaccheria, F.; Ravasio, N.; Fusi, A.; Rodondi, M.; Psaro, R. Tuning selectivity in terpene chemistry: Selective hydrogenation versus cascade reactions over copper catalysts. *Adv. Synth. Catal.* **2005**.

69. Azzena, U.; Carraro, M.; Pisano, L.; Monticelli, S.; Bartolotta, R.; Pace, V. Cyclopentyl Methyl Ether: An Elective Ecofriendly Ethereal Solvent in Classical and Modern Organic Chemistry. *ChemSusChem* 2019.

70. Watanabe, K.; Yamagiwa, N.; Torisawa, Y. Cyclopentyl methyl ether as a new and alternative process solvent. *Org. Process Res. Dev.* 2007.

71. Coeck, R.; De Vos, D.E. One-pot reductive amination of carboxylic acids: a sustainable method for primary amine synthesis. *Green Chem.* **2020**, *22*, 5105–5114.

72. Wang, L.; Wang, H.; Liu, F.; Zheng, A.; Zhang, J.; Sun, Q.; Lewis, J.P.; Zhu, L.; Meng, X.; Xiao, F.S. Selective catalytic production of 5-hydroxymethylfurfural from glucose by adjusting catalyst wettability. *ChemSusChem* **2014**, *7*, 402–406.

73. Lin, J.D.; Bi, Q.Y.; Tao, L.; Jiang, T.; Liu, Y.M.; He, H.Y.; Cao, Y.; Wang, Y.D. Wettability-Driven Palladium Catalysis for Enhanced Dehydrogenative Coupling of Organosilanes. *ACS Catal.* **2017**, *7*, 1720–1727.

74. Miura, H.; Kameyama, S.; Komori, D.; Shishido, T. Quantitative Evaluation of the Effect of the Hydrophobicity of the Environment Surrounding Brønsted Acid Sites on Their Catalytic Activity for the Hydrolysis of Organic Molecules. *J. Am. Chem. Soc.* **2019**, *141*, 1636–1645.

75. Li, Z.; Zhu, Z.; Cao, C.; Jiang, L.; Song, W. Bioinspired Hollow Nanoreactor: Catalysts that Carry Gaseous Hydrogen for Enhanced Gas-Liquid-Solid Three-Phase Hydrogenation Reactions. *ChemCatChem* **2020**, *12*, 459–462.

76. Li, Z.; Cao, C.; Zhu, Z.; Liu, J.; Song, W.; Jiang, L. Superaerophilic Materials Are Surprising Catalysts: Wettability-Induced Excellent Hydrogenation Activity under Ambient H2 Pressure. *Adv. Mater. Interfaces* **2018**, *5*, 1–6.

77. Cavuoto, D.; Zaccheria, F.; Marelli, M.; Evangelisti, C.; Piccolo, O.; Ravasio, N. The Role of Support Hydrophobicity in the Selective Hydrogenation of Enones and Unsaturated Sulfones over Cu/SiO2 Catalysts. *Catalysts* **2020**, 515.

78. Kim, H.J.; Brunelli, N.A.; Brown, A.J.; Jang, K.S.; Kim, W.G.; Rashidi, F.; Johnson, J.R.; Koros, W.J.; Jones, C.W.; Nair, S. Silylated mesoporous silica membranes on polymeric hollow fiber supports: Synthesis and permeation properties. *ACS Appl. Mater. Interfaces* **2014**, *6*, 17877–17886.

79. Yismaw, S.; Ebbinghaus, S.G.; Wenzel, M.; Poppitz, D.; Gläser, R.; Matysik, J.; Bauer, F.; Enke, D. Selective functionalization of the outer surface of MCM-48-type mesoporous silica nanoparticles at room temperature. *J. Nanoparticle Res.* **2020**, *22*.

80. Bauer, F.; Meyer, R.; Bertmer, M.; Naumov, S.; Al-Naji, M.; Wissel, J.; Steinhart, M.; Enke, D. Silanization of siliceous materials, part 3: Modification of surface energy and acid-base properties of silica nanoparticles determined by inverse gas chromatography (IGC). *Colloids Surfaces A Physicochem. Eng. Asp.* **2021**, *618*, 126472.

81. Silverstein, R.M.; Webster, F.X.; Kiemle, D.J.; Bryce, D.L. *Spectrometric Identification of Organic Compounds*; 8th Editio.; John Wiley & Sons, Inc., 2014; ISBN 978-0-470-61637-6.

82. Cavuoto, D.; Ravasio, N.; Zaccheria, F.; Marelli, M.; Cappelletti, G.; Campisi, S.; Gervasini, A. Tuning the Cu/Sio2 Wettability Features for Bio-Derived Platform Molecules Valorization. *SSRN Electron. J.* **2022**, *528*, 112462.

83. Alam, A.U.; Howlader, M.M.R.; Deen, M.J. Oxygen Plasma and Humidity Dependent Surface Analysis of Silicon, Silicon Dioxide and Glass for Direct Wafer Bonding. *ECS J. Solid State Sci. Technol.* **2013**, *2*, P515–P523.

84. Ma, J.W.; Lee, W.J.; Bae, J.M.; Jeong, K.S.; Oh, S.H.; Kim, J.H.; Kim, S.H.; Seo, J.H.; Ahn, J.P.; Kim, H.; et al. Carrier Mobility Enhancement of Tensile Strained Si and SiGe Nanowires via Surface Defect Engineering. *Nano Lett.* **2015**, *15*, 7204–7210.

85. Kitao, A.; Imakita, K.; Kawamura, I.; Fujii, M. An investigation into second harmonic generation by Si-rich SiNx thin films deposited by RF sputtering over a wide range of Si concentrations. *J. Phys. D. Appl. Phys.* **2014**, *47*.

86. Pargoletti, E.; Verga, S.; Chiarello, G.L.; Longhi, M.; Cerrato, G.; Giordana, A.; Cappelletti, G. Exploring SNx ti1−x o2 solid solutions grown onto graphene oxide (GO) as selective toluene gas sensors. *Nanomaterials* **2020**, *10*.

87. Dietrich, P.M.; Glamsch, S.; Ehlert, C.; Lippitz, A.; Kulak, N.; Unger, W.E.S. Synchrotron-radiation XPS analysis of ultra-thin silane films: Specifying the organic silicon. *Appl. Surf. Sci.* **2016**, *363*, 406–411.

88. Post, P.; Wurlitzer, L.; Maus-Friedrichs, W.; Weber, A.P. Characterization and applications of nanoparticles modified in-flight with silica or silica-organic coatings. *Nanomaterials* **2018**, *8*, 1–19.

89. Su, D.; Wang, L.; Liang, K.; Zhang, F.; Lin, D.; Hu, Y.; Ji, H.; Li, X.; Chen, S.; Yan, X. Silicon oxycarbide/titanium dioxide fibers with wrinkle-like surface by electrospinning.

Mater. Lett. **2016**, *172*, 202–206.

90. Zhao, Y.; Zhao, J.; Su, Z.; Hao, X.; Li, Y.; Li, N.; Li, Y. SiO2 capsulized Cu active nanoparticles: Synthesis and activity study. *J. Mater. Chem. A* **2013**, *1*, 8029–8036.

91. McCafferty, E.; Wightman, J.P. Determination of the concentration of surface hydroxyl groups on metal oxide films by a quantitative XPS method. *Surf. Interface Anal.* **1998**, *26*, 549–564.

92. Hashemi, A.; Bahari, A. Structural and dielectric characteristic of povidone–silica nanocomposite films on the Si (n) substrate. *Appl. Phys. A Mater. Sci. Process.* **2017**, *123*, 1–7.

93. Watanabe, T.; Hasegawa, S.; Wakiyama, N.; Usui, F.; Kusai, A.; Isobe, T.; Senna, M. Solid state radical recombination and charge transfer across the boundary between indomethacin and silica under mechanical stress. *J. Solid State Chem.* **2002**, *164*, 27–33.

94. Milanesi, F.; Cappelletti, G.; Annunziata, R.; Bianchi, C.L.; Meroni, D.; Ardizzone, S. Siloxane-TiO2 hybrid nanocomposites. the structure of the hydrophobic layer. *J. Phys. Chem. C* **2010**, *114*, 8287–8293.

95. Rytter, E.; Salman, A. ul R.; Tsakoumis, N.E.; Myrstad, R.; Yang, J.; Lögdberg, S.; Holmen, A.; Rønning, M. Hydrophobic catalyst support surfaces by silylation of Γ-alumina for Co/Re Fischer-Tropsch synthesis. *Catal. Today* **2018**, *299*, 20–27.

96. Castellano, M.; Marsano, E.; Turturro, A.; Conzatti, L.; Busca, G. Dependence of surface properties of silylated silica on the length of silane arms. *Adsorption* **2012**, *18*, 307–320.

97. Protsak, I.S.; Morozov, Y.M.; Dong, W.; Le, Z.; Zhang, D.; Henderson, I.M. A 29Si, 1H, and 13C Solid-State NMR Study on the Surface Species of Various Depolymerized Organosiloxanes at Silica Surface. *Nanoscale Res. Lett.* **2019**, *14*.

98. Bui, T. V.; Umbarila, S.J.; Wang, B.; Sooknoi, T.; Li, G.; Chen, B.; Resasco, D.E. High-Temperature Grafting Silylation for Minimizing Leaching of Acid Functionality from Hydrophobic Mesoporous Silicas Used as Catalysts in the Liquid Phase. *Langmuir* **2019**, *35*, 6838–6852.

99. Nam, K.H.; Lee, T.H.; Bae, B.S.; Popall, M. Condensation reaction of 3-(methacryloxypropyl)-trimethoxysilane and diisobutylsilanediol in non-hydrolytic sol-gel process. *J. Sol-Gel Sci. Technol.* **2006**, *39*, 255–260.

100. Escribano, V.S.; del Hoyo Martínez, C.; Fernández López, E.; Gallardo Amores, J.M.; Busca, G. Characterization of a ceria-zirconia-supported Cu oxides catalyst: An FT-

IR study on the catalytic oxidation of propylene. *Catal. Commun.* **2009**, *10*, 861–864.

101. Busca, G. Spectroscopic characterization of the acid properties of metal oxide catalysts. *Catal. Today* **1998**, *41*, 191–206.

102. Freitas, C.; Barrow, N.S.; Zholobenko, V. Accessibility and Location of Acid Sites in Zeolites as Probed by Fourier Transform Infrared Spectroscopy and Magic Angle Spinning Nuclear Magnetic Resonance. *Johnson Matthey Technol. Rev.* **2018**, *62*, 279–290.

103. Busca, G.; Gervasini, A. *Solid acids, surface acidity and heterogeneous acid catalysis*; 1st ed.; Elsevier Inc., 2020; Vol. 67; ISBN 9780128203705.

104. Yang, Y.; Xie, Y.; Zhang, J.; Li, D.; Deng, D.; Duan, Y. Fabrication of Pd/SiO2 with Controllable Wettability for Enhanced Catalytic Hydrogenation Activity at Ambient H2 Pressure. *ChemCatChem* **2019**, *11*, 5430–5434.

105. Mrowiec-Bialoń, J. Determination of hydroxyls density in the silica-mesostructured cellular foams by thermogravimetry. *Thermochim. Acta* **2006**, *443*, 49–52.

3 AMINATION OF BIODERIVED SUBSTRATES WITH Cu CATALYST

In this chapter the amination of some bioderived alcohols and lactones with heterogeneous supported copper catalysts will be deeply discussed. In a previous work [1,2] Cu catalysts with low metal loading deposited with CH method on different supports has demonstrated to be effective in the amination of ketones and alcohols.

The aim of this chapter is to face the challenging synthesis of N-containing chemicals starting from biobased alcohols and lactones using similar supported copper catalysts.

3.1   Amination of alcohols

3.1.1   Amination of alcohols with heterogeneous metal catalysts: recent work

Amines are important class of molecules that are useful as intermediates in the chemical industry for the production of drugs, agrochemicals, polymers and solvents. Traditionally, amines are produced through the direct reaction of alkyl halides and ammonia or through the reduction of nitro and nitriles compounds. These processes produce harmful byproducts and wastes, while also using stoichiometric amounts of reducing agents.

Nevertheless, amines can be prepared also starting from alcohols and ammonia (or other amines) through the so-called "hydrogen borrowing" "hydrogen auto-transfer" mechanism (Scheme 3.1) that can be achieved also using heterogeneous catalysts.
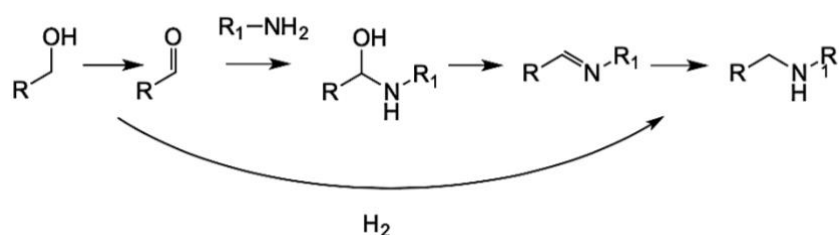
Scheme 3.1. Amination of alcohol using hydrogen borrowing mechanism.

In this process, the alcoholic moiety is dehydrogenated to give the corresponding carbonyl group: this condenses with ammonia (or amine) to form an imine that is in turn hydrogenated by the hydrogen obtained from the first step to obtain a primary amine. This process could be really convenient especially considering that exogenous hydrogen pressure is not required in the reaction mechanism and it can be suitable to produce amines

starting from biomass-derived alcohol substrates. Several reviews [3,4] have extensively discussed about this topic. However, despite the numerous benefits, the heterogeneously catalyzed synthesis of primary amines starting from alcohols and ammonia still gives raise to many challenges. In fact, ammonia is a poor amination reagent compared to the readily generated primary amine, thus resulting in lack of selectivity. In a work of Sautet and Pera-Titus groups [5], a deep computational study on the factors ruling on catalyst activity and selectivity in this process was carried out. The results enlighten that the catalytic activity was mainly controlled by the oxophilic nature of the metal catalysts that determines the adsorption energy of oxygen. Moreover, they discovered that the major reason for the loss in primary amines selectivity was the low activation energy of the surface mediated C-N bond coupling between two N-containing intermediates CH_3-NH and CH_2-NH that was small enough to compete with the hydrogenation towards the amine product. The more the metal is oxophilic, the higher is this activation energy and, as a consequence, the selectivity towards the primary amines [5].

Non-noble metal heterogeneous catalysts for amination of alcohols

Noble metal heterogeneously catalyzed amination of alcohols has been extensively studied. In particular, ruthenium has been demonstrated to be particularly active and selective towards the primary amine [6–8]. Nevertheless, in the next section some recent examples relying on non-noble metal heterogeneous catalysts used for this aim will be discussed (table 3.1).

Propylamine can be efficiently prepared from propanol and ammonia using hydroxyapatite (HAP) supported nickel catalysts [9]. The reaction pathway proceeds through a hydrogen transfer mechanism and the rate limiting step is the α-H-abstraction from propanol. The Ni/HAP showed an excellent activity with a selectivity towards the primary amine of 92%. The good catalytic performances of this system were ascribed to the high density of basic sites on HAP that stabilizes the alkoxide intermediates and avoids the subsequent alkylation to secondary amine. Notably, Ni/HAP showed a turnover frequency of an order of magnitude greater than Ni/SiO_2 catalysts that have a selectivity of 74% [9]. In a similar way, basic sites of USY@Ni-3 catalyst [10] derived from NiAl-Layered-Double-hydroxides precursors ensured the stabilization of the alkoxide intermediate during amination of 1-octanol with ammonia. This was combined with highly dispersed metallic Ni active sites reaching up to 77% conversion with a selectivity to the primary amine of 82% ($P(H_2) = 5$ bar; T = 180 °C; t = 16 h) [10].

As already mentioned, heterogeneous catalyzed amination strategy can be utilized also for the valorization of bioderived alcohols. In a paper of 2021, hydrotalcite-derived nickel catalysts Ni_xAl-CT demonstrated to be suitable for the valorization of furfuryl alcohol and aminomethyl-2-furanmethanol with ammonia [11]. Particularly, Ni_2Al-600 catalyst with a high quantity of Ni^0 sites and properly tuned acid-basic site density showed the best catalytic performance that was related to a high dehydrogenation activity reaching 84% yield in furfurylamine at 180 °C, 4 bar of hydrogen pressure in 36 hours of reaction [11].

Nickel and copper can be efficiently combined to prepare CuNiAlOx bifunctional catalysts that are active in the amination of biomass-derived 5-hydroxymethylfurfural (5-HMF) into 2,5-bis(aminomethyl)furan with ammonia obtaining 86% of yield in the amine. The process proceeded through two catalytic steps: reductive amination of hydroxymethylfurfural at 90 °C followed by the hydrogen-borrowing of its alcoholic group at 210 °C ($P(H_2)$ = 45 bar, Na_2CO_3 used as H-borrowing promoting agent) [12].

Table 3.1 Catalytic amination of alcohols with ammonia using non-noble heterogeneous catalysts.

Alcohol substrate	Catalyst	T (°C)	Conversion (%)	Selectivity to R-NH_2 (%)	Ref.
Propanol	Ni/HAP	150	TOF = 1.7 s^{-1}	92	[9]
1-octanol	USY@Ni-3	180	77	82	[10]
furfuryl alcohol	Ni_2Al-600	180	100	84	[11]
5-HMF	$Cu_4Ni_1Al_4O_x$	90-210	100	86 (diamine)	[12]
1,6-hexanediol	Cu/ZnO/γ-Al_2O_3	200	100	93 (diamine)[a]	[13]
3-(3,4-dimethoxyphenyl)-1-propanol	Cu/ZrO_2	190	95	97 (tertiary amine)[a]	[14]

[a]dimethylamine was used instead of ammonia.

Nevertheless, copper can be also used alone to prepare active catalysts in bioderived alcohol amination. Cai et al. [13] developed Cu/ZnO/γ-Al_2O_3 catalysts by co-precipitation method and used them in the amination of 1,6-hexanediol with dimethylamine to N, N, N', N'-tetramethyl-1,6-hexanediamine in a fixed-bed reactor under the reaction conditions of 200 °C of temperature and a hydrogen pressure of 30 bar, obtaining a yield in diamine of 93%. The high dispersion of copper, promoted by ZnO doping, was the reason of the

excellent activity showed by the catalyst due to the strong interaction between the metal and the doping agent [13]. Finally, tertiary amine can be prepared from a lignin model monomer 3-(3,4-dimethoxyphenyl)-1-propanol with dimethylamine using Cu/ZrO_2 prepared with incipient wetness impregnation with a conversion and a selectivity up to 95% and 97% respectively [14].

The Role of Hydrogen pressure

Although hydrogen pressure wouldn't be required for the proceeding of amination through hydrogen borrowing (scheme 3.1), several works have demonstrated that not using hydrogen compromises the activity and the selectivity of the catalyst particularly when ammonia or short-chained amines are used [13–15]. In a work of Baiker [15], it was demonstrated that the reactant amine can undergo disproportionation on amination catalysts under normal amination process conditions (Scheme 3.2):

$$2R_2NH \rightleftharpoons RNH_2 + R_3N$$
$$2RNH_2 \rightleftharpoons R_2NH + NH_3$$
$$R_3N + NH_3 \rightleftharpoons R_2NH + RNH_2$$
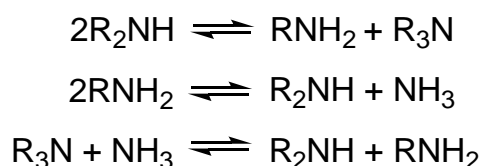
Scheme 3.2. Amine disproportionation on amination catalyst.

This can cause nitride formation on the metal catalyst surface, namely copper or nickel, caused by ammonia itself or originated from disproportionation of another reactant amine (scheme 3.3) that causes catalysts deactivation adsorbing on catalyst active sites.

$$NH_3 + 3Cu \rightleftharpoons Cu_3N + 3/_2H_2$$

Scheme 3.3. Nitride formation on copper catalyst.

Introducing an exogenous hydrogen pressure allows one to avoid the deactivation of the catalyst due to the immediate regeneration of the metal phase. Furthermore, the presence of hydrogen creates a reducing environment, stabilizing the active metallic Cu^0 sites for dehydrogenation [14].

3.1.2 Aim of the work

Herein, some preliminary results of preparation of amines starting from alcohols and ammonia using copper catalysts through an hydrogen borrowing strategy is reported. As already mentioned, supported copper catalysts have demonstrated to be effective in the

amination of ketones and alcohols [1,2]. The final aim is to obtain primary diamines starting from diols coming from renewable resources. Diamines are actually highly useful as monomers in the production of biobased polymers.

3.1.3 Results and discussion

In the first place, some bioderived monoalcohol substrates were chosen for the amination tests namely 1-octanol, 2-octanol, 1-butanol. Moreover cyclooctanol (Scheme 3.4) and diisopropylcarbinol were chosen for the sake of comparison. As catalytic materials, Cu/Al_2O_3 at 16% wt/wt Cu loading prepared with the CH method (see section 1.1.4) was chosen following the previously obtained results [1,2] using a reduction pre-treatment before any reaction (see experimental section 5.3). After some screening, the best reaction conditions were found to be temperature of 180 °C, using ammonia ($P(NH_3) = 3$ bar), heptane as the solvent under hydrogen atmosphere ($P(H_2) = 10$ bar) at 2 hours of reaction. The catalytic tests results are shown in table 3.2.
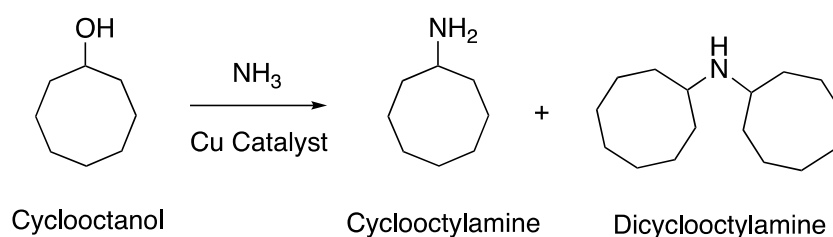
Scheme 3.4. Amination of cyclooctanol with ammonia using copper catalyst.

Under these conditions, the results were quite different depending on the alcohol used as the substrate. Considering the C_8 alcohols, the most prone to react were the secondary and the cyclic one, allowing to reach a conversion up to 98%. On the contrary when using the linear primary alcohol, the conversion was not higher than 49%, that means the half of the previous described. Besides, using *n*-butanol as the substrate a 100% conversion was reached while no conversion was obtained with diisopropylcarbinol. For the sake of comparison, a moderately acidic Cu/SiO_2 (16% wt/wt Cu) catalyst, prepared with the same method, was tested in the amination of 1-octanol and cyclooctanol under the same conditions obtaining 44% and 66% of conversion respectively. The lower activity of the silica supported catalyst could be searched in the surface acid-base properties of the material. In fact, the fine tuning of the acidity and basicity of the catalysts has shown to be pivotal in the amination of alcohols: it was demonstrated that amphoteric supports contribute to the high

conversion of the substrates stabilizing the alkoxide intermediates [9,10], thus explaining the higher activity of Cu/Al$_2$O$_3$.

Exogenous hydrogen pressure was employed even if not required by the reaction pathway. In fact, reactions that were carried under nitrogen atmosphere did not show any conversion of the substrate. The reason could be searched in the deactivation of the catalyst by nitride formation as already explained in the 3.1.1. paragraph. The hydrogen pressure maybe well regenerates the copper phase from the nitride adsorption on the surface. Moreover, hydrogen preserves the copper reduced and active for the dehydrogenation a hydrogenation steps [15].

From the catalytic results it was clear that the amination reactions suffered from poor selectivity towards the primary amine. In most of the cases the selectivity was almost total towards the secondary amine, such as 1-octanol and 2-octanol (94% and 86% selectivity respectively) or even for the tertiary amine as in the case of the short-chained *n*-butanol. Cyclooctanol was the only substrate that allowed us to isolate the primary cyclooctylamine with a 40% yield.

Table 3.2. Amination of various alcohols with ammonia using Cu/Al$_2$O$_3$ catalyst. Reaction conditions: T=180 °C, P(NH$_3$) = 3 bar, P(H$_2$) = 10 bar, t =2 h heptane as solvent.

Alcohol Substrate	Conversion (%)	R-NH$_2$ (%)	R-NH-R	R-NR$_1$R$_2$
Cyclooctanol	98	41	57	0
1-Octanol	49	0	94	2
2-Octanol	98	0	86	0
n-BuOH	100	0	0	99
Diisopropylcarbinol	0			

The main reason of the poor selectivity to the primary amine, in particular for linear alcohols, could be related to the fact that ammonia is a poor nucleophile if compared to primary amines: as soon as the latter forms on the catalyst surface, it is readily alkylated by another alcohol molecule. This could be enhanced by the moderately low oxophilicity of copper [16] that decreases the activation energy of the C-N bound coupling between two primary amines intermediates [5]. Moreover, the high steric hindrance of the cyclooctylamine could be a detrimental factor for further alkylation to secondary amine. In order to investigate the effect of time on the product distribution, 1-octanol was let to react under the same

conditions for 30 minutes only reaching 50% of conversion but with almost no effect in selectivity to the primary amine. This could confirm the fact that the latter is alkylated as soon as it forms.

From the obtained results, it was clear that primary amines could not be obtained easily from monoalcohols using this catalytic system. For comparison, it was decided to test biobased diols, namely isosorbide and 1,4-butanediol, in the amination with ammonia with the same catalytic set up. While isosorbide didn't react under this conditions, 1,4-butanediol was almost quantitatively converted into the product 3-(pyrrolidin-1-yl)propanol (Scheme 3.5). Even though the obtained product was not the desired one, namely the corresponding primary diamine, N-substituted pyrrolidines are a class of valuable intermediates and solvents.
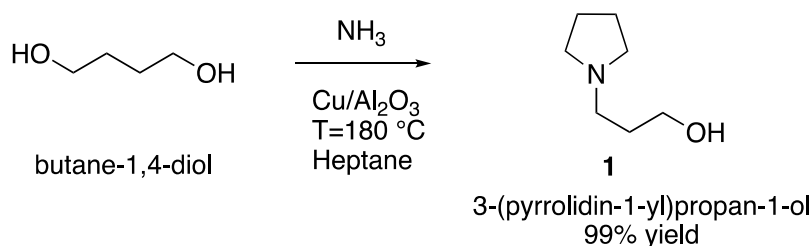
Scheme 3.5. Amination of 1,4-butanediol with ammonia using copper catalyst.

Therefore, considering the interesting result obtained, a deep investigation on the catalytic synthesis of N-substituted N-heterocycles starting from biobased molecules was carried out. The main results obtained are described in the following section.

3.2 Synthesis of N-alkylpyrrolidinones with Cu catalyst

Herein, we wish to report that heterogeneous copper catalyst can promote lactamization of GVL and other bioderived lactones with butylamine under mild reaction conditions (scheme 3.6). Using this methodology, it is possible to obtain N-alkylated pyrrolidinones and pyrrolidines, that are important class of molecules: the formers can be used as green solvents substitutes, while the latter class can be used as drug synthesis scaffolds.

3.2.1 N-containg Green Solvents: N-alkylpyrrolidinones

One of the main objectives and challenges presented by green chemistry is to reduce or replace the use of hazardous substances and processes. In particular, solvents are substances involved ubiquitously in the chemical industry with a broad range of applications. In recent times, solvent emissions or usage of harmful chemical substances has been limited by environmental legislation [17]. As a consequence, the academic and industrial field has grown the interest into find green alternatives or technologies to replace toxic, non-renewable solvents. In this regards, bio-derived substances obtained from renewable biomass feedstock could be an excellent alternative.

N-Methylpyrrolidinone (NMP) is a polar aprotic solvent extensively used in pharmaceutical and chemical industrial processes and formulations. However, it is reported in the candidate list of substances of very high concern due to its toxicity and reprotoxicity [18,19], therefore, its replacement is highly desirable [20,21].

Several alternative solvents have been proposed as renewable, biobased substitutes of NMP, in particular, γ-valerolactone (GVL) [22,23] and dihydrolevoglucosenone, with the trademark of Cyrene® [24,25] could be a sustainable and less harmful substitutes. Besides, N-butylpyrrolidinone (NBP) has showed to be non-reprotoxic, non-mutagenic and biodegradable and, therefore, could be a promising candidate [26]. In fact, it has been employed successfully in organic [27,28], solid phase peptide synthesis [29] and polymers synthesis [30].

N-alkyl-5-methyl-2-pyrrolidinones (NAMP) are also remarkably attractive to be used as industrial solvents due to their similarities to NMP and NBP. These compounds can be synthetized through reductive amination of levulinic acid (LA), ethyl levulinate (EL) or GVL using mostly noble metal based heterogeneous catalysts.

NAMP synthesis from levulinates

LA is a suitable substrate for the production of pyrrolidinones. In particular, it can be aminated with ammonia to produce 5-methyl-2-pyrrolidinones with yields higher than 95% by using Pd/C catalyst [31]. Furthermore, a similar catalytic system with low metal content was used to produce the same product using LA and ammonium formate as a source of hydrogen and nitrogen [32]. Reductive amination of LA with different amines can be achieved using cellulose-derived carbon supported Pt nano-catalyst in mild conditions (T = 30 °C, PH_2 = 1 atm) obtaining yield from 84% to 100% [33]. Another evidence found in the literature is the synthesis of various N-alkyl pyrrolidinones starting from LA using Pt nanoparticles catalyst supported on TiO_2 nanosheets achieving yields up to 89% at T = 25 °C and PH_2 = 1 atm [34]. Similarly, AuPd alloy nanoparticles demonstrated their efficacy in catalyzing the reductive amination of EL with different aliphatic amines obtaining a yield in isolated product >90% [35].

The aforementioned examples are related to the use of noble metal catalysts. Nonetheless there are only few reported cases in the literature relying on non-noble metal catalytic processes, in particular, copper catalysts. A non-conventional $CuPr/Al_2O_3$ prepared through incipient-wetness impregnation method was used to achieve the reductive amination of LA with various amines reaching up to 94% yield at T = 175 °C and PH_2 = 50 atm [36]. A 90% yield of pyrrolidinone products can be achieved using 5% Cu/H-ZSM-5 prepared with the wet impregnation method in the reductive amination of LA with different amines using also NH_3-BH_3 as the reducing agent [37].

3.2.2 Pyrrolidine: a useful scaffold in medicinal chemistry

 Pyrrolidine ring is one of the most used nitrogen-containing heterocycles used in medicinal chemistry field to obtain compounds for the treatment of human diseases. Pyrrolidine appears to be a ubiquitous and versatile scaffold found in molecules that exhibit a wide variety of biological activities. Particularly, they are useful to synthetize compounds

that have anti-cancer, anti-microbial properties and are active for the treatment of metabolic diseases [38]. It is also found in many other pharmaceuticals such as procyclidine and bepridil [39].

As already shown in the previous section, the combination of a reductive amination of levulinic acid is a convenient approach to synthetize pyrrolidinones and pyrrolidines, with a subsequent deoxygenation step. However, while significant efforts have been made for the synthesis of N-substituted methyl-2-pyrrolidinones in the presence of H_2 or as reducing agent by the reductive amination of LA, the production of N-substituted pyrrolidines have been hardly addressed. In the literature, few examples reporting the synthesis of pyrrolidine starting from LA can be found and they mainly relying on homogeneous catalysis. Moreover, these studies are focused on the switchable synthesis of pyrrolidines and pyrrolidinones. For instance, Sakai and co-workers proposed a direct switch from lactam synthesis to pyrrolidines changing the catalyst from $In(OAc)_3$ to InI_3. This approach was allowed by the reduction of the lactam using the indium/silane pair. The reason was found in the stronger Lewis acidity of InI_3 than the one of $In(OAc)_3$. This results in an over-reduction of the lactam to give N-substituted pyrrolidines [40]. $AlCl_3$ and $RuCl_3$ can be effectively used in the reductive amination of levulinic acid using phenylsilane to selectively synthetize pyrrolidinones or pyrrolidines under mild conditions. In fact, using $AlCl_3$ as the catalyst, pyrrolidinones were obtained with complete selectivity at room temperature, while the use of $RuCl_3$ as the catalyst allowed one to selectively obtain pyrrolidines in high yields at 45 °C [41].

Another example was the use of iron catalysts for the synthesis of N-substituted pyrrolidinones and pyrrolidines starting from levulinic acid and esters and a variety of amines *via* reductive amination using phenylsilane as the reducing agent. Particularly, by changing two diverse N-heterocyclic carbene iron complexes allowed to obtain selectively to a single derivative: pyrrolidinones or pyrrolidines [39].

Conversely to its precursor LA, GVL is more prone to react with heterogeneous non-noble metal catalysts [42]. In fact, its physico-chemical properties make it a stable but at the same time a reactive compound, therefore, it can be a suitable starting material to synthetize a wide variety of chemicals. Besides, lactamization of lactones with amine is an appropriate way to produce lactams. Nevertheless, there are only few examples of homogeneous catalysts in the literature.

3.2.3 Results and discussion

The effectiveness of supported copper catalysts in reactions that entail carbonyl group activation and amination was already demonstrated in previous works. Thus, it has already been reported the efficacy of supported copper catalysts in reactions involving carbonyl group activation [43–45] and amine-coupling. In particular, Cu/Al_2O_3 resulted to enable the synthesis of amines starting from ketones [2] and alcohols [1].

Considering these achievements, the amination of γ-valerolactone with butylamine to obtain N-butyl-5-methylpyrrolidinone (NBPO) as the main product was studied in the present thesis using the same class of materials (Scheme 3.6). In particular, copper was initially deposited on three different supports: one amphoteric, namely hydroxyapatite (HAP), one acidic, namely SiO_2-Al_2O_3 and one moderately acidic, namely SiO_2. See appendix section 6.4 for the textural properties of the supports.
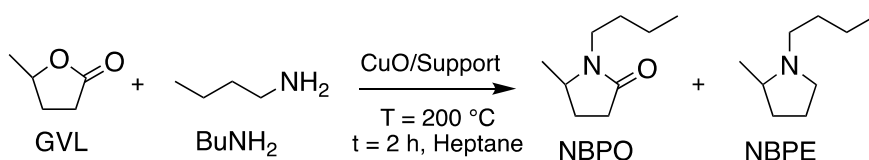
Scheme 3.6. Lactamization of GVL with butylamine using supported copper catalysts.

3.2.4 Characterization of the catalysts

Copper was deposited using the Chemisorption-Hydrolysis method. The textural properties (SSA and PV) and the copper loading determined by Inductively Coupled Plasma Optical Emission Spectroscopy (ICP-OES) analyses are showed in table 3.3. The copper content of the materials is slightly different among the samples. This was expected because catalysts were prepared to reach at least 8% wt/wt of Cu content in the solids with a procedure optimized for SiO_2 support.

Table 3.3 Textural properties (1st and 2nd column) and copper content (3rd column) of the copper catalysts

	SSA (m²/g)	PV (cm³/g)	% Cu (ICP-OES)
CuO/HAP	77	0.72	10
CuO/SiO$_2$	271	1.23	8
CuO/SiO$_2$ – Al$_2$O$_3$	302	0.57	11
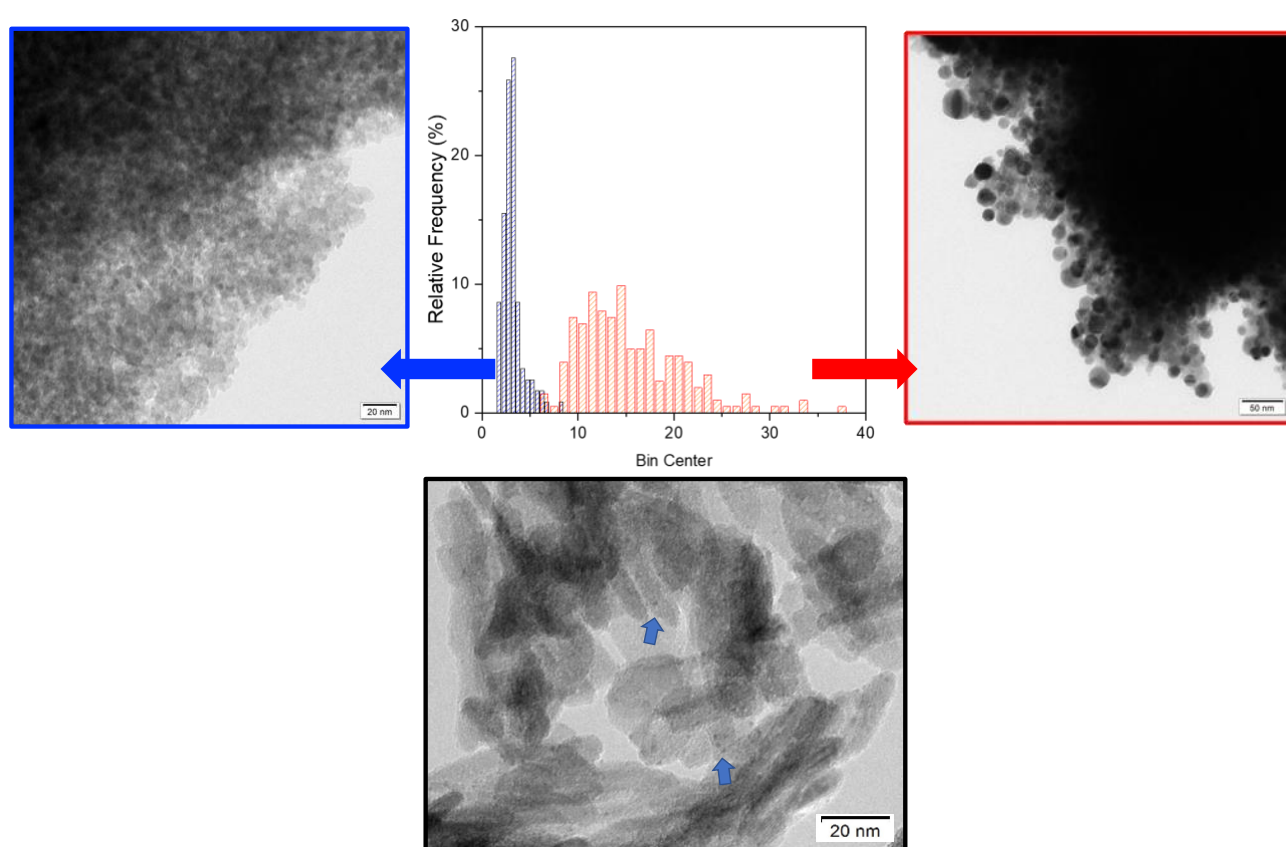
Figure 3.1. TEM images of Top: CuO/SiO$_2$-Al$_2$O$_3$ sample with relative particle size distribution. Bottom: CuO/HAP sample.

To have an outlook of the copper morphology TEM micrograph of the samples were acquired. Surprisingly, CuO/SiO$_2$-Al$_2$O$_3$ (figure 3.1, top) showed a bimodal Cu nanoparticle size distribution: on the same sample the micrographs enlightened the presence of two different particle populations: one between 1.7 and 6 nm with a mean value of 3.2 nm and another one with a really broader distribution of larger size, between 9 to 25 nm. Moreover, larger nanoparticles of 30 nm up to 70 nm size were also identified. On the other hand, CuO/HAP (figure 3.1, bottom) presented a very different nanoparticle morphology: the nanoparticles were much smaller (mean value 2-3 nm) and very well dispersed. A similar situation was found for CuO/SiO$_2$ as enlighten by STEM micrographs which showed the presence of highly dispersed small Cu nanoparticles of mean size value of 2.4 nm [46].

Successively, a characterization work focused on the copper phase and acidity properties of the materials was carried out. To investigate the coordination environment of the copper species on the catalysts surfaces, UV–vis Diffuse Reflectance (UV-DR) spectra were recorded in the 200–1200 cm^{-1} range. Due to their enlargement, absorption bands

were deconvoluted to understand the different speciation contributions and the spectra and the deconvolution results are shown in figure 3.2.
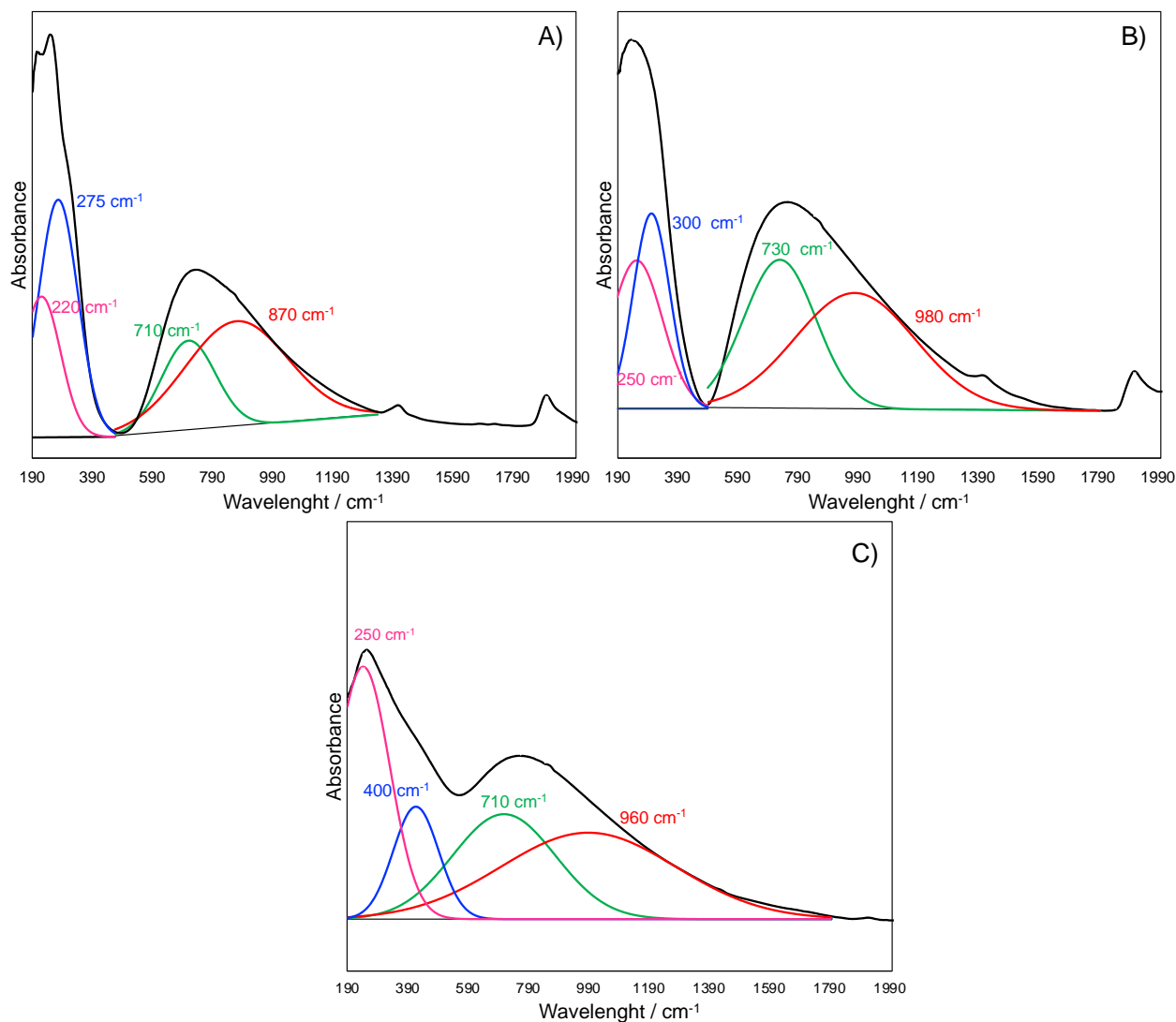
Figure 3.2. UV-DR spectra of the A) CuO/SiO$_2$, B) CuO/ SiO$_2$-Al$_2$O$_3$ and C) CuO/HAP catalysts.

The UV-DR spectra of the samples presented mainly two absorption bands one with a peak around 270 cm^{-1} and one broader in the range 600-1400 cm^{-1}. According to the literature, the band at around 270 cm^{-1} can be ascribed to the ligand-to-metal charge-transfer (Cu^{2+} ← O^{2-}) [47]. If a deconvolution of the bands is performed, some other contribution bands can be acknowledged. In the case of the CuO/SiO$_2$, it can be observed a small band at 220 cm^{-1} that could be ascribed to the presence of some Cu$^+$ [48]. It is also noticeable, in the case of CuO/HAP, a contribution band at 403 cm^{-1} that indicates the presence of Cu$^+$ in three dimensional clusters in the CuO matrix [47,49]. The presence of Cu$^+$ could be ascribable to the electron-rich environment produced by the phosphate groups

that could partially cause the reduction of the Cu^{2+}. The large absorption band from 600 to 1400 cm^{-1} is assigned to d-d ($2E_g \rightarrow 2T_{2g}$) transitions of Cu^{2+} located in more or less tetragonally distorted octahedral environment with an distorted O_h symmetry. Moreover, this band is shifted to lower wavelength with a more distorted symmetry [47,50]. As observable, the band presents two components at different wavelengths if we compare the catalysts. In the case of CuO/SiO_2 the bands are at lower wavenumbers meaning that the CuO presents a quite distorted symmetry with a contribution of square pyramid valency (870 cm^{-1}) [47]. On the other hand, the other two sample display a higher contribution at wavelengths >950 cm^{-1} suggesting an increase in crystallinity and the formation of bulk CuO, that it is also in agreement with a higher Cu loading shown by the samples. In any case, both CuO/SiO_2 and CuO/SiO_2-Al_2O_3 present a shoulder at 1400 cm^{-1} typical of the tetrahedral symmetry.

Copper reducibility was investigated by Temperature Programmed Reduction (TPR) to have more information about the copper phase morphology and its reducibility and the profiles are showed in figure 3.3. The three materials presented a remarkably different reduction behavior. The CuO/SiO_2 catalysts presents a sharp peak centered at around 242 °C that can be ascribed to the reduction of a well dispersed and highly uniform single CuO phase into Cu(0) that was already observed in the case of copper catalysts prepared with the CH method [51].
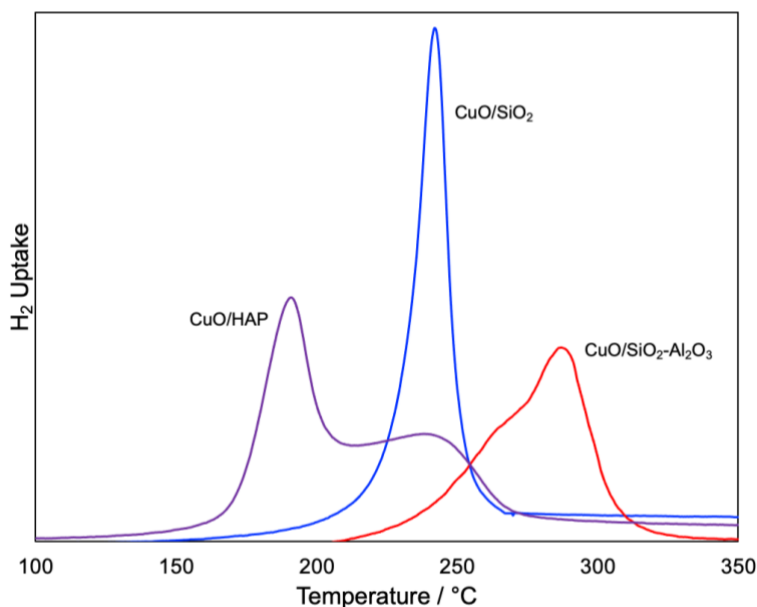
Figure 3.3. TPR profiles of the catalysts.

On the other hand, CuO/SiO_2-Al_2O_3 sample presents a broader peak centered at around 287 °C with a shoulder at around 267 °C, indicating a copper phase less prone to be reduced. This reduction profile, was coherent with the bimodal size distribution found

through TEM analysis: the two reduction events could be ascribed to the two different particle size population. This was also in accordance with previous work results showing that on $CuO/SiO_2-Al_2O_3$ prepared with CH method, Cu isolated ions likely belonging to a surface Cu-aluminate-like phase and strongly resistant to reduction were observed, while on SiO_2 small and well dispersed CuO particles were formed [53]. In fact, an explanation of the higher reduction temperature values could be due to the electron withdrawing capacity of aluminum that hampers the copper reduction. An even different situation was found for the CuO/HAP sample: the reduction profile presents one broad peak centered at 192 °C with one shoulder at around 250 °C once again diagnostic of the presence of two well dispersed copper species [54]. The lower reduction temperature peak could be ascribable to the presence of Cu^+ clusters in the CuO matrix that was also detected in the UV DRs spectrum. In both CuO/HAP and $CuO/SiO_2-Al_2O_3$ cases, this phenomenon could be due to a strong interaction between the copper species and the supports [53].

To understand the surface acidic features of the samples, two different characterization techniques has been utilized, in particular, FT-IR after pyridine adsorption and solid-liquid acid-base titration using phenylethylamine (PEA) as basic probe molecule (see experimental section 5.4.6).

Liquid-solid acid-base titration of the samples using PEA as probe molecule. Were carried out to have a clue of the *effective* acidity in the reaction solvents, namely *n*-heptane performing two titration runs. The first run quantifies the total amount of acid sites saturating the surface with PEA; the second run gives account to the weak acid sites obtained with a new titration after desorption of physisorbed PEA. The difference in adsorbed PEA between the two runs is therefore related to the number of strong acid sites (see 5.4.6 section). The quantification of the acidic sites normalized for the mass and the area of the samples is shown in table 3.5 and the Langmuir linearization of the strong sites in figure 3.4 See appendix section 6.8 for a detailed explanation of data curing. Interestingly, the strength of the acidic sites of the samples was quite different: the 82% of the acidic sites density of $CuO/SiO_2-Al_2O_3$ are strong acid sites while CuO/SiO_2 and CuO/HAP presents only 62%. Moreover, if the strong acid sites are normalized according to the mass of the sample (figure 3.4) we obtain an acidity strength ranking $CuO/SiO_2-Al_2O_3$ > CuO/SiO_2 > CuO/HAP.

Table 3.5 Total sites quantification normalized for the mass (1st column) and for the surface area (2nd column) for the copper catalysts.

	Total Acidic Sites Density $\mu mol_{PEA}/m^2$	*Strong Acidic Sites Density* $\mu mol_{PEA}/m^2$
CuO/SiO$_2$	1.6 ± 0.3	0.98 ± 0.27
CuO/SiO$_2$ - Al$_2$O$_3$	2.8 ± 0.1	2.33 ± 0.11
CuO/HAP	2.9 ± 0.1	1.81 ± 0.03
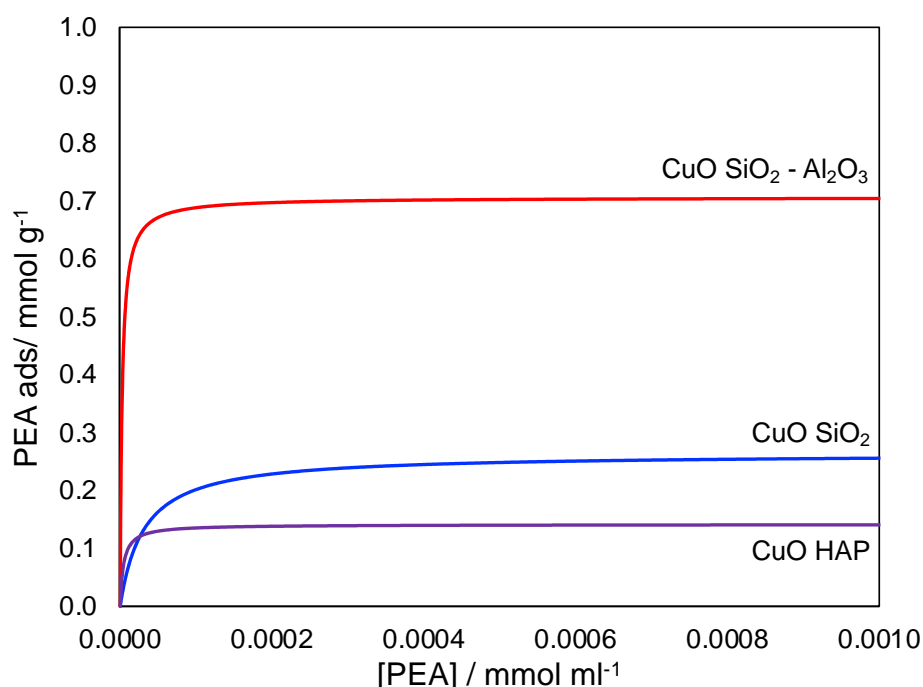
Figure 3.4. Adsorption isotherms (modeled through Langmuir linearization) of strong acid sites of the copper catalysts obtained performing liquid-solid titration usin PEA as probe molecule (T=30 °C)

FT-IR after pyridine adsorption is useful to discriminate the nature of the acidic sites, namely Brønsted and Lewis ones, and to quantify them according to the different diagnostic absorption bands of each site. Bands around 1450 cm^{-1} and 1610 cm^{-1} can be ascribed to pyridine bounded to Lewis acid sites, while absorption at 1550 cm^{-1} together with peaks near 1620 cm^{-1} and 1640 cm^{-1} are related to the presence of Brønsted acid sites [55].

CuO/HAP presented some issue during the experiment of pyridine adsorption. In fact, HAP materials presents a high surface concentration of CO$_3^{2-}$ which absorbs in the 1600-

1400 cm^{-1} region [56], the same of the pyridine adsorbed on the acidic sites present onto a solid surface (see figure S22 for the spectra). To overcome this problem, CuO/HAP was dispersed with a non-acidic matrix such as pyrogenic SiO_2, to limit the signal carbonates absorption band (see experimental section 5.4.7 for the procedure and figure 2.6 for the spectrum of SiO_2 A). The FT-IR spectra after pyridine adsorption of the catalysts are shown in figure 3.5.
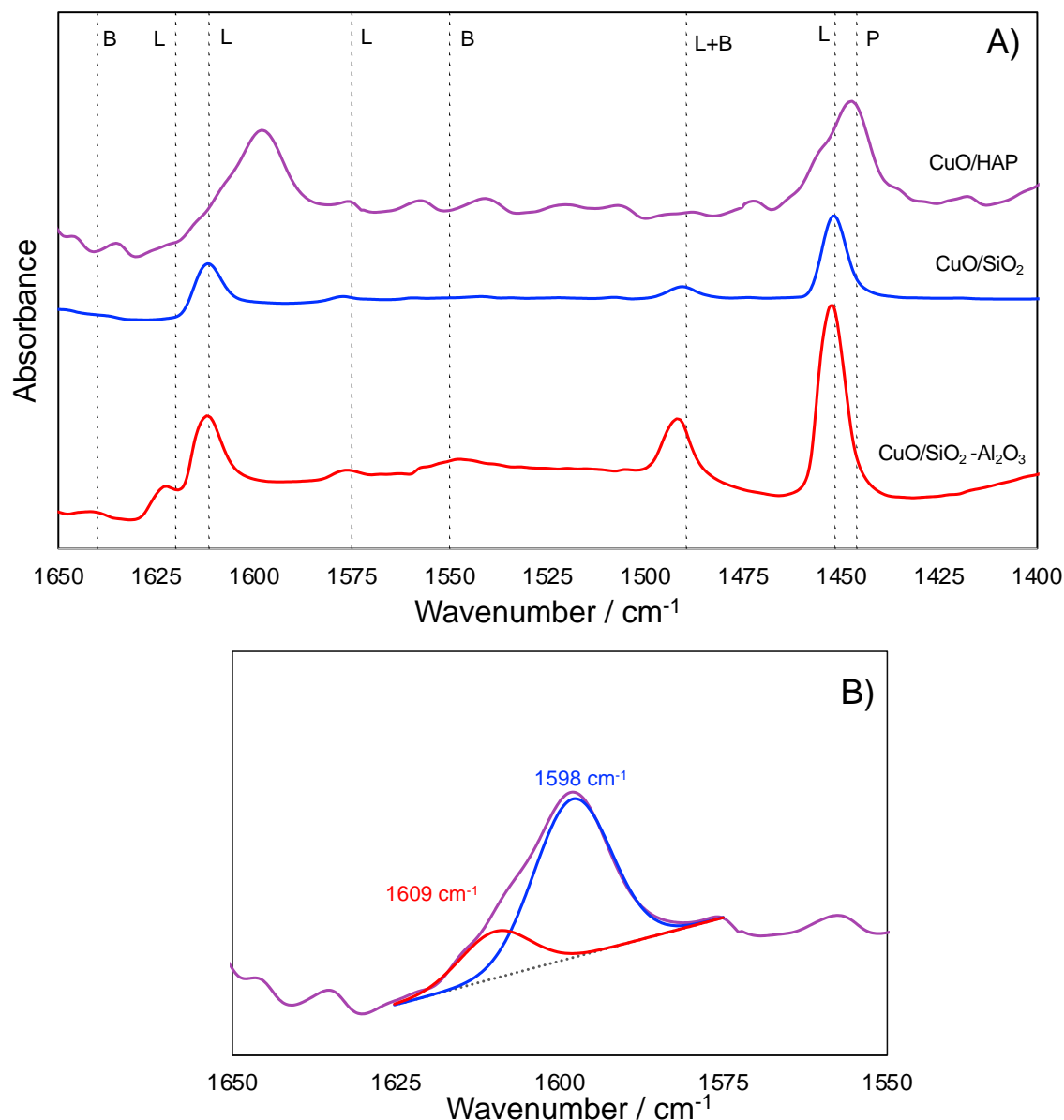
Figure 3.5. A) FT-IR spectra after pyridine adsorption of the solid catalysts. B) Magnification if the deconvoluted Lewis peak of CuO/HAP sample.

As observable, the samples show the presence of Lewis acidic sites as expected from the copper catalysts prepared with the CH method [51]. Brønsted sites that are typical of HAP and SiO_2-Al_2O_3 are no longer present or just in negligible amounts in the case of

CuO/SiO$_2$-Al$_2$O$_3$. Interestingly, CuO/SiO$_2$-Al$_2$O$_3$ and CuO/HAP, after deconvolution, presents two contributions in the 1610 cm^{-1} region. This could be ascribable to the presence of two different Lewis sites center, namely Al and Cu in the case of CuO/SiO$_2$-Al$_2$O$_3$ and Ca and Cu for CuO/HAP. Similarly, it was observed by Zaccheria *et al.* in the spectra of SiO$_2$-Al$_2$O$_3$ and CuO/SiO$_2$-Al$_2$O$_3$: the support presented a Lewis band at 1623 cm^{-1} ascribable to Al^{3+} while the copper catalyst presented not only the same band but also a band at 1610 cm^{-1} ascribable to Cu centers [57]. According to the quantification method proposed by Emeis [55], the integration of the characteristic Lewis band is normalized for the mass of the sample disk. Notably, CuO/SiO$_2$-Al$_2$O$_3$ presented the highest number of acidic sites followed by CuO/HAP and CuO/SiO$_2$ (table 3.4, first column). However, if the density is considered (table 3.4, second column), namely normalized for the area of the materials, CuO/HAP presented consistently higher acidic sites quantity on the surface compared to the other samples. This is due to the presence of many functional groups exposed on a considerably low surface area (see appendix section 6.2). However, it is possible to observe a shift to lower wavelength of the Lewis band from 1611 cm^{-1} to 1609 cm^{-1} and 1595 cm^{-1} for CuO/SiO$_2$-Al$_2$O$_3$, CuO/SiO$_2$, and CuO/HAP respectively. This could be an indication for the strength of the acidic sites: a lower wavelength is associated with a lower strength of the site [57,58]. This is in agreement with the strong acid sites quantification ranking obtained from titration with PEA.

Table 3.4. Quantification of Lewis acidic sites of the samples according to Emeis method at outgassing temperature of pyridine of 150 °C [55].

Sample	Adsorbed pyridine $mmol_{py} \, g_{cat}^{-1}$	Adsorbed pyridine $\mu mol_{py}/m^2$
CuO/SiO$_2$	0.047	0.18
CuO/SiO$_2$-Al$_2$O$_3$	0.119	0.39
CuO/HAP	0.088	1.13

3.2.5 Catalytic test and discussion

After the characterization of the morphological and acidic properties, the catalysts were tested in the lactamization of GVL with butylamine. The reaction conditions were optimized and they were found to be T=200 °C, $P(H_2)$ = 10 bar and GVL:BuNH$_2$ molar ratio of 1:1. The materials were tested up to 6 h of reaction when the conversion and yield of the products reached a plateau. In fact, carrying out the reaction for longer time (up to 24 h) did not significantly improve the catalytic performances. Again, the reactions were performed under a hydrogen atmosphere to prevent catalysts poisoning, as deeply explained in section 3.1. Notably, if the reaction is performed under N$_2$ atmosphere with no H$_2$, the conversion of GVL was almost 0. The results of the catalytic tests are shown in figure 3.6. As observable, the materials showed different performances in terms of activity and selectivity: CuO/HAP was found to be the most active catalyst with the highest selectivity towards the green solvent NBPO, reaching a conversion of 77% of GVL and a yield of NBPO of about 50%.
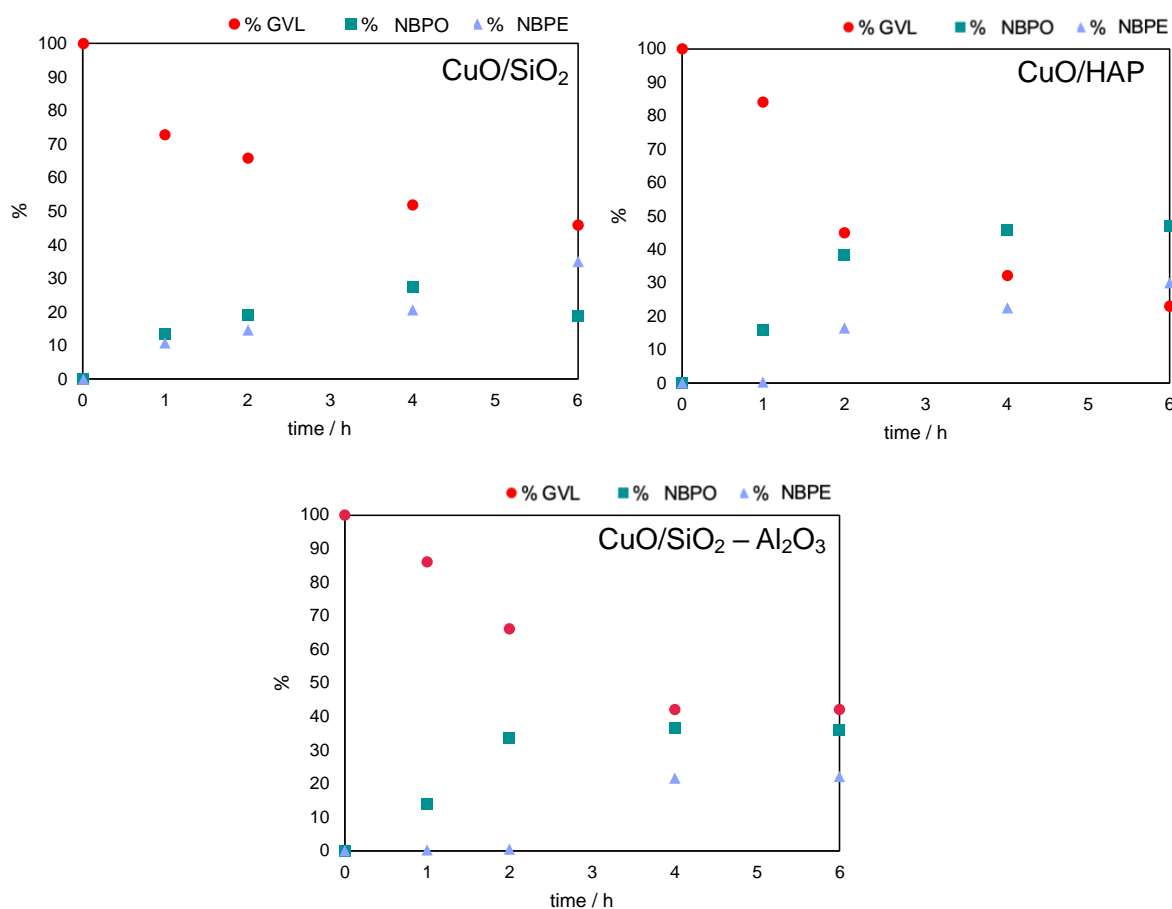
Figure 3.6. Catalytic tests performed with the copper catalysts. Reaction conditions: T=200°C, $P(H_2)$ = 10 bar.

To the best of our knowledge, in the literature, there are no evidences of heterogeneously catalyzed lactamization of GVL with amines. Moreover, as deeply explained in the section 3.2.1, when N-substituted pyrrolidinones are prepared starting from LA harsh conditions [31,36], precious noble or toxic metal catalysts [59–61] or auxiliaries [37] are required to achieve high yields in the desired product. Some instances of homogeneous catalyzed lactamization of various lactones could be found as in the case of an Ir complex [62] or a Zn based catalyst for the reaction of GVL with different amines [63].

The reasons of the different catalytic activity of the materials could be searched in the surface properties. In particular, the role of Lewis acid sites is pivotal in promoting both activity and selectivity in the hydrogenation of carbonyl compounds [43–45]. Thus, they can coordinate with the Lewis basic C=O group *via* one of the oxygen lone pairs, activating the GVL to the amine nucleophilic attack (figure 3.7). This could be enhanced also by an appropriate morphology of the copper phase.
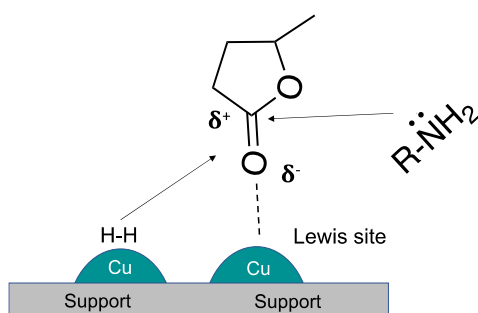
Figure 3.7. GVL carbonyl group activation of the copper Lewis sites.

CuO/HAP and CuO/SiO$_2$-Al$_2$O$_3$ had shown to be markedly acidic when analyzed both in-vacuum after pyridine adsorption and in solvent with PEA titration with the contribution of both Ca^{2+} and Cu^{2+} and Al^{3+} and Cu^{2+} in imparting Lewis acidity respectively. These elements ensure high catalytic activity: a proper amount of acidity is fundamental int activating the C=O group of GVL towards the nucleophilic attack of the amine. However, CuO/HAP presented weaker acidic sites compared to CuO/SiO$_2$-Al$_2$O$_3$. In this respect, it can be hypothesized that a weaker acidity of the copper sites could prevent a strong amine-copper adsorption, responsible for the formation of nitride species that poison the catalytic active sites (see section 3.1.1). A clue can be found in a faster deactivation of the CuO/SiO$_2$-Al$_2$O$_3$ catalysts, reaching a plateau in conversion just after 4 hours of reaction. Besides, the presence of smaller and well dispersed Cu nanoparticles present on CuO/HAP could be the reason for its higher activity.

Meanwhile, CuO/SiO$_2$ presented a lower acidic sites density according to both the characterization techniques. In this case, this could be detrimental for the catalytic activity of the material. Nevertheless, despite being the less active material, CuO/SiO$_2$ was the most selective towards product NBPE namely the deoxygenated one. This result was not unexpected: the efficacy of silica supported copper catalyst in the deoxygenation of aromatic ketones was demonstrated in a previous work [64]. The fine tuning of copper morphology has shown to be a pivotal tool in achieving high conversion of the substrates and selectivity toward a desired product [65] (See chapter 2). In fact, despite the fact that unreduced catalysts were used in the reaction, the high selectivity of CuO/SiO$_2$ towards the deoxygenated product could be ascribed to the presence on lone Cu Lewis sites centers that are more prone also to be reduced from Cu(II) to Cu(0) *in situ* by the reaction hydrogen atmosphere and, due to the Cu(0) nature, have an higher hydrogenating power. This was confirmed by the TPR qualitative profile of the samples: CuO/SiO$_2$ presents a single and very sharp peak ascribed to the reduction of a well dispersed and highly uniform CuO phase into Cu(0). Conversely, the other two samples present broader peaks with shoulders indicating the presence of diverse copper species making the *in situ* reduction more complex.

With the aim to furtherly reduce the impact of the reaction conditions and study the effect of hydrogen pressure on the selectivity, the catalytic tests were performed lowering the hydrogen pressure from 10 bar to 1 bar (figure 3.8).

It is readily observable that all the samples show a dramatic increase in selectivity to the product NBPO while also keeping good conversion performances. Once again, the best performances in terms of yield in product NBPO was the CuO/HAP catalyst. It can be hypothesized that 1 bar of hydrogen pressure is not sufficient to enable the deoxygenation of the product NBPO to product NBPE but it is enough to preserve the copper phase activity necessary for the lactamization reaction. This allows one to raise the yield towards the desired pyrrolidinone product making the process really convenient in terms of product recovery.
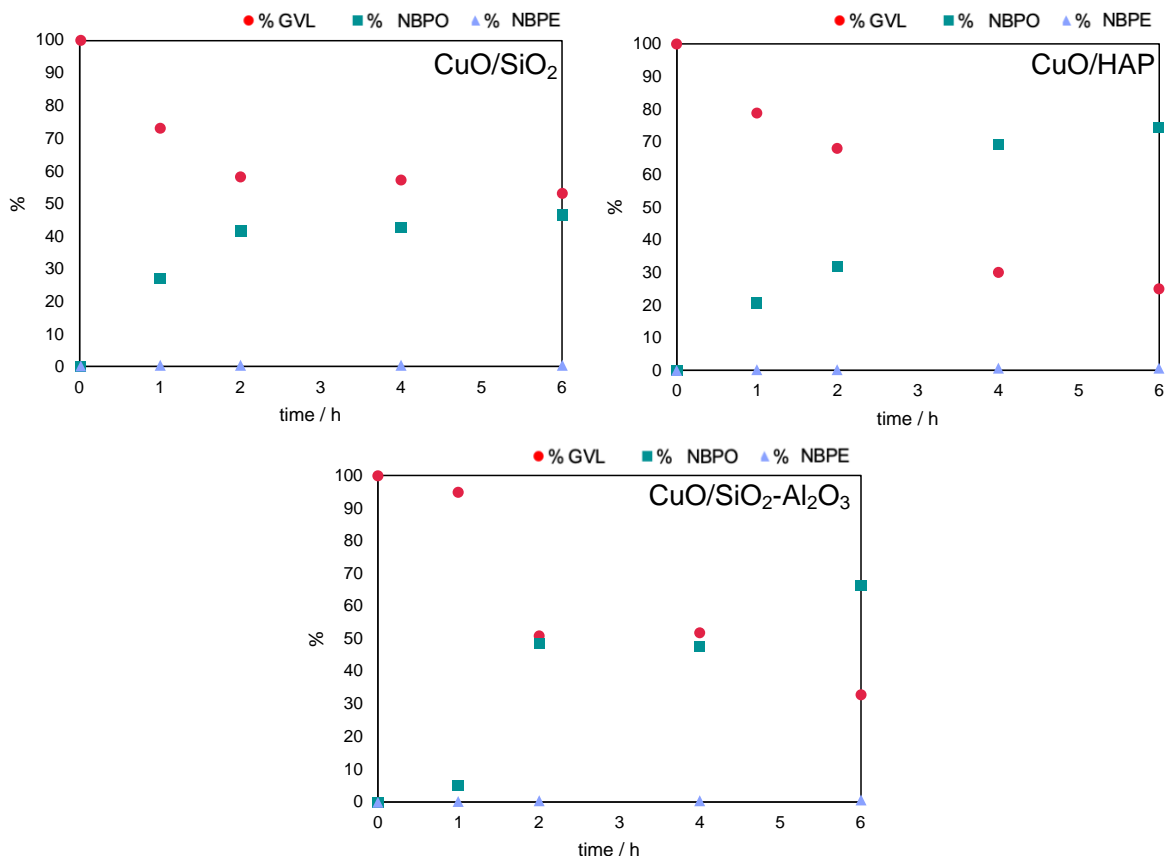
Figure 3.8. Catalytic tests performed with the copper catalysts. Reaction conditions: T=200°C, $P(H_2)$ = 1 bar.

3.2.6 Comparison with other materials

Considering the catalytic tests results, it can be observed that a milder acidic support with low acid strength was the key to achieve higher catalytic activity and selectivity even at low hydrogen pressures. For the sake of comparison and catalytic processes performances improvement other amphoteric supports were chosen to prepare another series of Cu catalyst. In the first place, two different aluminas (Al_2O_3 A, Al_2O_3 B), ZrO_2 and TiO_2, were selected for their properties [66–68] (see appendix section 6.2) for the preparation of the corresponding copper 8 wt% catalysts utilizing the CH method [51]. The textural properties, namely SSA and PV, of the prepared catalysts are listed in table 3.6.

Table 3.6. Textural properties of the catalysts.

	SSA (m^2/g)	PV (cm^3/g)
CuO/Al$_2$O$_3$ A	118	0.46
CuO/Al$_2$O$_3$ B	283	0.46
CuO/TiO$_2$	60	0.38
CuO/ZrO$_2$	286	0.27

Successively, the four materials were tested in the reaction and compared at 2 hours of time. Results of the catalytic tests are shown in the figure 3.9.A). The best material in terms of performances was found to be CuO/Al$_2$O$_3$ B achieving 72% conversion of GVL with a selectivity towards product NBPO of 75%, higher if compared to the 55% of conversion and 70% of selectivity obtained with CuO/HAP. Again, NBPE was the main byproduct detected.
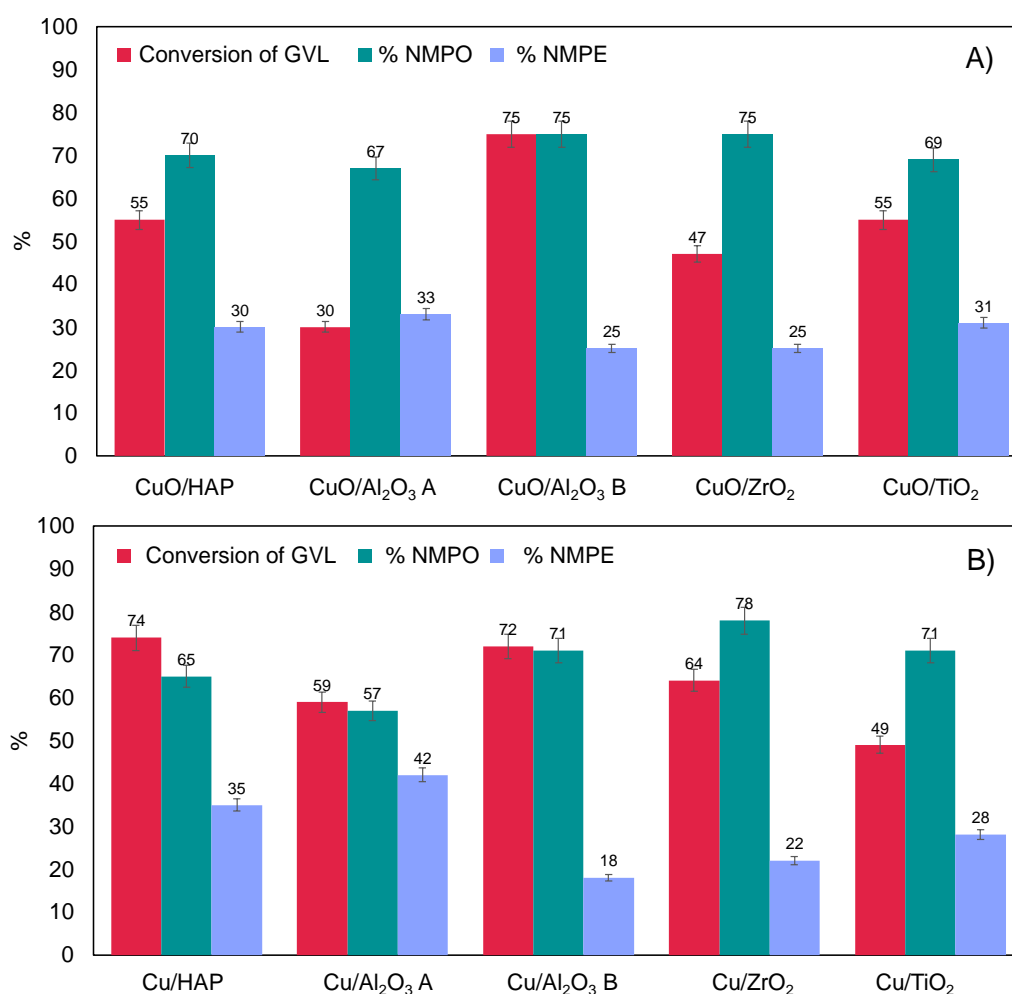
Figure 3.9. Catalytic tests performed with A) the fresh calcined and B) the pre-reduced catalysts. Reaction conditions were the same: T=200°C, P(H$_2$) = 10 bar, t = 2h.

Subsequently to preliminarily optimize the reaction conditions optimization, the investigation of other different variables was performed. Therefore, the catalysts were tested performing a reduction pre-treatment and the results are displayed in figure 3.9.B).

Interestingly, Cu/Al$_2$O$_3$ B was again the best catalyst but the catalytic performance of the pre-reduced catalyst (Conversion = 72% and molar % 1= 71% in 2h) was very similar to the fresh calcined catalyst. However, under these conditions, Cu/HAP showed excellent catalytic performances too (Conversion = 74% and molar % 1= 65%). At the same time, the activity of the calcined Cu/TiO$_2$ decreased slightly from 55% to 49% in terms of conversion, while Cu/ZrO$_2$ and in particular Cu/Al$_2$O$_3$ A show a marked increase in performances.

These results are quite promising in terms of sustainability: in fact, using CuO/Al$_2$O$_3$ B as the catalyst we can still obtain good yield of the N-butyl-5-methylpyrrolidinone product, thus avoiding the high temperature and hydrogen consumption of the pre-treatment. It is noticeable that the activity of the catalysts prepared with the two different aluminas was quite diverse. Particularly, CuO/Al$_2$O$_3$ B, when used in the non-reduced form, was the most active and selective material. Furthermore, the reduction pre-treatment did not increase its catalytic performances. Conversely, CuO/Al$_2$O$_3$ A was the less active in the non-reduced form but, after the reduction pretreatment, it doubled the conversion and increased the selectivity towards product NBPE.

To investigate the reasons of the different activity some studies about the copper phase has been performed, in particular, using XRD and TEM characterization techniques. The presence of a monoclinic phase of CuO was detected in both the XRD patterns of CuO/Al$_2$O$_3$ A and CuO/Al$_2$O$_3$ B. Specifically, the CuO crystallite size was estimated to be around 7 nm in the case for the CuO/Al$_2$O$_3$ A sample (figure 3.10). On the contrary, the presence of smaller nanoparticle was suggested by the XRD signal on Al$_2$O$_3$ B but the wide peak broadening prevents a reliable crystallite size determination using the method used (see experimental section 5.4.12).
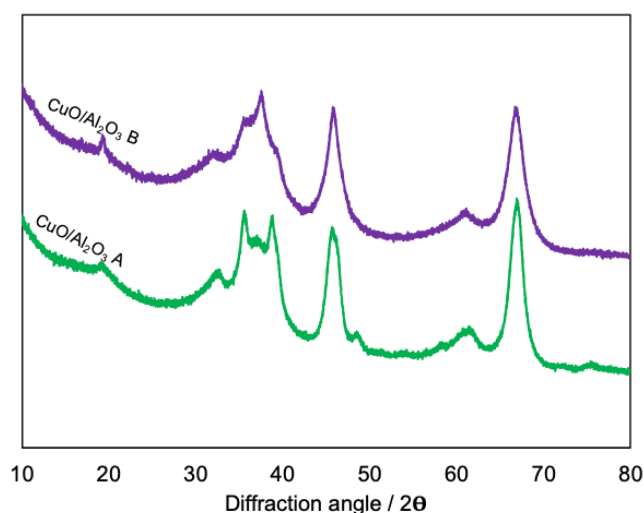
Figure 3.10. XRD patterns of the CuO/Al$_2$O$_3$ A and CuO/Al$_2$O$_3$ B catalysts.

Analogously, TEM measurements (figure 3.11) highlighted a similar morphology for the two CuO/Al$_2$O$_3$ A and B catalysts where a heterogeneous crystalline support morphology alternated roundish grain to acicular structures. Nevertheless, the CuO nanoparticles were different at nanoscale. On sample CuO/Al$_2$O$_3$ A nanoparticles with a mean size of 3.6 nm were detected, but with a broader distribution through a range of 1.5 to 6.5 nm. In fact, almost 50% of the particles are bigger than the mean size, and nanoparticles larger than 6 nm were found. Conversely, on sample CuO/Al$_2$O$_3$ B, smaller nanoparticles were in general detected, with a mean size of 2.8 nm and a narrower distribution where 72% of nanoparticles were smaller than 3 nm. In both cases no huge aggregates were detected.
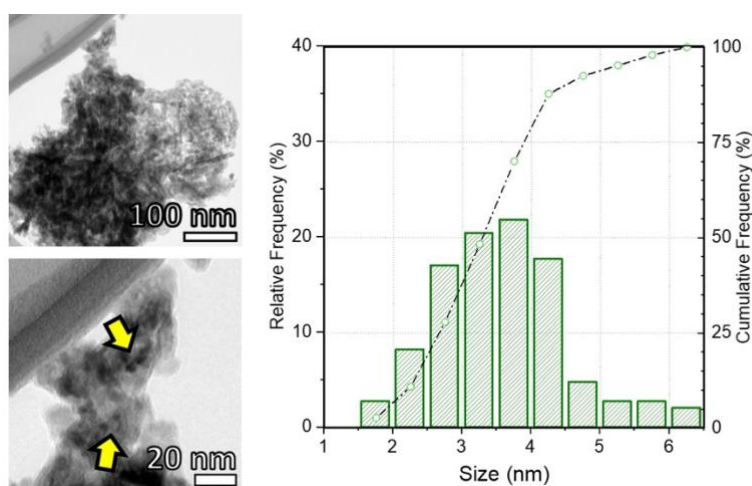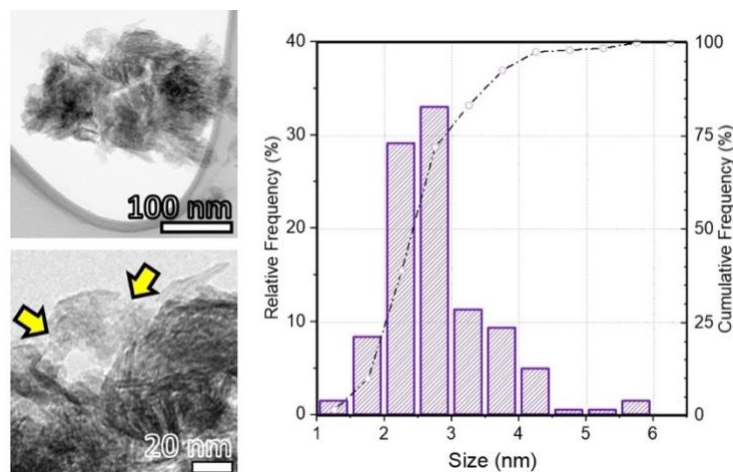
Figure 3.11. Representative TEM micrograph and related CuO nanoparticles size distribution of the CuO/Al$_2$O$_3$ A (Above) and CuO/Al$_2$O$_3$ B catalysts (Bottom). In the magnified images the arrows point out some nanoparticles.

Again, with the sustainability goal in mind, the catalytic tests were performed lowering the hydrogen pressure from 10 bar to 1 bar (figure 3.12) to see also how it affected the catalytic performances. Results were also compared to the ones achieved previously with CuO/HAP. As it can be noticed, the activity of the catalysts regarding GVL conversions slightly decreases for the CuO/Al$_2$O$_3$ B, CuO/ZrO$_2$ and CuO/TiO$_2$ catalysts but a total selectivity towards the product NBPO (> 99%) was achieved. Once again, despite a slight decrease in activity, these results were convenient in terms of selectivity, and in turn of product recovery.
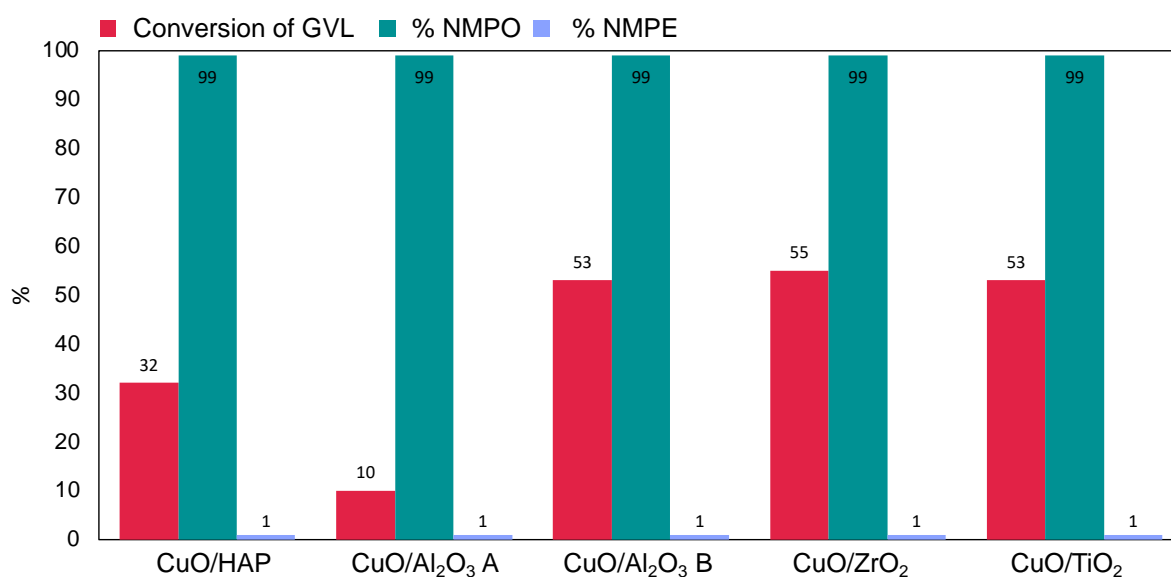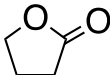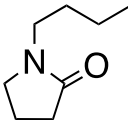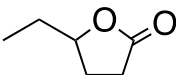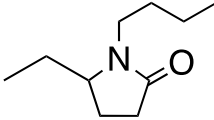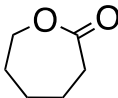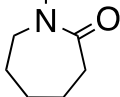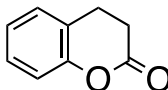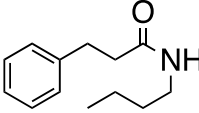

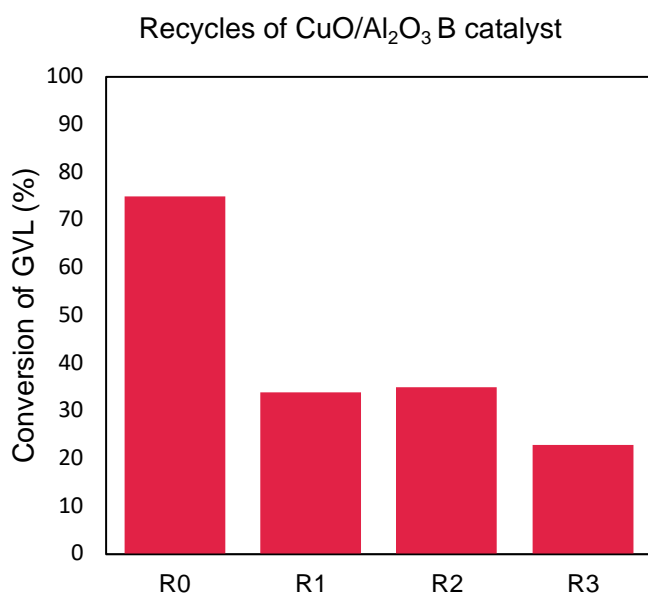**Figure 3.12.** Catalytic tests performed with the fresh calcined catalysts. Reaction conditions: T=200°C, P(H$_2$) = 1 bar, t = 2h.

A Quantitative Structure Toxicity Relationship (QSTR) analysis was performed in order to evaluate the potential health effects of NMP, of the mutagenicity and developmental effects. Neither developmental toxicity nor Ames mutagenicity was specified for N-butyl-5-methyl-pyrrolidinone by the Discovery Studio module TOPKAT which provides a probability value of toxicological outcomes of novel structures [69,70].

Considering the outstanding catalytic performances of the CuO/Al_2O_3 B system, the lactamization of other bioderived lactones such as γ-butyrolactone (GBL), γ-caprolactone (γ-CPL), ε-caprolactone (ε-CPL) and dihydrocoumarin (DHC) with butylamine under the same reaction conditions utilized for GVL was performed (table 3.7). From the results, the catalytic system showed to be appropriate for the lactamization of different lactone substrates, particularly, a conversion of 77% was achieved for the ε-CPL with total selectivity towards the ε-N-butyl-caprolactam (table 3.7, entry 3). This is a promising result: in fact, caprolactams are important platform molecules for the production of polymers such as nylon 6 and nylon 6.6 [71] and the synthesis of deep eutectic solvents [72].

Table 3.7. Lactamization of different lactones with and CuO/Al_2O_3 B catalyst. Reaction conditions: T = 200 °C, t = 2 h, $P(H_2)$=10 bar.

Entry	Substrate	Conversion (%)	Mol % product (%)	
1		56		65
2		62		23
3		77		100
4		>99		100

To test the catalyst reusability, recycle tests were conducted with CuO/Al_2O_3 B catalysts under the optimal reaction conditions using GVL and butylamine and the results are shown in figure 3.13. In between the recycle steps the reaction solution was removed

and the fresh solution was added to the reactor without any catalyst washing or treatment. After one cycle, the catalyst loses catalytic activity passing from 75% to 35% of conversion and it keeps constant for another step. After three recycle steps, the conversion was 15%. The reasons for the deactivation could be searched in the nitride formation on the copper surface explained in 3.1. section. In this case, hydrogen pressure introduced in the new step could be not enough to enable the catalyst regeneration and some permanent poisoning could occur.

Figure 3.13. Catalytic tests performed with the fresh calcined catalysts. Reaction conditions: T=200°C, $P(H_2)$ = 1 bar, t = 2h.

3.3 Conclusions

The synthesis of green N-alkylpyrrolidinone solvents and pyrrolidine scaffold were achieved using simple non-noble, supported copper catalysts with a facile protocol that avoids high energy and hydrogen consumption pre-treatment of the catalysts. These materials were prepared depositing copper on various materials with different acidic properties. A high dispersion with a low particle size together with a mild acidity, in particular a lower strength, of CuO/HAP and CuO/Al$_2$O$_3$ was the key to achieve high conversion of the GVL and selectivity towards the NMPO product respectively. Exogenous hydrogen was necessary to preserve the copper phase of the catalysts from deactivation, however, lowering the H$_2$ pressure from 10 to 1 bar totally diverted the selectivity to NMPO. Besides, modulation of the selectivity was also possible choosing the appropriate support material:

CuO/SiO$_2$ was the most selective towards the pyrrolidine product due to its high hydrogenating power and inclination to be reduced *in situ*.

The substrate scope was extended to the lactamization of other lactones, in particular, for the production of ε-N-butyl-caprolactame, suitable for the synthesis of polymers and deep eutectic solvents.

3.4 References

1. Santoro, F.; Psaro, R.; Ravasio, N.; Zaccheria, F. N-Alkylation of amines through hydrogen borrowing over a heterogeneous Cu catalyst. *RSC Adv.* **2014**, *4*, 2596–2600.

2. Santoro, F.; Psaro, R.; Ravasio, N.; Zaccheria, F. Reductive Amination of Ketones or Amination of Alcohols over Heterogeneous Cu Catalysts: Matching the Catalyst Support with the N-Alkylating Agent. *ChemCatChem* **2012**, *4*, 1249–1254.

3. Hameury, S.; Bensalem, H.; Vigier, K.D.O. Sustainable Amination of Bio-Based Alcohols by Hydrogen Borrowing Catalysis. *Catalysts* **2022**, *12*.

4. Yue, C.; Gu, L.; Zhang, Z.; Wei, X.; Yang, H. Nickel- and cobalt-based heterogeneous catalytic systems for selective primary amination of alcohol with ammonia. *Arab. J. Chem.* **2022**, *15*, 103865.

5. Wang, T.; Ibañez, J.; Wang, K.; Fang, L.; Sabbe, M.; Michel, C.; Paul, S.; Pera-Titus, M.; Sautet, P. Rational design of selective metal catalysts for alcohol amination with ammonia. *Nat. Catal.* **2019**, *2*, 773–779.

6. Kita, Y.; Kuwabara, M.; Yamadera, S.; Kamata, K. Effects of ruthenium hydride species on primary amine synthesis by direct amination of alcohols over a heterogeneous Ru catalyst. *Chem. Sci.* **2020**, 9884–9890.

7. Fu, X.P.; Han, P.; Wang, Y.Z.; Wang, S.; Yan, N. Insight into the roles of ammonia during direct alcohol amination over supported Ru catalysts. *J. Catal.* **2021**, *399*, 121–131.

8. Niemeier, J.; Engel, R. V.; Rose, M. Is water a suitable solvent for the catalytic amination of alcohols? *Green Chem.* **2017**, *19*, 2839–2845.

9. Ho, C.R.; Defalque, V.; Zheng, S.; Bell, A.T. Propanol Amination over Supported Nickel Catalysts: Reaction Mechanism and Role of the Support. *ACS Catal.* **2019**, *9*, 2931–2939.

10. Wang, B.; Ding, Y.; Lu, K.; Guan, Y.; Li, X.; Xu, H.; Wu, P. Host-guest chemistry immobilized nickel nanoparticles on zeolites as efficient catalysts for amination of 1-octanol. *J. Catal.* **2020**, *381*, 443–453.

11. Zhou, K.; Xie, R.; Xiao, M.; Guo, D.; Cai, Z.; Kang, S.; Xu, Y.; Wei, J. Direct Amination of Biomass-based Furfuryl Alcohol and 5-(Aminomethyl)-2-furanmethanol with NH3 over Hydrotalcite-derived Nickel Catalysts via the Hydrogen-borrowing Strategy. *ChemCatChem* **2021**, *13*, 2074–2085.

12. Yuan, H.; Kusema, B.T.; Yan, Z.; Streiff, S.; Shi, F. Highly selective synthesis of 2,5-

bis(aminomethyl)furan: Via catalytic amination of 5-(hydroxymethyl)furfural with NH3 over a bifunctional catalyst. *RSC Adv.* **2019**, *9*, 38877–38881.

13. Cai, X.; Ke, Y.; Wang, B.; Zeng, Y.; Chen, L.; Li, Y.; Bai, G.; Yan, X. Efficient catalytic amination of diols to diamines over Cu/ZnO/γ-Al2O3. *Mol. Catal.* **2021**, *508*, 111608.

14. Ruijten, D.; Narmon, T.; De Weer, H.; van der Zweep, R.; Poleunis, C.; Debecker, D.P.; Maes, B.U.W.; Sels, B.F. Hydrogen Borrowing: towards Aliphatic Tertiary Amines from Lignin Model Compounds Using a Supported Copper Catalyst. *ChemSusChem* **2022**.

15. Baiker, A. Catalytic Amination of Aliphatic Alcohols. The Role of Hydrogen as Inhibitor for Catalyst Deactivation. *Ind. Eng. Chem. Process Des. Dev.* **1981**, *20*, 615–618.

16. Kepp, K.P. A quantitative scale of oxophilicity and thiophilicity. *Inorg. Chem.* **2016**, *55*, 9461–9470.

17. Kerton, F.; Marriott, R. Chapter 2 Green Solvents – Legislation and Certification. In *Alternative Solvents for Green Chemistry (2)*; The Royal Society of Chemistry: Cambridge, 2013; pp. 31–50 ISBN 978-1-84973-595-7.

18. Sherwood, J.; Farmer, T.J.; Clark, J.H. Catalyst: Possible Consequences of the N-Methyl Pyrrolidone REACH Restriction. *Chem* **2018**, *4*, 2010–2012.

19. Khera, N.; Ghayor, C.; Pavlova, E.; Atanassova, N.; Weber, F.E. Exposure to the bromodomain inhibitor N-methyl pyrrolidone blocks spermatogenesis in a hormonal and non-hormonal fashion. *Toxicol. Appl. Pharmacol.* **2021**, *423*, 115568.

20. European Chemicals Agency (ECHA), Candidate list of substances of very high concern for authorisation Available online: https://echa.europa.eu/it/candidate-list-table (accessed on Aug 23, 2022).

21. Gao, F.; Bai, R.; Ferlin, F.; Vaccaro, L.; Li, M.; Gu, Y. Replacement strategies for non-green dipolar aprotic solvents. *Green Chem.* **2020**, *22*, 6240–6257.

22. Strappaveccia, G.; Ismalaj, E.; Petrucci, C.; Lanari, D.; Marrocchi, A.; Drees, M.; Facchetti, A.; Vaccaro, L. A biomass-derived safe medium to replace toxic dipolar solvents and access cleaner Heck coupling reactions. *Green Chem.* **2015**, *17*, 365–372.

23. Clarke, C.J.; Tu, W.C.; Levers, O.; Bröhl, A.; Hallett, J.P. Green and Sustainable Solvents in Chemical Processes. *Chem. Rev.* **2018**, *118*, 747–800.

24. Sherwood, J.; De bruyn, M.; Constantinou, A.; Moity, L.; McElroy, C.R.; Farmer, T.J.; Duncan, T.; Raverty, W.; Hunt, A.J.; Clark, J.H. Dihydrolevoglucosenone (Cyrene) as a bio-based alternative for dipolar aprotic solvents. *Chem. Commun.* **2014**, *50*, 9650–

9652.

25. Germán, L.; Cuevas, J.M.; Cobos, R.; Pérez-Alvarez, L.; Vilas-Vilela, J.L. Green alternative cosolvents toN-methyl-2-pyrrolidone in water polyurethane dispersions. *RSC Adv.* **2021**, *11*, 19070–19075.

26. Vandeputte, B.; Moonen, K.; Roose, P. WO2013107822A1 2013.

27. Sherwood, J.; Parker, H.L.; Moonen, K.; Farmer, T.J.; Hunt, A.J. N -Butylpyrrolidinone as a dipolar aprotic solvent for organic synthesis. *Green Chem.* **2016**, *18*, 3990–3996.

28. Bisz, E.; Koston, M.; Szostak, M. N -Butylpyrrolidone (NBP) as a non-toxic substitute for NMP in iron-catalyzed C(sp2)-C(sp3) cross-coupling of aryl chlorides. *Green Chem.* **2021**, *23*, 7515–7521.

29. Lopez, J.; Pletscher, S.; Aemissegger, A.; Bucher, C.; Gallou, F. N -Butylpyrrolidinone as Alternative Solvent for Solid-Phase Peptide Synthesis. *Org. Process Res. Dev.* **2018**, *22*, 494–503.

30. Winters, J.; Dehaen, W.; Binnemans, K. N-butyl pyrrolidone/ionic liquid mixtures as benign alternative solvents to N-methyl pyrrolidone for the synthesis of polyaramids. *Mater. Today Commun.* **2021**, *29*, 102843.

31. Louven, Y.; Haus, M.O.; Konrad, M.; Hofmann, J.P.; Palkovits, R. Efficient palladium catalysis for the upgrading of itaconic and levulinic acid to 2-pyrrolidones followed by their vinylation into value-added monomers. *Green Chem.* **2020**, *22*, 4532–4540.

32. Liu, Y.; Wang, Y.; Cheng, Y.; Wei, Z. Sustainable Efficient Synthesis of Pyrrolidones from Levulinic Acid over Pd / C Catalyst. **2022**, *202201191*.

33. Wu, Y.; Wu, Y.; Zhao, Y.; Zhao, Y.; Wang, H.; Wang, H.; Zhang, F.; Zhang, F.; Li, R.; Li, R.; et al. Ambient reductive synthesis of N-heterocyclic compounds over cellulose-derived carbon supported Pt nanocatalyst under H2atmosphere. *Green Chem.* **2020**, *22*, 3820–3826.

34. Xie, C.; Song, J.; Wu, H.; Hu, Y.; Liu, H.; Zhang, Z.; Zhang, P.; Chen, B.; Han, B. Ambient Reductive Amination of Levulinic Acid to Pyrrolidones over Pt Nanocatalysts on Porous TiO2 Nanosheets. *J. Am. Chem. Soc.* **2019**, *141*, 4002–4009.

35. Muzzio, M.; Yu, C.; Lin, H.; Yom, T.; Boga, D.A.; Xi, Z.; Li, N.; Yin, Z.; Li, J.; Dunn, J.A.; et al. Reductive amination of ethyl levulinate to pyrrolidones over AuPd nanoparticles at ambient hydrogen pressure. *Green Chem.* **2019**, *21*, 1895–1899.

36. Cao, P.; Ma, T.; Zhang, H.Y.; Yin, G.; Zhao, J.; Zhang, Y. Conversion of levulinic acid to N-substituted pyrrolidinones over a nonnoble bimetallic catalyst Cu15Pr3/Al2O3. *Catal. Commun.* **2018**, *116*, 85–90.

37. Boosa, V.; Varimalla, S.; Dumpalapally, M.; Gutta, N.; Velisoju, V.K.; Nama, N.; Akula, V. Influence of Brønsted acid sites on chemoselective synthesis of pyrrolidones over H-ZSM-5 supported copper catalyst. *Appl. Catal. B Environ.* **2021**, *292*, 120177.

38. Li Petri, G.; Raimondi, M.V.; Spanò, V.; Holl, R.; Barraja, P.; Montalbano, A. *Pyrrolidine in Drug Discovery: A Versatile Scaffold for Novel Biologically Active Compounds*; Springer International Publishing, 2021; Vol. 379; ISBN 0123456789.

39. Wei, D.; Netkaew, C.; Darcel, C. Iron-Catalysed Switchable Synthesis of Pyrrolidines vs Pyrrolidinones by Reductive Amination of Levulinic Acid Derivatives via Hydrosilylation. *Adv. Synth. Catal.* **2019**, *361*, 1781–1786.

40. Ogiwara, Y.; Uchiyama, T.; Sakai, N. Reductive Amination/Cyclization of Keto Acids Using a Hydrosilane for Selective Production of Lactams versus Cyclic Amines by Switching of the Indium Catalyst. *Angew. Chemie - Int. Ed.* **2016**, *55*, 1864–1867.

41. Liu, Z.; Wu, C.; Luo, X.; Zhang, H.; Liu, X.; Ji, G.; Liu, Z. Reductive amination/cyclization of levulinic acid to pyrrolidones: Versus pyrrolidines by switching the catalyst from AlCl3 to RuCl3 under mild conditions. *Green Chem.* **2017**, *19*, 3525–3529.

42. Xue, Z.; Liu, Q.; Wang, J.; Mu, T. Valorization of levulinic acid over non-noble metal catalysts: Challenges and opportunities. *Green Chem.* **2018**, *20*, 4391–4408.

43. Chan-Thaw, C.E.; Marelli, M.; Psaro, R.; Ravasio, N.; Zaccheria, F. New generation biofuels: γ-Valerolactone into valeric esters in one pot. *RSC Adv.* **2013**, *3*, 1302–1306.

44. Scotti, N.; Finocchio, E.; Evangelisti, C.; Marelli, M.; Psaro, R.; Ravasio, N.; Zaccheria, F. Some insight on the structure/activity relationship of metal nanoparticles in Cu/SiO2 catalysts. *Chinese J. Catal.* **2019**, *40*, 1788–1794.

45. Ravasio, N.; Zaccheria, F.; Fusi, A.; Psaro, R. One pot selective hydrogenation and dynamic kinetic resolution over Cu/Al2O3: A way to (-)-menthol starting from low value mint oils. *Appl. Catal. A Gen.* **2006**, *315*, 114–119.

46. Cavuoto, D.; Zaccheria, F.; Marelli, M.; Evangelisti, C.; Piccolo, O.; Ravasio, N. The role of support hydrophobicity in the selective hydrogenation of enones and unsaturated sulfones over Cu/SiO$_2$ catalysts. *Catalysts* **2020**, *10*.

47. Praliaud, H.; Mikhailenko, S.; Chajar, Z.; Primet, M. Surface and bulk properties of Cu-ZSM-5 and Cu/Al2O3 solids during redox treatments. Correlation with the selective reduction of nitric oxide by hydrocarbons. *Appl. Catal. B Environ.* **1998**, *16*, 359–374.

48. Singh, L.; Rekha, P.; Chand, S. Cu-impregnated zeolite Y as highly active and stable heterogeneous Fenton-like catalyst for degradation of Congo red dye. *Sep. Purif.*

Technol. **2016**, *170*, 321–336.

49. Chanquía, C.M.; Sapag, K.; Rodríguez-Castellón, E.; Herrero, E.R.; Eimer, G.A. Nature and location of copper nanospecies in mesoporous molecular sieves. *J. Phys. Chem. C* **2010**, *114*, 1481–1490.

50. Chary, K.V.R.; Sagar, G.V.; Srikanth, C.S.; Rao, V.V. Characterization and catalytic functionalities of copper oxide catalysts supported on zirconia. *J. Phys. Chem. B* **2007**, *111*, 543–550.

51. Zaccheria, F.; Scotti, N.; Marelli, M.; Psaro, R.; Ravasio, N. Unravelling the properties of supported copper oxide: Can the particle size induce acidic behaviour? *Dalt. Trans.* **2013**, *42*, 1319–1328.

52. Jouguet, B.; Gervasini, A.; Auroux, A. Optimal experimental procedures in a combined TPR/TPO apparatus. *Chem. Eng. Technol.* **1995**, *18*, 243–247.

53. Gervasini, A.; Manzoli, M.; Martra, G.; Ponti, A.; Ravasio, N.; Sordelli, L.; Zaccheria, F. Dependence of copper species on the nature of the support for dispersed CuO catalysts. *J. Phys. Chem. B* **2006**, *110*, 7851–7861.

54. Campisi, S.; Galloni, M.G.; Bossola, F.; Gervasini, A. Comparative performance of copper and iron functionalized hydroxyapatite catalysts in NH3-SCR. *Catal. Commun.* **2019**, *123*, 79–85.

55. Emeis, C.A. Determination of integrated molar extinction coefficients for infrared absorption bands of pyridine adsorbed on solid acid catalysts. *J. Catal.* **1993**, *141*.

56. Silvester, L.; Lamonier, J.F.; Vannier, R.N.; Lamonier, C.; Capron, M.; Mamede, A.S.; Pourpoint, F.; Gervasini, A.; Dumeignil, F. Structural, textural and acid-base properties of carbonate-containing hydroxyapatites. *J. Mater. Chem. A* **2014**, *2*, 11073–11090.

57. Zaccheria, F.; Shaikh, N.I.; Scotti, N.; Psaro, R.; Ravasio, N. New concepts in solid acid catalysis: Some opportunities offered by dispersed copper oxide. *Top. Catal.* **2014**, *57*, 1085–1093.

58. Busca, G. The surface acidity of solid oxides and its characterization by IR spectroscopic methods. An attempt at systematization. *Phys. Chem. Chem. Phys.* **1999**, *1*, 723–736.

59. Bukhtiyarova, M. V.; Bukhtiyarova, G.A. Reductive amination of levulinic acid or its derivatives to pyrrolidones over heterogeneous catalysts in the batch and continuous flow reactors: A review. *Renew. Sustain. Energy Rev.* **2021**, *143*, 110876.

60. Amarasekara, A.S.; Lawrence, Y.M. Raney-Ni catalyzed conversion of levulinic acid to 5-methyl-2-pyrrolidone using ammonium formate as the H and N source.

Tetrahedron Lett. **2018**, *59*, 1832–1835.

61. Zhang, T.; Ge, Y.; Wang, X.; Chen, J.; Huang, X.; Liao, Y. Polymeric Ruthenium Porphyrin-Functionalized Carbon Nanotubes and Graphene for Levulinic Ester Transformations into γ-Valerolactone and Pyrrolidone Derivatives. *ACS Omega* **2017**, *2*, 3228–3240.

62. Kim, K.; Hong, S.H. Iridium-Catalyzed Single-Step N-Substituted Lactam Synthesis from Lactones and Amines. *J. Org. Chem.* **2015**, *80*, 4152–4156.

63. Kong, Q.; Li, X.; Xu, H.; Fu, Y. Study on Reaction of γ-Valerolactone and Amine Catalyzed by Zirconium-Based Lewis Acids. *Chinese J. Org. Chem.* **2020**, *40*, 2062–2070.

64. Zaccheria, F.; Ravasio, N.; Ercoli, M.; Allegrini, P. Heterogeneous Cu-catalysts for the reductive deoxygenation of aromatic ketones without additives. *Tetrahedron Lett.* **2005**, *46*, 7743–7745.

65. Cavuoto, D.; Ravasio, N.; Scotti, N.; Gervasini, A.; Campisi, S.; Marelli, M.; Cappelletti, G.; Zaccheria, F. A green solvent diverts the hydrogenation of γ – valerolactone to 1 , 4 - pentandiol over Cu / SiO 2. *Mol. Catal.* **2021**, *516*, 111936.

66. Fahmi, A.; Minot, C. A theoretical investigation of water adsorption on titanium dioxide surfaces. *Surf. Sci.* **1994**, *304*, 343–359.

67. Rigney, M.P.; Funkenbusch, E.F.; Carr, P.W. Physical and chemical characterization of microporous zirconia. *J. Chromatogr. A* **1990**, *499*, 291–304.

68. Patnaik, P. *Handbook of Inorganic Chemicals*; The McGraw-Hill Companies, Inc: New York; Vol. s8-X; ISBN 0-07-049439-8.

69. Enslein, K.; Gombar, V.K.; Blake, B.W. Use of SAR in computer-assited prediction of carcinogenicity and mutagenicity of chemicals by the TOPKAT program. *Mutat. Res. Mol. Mech. Mutagen.* **1994**, *305*, 47–61.

70. Gomba, V.K.; Enslein, K.; Blake, B.W. Assessment of developmental toxicity potential of chemicals by quantitative structure-toxicity relationship models. *Chemosphere* **1995**, *31*, 2499–2510.

71. Beerthuis, R.; Rothenberg, G.; Shiju, N.R. Catalytic routes towards acrylic acid, adipic acid and ε-caprolactam starting from biorenewables. *Green Chem.* **2015**, *17*, 1341–1361.

72. Karibayev, M.; Shah, D. Comprehensive Computational Analysis Exploring the Formation of Caprolactam-Based Deep Eutectic Solvents and Their Applications in Natural Gas Desulfurization. *Energy and Fuels* **2020**, *34*, 9894–9902.

4 CONCLUDING REMARKS

The research work conducted in this Ph.D thesis investigated the use of supported non-noble copper catalysts for the valorization of biomass derived chemicals such as γ-valerolactone (GVL) and bioalcohols. The copper was deposited on various support materials with the Chemisorption-Hydrolysis method that ensures a high dispersion of the copper phase and low particle size that gives excellent hydrogenation power and imparts an unusual acidity to the Cu-centers. All the catalytic tests were supported by a deep physicochemical characterization work in order to clarify the structure-activity-relationship between the materials and their catalytic behavior.

CuO/SiO$_2$ was found to have an excellent activity in the hydrogenation of GVL to give 1,4-Pentandiol. This result was ascribable to the bifunctionality of the copper catalysts imparted by the preparation method. In fact, the moderate acidity of the copper phase activates the carbonyl group of the lactone towards the hydrogenation. Moreover, the modulation of wettability through the choice of the support or through post synthesis organosilane grafting was important to boost the selectivity towards the diol, allowing a better desorption of the product from the catalyst surface. The activity of the catalytic system was also diverted by the choice of the solvent: the use of the green cyclopentylmethylether was the key to achieve high conversion of GVL and selectivity to the diol due to finely tune of the surface acidity of the materials. The choice of the support was important also in the amination of GVL to obtain potential green solvents as N-alkylpyrrolidinones. In this case, CuO/HAP and CuO/Al$_2$O$_3$ were the best materials in terms of activity and selectivity thanks again to the well dispersed copper phase and to the mild, lower strength acidity without the need of pre-activation. These CuO systems had shown promising results also in the amination of bioalcohols to obtain primary amines that are benchmark chemicals in the chemical industry.

In conclusion, the results achieved during the Ph.D thesis work showed that cheap, simple, robust, bifunctional copper catalysts are applicable to the valorization of diverse biomass-derived platform molecules with the possibility to obtain different products. This is possible simply modulating the processes variables such as the catalyst support, the post-synthesis functionalization, the reaction conditions and the pre-treatment, thus making these materials promising catalysts for biomass valorization.

# 5 EXPERIMENTAL SECTION

5.1   Materials

Silica materials used as supports: SiO_2 A and SiO_2 C were obtained by Evonik, SiO_2 B was purchased by Fluka Chemicals, SiO_2 D was provided by Mitsubishi Chemicals. SiO_2-Al_2O_3 (Alumina content 13.5%) was purchased from Merck. γ-Al_2O_3 A was purchased by Sasol, ZrO_2 (3.5 % SiO_2) was provided by MELCAT, TiO_2 was purchased by Degussa. Highly pure (>99%) trietoxyoctylsilane (TEOCS), γ-valerolactone (GVL) with purity 99%, 1,4-pentanediol (1,4-PDO) with purity 99%, copper nitrate trihydrate with purity 99% and 1,4-dioxane with purity 99%, heptane (purity >99%) were purchased from Sigma Aldrich. Cyclopentyl methyl ether (CPME) stabilized with butylated hydroxy toluene at > 99.5% purity was purchased by Tokyo Chemical Industry. Urea (>99%) and aluminum isopropoxide (≥98%) were purchased by Merck.

5.2   Catalysts preparation

Hydroxyapatite preparation

Stoichiometric hydroxyapatite ($Ca_{10}(PO_4)_6(OH)_2$, atom/atom Ca/P ratio equal to 1.67 has been synthesized utilizing a coprecipitation method. A 0.1 M aqueous solution of $(NH_4)_2HPO_4$ (250 ml) was placed in a three-necked round flask equipped with a mechanical stirrer, a reflux condenser and an adaptor for peristaltic pump tube connection. The $(NH_4)_2HPO_4$ solution was heated to 80 °C under stirring (200 rpm) through an oil bath and pH was adjusted to 9.7 adding 50 ml of a 28-30% wt/wt NH_4OH solution. Subsequently,

250 mL of a 0.167 M aqueous solution of $Ca(NO_3)_2 \cdot 4H_2O$ were fed to the flask through a peristaltic pump (dropping rate = 1.5 mL min^{1}). During the addition, the pH of the solution was kept constant. All solutions were prepared from MilliQ water (15.0 MΩ, Millipore). Addition of the Ca(II) precursor solution leads to the formation of a milky suspension. HAP precipitates according to the following chemical equation:

$$10\ Ca(NO_3)_2 + 6\ (NH_4)_2HPO_4 + 8\ NH_3 + 2\ H_2O \rightarrow Ca_{10}(PO_4)_6(OH)_{2\downarrow} + 20\ (NH_4)NO_3$$
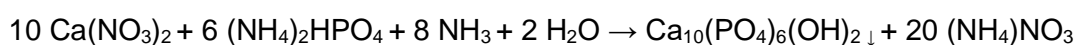
γ-Al₂O₃ B preparation

γ-Al₂O₃ B was prepared via sol-gel procedure assisted by sonication [1]. In detail, 0.22 g of urea were dissolved in 30 ml of deionized water. After complete dissolution, 3.18 g of aluminum isopropoxide were added to the solution. The resulting gel was stirred for 1 h at room temperature and then sonicated for 10 min. After sonication the gel was calcined under air flow (100 ml/min) for 4 h at 500 °C.

Copper deposition

Catalysts were prepared using the Chemisorption-Hydrolysis (CH) method [2] widely described in the paragraph 1.1.2. The following procedure and slight excess quantity of $Cu(NO_3)_2 \cdot 3\,H_2O$ was optimized to obtain 16% wt/wt of Cu deposited on SiO_2 material confirmed by ICP analysis in previous studies [3].

$$8 \text{ g of } Cu(NO_3)_2 \cdot 3\,H_2O \text{ for } 10 \text{ g of } SiO_2$$

$$8 \text{ g } [Cu(NO_3)_2 \cdot 3\,H_2O] / 241.6 \text{ g/mol } [\text{MW of } Cu(NO_3)_2 \cdot 3\,H_2O] =$$

$$0.033 \text{ mol of } Cu(NO_3)_2 \cdot 3\,H_2O = 0.0033 \text{ mol of Cu}$$

$$0.033 \text{ mol } [Cu] \times 63.55 \text{ g/mol } [\text{AW of Cu}] = 2.11 \text{ g of Cu}$$

$$2.11 \text{ g}/(2.11 \text{ g} + 10 \text{ g}) \times 100 = 17.4\%$$

Experimentally the catalyst is prepared by adding the SiO_2 support to an aqueous $[Cu(NH_3)_4]^{2+}$ solution prepared by dropping NH_4OH to a $Cu(NO_3)_2 \cdot 3H_2O$ solution (25 mL) with the desired concentration until pH 9 had been reached. After 20 minutes under stirring, the slurry was diluted with 3 L of water in an ice bath at 0 °C. The solid was separated by filtration with a Büchner funnel, washed with water, dried overnight at 110 °C and calcined in air atmosphere at 350 °C for 4 h. The following code was used in the discussion of this work: CuO in the case of calcined catalysts, Cu in the case of reduced catalyst slash the utilized support.

Organosilane grafting

A solution of TEOCS of the desired concentration was prepared (in the range 1%−15% wt/wt of nominal silane loading) with 80 mL isopropanol in which 1 g of dry catalyst was dispersed accurately. After 1 h of vigorous stirring (750 rpm) at room temperature, the isopropanol was evaporated under vacuum at 50 °C. The effective amount of organosilane

grafted was analyzed by elemental analysis determined on the bases of the C content of the samples. (1.7%, 6.5%, 6.9%, 9.8%).

5.3 Catalytic tests

Catalytic tests procedure of hydrogenation of GVL

Before any reaction the catalysts (100 mg) were pre-treated for 20 minutes at 270 °C under air and for 20 minutes under vacuum and then reduced through three hydrogen (1 bar) and vacuum cycles (5 mins each) at the same temperature. Generally, GVL (5 mmol) was dissolved in 20 mL of solvent. Then, the pre-reduced catalyst was suspended in the reaction mixture and they were loaded under nitrogen flow in a 100 mL Parr reactor under different H_2 pressure (30-50 bar) and temperatures (140-180 °C) for 22 h under mechanical stirring (750 rpm).

Reaction conversions and selectivity were determined by GC-FID analysis using an Agilent 6890 Gas 0,25 Chromatography system with a Alltech Heliflex AT-5 capillary column (30 m × 0.32 mm ID × 0.25 µm). Dodecane was used as internal standard (carbon balance >98%). Byproducts were qualitative determined with GC-MS analysis using an Agilent 5957C GC-MS chromatograph with an HP-5 column. See appendix section 6.10 for an example of chromatogram, method program and calibration lines.

Conversion was determined using the following equation (1):

$$\% \ C = \frac{n(t_0) - n(t)}{n(t_0)} \times 100 \qquad (1)$$

Where $n(t_0)$ are the initial moles of GVL introduced in the reactor and $n(t)$ are the unreacted moles of GVL determined with GC-FID analysis.
Selectivity was determined using this equation (2):

$$\% \ S = \frac{p(t)}{n(t_0) - n(t)} \times 100 \qquad (2)$$

Where $p(t)$ are the moles of products formed determined by GC-FID analysis.

Catalytic tests procedure of amination of alcohols

Before any reaction the catalysts (100 mg) were pre-treated for 20 min at 270 °C under air and for 20 min under vacuum and then reduced through three hydrogen (1 bar) and vacuum cycles (5 mins each) at the same temperature.

After the pretreatment, the catalyst was suspended in the reaction solvent (10 ml heptane) and loaded under nitrogen flow in a 100 mL Parr reactor together with the chosen alcohol (100 mg). Then, the autoclave was pressurized with H_2 (1-10 bar) and NH_3 (3 bar) and the temperature was brought to 180 °C for the desired time of reaction under magnetic stirring (750 rpm). Reaction conversions and selectivity were determined using GC-MS analysis using an Agilent 5957C GC-MS chromatograph with an HP-5 column using dodecane as standard.

Catalytic tests procedure of lactamization of GVL

Before any reaction the catalysts (100 mg) were pre-treated for 20 min at 270 °C under air and for 20 min under vacuum and then, in the case of pre-reduced catalysts, reduced through three hydrogen (1 bar) and vacuum cycles (5 mins each) at the same temperature. After the pretreatment, the catalyst was suspended in the reaction solvent (10 ml) and loaded under nitrogen flow in a 100 mL Parr reactor together with the chosen lactone (100 mg) and the butylamine (1 equivalent). Then, the autoclave was pressurized with H_2 (1-10 bar) and the temperature was brought to 200 °C for 2 h under magnetic stirring (750 rpm). Reaction conversions and selectivity were determined by GC-FID analysis using an Agilent 6890 Gas 0,25 Chromatography system with a Alltech Heliflex AT-5 capillary column. Dodecane was used as internal standard (carbon balance >98%). Products were qualitative determined with GCMS– analysis using an Agilent 5957C GC–MS chromatograph with an HP-5 column. See appendix section 6.10 for an example of chromatogram, method program and calibration lines.

Conversion was determined using the equation (1).

The molar percentage of the products was calculated using the following equation (3):

$$\text{Mol \%} = (n_p / \Sigma n) \times 100 \qquad (3)$$

Where n_p are the moles of the considered product and Σn is the sum of the moles of each formed products determined with GC-FID analysis.

5.4 Catalyst phyisco-chemical characterization

5.4.1 Static contact angle measurement

SCA of the tested solid supports were performed by means of a Krüss Easy instrument. Notably, molded thin disks (25-30 mg of the sample powders, 1-5 tons) were prepared by using a Specac manual hydraulic press to achieve a compact and flat surface. A 1,3-propanediol drop of 5 µL was gently placed on the surface disk; the drop profile was extrapolated using an appropriate fitting function to acquire the static contact angle (θ). Measurements were repeated ten times to obtain a statistically relevant population.

5.4.2 Specific Surface Area and Porosity

SSA and porosity (pore volume, pore size and pore size distribution) were determined by N_2 adsorption/desorption isotherms collected at -196 °C using automatic analyzers of surface area Micromeritics ASAP 2020 (V4.02). Prior to the analysis, the sample, was outgassed at 350 °C for 4 h under vacuum to remove water and other volatile organic compounds adsorbed on the surface. Specific surface area values were calculated by Brunauer-Emmet-Teller (BET) equation. Pore volume (PV), pore size and pore size distribution were determined by Barrett-Joyner- Halenda (BJH) model from the desorption branch of the collected isotherms.

5.4.3 Water adsorption isotherms

The water adsorption isotherms were collected on the same instrument and exploiting the same pre-treatment method of the samples adopted for the morphologic analyses above detailed. Adsorption of water was performed with 20 mL reservoir of ultrapure water MilliQ water (15.0 MΩ, Millipore) as a vapor source and held at 40 °C. The adsorption experiments were carried out at 22 °C and the saturation pressure was 25 mmHg.

5.4.4 Thermogravimetric Analysis

Mass loss of bare silica supports was determined by thermogravimetric analysis (TGA 7, Perkin Elmer analyzer) with targeted experiments aimed at determining the amount of the surface hydroxyl groups. Prior to the analysis, the sample was stored in a vessel with

water vapor at room temperature overnight for saturating the surface. Then, a weighted amount of the saturated sample (ca. 10-15 mg) was loaded on the pan of the thermobalance. Each experiment was carried out under air flowing gas (60 mL min^{-1}). The thermal program comprised three steps: i) heating at rate of 5 °C min^{-1} from 25 to 200 °C; ii) maintenance of the temperature of 200 °C for 30 min and iii) heating at rate of 10 °C min^{-1} up to 900 °C [4].

The hydroxyl amount of each sample was evaluated through the determination of the loss of mass in the range 200°-900 °C (third step of the thermal program) using the following equation (4):

$$mmol_{OH}\ g_{cat}^{-1} = \frac{[(2 \times \Delta wt\ \%) \times 10]}{18\ g\ mol^{-1}} \qquad (4)$$

Mass loss of organosilane-grafted catalysts was determined on the same instrument but with a different experiment aimed at determining the stability of the silane groups. Prior to the analysis, the sample was stored in oven (110 °C) overnight. Then, a weighted amount of the sample (ca. 10–15 mg) was loaded on the pan of the thermobalance. Each experiment was carried out under nitrogen flowing gas (60 mL min^{-1}). The thermal program comprised three steps: (i) isothermal step at 50 °C for 10 min; (ii) heating at rate 20 °C min^{-1} up to 700 °C [5]. Weight loss percentage was determined in the 200°-700 °C interval. T_{onset} and T_{end} were determined performing the δTGA of the thermograms.

In any case, the calibration of temperature was performed by measuring the Curie transitions (T_C) of high-purity reference materials (alumel, nickel, perkalloy, and iron: T_C of 163, 354, 596, and 780 °C, respectively) at the same heating rate (β) employed for the analyses. The instrument accuracy is around few μg.

5.4.5 UV-vis Spectroscopy

UV spectroscopy was carried out using Shimadzu UV–3600 spectrophotometer equipped with quartz cuvettes to assess the linearity between 2-phenylethylamine (PEA) solution concentration and absorbance in the solvents using in the liquid-solid acid-base titrations (Cyclohexane, CPME, dioxane and heptane). The concentration range was chosen according to the operational concentration range used in the liquid-solid titration. After performing an auto-zero blank with the solvents, spectra of solution with PEA at different concentrations were acquired in the entire wavelength range (200-1100 nm) to assess the PEA absorption range (see appendix section 6.8 for the spectra figures). Subsequently, calibration lines were built using the Lambert-Beer law measuring the absorbance at the

typical absorption wavelength of PEA (254 nm) for each concentration in photometric mode with the aim to determine the molar extinction of PEA in each solvent and to check the effective PEA solution concentration (0.1 M) before each titration experiment. See appendix section 6.8 for more detail about data elaboration.

5.4.6 Liquid-solid acid-base titrations with PEA

The acid-base liquid-solid titrations on the samples were performed using 2-phenylethylamine (PEA, pKa = 9.90) as a probe in different solvents namely cyclohexane and heptane (aprotic-apolar), CPME and dioxane (both aprotic-polar). The experimental set up consisted in a HPLC line, comprising a pump (Waters, model 515), a reservoir and a monochromatic UV detector (Waters, model 2487, λ = 254 nm), coupled to a personal computer for the collection, storage, and processing of the data (figure 5.1 A).
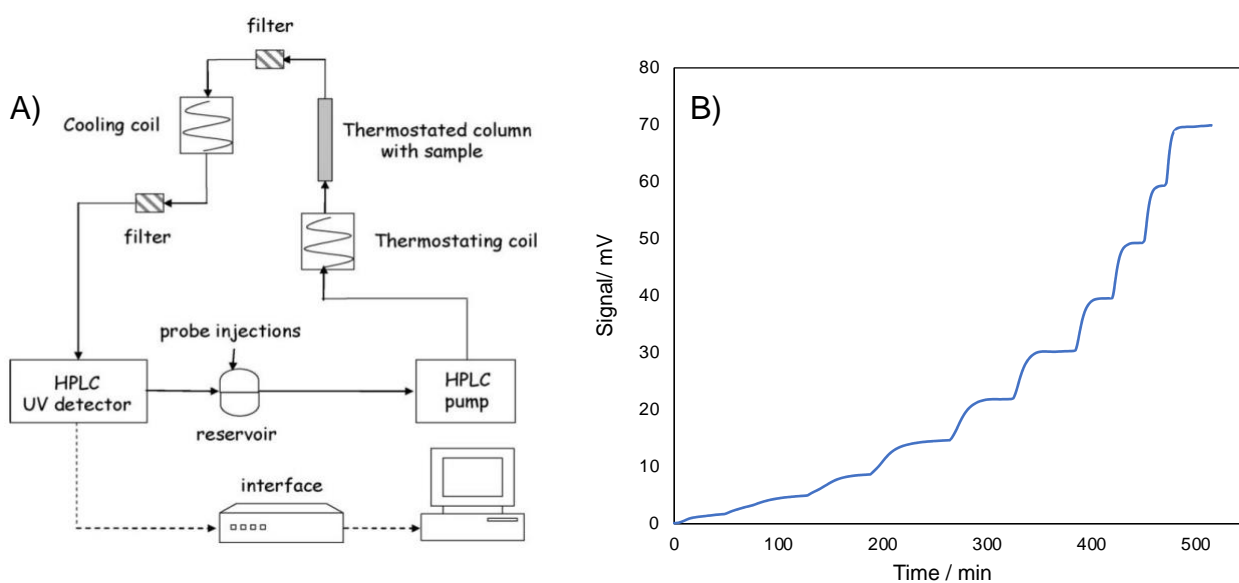
Figure 5.1. A) Titrations experimental apparatus. B) Example of chromatogram obtained during the liquid-solid acid-base titrations. Each step represents the achievement of the equilibrium at the injected PEA concentration.

The sample (0.050–0.100 g, crushed and sieved as 80–200 mesh particles) was placed in a small stainless tubular sample holder between two sand pillows. The sample was successively activated at 350 °C for 16 h in flowing air (8 mL min^{-1}), then evacuated and eventually filled with the operating solvent. The sample holder, inserted in a glass jacket connected with a water thermostat to maintain a constant temperature (± 0.1 °C), was placed instead of the chromatographic column. The titrations were carried out by injecting

successive dosed amount of PEA in the operating solvents (20 50 mL, 0.10 0.15 M) into the line in which the solution continuously circulated. For each injection, the PEA solution recirculated onto the sample until adsorption equilibrium was achieved, revealed by the attainment of the UV-detector signal stability (figure 2.21 B). Assuming a 1:1 stoichiometry for the PEA adsorption on the acid site, the number of acid sites per sample mass titrated at each equilibrium PEA concentration was evaluated, obtaining adsorption isotherms for the various samples. During the first run, the injections of PEA solution were done until surface saturation; then, clean solvent was flowed through the sample to remove the physisorbed PEA, and the second run adsorption was collected. Subtraction of the second run from the first gives the chemisorption isotherm, from which the strong acid sites can be computed. Total amount of acidic sites and strong acidic sites per mass of solvent were obtained through Langmuir linearization model of the experimental adsorption isotherms. The detailed mathematical elaboration method is displayed in the appendix section 6.8.

5.4.7 Infrared Spectroscopy

The Fourier Transform-Infrared (FT-IR) studies of the adsorption of the pyridine probe molecule were carried out on an FTS-60 spectrophotometer equipped with mid-IR MCT detector purchased from BioRad. The experiments were performed in all cases except for CuO/HAP sample on a thin disk of sample (20–30 mg, pressed at 1–2 tons) after a reduction pre-treatment consisting in 20 min at 270° at air followed by 20 min at 270 °C under vacuum and finally a reduction under H_2 through three hydrogen (1 bar) and vacuum cycle at the same temperature. The first spectrum was collected before pyridine adsorption as a blank and it was subtracted to each spectrum prior to data curation. Then, pyridine vapors were adsorbed at room temperature and then desorbed in steps of 30 min until 250 °C at the given vacuum (10^{-5} bar). The spectrum of each desorption step was collected every 50 °C up to 250 °C. See figure S23 and S24 in the appendix section 6.9 for examples of pyridine adsorption spectra at different outgassing temperature for sample CuO/SiO_2 and $CuO/SiO_2\text{-}Al_2O_3$. For quantitative analysis the amount of absorbed pyridine ($mmol_{py}\ g_{cat}^{-1}$) was calculated on the basis of the relationship (equation (5)) reported by Emeis [6] namely:

Pyridine Concentration of Lewis Sites ($mmol\ g^{-1}$) = $(1.42 \times IA \times R^2) / W$ (5)
Where:
R = radius of the catalyst disk (cm) = 0.65 cm

W= weight of the disk (mg)

IA = Integrated Absorbance Band at 1449 cm^{-1}

CuO/HAP sample was prepared dispersing the catalysts in an inert, non-acidic matrix, namely SiO_2 A, in a mass ratio of 1:15 wt/wt. This mixed powder was pressed and pre-treated and analyzed with the same procedure of the other sample. This had the aim to limit the CO_3^{2-} signal which absorbs in the 1600-1400 cm^{-1} region. Equation (5) was still applied but W was only the weight of CuO/HAP contained in the disk. The Lewis site band at 1600 cm^{-1} was deconvoluted and fitted by using a Gaussian function.

Attenuated Total Reflection (ATR) experiments of the silanized catalyst were acquired with the same instrument equipped with Specac Golden Gate ATR platform with diamond crystal. The ATR experiments of the pre and post reaction catalyst were performed on a Nicolet iS50 FT-IR purchased from Thermo Scientific using diamond crystal also.

5.4.8 X-ray Photoelectron Spectroscopy

Surface composition of all the samples was analyzed by X-ray Photoelectron Spectroscopy (XPS) by means of an M-PROBE Surface Spectrometer with an Al (Ka) source and a spot size from 0.15 mm to 1 mm in diameter. An applied voltage of 10 V and a vacuum of 10^{-8} –10^{-7} Torr were used. The survey scans were investigated in 0-1100 eV binding energy range, using a spot size of 800 microns with an energy resolution of 4 eV (scan rate of 1 eV per step). The samples were pre-treated with the same procedure of FT-IR analysis. ESCA Hawk Software was used for data curation. All the resulting binding energy values were corrected using the C 1s peak (C–C) fixed at 284.6 eV, as a reference. Normalized surface concentrations of all the species were computed by ruling out only the contribution of adventitious carbon (C–C at 284.6 eV).

5.4.9 Transmission Electron Microscopy

TEM analysis was performed using a ZEISS LIBRA200FE. The samples were gently smashed in an agate mortar, suspended in isopropyl alcohol for 20 min in an ultrasonic bath and dropped onto a lacey carbon-coated copper TEM grid. The samples were analyzed after

complete solvent evaporation. Histograms of the particle size distribution were obtained by counting onto the micrographs at least 500 particles; the mean particle diameter (d_m) was calculated by using the equation (6):

$$d_m = \Sigma d_i n_i / \Sigma n_i \qquad (6)$$

where n_i was the number of particles of diameter d_i.

5.4.10 Cross-Polarization Magic Angle Spinning Nuclear Magnetic Resonance

Solid state NMR spectra of bare CuO/SiO_2 B and organosilane grafted samples were obtained at 99.36 (^{29}Si) MHz on a Bruker Avance 500 spectrometer, equipped with a 4 mm magic angle spinning (MAS) broad-band probe (spinning rate vR up to 6 kHz). The MAS spectra were recorded on solid samples, typically around 150 mg. Each sample was packed into a 4-mm MAS rotor (50 µL sample volume) spinning at 6 kHz and at a temperature of 303 K with a contact time of 6 ms and accumulation time of 68 h; no resolution improvement was found at higher rate spinning and/or temperature. The experimental data were deconvoluted and fitted by using a Gaussian function [7].

5.4.11 Total Acidity determined through NH_3 adsorption tests

NH_3 adsorption tests of bare CuO/SiO_2 B and organosilane grafted samples were carried out in flowing dynamic experiments. Each dried and weighed sample (*ca.* 0.15 g, previously sieved to have particles of 45-60 mesh, corresponding to 250-355 µm) was activated at 150°C under air flow (3 $NL \cdot h^{-1}$) for 30 min in a quartz reactor. Then, a NH_3/N_2 mixture (NH_3 concentration of *ca.* 500 ppm) flowed at 6 $NL \cdot h^{-1}$ through the reactor and reached a gas cell (path length 2.4 m multiple reflection gas cell) in the beam of an online FT-IR spectrometer (Bio-Rad with DTGS detector). The NH_3 line (at 966 cm^{-1}) was monitored along with time. On each sample, NH_3 was completely adsorbed, as observed from the NH_3-signal profile, which exponentially decreased and remained to zero for a given measured time. When saturation of sites by NH_3 was attained, the signal was restored at the same value of its starting concentration. From the evaluation of the time during which the NH_3-signal was not at the level corresponding to its starting concentration, the amount of total acid sites in excess was evaluated using the following equation (7):

$$\frac{\text{moles of } NH_{3\,(Ads)}}{m_{sample}} = \frac{[NH_3]_{fed} \times F \times t \times P}{RT \times m_{sample}} \qquad (7)$$

Where:

[NH3]fed (ppm) = flowing NH3 concentration, in ppm;

F (NL·h⁻¹)= total flow rate of the NH3/N2 mixture in;

t (min) = time during which NH3 was completely adsorbed,

P(atm) = pressure

msample (g) = sample mass

Assuming a 1:1 stoichiometry for the NH3 adsorption on the surface site, the quantity of total acid sites per sample mass (in $\mu mol \cdot g^{-1}$), or per surface unit (in $\mu mol \cdot m^{-2}$) was evaluated by integration of the NH3 signal profile.

5.4.12 X-Ray Diffraction Spectroscopy

X-ray diffraction (XRD) patterns were recorded at room temperature (26 °C) with an Aeris (PANalytical, Almelo, The Netherlands) diffractometer in the Bragg-Brentano geometry and using Cu-Kα equipped with a PIXcel1D detector. Measurement range was 2θ = 8° - 80°, with a step size of 0.0109° and acquisition time of 79 s per step. The identification of crystalline phases was performed using the High Score Plus software including the PDF-4+ and ICSD databases. Crystallite size (DV) of synthetized CuO nanoparticles was estimated from the profile parameter of Rietveld refinement by the following equation (8):

$$Dv = \frac{36000\lambda}{\pi 2 LX} \qquad (8)$$

Where LX parameter is the profile parameter representing the 1/cosq like contribution to the Lorentzian part of the pseudo-Voigt. In particular, the Rietveld analysis was performed through the GSAS program [8] by using the γ-Al2O3 cubic Fd-3m s.g. and the CuO tenorite monoclinic C2/c s.g. structural models. During the refinement, the background was subtracted using shifted Chebyshev polynomials and the diffraction peak profiles were fitted with a modified pseudo-Voigt function. In the last calculation cycles, all the parameters were refined: cell parameters, isotropic thermal parameters, profile broadening parameter, background and diffractometer zero point. A discussion of the application of relation (1) is reported in reference [9].

5.4.13 UV-vis Diffuse Reflectance Spectroscopy

UV-vis Diffuse Reflectance (UV-DR) spectra were collected at room temperature in 200-2600 nm interval through a double beam UV–vis–NIR scanning spectrophotometer (Shimadzu UV-3600 plus, Japan) equipped with a diffuse reflectance accessory (integrating sphere from BIS-603). Each sample was pretreated in oven (110 °C) overnight and finely ground, uniformly pressed in a circular disk (diameter of *ca.* 4 cm) and placed in the sample-holder. This was inserted in a special quartz cuvette and placed on the window of the integrating sphere for reflectance measurements. Spectra were measured using ultrafine $BaSO_4$ as the reference. The measured reflectance values ($R\infty\%$) were converted to absorbance (Abs, a.u.) by the equation (9):

$$Abs = Log\ (1/\ R\infty/100) \qquad (9)$$

To discriminate each contribution the collected UV-vis-DR spectra (Absorbance, a.u., vs. wavelength, nm) in 200-1800 nm and 200-800 nm ranges were deconvoluted using a peak type Gaussian method.

5.4.14 Inductive Coupled Plasma Analysis

Cu loading of the catalysts samples was determined by ICP-OES, AAS, and IC analyses by means of an «Activa », Jobin Yvon ICP-OES instrument, or a PinAAcle 900T, S/N PTDS11062202, Perkin Elmer, Waltham, MA, USA, or a Dionex DX-120 instrument. It was double checked both on digested solids (*ca.* 50 mg of sample treated in concentrated HNO_3 for each analysis), and on the filtration solutions.

In particular, IC analyses were carried out by means of an IonPac CS5A analytical column from Dionex, using a solution of 50 mM oxalic acid/95 mM lithium hydroxide (pH 4.8) as eluent, and a solution of 0.4 mM PAR in 3 M NH_4OH and 1 M acetic acid as colorimetric indicator for UV-vis detection (at 520 nm) of metal ions (reagent flow rate of 0.6 mL·min-1). Calibration lines for Cu determination were built by analyzing standard solutions with concentration in 1-10 ppm interval prepared by a commercial multistandard certified by Areachem.

5.4.15 Temperature programmed reduction

Temperature-programmed reduction analysis was performed with a modified version of the Pulse Chemisorb 2700 apparatus from Micromeritics. Catalysts (samples containing ca. 2 mg of Cu) were diluted with quartz, calcined at 300 °C under O_2 (40 mL/min) with a thermal program consisting in: i) heating 10 °C/min until 300 °C ii) hold the temperature for 60 min. After calcination, catalysts were reduced at 8 °C/min under a flow (15 mL/ min) of an 8% H_2/Ar mixture. The H_2 consumption was detected by a thermal conductivity detector (TCD).

5.5 References

[1]   A. Sacco, A. Lamberti, M. Gerosa, C. Bisio, G. Gatti, F. Carniato, N. Shahzad, A. Chiodoni, E. Tresso, L. Marchese, Toward quasi-solid state Dye-sensitized Solar Cells: Effect of γ-Al2O3 nanoparticle dispersion into liquid electrolyte, Sol. Energy. 111 (2015) 125–134. https://doi.org/10.1016/j.solener.2014.10.034.

[2]   F. Zaccheria, N. Scotti, M. Marelli, R. Psaro, N. Ravasio, Unravelling the properties of supported copper oxide: Can the particle size induce acidic behaviour?, Dalt. Trans. 42 (2013) 1319–1328. https://doi.org/10.1039/c2dt32454g.

[3]   N. Scotti, M. Dangate, A. Gervasini, C. Evangelisti, N. Ravasio, F. Zaccheria, Unraveling the role of low coordination sites in a cu metal nanoparticle: A step toward the selective synthesis of second generation biofuels, ACS Catal. 4 (2014) 2818–2826. https://doi.org/10.1021/cs500581a.

[4]   J. Mrowiec-Bialoń, Determination of hydroxyls density in the silica-mesostructured cellular foams by thermogravimetry, Thermochim. Acta. 443 (2006) 49–52. https://doi.org/10.1016/j.tca.2005.12.014.

[5]   M. Castellano, E. Marsano, A. Turturro, L. Conzatti, G. Busca, Dependence of surface properties of silylated silica on the length of silane arms, Adsorption. 18 (2012) 307–320. https://doi.org/10.1007/s10450-012-9402-6.

[6]   C.A. Emeis, Determination of integrated molar extinction coefficients for infrared absorption bands of pyridine adsorbed on solid acid catalysts, J. Catal. 141 (1993) 347–354. https://doi.org/10.1006/jcat.1993.1145.

[7]   F. Milanesi, G. Cappelletti, R. Annunziata, C.L. Bianchi, D. Meroni, S. Ardizzone, Siloxane-TiO2 hybrid nanocomposites. the structure of the hydrophobic layer, J. Phys. Chem. C. 114 (2010) 8287–8293. https://doi.org/10.1021/jp1014669.

[8]   A.C. Larson and R.B. Von Dreele, General Structure Analysis System (GSAS), 2004.

[9]   P. Karen, P.M. Woodward, Liquid-Mix Disorder in Crystalline Solids: ScMnO3, J. Solid State Chem. 141 (1998) 78–88. https://doi.org/10.1006/JSSC.1998.7918.

6 APPENDICES

6.1 Copper as raw material

Copper is a chemical element that is a soft, malleable, and ductile metal with very high thermal and electrical conductivity. Copper naturally occurs in the mineral cuprite, chalcopyrite, azurite, chalcocite, malachite and bornite that mostly are sulfides or oxides. Pure copper contains the metal in uncombined form. Copper production can be divided into the three main process steps, which are mining, processing and metallurgy. Each process step can be done using different methods and in the majority of industrial processes, copper is produced from the ore chalcopyrite, a mixed copper-iron sulfide mineral, or from the carbonate ores azurite and malachite [1]. The use of copper has to be date back to prehistoric times where it had numerous applications in every aspect of life. Due to its properties, it has been employed in the metallic form to create alloys to manufacture various objects and tools. Besides, thanks to its high conductivity, it has used in electric wiring, switches and electrode production. Moreover, copper compounds, such as oxide, sulfates and chlorides have diverse commercial application [2,3].

The majority of copper production has been historically held by Chile (21.5% world production, followed by USA (18.5%). However, if potential copper resources are considered Chile has again the largest reserves followed by Peru (13%), Australia and USA [4] (see figure S1).
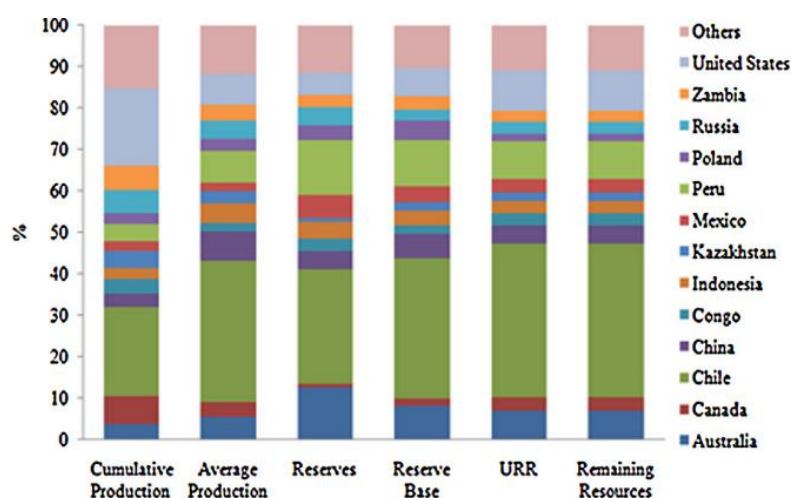
Figure S1. Copper historical production and resources by country or region (per cent of global total). This material was published in Ref. [4]. Copyright Elsevier.

Global copper demand has increased in the last 10 years and it is expected to keep rising concerning every production sector (figure S2). In fact, copper had earned a crucial

134

role in modern processes and technologies and the always increasing demand will deplete copper natural resources intensify the energy requirement for mining causing a high environmental impact [5].
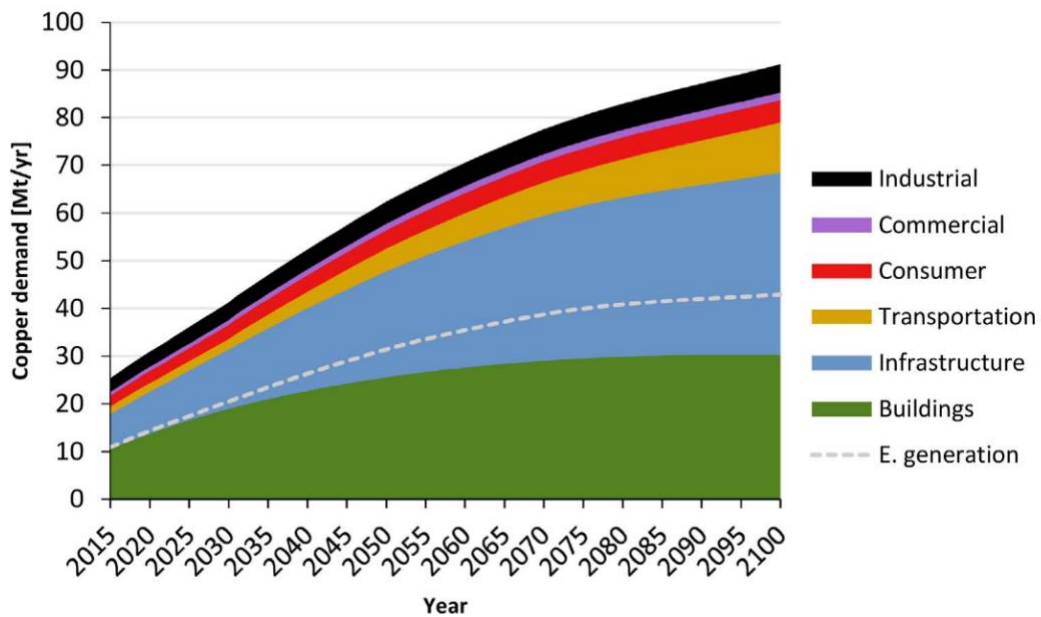
Figure S2. Global copper demand by product category extimated for a eterogeneous development due to isolated economies. High social inequalities scenario The dotted line for electricity generation. This material was published in Ref. [5]. Copyright Elsevier.

Accordingly, copper prices have tripled between 2005 and 2009. This exponential increase of copper price was coinciding with China economic development that restart copper demand. Between 2010 and 2011 copper prices reached a maximum as result of an increase in world demand (6.5%) and a decline in stocks [6]. Copper prices is estimated to increase furtherly due to the growth of the demand (figure S3). To overcome the copper supply and prices and limit the environmental impact of copper mining, circular economy of copper could provide a possible solution that represents the secondary production.
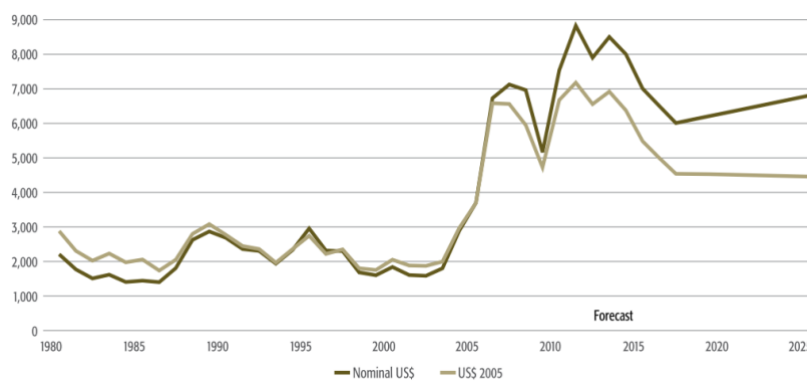
Figure S3. Variation in and Forecast for Copper price (US$/million tons; prices expressed in constant 2005 US$). Adapted from ref. [6].

135

As already mentioned, copper founds application in many diverse industrial processes and technologies. This, obviously, includes heterogeneous catalysis field. In truth, noble metals had found many applications as catalysts active phase due to their good catalytic properties. However, these metals are expensive, toxic and have a low availability in nature. These reasons press the industrial research into find inexpensive and more abundant metals such as copper, iron, nickel, cobalt and so on. Copper based catalysts are widely used in industrial catalysis compared to other metals because they present similar activity and performances without the high costs of noble metals (*i.e.* $/ounce 0.26 cost of copper compared to platinum cost = $/ounce 1011 at January 2023) and high toxicity problems of nickel [3]. Some examples of industrial processes that uses copper catalysts are acrylamide manufacture, dehydrogenation of cyclohexane and hydrogenolysis of ethane to methane. Recently, copper chromite spinel catalysts have been employed successfully in the direct hydrogenation of fats to fatty alcohols that is suitable also for lower quality, acid-containing fats and oil [7].

6.2 Characteristic of the support materials

Silica (silicon dioxide, SiO_2) are amorphous materials that are widely employed in the industry field with many different purposes such as filler, as semiconductor, as insulator *etc.* Due to its inert nature and high surface area, silica is often used as support for heterogeneous metal catalysts. SiO_2 is constituted by interlinked tetrahedral SiO_4 and the structure pattern can end with a siloxane group (Si-O-Si) or with a silanol group (Si-OH). The latter assumes different definitions depending on its location: the silanol is isolated if there are no adjacent silanols, it is vicinal if another silanol, present on an adjacent silicon atom, is close enough to make a hydrogen bond and, eventually, it is geminal if the silanol is bonded to the same Si atom that bears another silanol [8]. The density of the silanol groups present on the surface influences the hydrophilicity of the silica materials. However, depending on the preparation method, silicas can possess different surface and textural properties. Silica can derive from natural resource but usually when it is used with chemical application is obtained from synthetic procedures. There are several methods to synthetize amorphous silica materials. In this thesis, two classes of silica were utilized for the catalyst preparation: silica gel and pyrogenic silica. The former is prepared solubilizing a soluble silicate, *i. e.* alkoxysiloxane, in water and then acid is added. In this way, stable particles of colloidal size are formed by condensation. As condensation proceeds, a gel is formed that is successively dried and washed. Silica gels result in a coherent, rigid, 3D network of contiguous particles of colloidal silica [8]. Silica could be also synthetized using high temperature processes burning $SiCl_4$ with oxygen or hydrogen. In this way, pyrogenic silicas are formed in which primary particles are connected into linear chains and a non-porous structure is formed [8].

Amorphous silica-aluminas (SiO_2-Al_2O_3) are a class of materials that are ubiquitous in the chemical process fields that, thanks to their high surface area and acidic properties, could be utilized as heterogeneous catalysts themselves or as support for metal catalysts.

Low aluminum content SiO_2-Al_2O_3 (Al content between 12-15% wt/wt) are usually fully amorphous. They show the predominant presence of tetrahedral Al ions with small amounts of octahedral Al ions, without significant detection of pentacoordinated Al that increase with the increase of Al quantity. Besides, Si is in the typical silica configuration namely a silicates tetrahedral bonded to four other silicate tetrahedral (Q^4 strucure) that have the tendency to shift to higher ppm positions with the increase of Al content [9].

$SiO_2-Al_2O_3$ can be prepared with different methods both in laboratory and in industrial scale. In the latter case, the cheapest precursor is represented by sodium silicate and sodium aluminate and in this way low Al content, low acidic $SiO_2-Al_2O_3$ can be achieved. Aluminum salts such as aluminum chloride or sulphate can be used instead of sodium aluminate [10].

The peculiar catalytic activity of amorphous $SiO_2-Al_2O_3$ is attributed to their marked acidic character. In spite of their wide applicability, both the structure of these largely or completely amorphous materials and the origin of their acid properties are still not fully clarified and somehow under studies. Characterization techniques had shown the presence of strong Lewis acid sites attributed to Al^{3+} and a limited number of Brønsted acidic sites. In this case, the latter are attributed not, as in zeolitic structures, to bridged -OH groups but to terminal silanols activated by Al^{3+} but not bridged [11] (see Scheme S1).
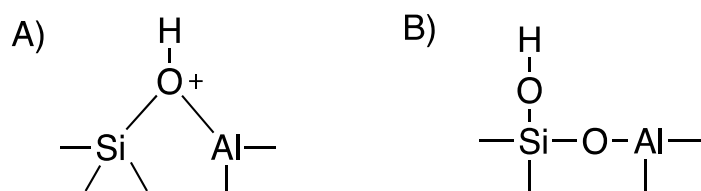
Scheme S1. A) bridged -OH groups in zeolitic materials *vs* B) terminal silanol -OH group.

Other characterization techniques showed that $SiO_2-Al_2O_3$ don't display any type of basic or nucleophilic behaviour, in particular, CO_2 adsorption does not produce any carbonate or bicarbonate species [9].

Hydroxyapatite (HAP), are calcium dibasic phosphate materials with chemical formula $Ca_{10}(PO_4)_6(OH)_2$, that found many different applications in the field of catalysis thanks to its peculiar structure and properties. Its unit cell is composed by a total of ten calcium atoms, organized in two non-equivalent calcium sites: four of them are Ca(I)-type, whereas the remaining six are Ca(II)-type. Considering this, the chemical formula of HAP can be written also as $Ca(I)_4Ca(II)_6(PO_4)_6(OH)_2$. Moreover, the HAP network is characterized by a three-dimensional network of hexagonally packed tetrahedral PO_4^{3-} ions.

Several methods for production of HAP powders exist and they can be classified under four different procedures: dry methods, wet methods, microwave-assisted methods, ball-millingor ultrasound and miscellaneous methods [12].

HAP is characterized by a unique compositional and structural flexibility: it can possess a high number of defects or it can be modified by ionic substitution without changing

its lattice and structural properties. According to these features HAP can be classified as stoichiometric with a Ca/P ratio of *ca.* 1.67; calcium deficient with a Ca/P ratio less than 1.67 or carbonate-rich [13]. Due to these features, it presents a marked adsorption capacity and peculiar surface functionalization that confers acid-basic properties. The surface hosts different functional groups, organized as acid and basic sites of different interaction strength: Ca^{2+} and HO^- vacancies impart Lewis acidity, Ca^{2+} vacancies and O^{2-}, PO_4^{3-} and HO^- confers basicity while Brønsted acidity could be ascribable to HPO_4^{2-} groups [14].

Aluminas, (Al_2O_3, namely aluminum oxide) is an important class of materials that founds many different industrial applications. It is available in different structural configuration that possess diverse properties. Some of these are $\alpha-Al_2O_3$ (corundum), and metastable phase aluminas, such as, $\gamma-Al_2O_3$, $\eta-Al_2O_3$ and $\rho-Al_2O_3$ [2,15]. $\gamma-Al_2O_3$ is the most used in catalysis mainly as support for catalysts synthesis due to its high mechanical strength, surface area and low cost. Moreover, $\gamma-Al_2O_3$ can be used as catalysts itself thanks to its surface acidic and basic groups. It is produced through thermal dehydration of the mineral boehmite that change structure with the increase of temperature (Boehmite → γ → δ → θ → α, α- Al_2O_3 (corundum) being the most thermodynamically stable phase) [16].

Despite the wide research into $\gamma-Al_2O_3$, the precise definition of its structure is still unresolved. One model proposes that it consists of irregularly stacked nanocrystals with all Al^{3+} cations that occupies spinel positions, while one other that Al^{3+} cations occupy non-spinel positions and, finally, a third model proposes that γ- Al_2O_3 does not have a spinel structure [15].

The surface properties of $\gamma-Al_2O_3$ have been widely studied like acidity, basicity and zero point charge. The latter has been reported to be in a range between pH 6-9 depending on the synthesis of the Al_2O_3 and the measuring technique used [16].

$\gamma-Al_2O_3$ is a bifunctional catalyst that possess acidic and basic sites that are able to catalyze a wide number of reactions. Surface acidity has been attributed doubtlessly to Al^{3+} while surface basicity to oxygen anions. Moreover, hydroxyl groups can have acidic as well as basic character (see Scheme S2). The surface concentration of these sites depends on the surface dehydration of the material: the more is the dehydration the lower the surface hydroxides [17].
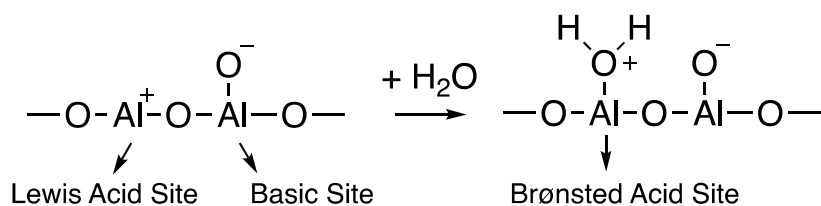
Scheme S2. Acid and basic sites on γ-Al$_2$O$_3$.

Zirconia (ZrO$_2$, zirconium oxide) is a polymorphic crystalline material with exceptional tensile strength, hardness and corrosion resistance. It can be found in nature as a mineral called baddeleyite that is purified by various processes. Alternatively, it is more commonly obtained as an intermediate in recovering zirconium from zircon, ZrSiO4. On laboratory scale, it is produced through thermal decomposition of zirconium hydroxide or zirconium carbonate [2].

It exists in four solid phases: monoclinic, tetragonal, orthorhombic, and a cubic fluorite structure depending on the temperature and pressure conditions [18]. The cubic structure can be stabilized at lower temperatures by the introduction of vacancies in the anion lattice adding other oxide such as SiO$_2$ [19]. The coordination of Zr and O are different depending on the phase state: for instance, the Zr^{4+} cation is octacoordinated, and the O^{2-} anion is tetracoordinated in a tetragonal phase, whereas the Zr^{4+} cation is heptacoordinated, and the O^{2-} anion is either tri or tetracoordinated in a monoclinic phase [20]. ZrO$_2$ can possess different acidic or basic properties. Brønsted basicity or acidity can be conferred by the amphoteric hydroxyl groups while Lewis basicity is attributable to of coordinately unsaturated O^{2-} species while the Lewis acidity is ascribable to Zr^{4+}. Moreover, this species could form acid-basic pairs.[21]. It was demonstrated that ZrO$_2$ can change the surface acidity or basicity varying calcination temperatures.

Titania (TiO$_2$, namely titanium dioxide) is a semiconduction material with a wide band gap (3.2 eV) under ultraviolet light. Furthermore, it possesses a high physical and chemical stability and due to its excellent properties it founds application in many fields such as solar cells, photocatalysis, electrochemistry and heterogeneous catalysis.

The naturally occurring TiO$_2$ exists in three crystalline forms: anatase, rutile and brookite. Rutile, the most common form, has an octahedral structure, meanwhile, Anatase and brookite have very distorted octahedral oxygen atoms surrounding each titanium atom. Titanium dioxide can be mined from natural resources. It also is produced from other

titanium minerals or prepared in the laboratory [2]. Due to its excellent properties, it founds more applications in particular as support for the synthesis of heterogeneous catalysts [2,22]. In addition, TiO_2 surface has a marked amphoteric nature. It was modeled that the strucure of the crystal leads to two types of -OH groups, one bounded to one Ti^{4+} terminal sites and one bridged between two Ti^{4+} sites. The former present a predominantely basic character wile the latter should be strongly polarized by cations and therefore be acidic [23]. Moreover Ti^{4+} presents a typical Lewis acidic character [24].

6.3   Chemisorption Hydrolysis method

Chemisorption-Hydrolysis is a method for Cu deposition on different supports that combine the easiness of impregnation techniques while ensuring high metal dispersion and low particle size. The nature of the support and the pH of the preparation solution have a pivotal role in shaping the metallic phase. Actually, the surface polarization of a solid material changes depending on the pH of the solution and on the isoelectric point of the solid. When the pH is below the isoelectric point, or Point of Zero Charge (PZC), of the surface polarization equation (1) of the support is:

$$S\text{-}OH + H^+A^- \Leftrightarrow S\text{-}OH_2^+ + A^- \qquad (1)$$
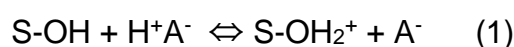
In this way the surface will be positively charged and, as consequence, will attract and adsorb anions for electrostatic reasons. On the other hand, if pH is above the PZC the equilibrium equation (2) is:

$$S\text{-}OH + B\text{-}OH^- \Leftrightarrow S\text{-}O\text{-}B^+ + H_2O \qquad (1)$$
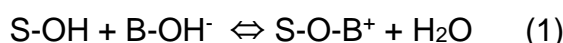
Thus, the surface will be negatively charged and will attract the surrounding cationic species that will be adsorbed.

According to this concept, the operation steps of the Chemisorption-Hydrolysis were set up in the following procedure (Figure 1.5):
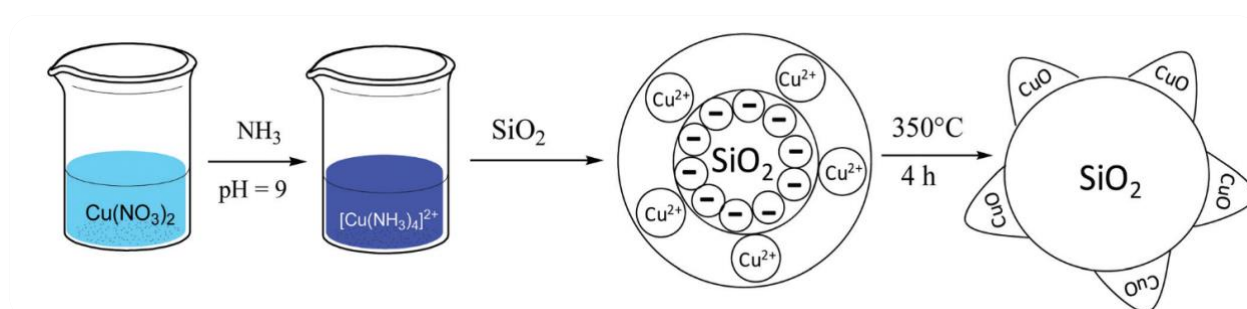
Figure S4. Chemisorption-Hydrolysis preparation scheme. Reproduced from Ref. [25] with permission from the Royal Society of Chemistry.

1. Preparation of $[Cu(NH_3)_4]^{2+}$ complex by dropping NH_4OH to a $Cu(NO_3)_2 \cdot 3H_2O$ solution at the desired concentration until pH 9 has been reached
2. Dispersion of support powder to the readily prepared solution
3. Hydrolysis of the $[Cu(NH_3)_4]^{2+}$ complex by diluition with distilled water at 0 °C

4. Filtration and calcination (350 °C, 4 h) of the solid to obtain CuO/support catalyst

With this procedure, it is possible to obtain high dispersion of the copper phase even at very high metal loading with low particle size (3-6 nm as average), while the impregnation methods, such as incipient wetness (IW), produces particle size ten times larger, thus forming bigger aggregates. This was confirmed using Temperature-Programmed-Desorption, X-Ray Diffraction (XRD) and Transmission Electronic Microscopy (TEM) as investigation techniques. [25,26] For instance, in figure 1.4 XRD patterns of CuO/SiO_2 (12 % Cu wt/wt) indicates the typical signal of CuO only for the samples prepared with IW samples (mean particle size estimated: 34 nm), while no signals are registered in the diffractogram of CH sample collected under the same conditions, suggesting that either the structure of copper species is amorphous or their size is very small. Increasing the counting time (Figure 1.6 c)) produces a very broad signal, caused by the finely dispersion of copper oxide.
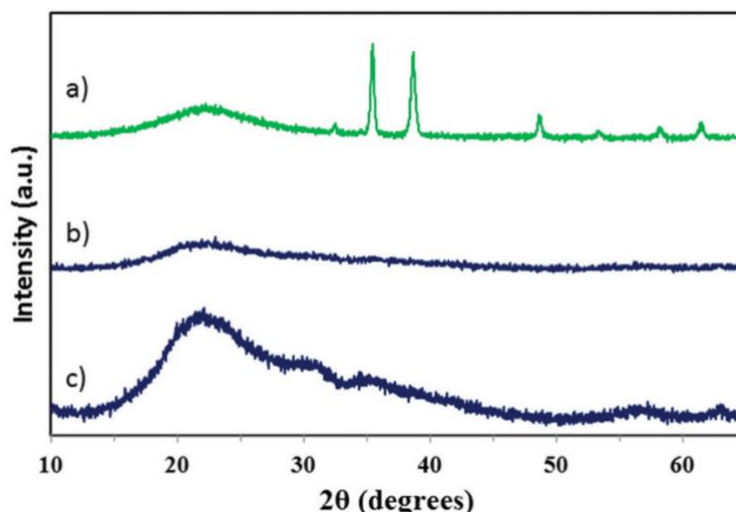
Figure S5. XRD analysis of (a) 12 % CuO/SiO2 (Incipient Wetness) (1 second per step); (b) 12% CuO/SiO_2 CH (1 second per step) and (c) 12% CuO/SiO_2 CH (4 seconds per step). Reproduced from Ref. [25] with permission from the Royal Society of Chemistry.

Moreover, High-Resolution TEM analysis micrograph and FT patterns of a CuO/SiO_2 (16% Cu wt/wt) were in good accordance with the presence of cuboctahedron copper particles. The metallic phase was again high dispersed with small and highly defective Cu nanoparticles [27].

The peculiar feature of the copper phase deposited with CH method confers outstanding reactivity to the copper oxide nanoparticles, particularly, an unexpected Lewis

acidic character. In fact, FT-IR spectra after pyridine desorption of CuO/SiO_2 (12 % Cu wt/wt) prepared with CH showed the presence of Lewis acid sites on its surface while the spectra of the sample prepared with IW was mute [25]. This feature can be ascribed to the high dispersion of the metallic phase and surface defectivity. Moreover, if the CuO phase is reduced to Cu^0 the material not only preserves the acidity of the non-reduced precursor but also show an increase in Lewis acidity [27].

All the described features, confers the Cu catalyst prepared with CH method excellent catalytic properties, especially if compared with the IW samples. For example, a pronounced difference in activity was observed in the hydrogenation of 1,3-cyclooctadiene to cyclooctene if catalysts prepared with CH and IW are compared. In fact, the former showed turnover frequencies 100 times greater than the latter [28]. More recently, it was reported that a 75% yield of sorbitol and dulcitol can be obtained by CuO/SiO_2 CH in the one-pot hydrolysis and hydrogenation of lactose in water while only 6% yield can be reached with the IW catalyst with the formation of important decomposition products under the same reaction conditions and Cu loading [29].

Considering these results, it can be derived that CH method offers the possibility to prepare supported metal catalysts that on one hand have the characteristic catalytic features of a metallic phase such as hydrogenation or dehydrogenation with higher performances with respect to the catalysts prepared with traditional techniques and on the other also show unusual moderate acidity properties that are preserved even if the copper phase is reduced. This makes CH Copper Catalyst perfect examples of robust bifunctional materials easy to prepare and suitable for biomass valorization catalytic processes.

6.4 Nitrogen adsorption and desorption isotherms of the materials
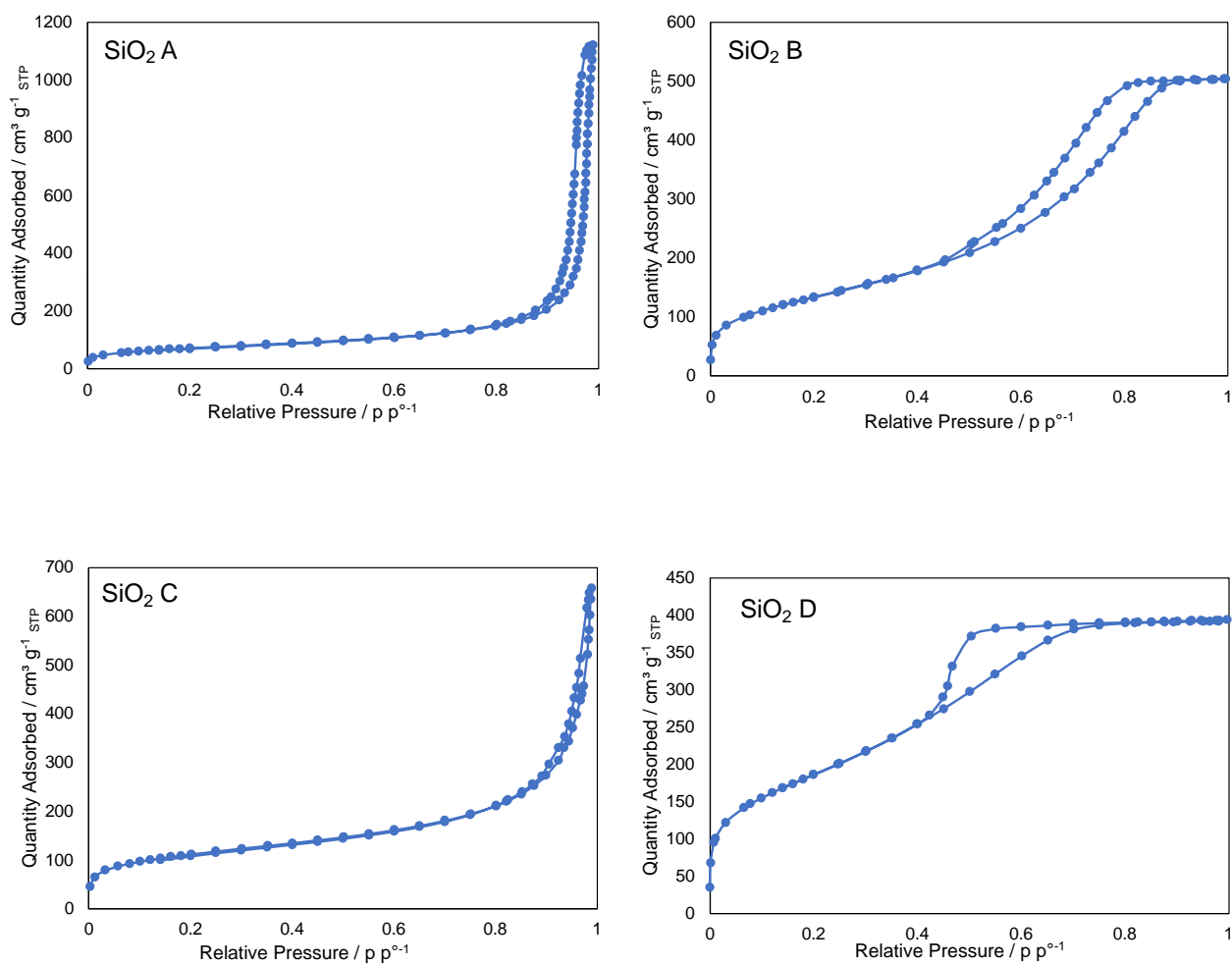
Figure S6. N_2 adsorption and desorption isotherms of the silica materials collected at T = -176 °C. Top left: SiO_2 A, top right: SiO_2 B, bottom left: SiO_2 C, bottom right: SiO_2 D.
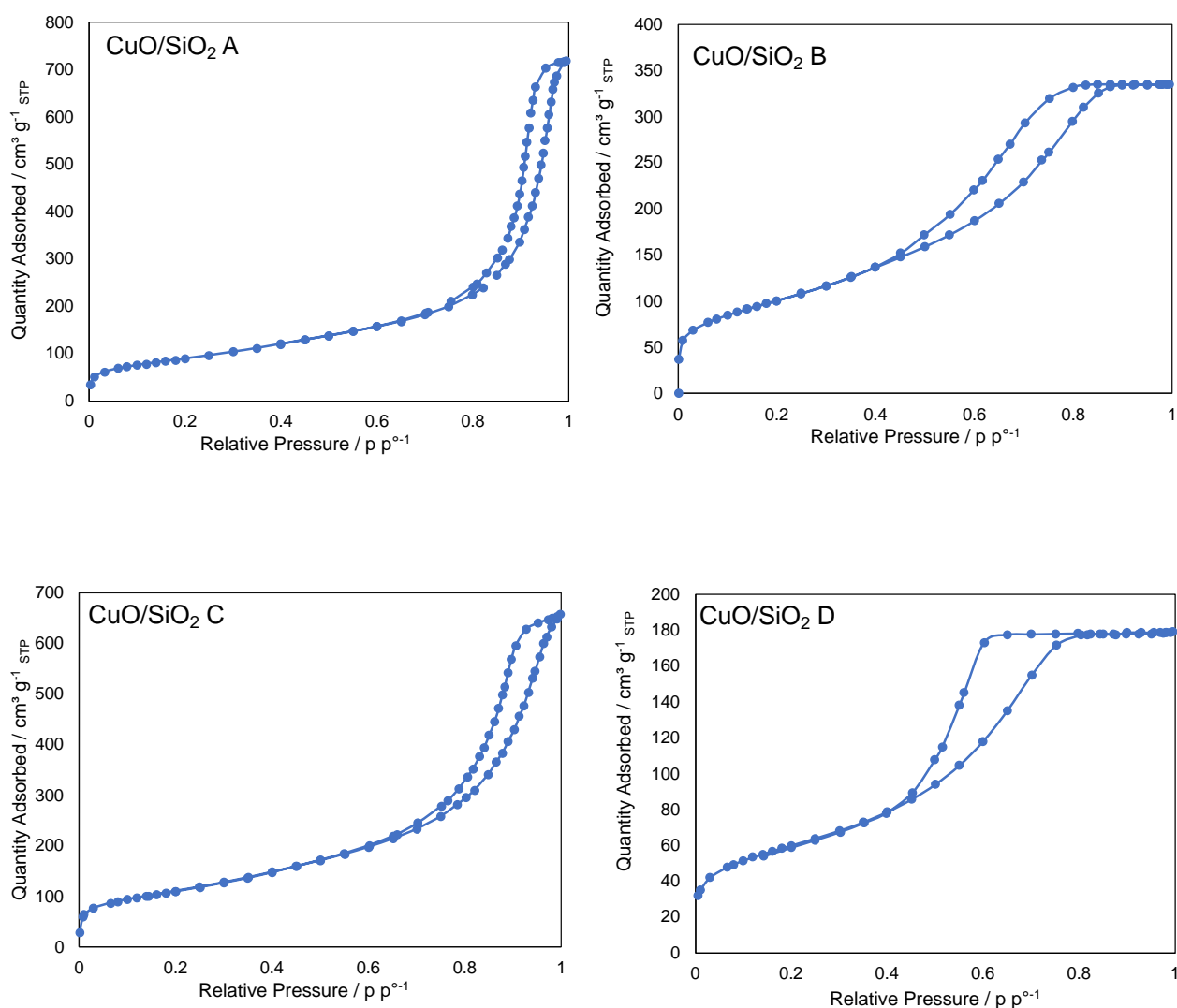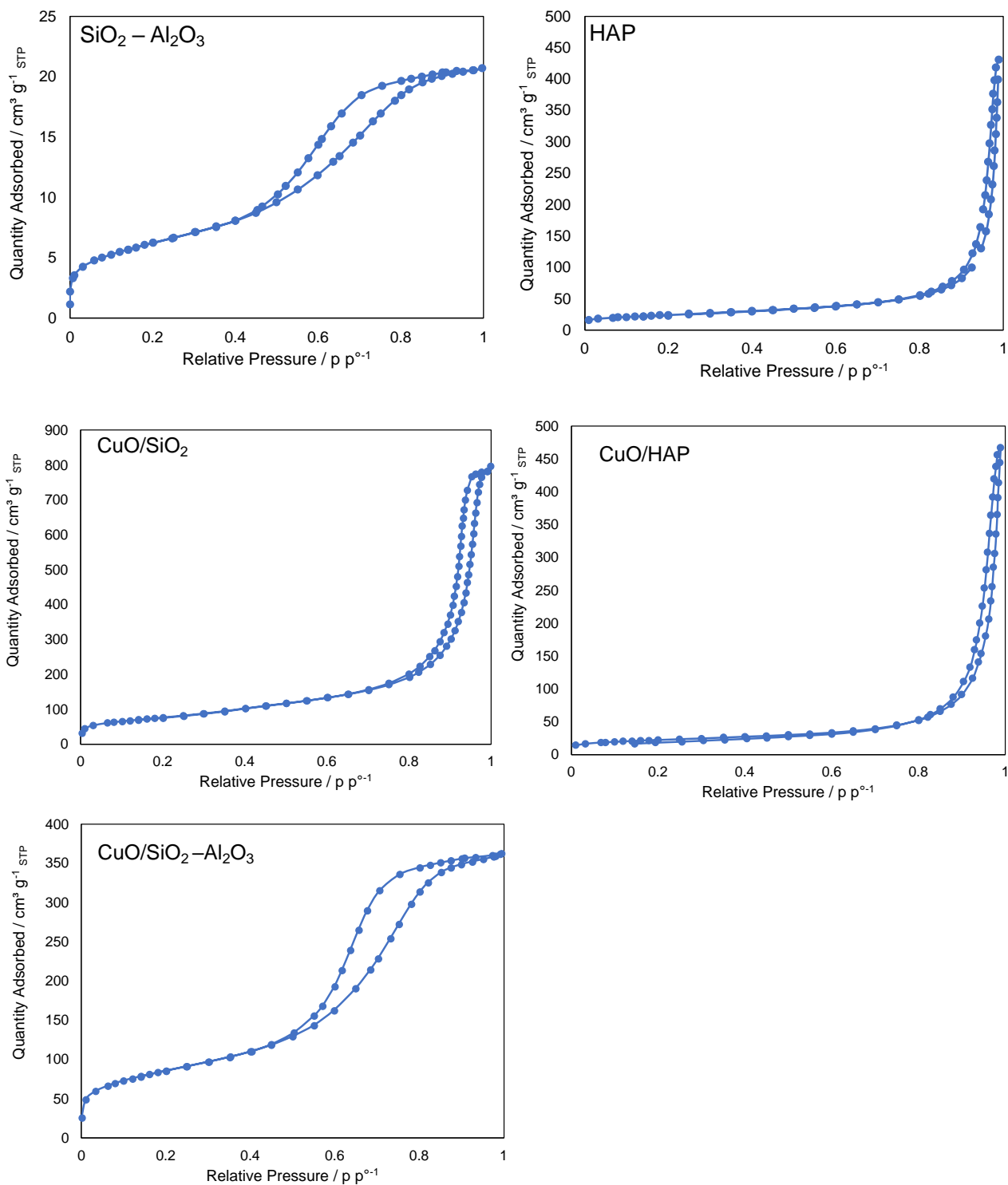
Figure S7. N$_2$ adsorption and desorption isotherms of the CuO/SiO$_2$ catalysts collected at T = -176 °C. Top left: CuO/SiO$_2$ A, top right: CuO/SiO$_2$ B, bottom left: CuO/SiO$_2$ C, bottom right: CuO/SiO$_2$ D.
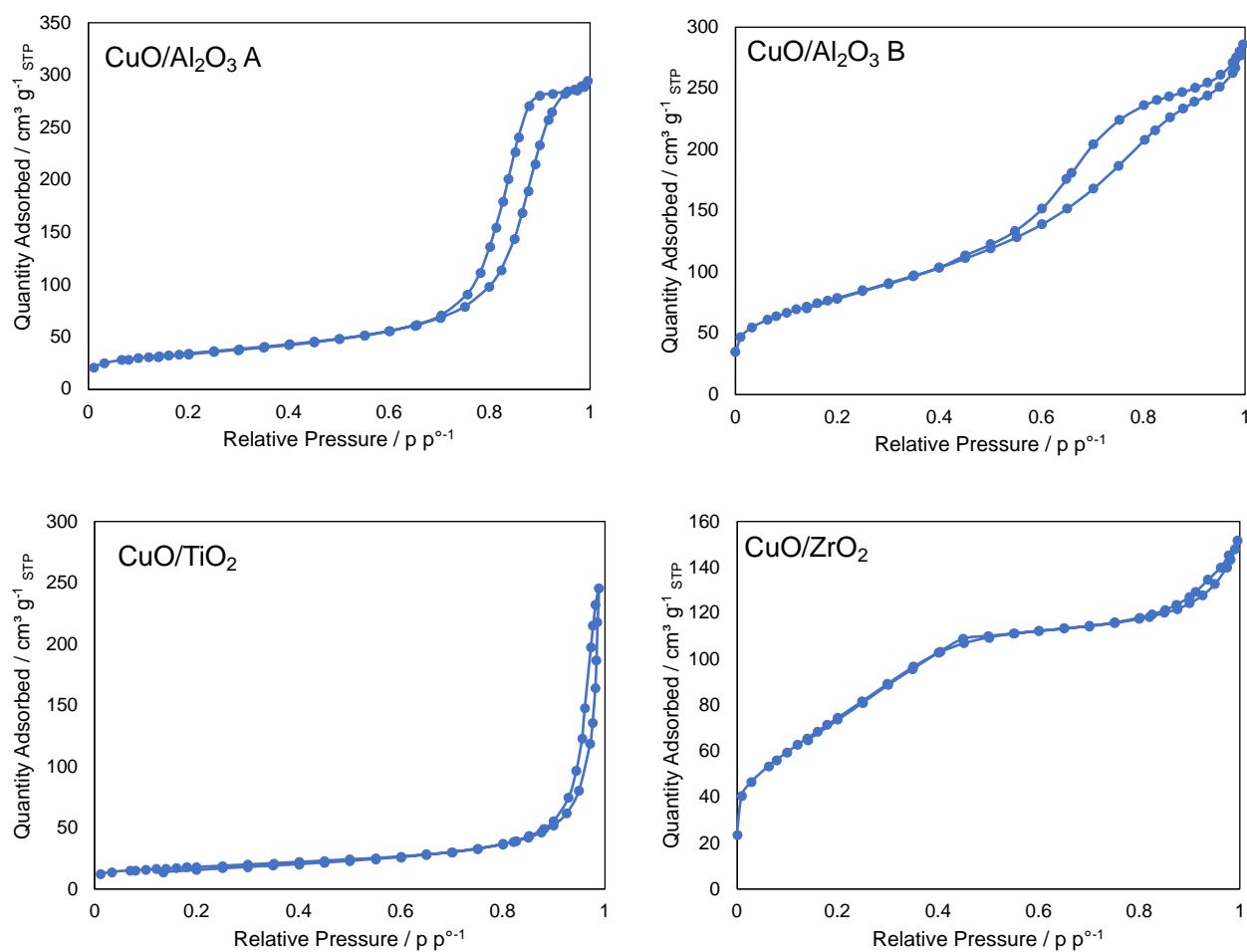
Table S1 Specific Surface Area (SSA) and Pore Volume (PV) of the CuO/SiO$_2$ catalysts.

	SSA / m^{2}g^{-1}	PV / cm^{3}g^{-1}
CuO/SiO$_2$ A	323	1.12
CuO/SiO$_2$ B	364	0.53
CuO/SiO$_2$ C	396	1.01
CuO/SiO$_2$ D	211	0.28
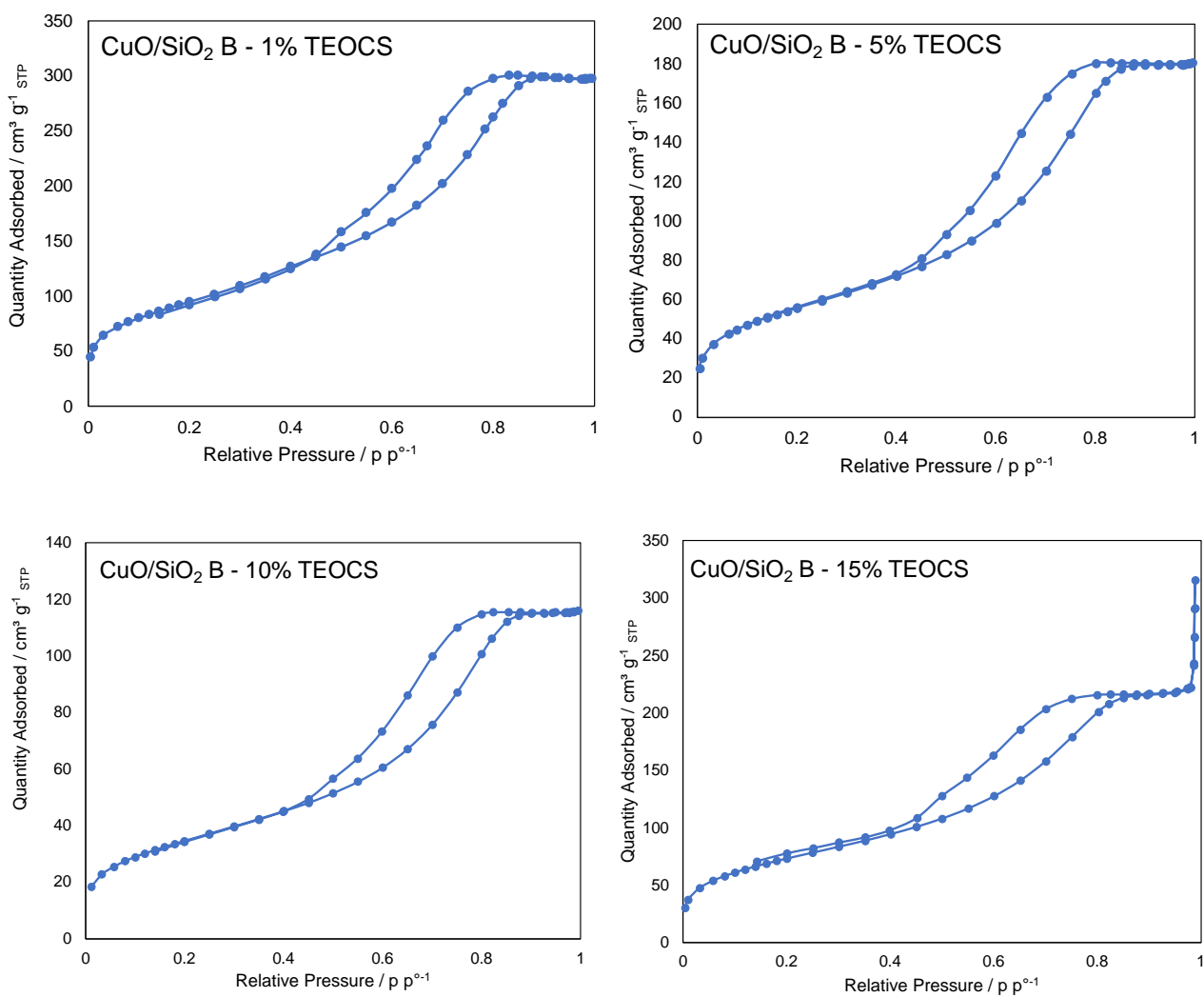
Figure S8. N_2 adsorption and desorption isotherms of the TEOCS functionalized CuO/SiO$_2$ B catalysts collected at T = -176 °C. Top left: CuO/SiO$_2$ - 1% TEOCS, top right: CuO/SiO$_2$ - 5% TEOCS, bottom left: CuO/SiO$_2$ -10% TEOCS, bottom right: CuO/SiO$_2$ -15% TEOCS.

Figure S9. N_2 adsorption and desorption isotherms of the CuO catalysts collected at T = -176 °C. Top left: CuO/SiO_2, top right: CuO/HAP, bottom left: CuO/SiO_2 -Al_2O_3.
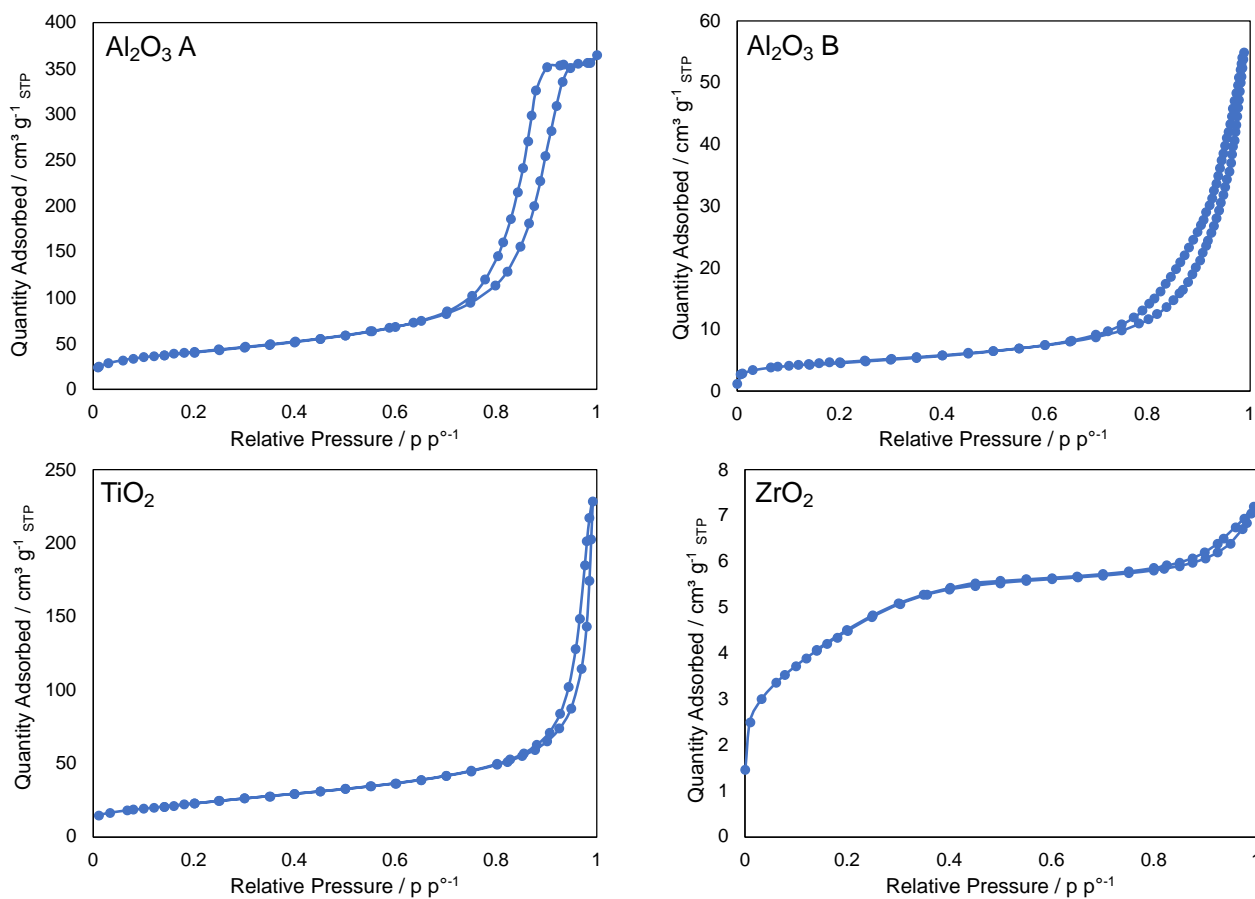
Figure S10. N_2 adsorption and desorption isotherms of the CuO catalysts collected at T = -176 °C. Top left: Al_2O_3 A, top right: Al_2O_3 B, bottom left: TiO_2, bottom right ZrO_2 .

Figure S11. N$_2$ adsorption and desorption isotherms of the CuO catalysts collected at T = -176 °C. Top left: CuO/Al$_2$O$_3$ A, top right: CuO/ Al$_2$O$_3$ B, bottom left: CuO/TiO$_2$, bottom right CuO/ZrO$_2$.

Table S2 Specific Surface Area (SSA) and Pore Volume (PV) of support used for catalyst preparation.

	SSA / m^{2}g^{-1}	*PV / cm^{3}g^{-1}*
HAP	84	0.67
SiO$_2$ – Al$_2$O$_3$	496	0.74
Al$_2$O$_3$ A	147	0.56
Al$_2$O$_3$ B	363	1.90
TiO$_2$	81	0.36
ZrO$_2$	357	0.20

6.5 X-Ray Photolectron Spectroscopy

Table S3. Binding energies of deconvoluted Cu 2p spectra of CuO/SiO_2 A and CuO/SiO_2 B before and after reduction.

CuO/SiO_2 A			
Cu 2p$^{3/2}$ (eV)		Cu 2p$^{1/2}$ (eV)	
Peak 1	935.5	Peak 4	955.3
Peak 2	937.7	Peak 5	958.1
Peak 3	944.5	Peak 6	964.2
CuO/SiO_2 B			
Cu 2p$^{3/2}$		Cu 2p$^{1/2}$	
Peak 1	933.6	Peak 4	953.4
Peak 2	935.8	Peak 5	955.5
Peak 3	943.9	Peak 6	963.5
Cu/SiO_2 A			
Cu 2p$^{3/2}$		Cu 2p$^{1/2}$	
Peak 1	933.1	Peak 3	952.9
Peak 2	934.6	Peak 4	954.5
Cu/SiO_2 B			
Cu 2p$^{3/2}$		Cu 2p$^{1/2}$	
Peak 1	932.7	Peak 3	952.3
Peak 2	934.5	Peak 4	954.2

6.6 Thermogravimetric Analysis
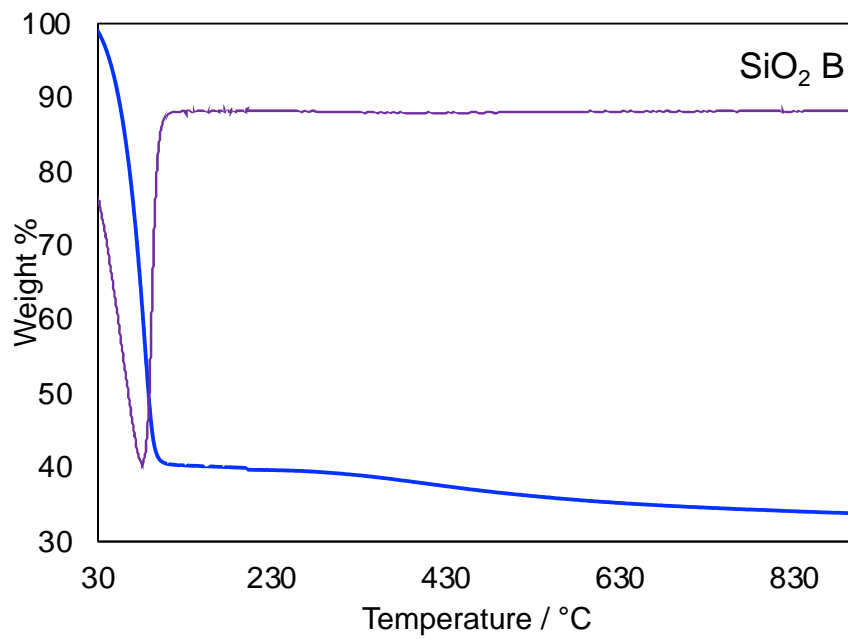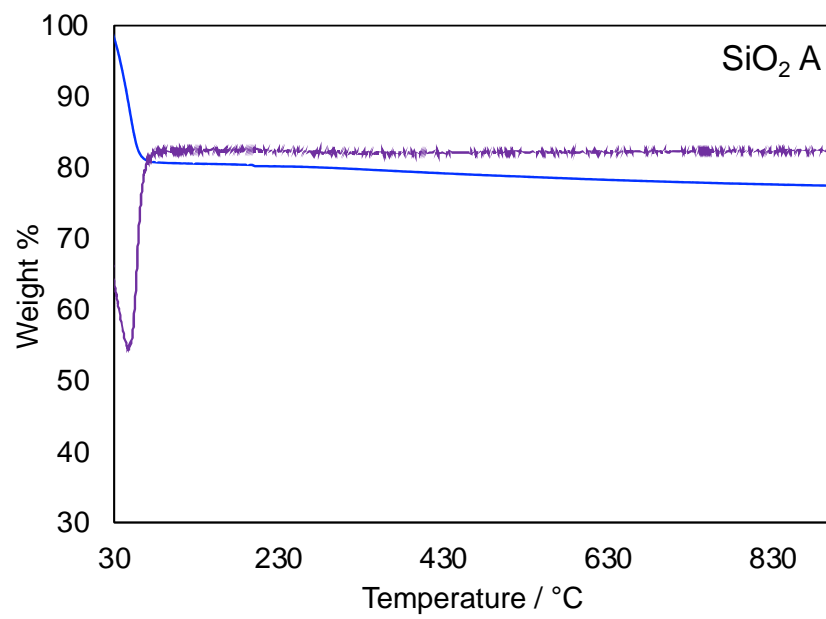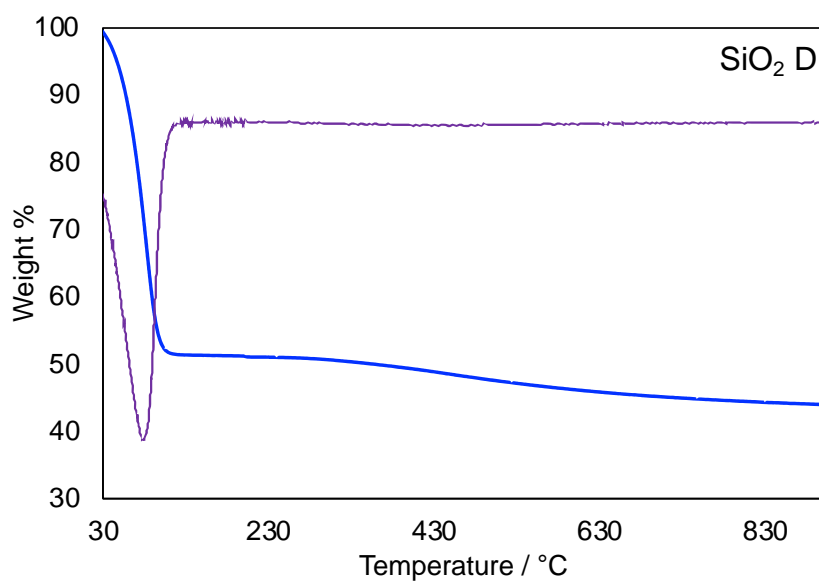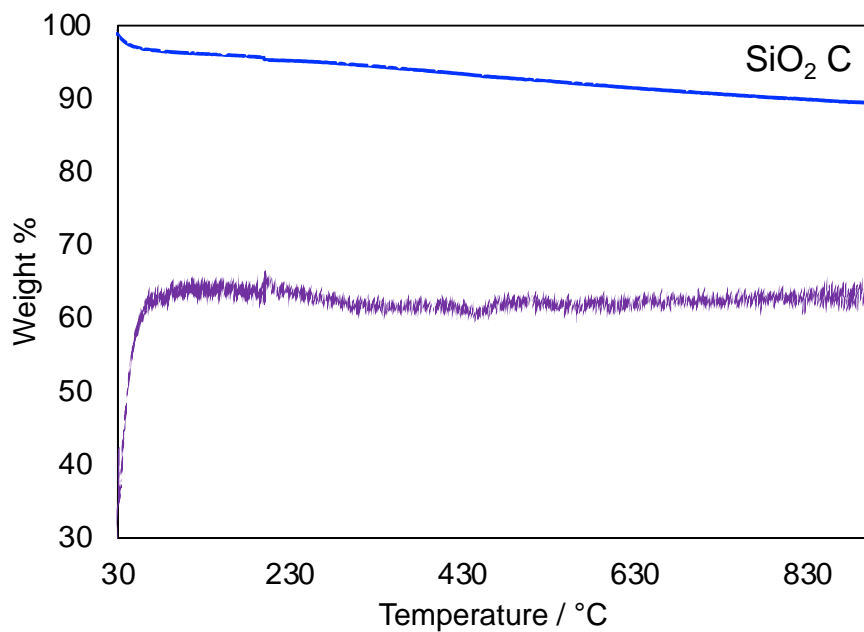
Figure S12. Thermogravimetric analysis thermograms of the SiO_2 materials recorded as following: (i) heating at rate of 5 °C min^{-1} from 25 to 200 °C; ii) maintenance of the temperature of 200 °C for 30 min and iii) heating at rate of 10 °C min^{-1} up to 900 °C
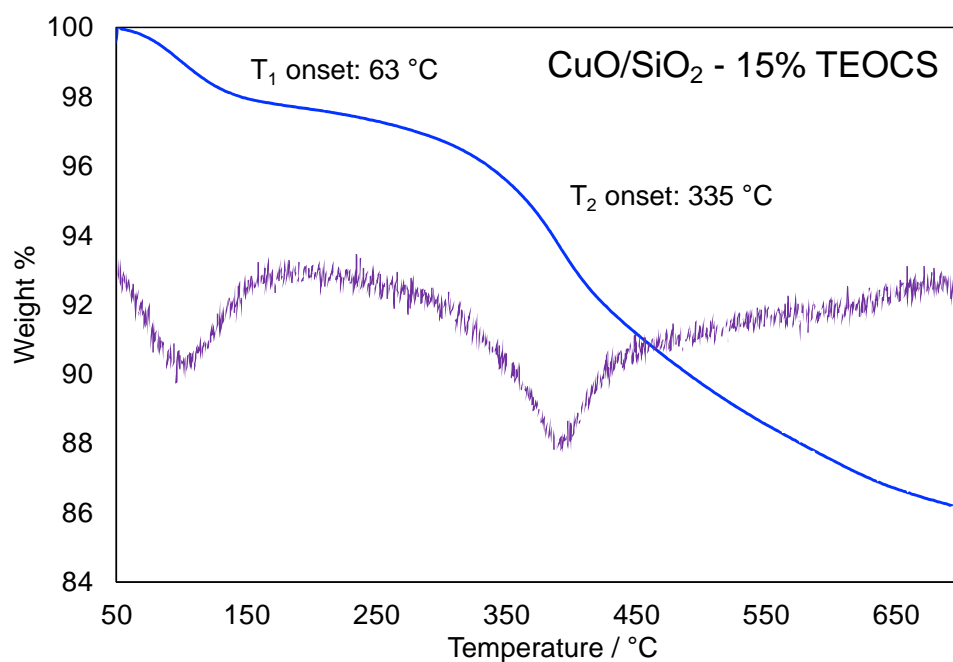
CuO/SiO$_2$ - 5% TEOCS

T$_1$ onset: 68 °C

T$_2$ onset: 320 °C

CuO/SiO$_2$ - 10% TEOCS

T$_1$ onset: 63°C

T$_2$ onset: 322 °C
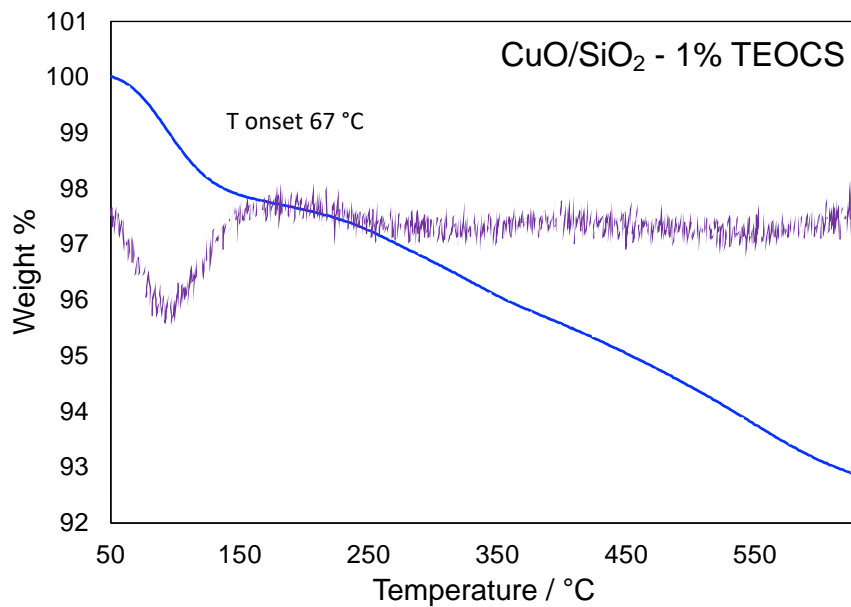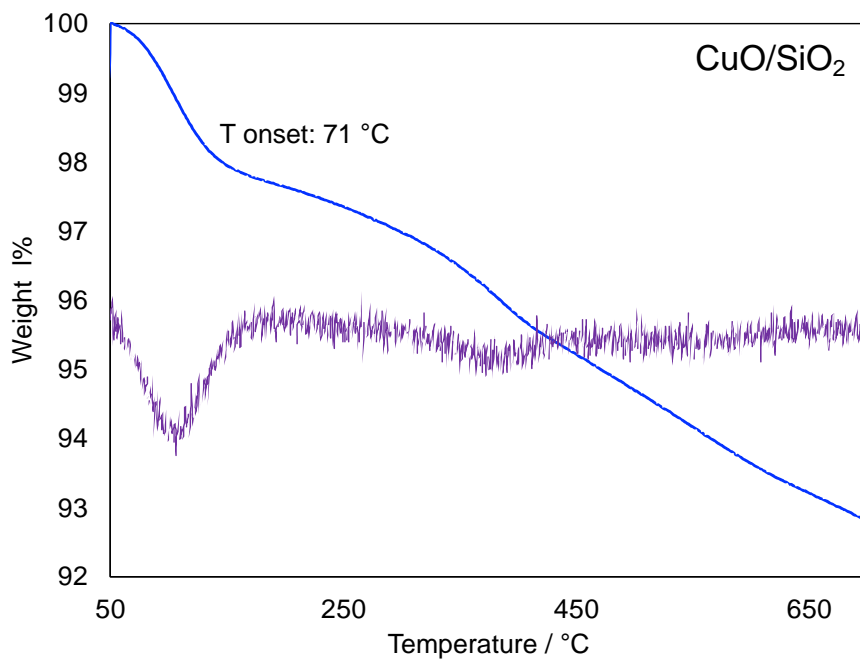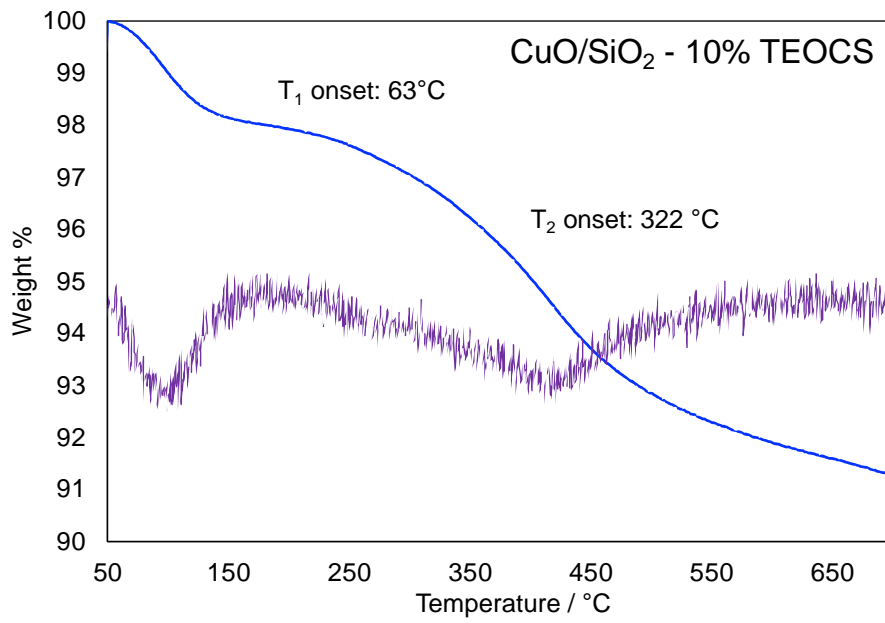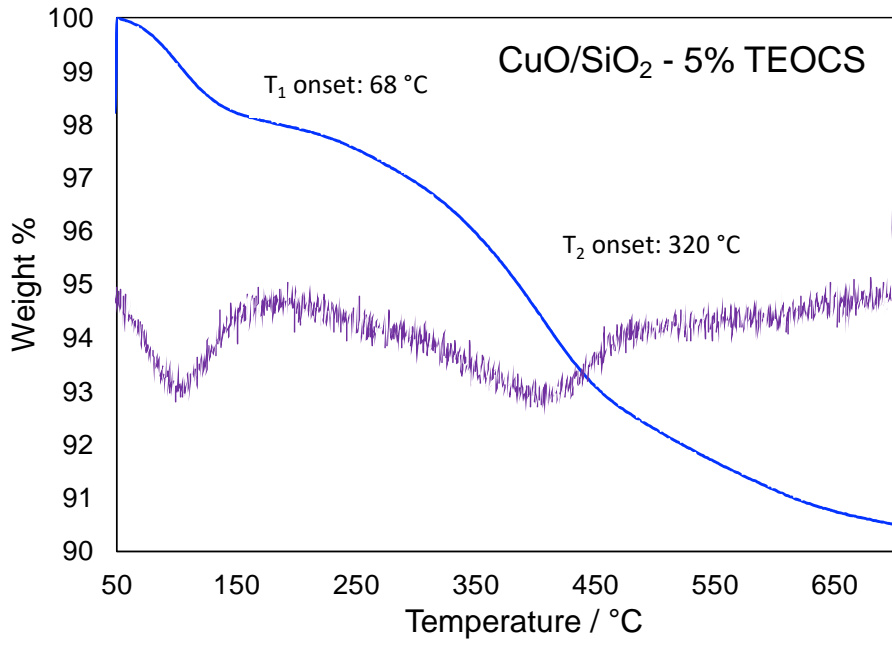
Figure S13. Thermogravimetric analysis thermograms of the TEOCS functionalized CuO/SiO_2 B catalysts recorded as following: (i) isothermal step at 50 °C for 10 min; (ii) heating at rate 20 °C min^{-1} up to 700 °C.

Table S4. TGA results from 200 ° to 700 °C for the catalysts sample.

Sample	T^a_{onset} /°C	T^b_{onset} /°C	T^b_{end} /°C	Δm % (200-700 °C)
CuO/SiO_2	71	-		4.5
CuO/SiO_2 - 1% TEOCS	67	-		4.6
CuO/SiO_2 - 5% TEOCS	68	320	492	6.7
CuO/SiO_2 - 10% TEOCS	63	322	508	6.1
CuO/SiO_2 - 15% TEOCS	63	335	>650	10.1

6.7 Transmission electron microscopy
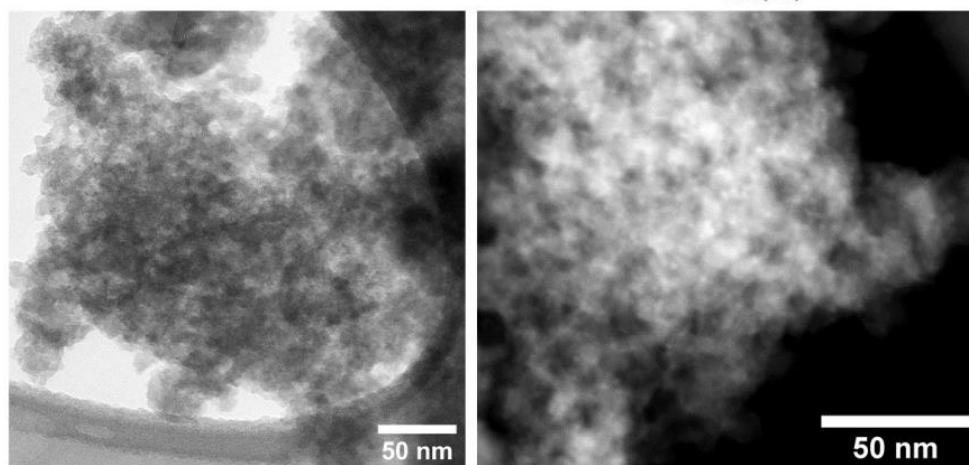
Figure S14. Representative micrographs for sample CuO/SiO_2 - 15 % TEOCS. On the left bright field TEM image and on the right side HAADF-STEM image (copper particles are the brighter roundish spots). Adapted from ref. [30], Copyright Elsevier.

6.8 Liquid-solid acid-base titration – Langmuir modelization

6.8.1 Langmuir isotherm

Langmuir adsorption isotherm model was developer to describe gas-solid adsorption phenomena. According to Langmuir theory, adsorption process of a gas adsorbate onto a solid surface is based on a kinetic principle according to which a continuos adsorption process of molecules onto the surface that corresponds to immediate desorption from the surface with zero accumulation rate at the surface [31]. Postulates of the model are the homogeneity of the sorbent sites toward the target species, the absence of interaction between adsorbate species on the surface, mono-layer coverage of the surface and constant heat of adsorption [31].

The linear form of Langmuir adsorption isotherm is described by the following equation (1):

$$\bullet \quad \frac{C_e}{q_e} = \frac{1}{n_{max}\, b} + \frac{C_e}{n_{max}} \quad (1)$$

- C_e is the equilibrium concentration of the adsorbate in the bulk phase (mmol L^{-1});
- q_e is the equilibrium concentration of the adsorbate on the sorbent (mmol g^{-1});
- n_{max} is the maximum monolayer coverage of the adsorbate on the sorbent (mmol g^{-1});
- b_{ads} is the Langmuir constant, indicative of the adsorbate-sorbent interaction strength (L mmol^{-1}).

6.8.2 Data curation

Experimental adsorption isotherms obtained by liquid-solid titration of the sample using phenylethylamine (PEA) collected in I and II runs have been modeled according to Langmuir model equation. In this case C_e represents the PEA probe concentration in the solution while q_e represent the PEA concentration adsorbed onto the sample surface. Adsorbed PEA can be calculated subtracting the moles of PEA in the operating solution to the ones actually injected by the operator (see experimental section for the operating procedure). After calculating C_e and q_e at each equilibrium steps, a linear regression is

performed to obtain n_{max}, that is the maximum amount of absorbed probe ($mol_{PEA} g_{cat}^{-1}$), and b_{ads}, that is the adsorption constant (M^{-1}). Notably, n_{max} can be considered equal to the number of acidic sites present on the sample surface, if a 1:1 stoichiometry is assumed between the PEA molecule and adsorption site.

The I run experimental isotherm can be associated with PEA adsorption on the total acid sites of the sample surface, namely weak and strong. Hence, its linear regression returns the total number of surface acid sites. Meanwile, II run experimental adsorption isotherms concearns only weak acid sites. In fact, washing with fresh solvent between the two runs is insufficient to desorb PEA probe from the strong acid sites. With its linear regression, it is possible to obtain weak acid sites quantification.

Subsequently, at given probe concentrations, a subtraction of the quantity of probe adsorbed in II run from the one adsorbed in I run was made. In this way, a new set of data is obtained: a set of PEA C_e concentration corresponding to the equilibrium steps of the I run to which each computed q_e is associated. Again, the data are linearly regressed according to equation (1) to obtain n_{max} that corresponds to the quantity of strong acid sites.

6.8.3 Calibrations

The linearity between the absorbance and PEA probe concentration in the titration solvents, namely cyclohexane, cyclopentyl methyl ether (CPME), dioxane and heptane, was evaluated performing UV spectra of various solutions of PEA in the solvents and elaborating them with the Lambert-Beer equation (2)

$$A = \varepsilon LC \quad (2)$$

Where:
- A = absorbance of the solution measured at λ = 254 nm that is the characteristic absorption wavelenght of PEA
- L = path length of the beam
- C = PEA solution concentration
- ε = molar attenuation coefficient

Calibration lines were realized to obtain the molar attenuation coefficient of PEA in each solvent.
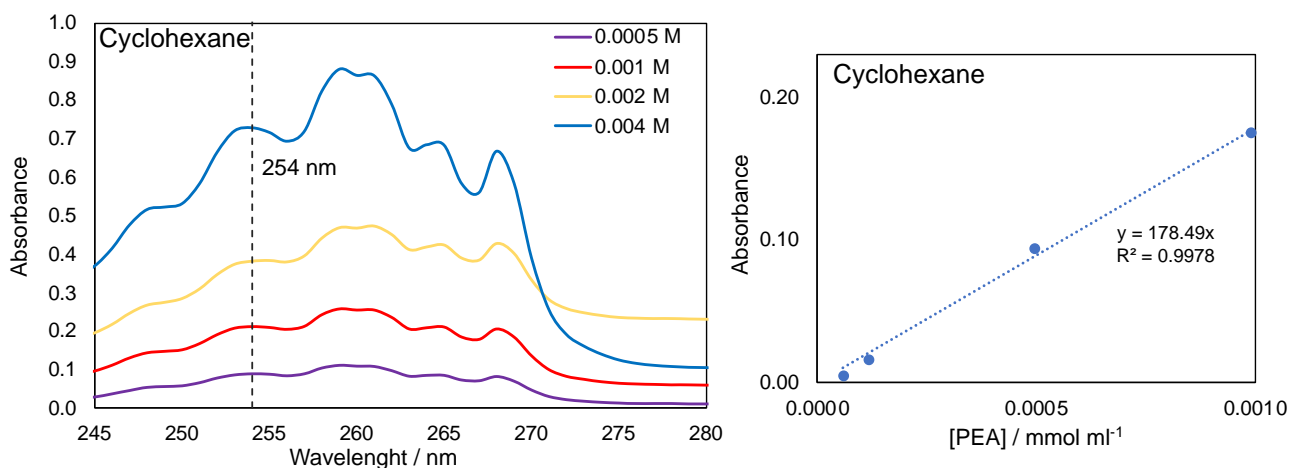
Figure S15. Left: UV spectra of various solutions with concentration of PEA in cyclohexane. Right: calibration line A *vs* Concentration of PEA in cyclohexane.
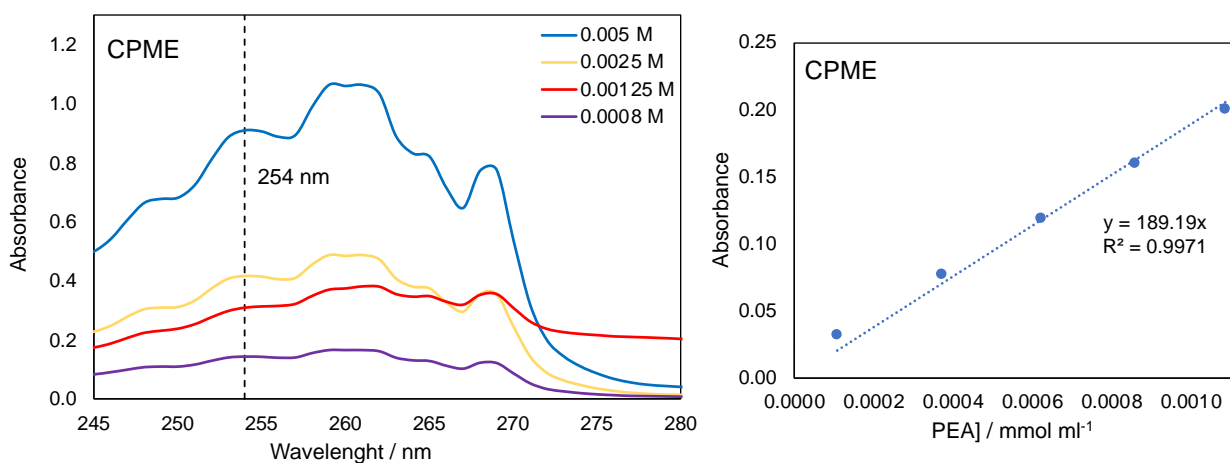

Figure S16. Left: UV spectra of various solutions with concentration of PEA in CPME. Right: calibration line A *vs* Concentration of PEA in CPME.
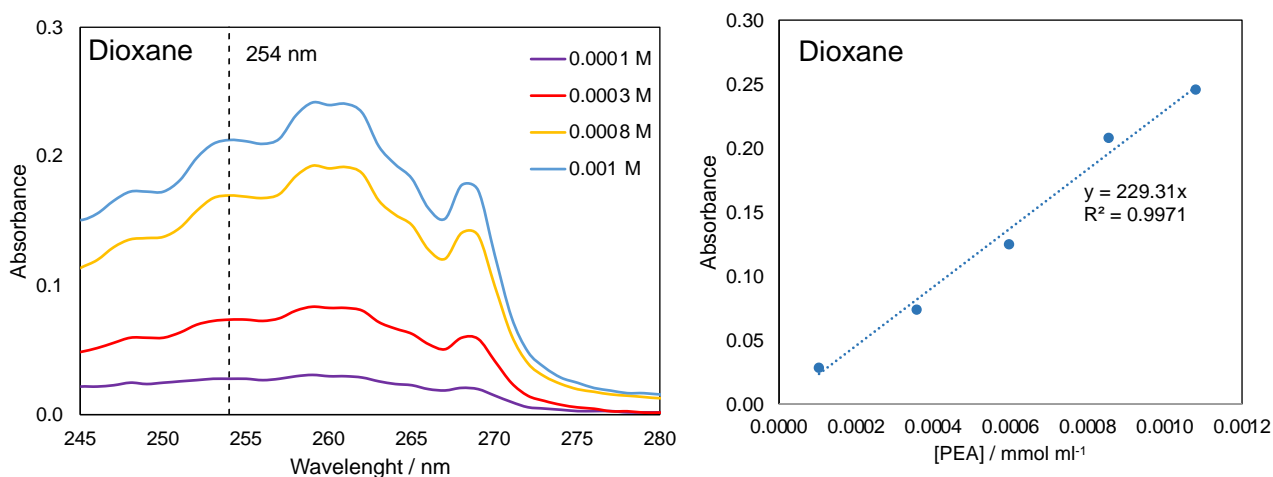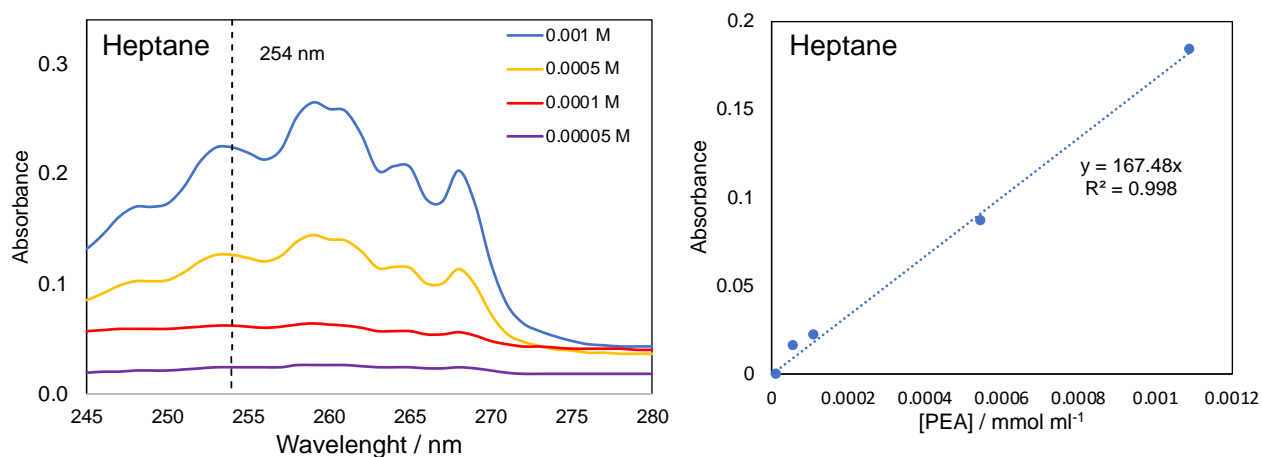
Figure S17. Left: UV spectra of various solutions with concentration of PEA in dioxane. Right: calibration line A *vs* Concentration of PEA in dioxane.

Figure S18. Left: UV spectra of various solutions with concentration of PEA in heptane. Right: calibration line A *vs* Concentration of PEA in heptane.

Table S5. Molar extinction coefficients of PEA in the solvents of interest.

	Cyclohexane	CPME	Dioxane	Heptane
Molar extinction coefficient ε ($mol^{-1}L\ cm^{-1}$)	178.5 ± 4.3	189.2 ± 3.5	229.3 ± 6.2	167.5 ± 3.8

Successively, calibrations between the HPLC line detector signal and PEA concentration in the titration solvents were performed to obtain the characteristic response factor (RF) in each solvent (figure XX).
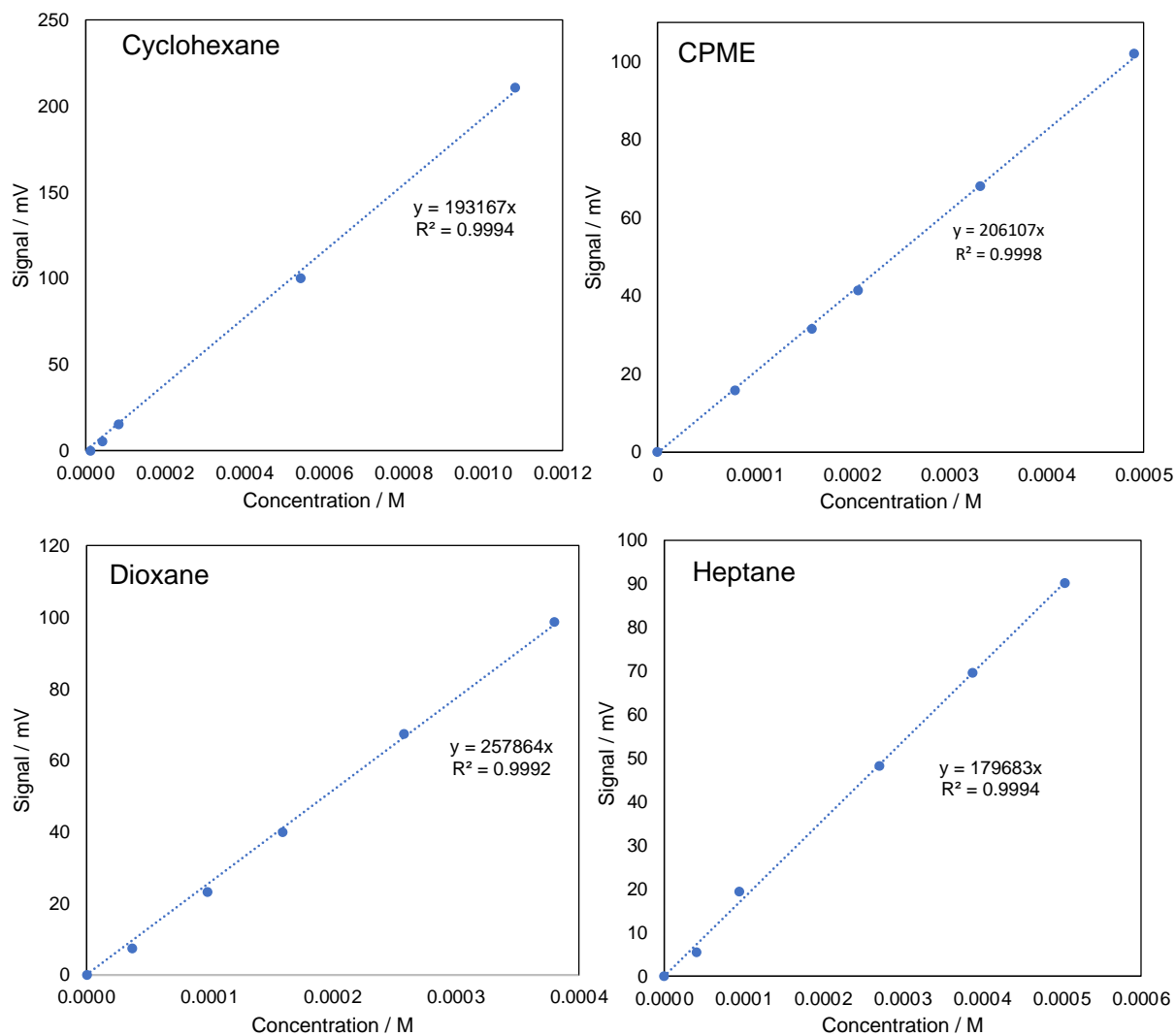

Figure S19. Calibration line between HPLC line detector signal and PEA concentration in the titration solvents.

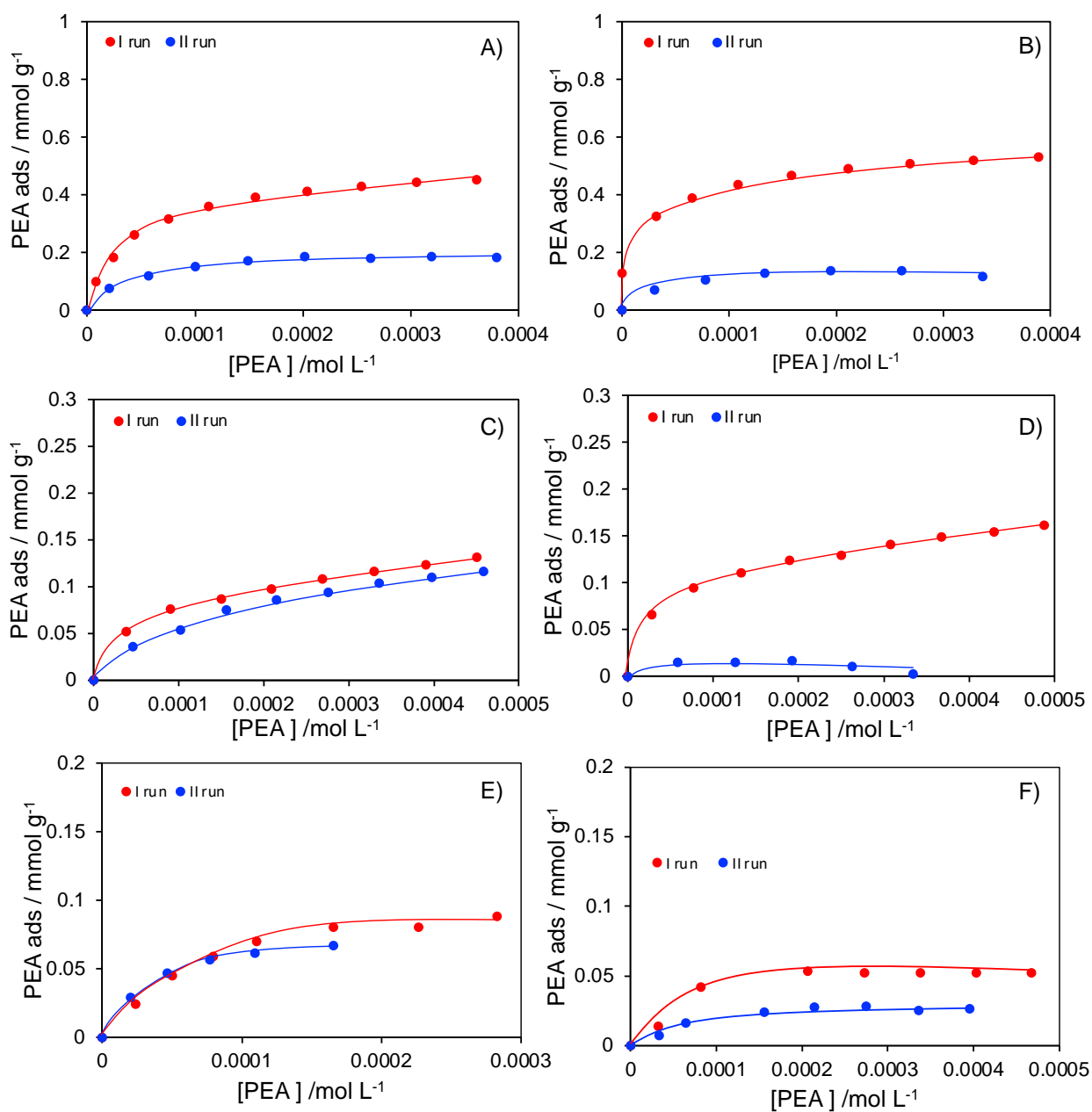## 6.8.4 Experimental adsorption isotherms

Figure S20. Experimental adsorption isotherm (T = 30.0 ± 0.1 °C) of PEA on CuO/SiO$_2$ catalysts. Top: *Intrinsic* acidity in cyclohexane of A) CuO/SiO$_2$ A and B) CuO/SiO$_2$ B. Bottom: *Effective* acidity in CPME of C) CuO/SiO$_2$ A and D) CuO/SiO$_2$ B and in dioxane of E) CuO/SiO$_2$ A and F) CuO/SiO$_2$ B. Adapted from reference [32]. Copyright Elsevier.
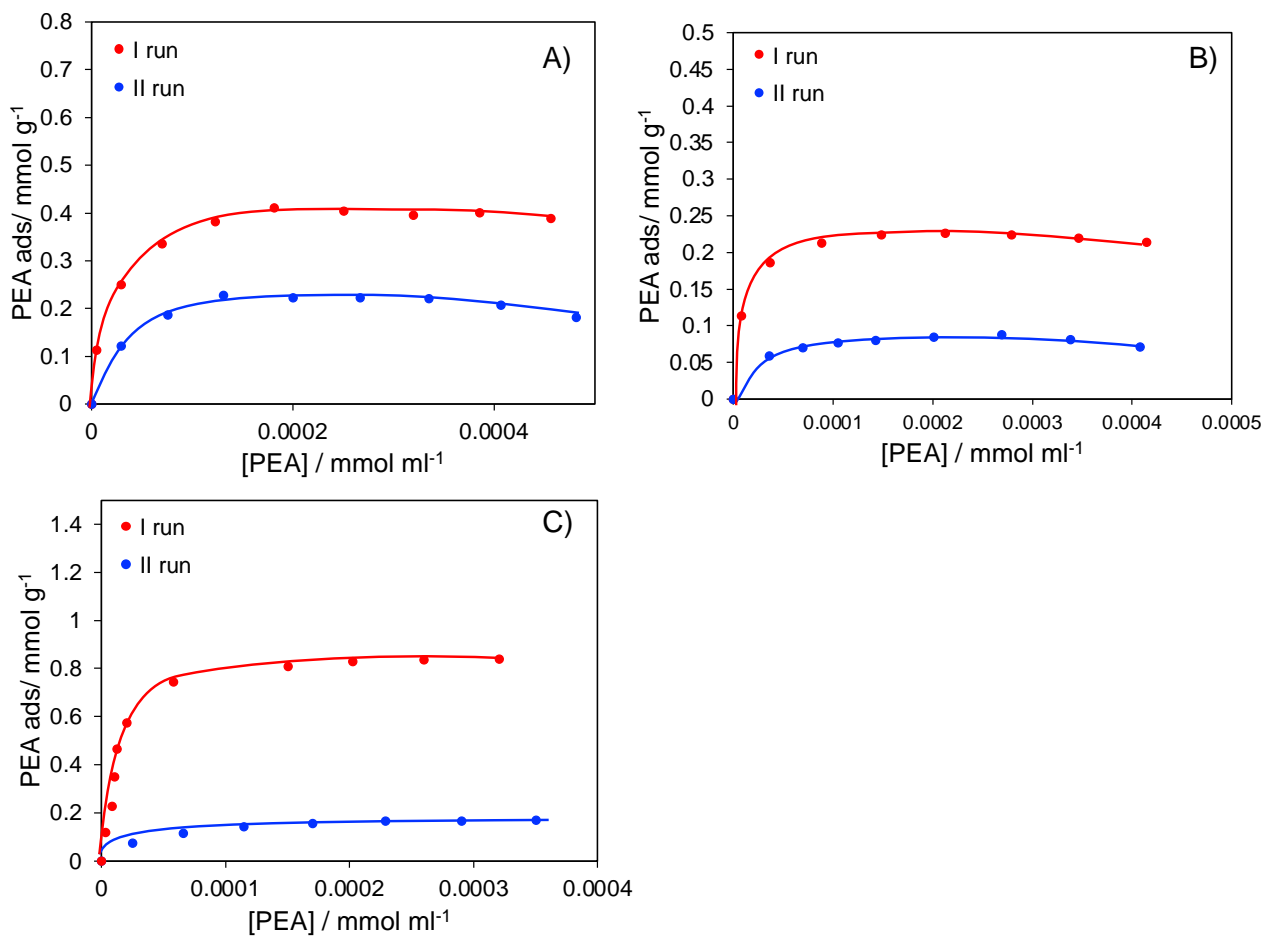
Figure S21. Experimental adsorption isotherm (T = 30.0 ± 0.1 °C) of PEA on CuO catalysts. in heptane A) CuO/SiO$_2$ and B) CuO/HAP.C) CuO/SiO$_2$ -Al$_2$O$_3$
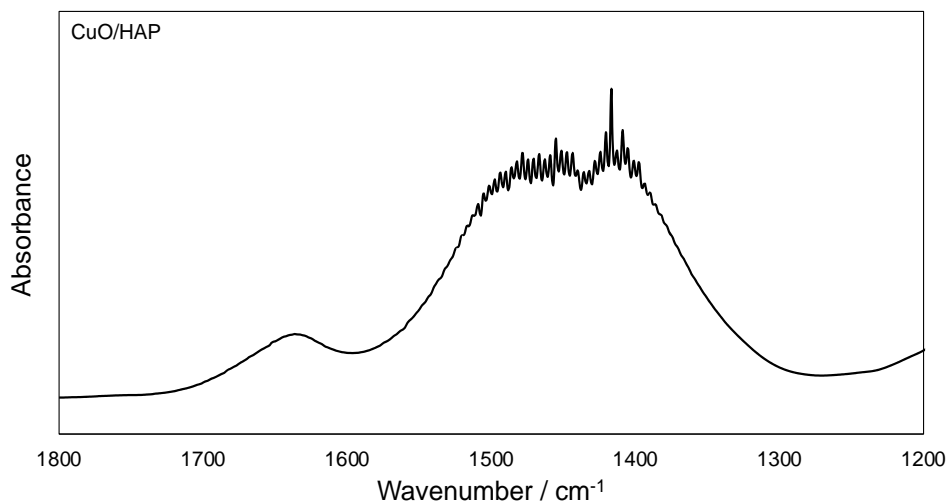
6.9 IR Spectroscopy

Figure S22. FT-IR spectrum of the CuO/HAP sample pretreated at 350 °C for 2 h under vacuum. It is possible to observe the CO_3^{2-} absorption band between 1600-1300 cm^{-1}. The intensity of the band is to such an extent that saturates the signal.
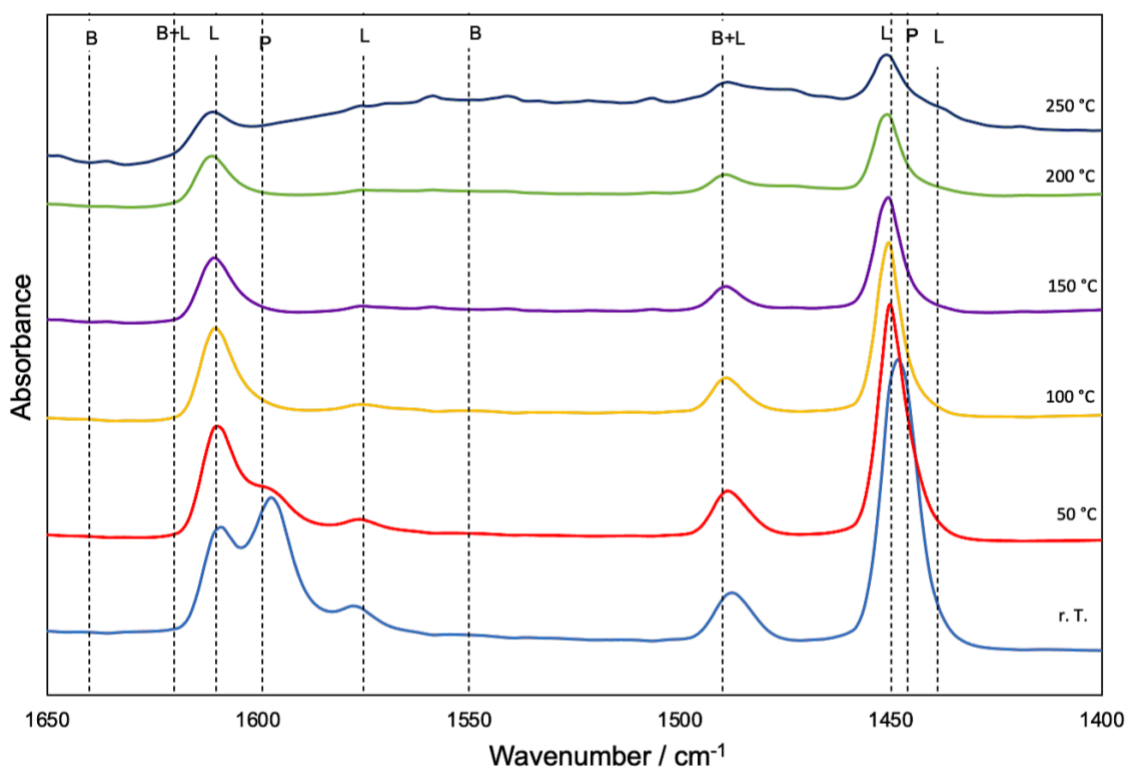

Figure S23. FT-IR spectra of the CuO/SiO$_2$ sample after pyridine adsorption at different outgassing temperatures.
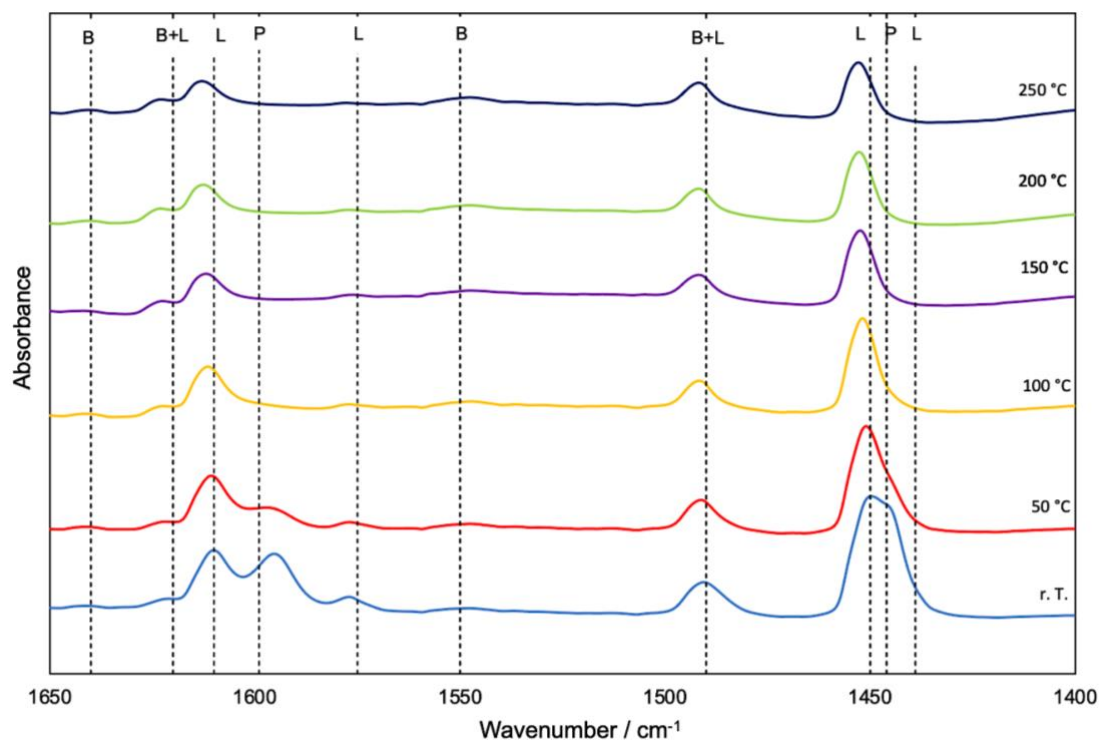
Figure S24. FT-IR spectra of the CuO/SiO$_2$-Al$_2$O$_3$ sample after pyridine adsorption at different outgassing temperatures.

Pyridine Absorption mode

For a molecule with "N" atoms there are 3N degrees of freedom. For a non-linear molecule 3 degrees of freedom can be signed to translations movement of a body as a whole (Tx, Ty, Tz) and 3 to rotations (Rx, Ry, Rz). The remaining motions of the atoms are displacements of the atoms from their mean positions while the center of gravity does not change. These fundamental vibrations are referred to as normal modes. Thus, a non-linear molecule has 3N-6 normal modes. Pyridine has 3N-6= 3 × 11 − 6 = 27 vibrational modes that depends on the atom orientation onto Cartesian coordinates and on the nature of the of the vibration that are similar to benzene ones. 8b mode (Figure S25) represent a stretching one and it can be sometimes observed in IR spectra at 1577 cm^{-1} but it is not commonly used for Lewis acid site strenght evaluation
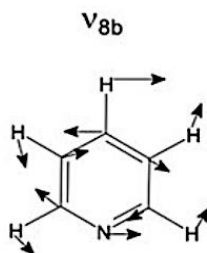
ν_{8b}

Figure S25. Schematic representation of pyridine 8b vibrational mode.

6.10 Gas Chromatography analysis and calibrations

$T_i = 50 \,°C$
$t_i = 4 \, min$
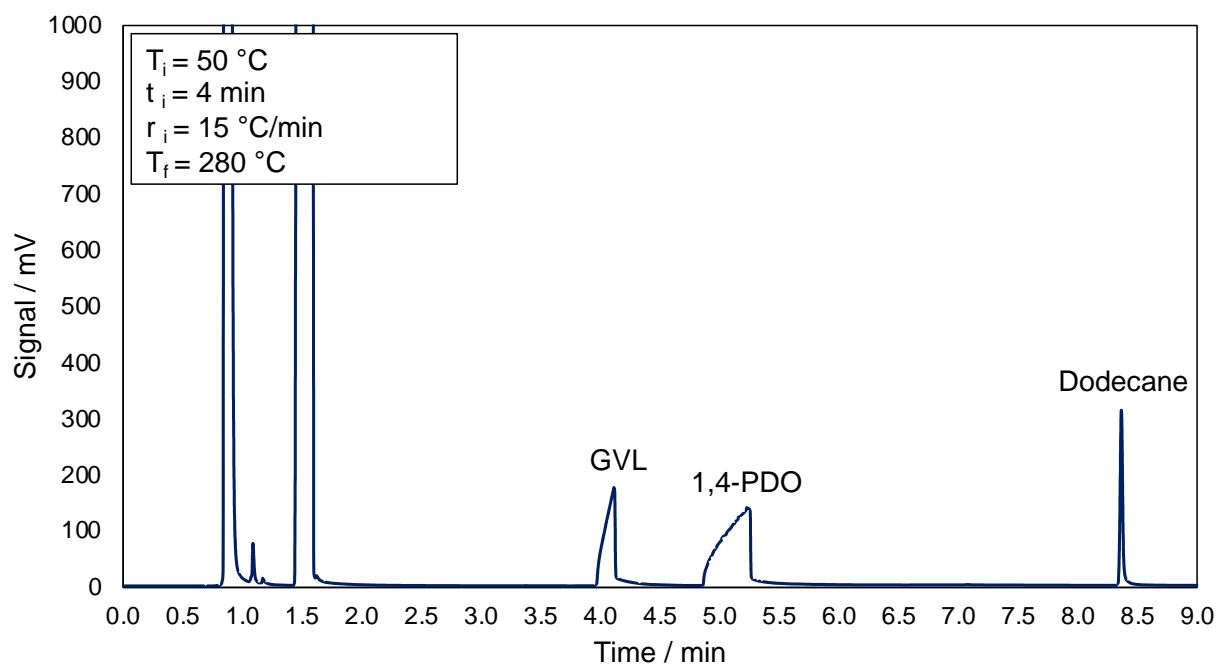$r_i = 15 \,°C/min$
$T_f = 280 \,°C$

Figure S26. Example of Chromatogram of GVL hydrogenation to 1,4-PDO post-reaction analysis of products and reagent.
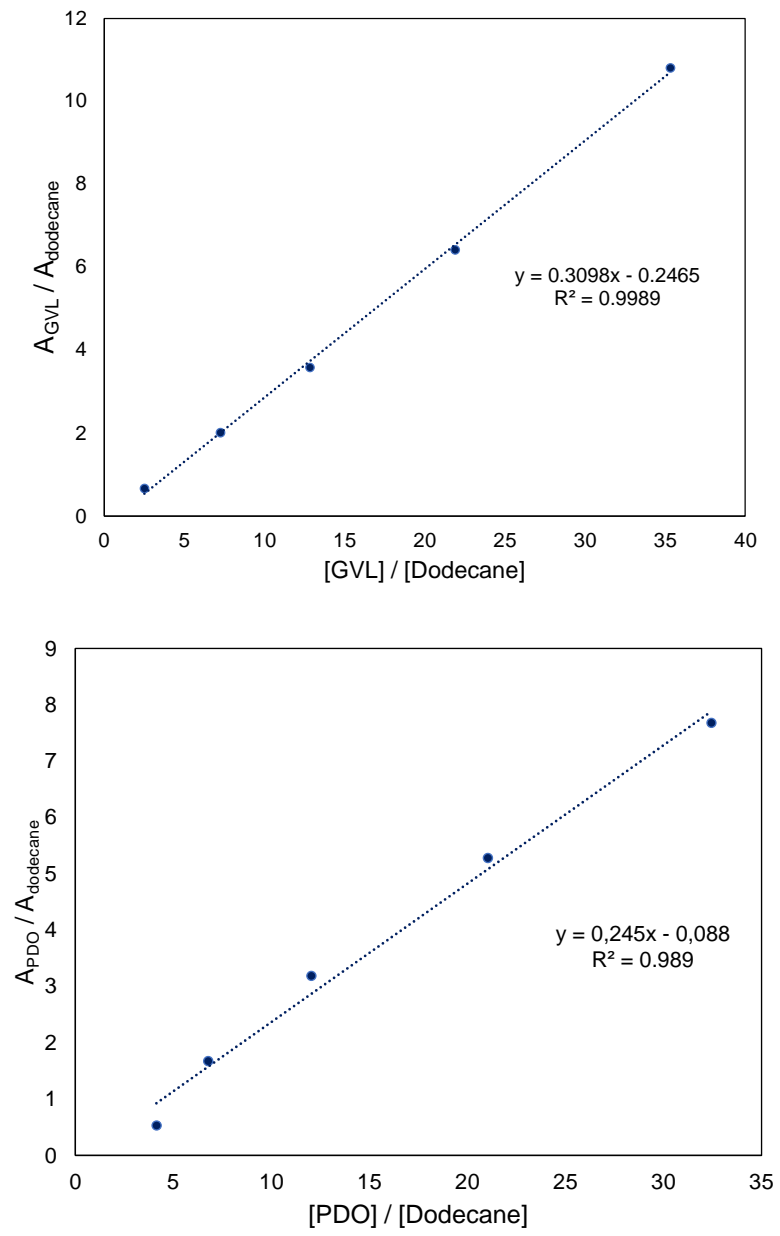
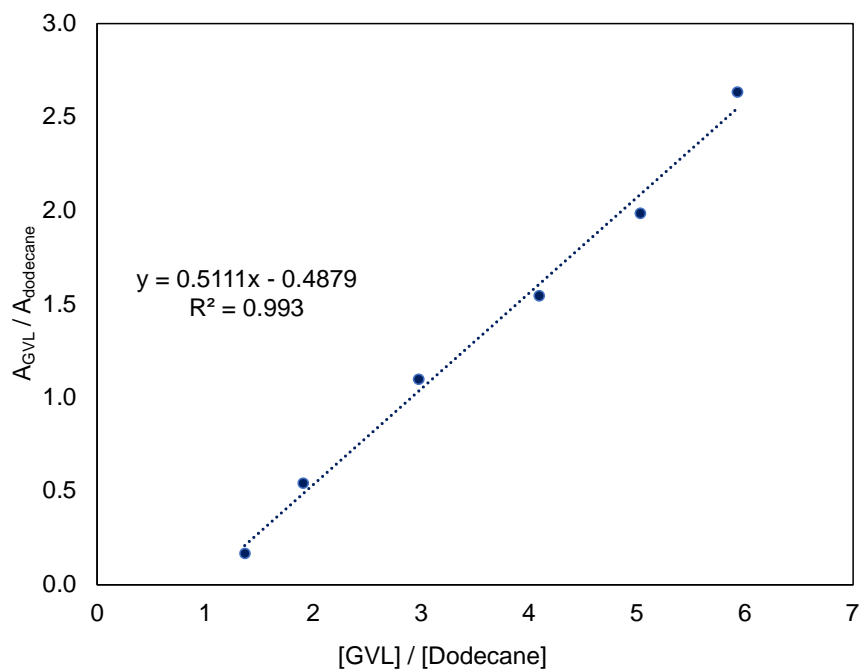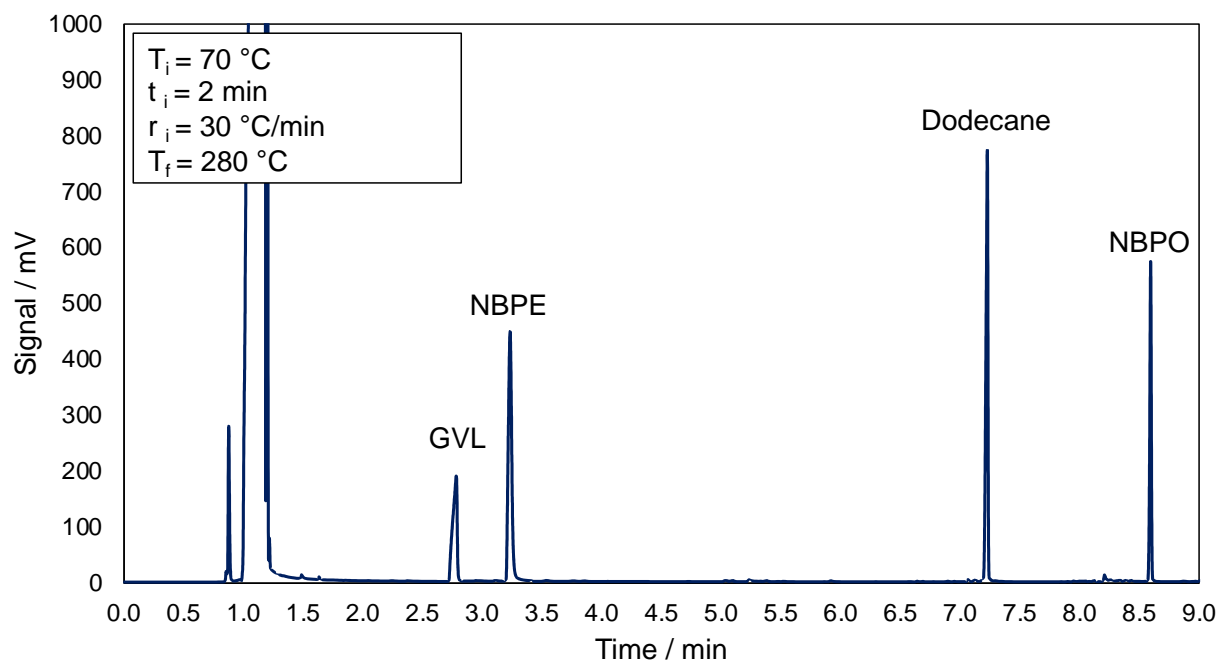**Figure S27**. Calibration lines of Top: GVL, Bottom: 1,4-PDO.

Figure S28. Top: Example of Chromatogram of GVL amination post-reaction analysis of products and reagent. Butylamine signal is overlapped with solvent's. Bottom: Calibration lines of GVL.

6.11 References

[1]   N. Rötzer, M. Schmidt, Historical, current, and future energy demand from global copper production and its impact on climate change, Resources. 9 (2020). https://doi.org/10.3390/RESOURCES9040044.

[2]   P. Patnaik, Handbook of Inorganic Chemicals, The McGraw-Hill Companies, Inc, New York, n.d.

[3]   S. Saranya, G. Anilkumar, Copper Catalysis, in: Copp. Catal. Org. Synth., John Wiley & Sons, Ltd, 2020: pp. 1–5. https://doi.org/https://doi.org/10.1002/9783527826445.ch1.

[4]   A. Elshkaki, T.E. Graedel, L. Ciacci, B. Reck, Copper demand, supply, and associated energy use to 2050, Glob. Environ. Chang. 39 (2016) 305–315. https://doi.org/10.1016/j.gloenvcha.2016.06.006.

[5]   B.W. Schipper, H.C. Lin, M.A. Meloni, K. Wansleeben, R. Heijungs, E. van der Voet, Estimating global copper demand until 2100 with regression and stock dynamics, Resour. Conserv. Recycl. 132 (2018) 28–36. https://doi.org/10.1016/j.resconrec.2018.01.004.

[6]   K. Hund, C. Megevand, E.P. Gomes, M. Miranda, E.W. Reed, Deforestation Trends in the Congo Basin Working Paper: Mining, 2013. https://doi.org/10.13140/RG.2.1.2957.4244.

[7]   J. Hagen, Industrial catalysis: A practical approach, 2015. https://doi.org/10.1002/9783527684625.

[8]   E.E. Vansant, P. Van Der Voort, K.C. Vrancken, Characterization and Chemical Modification of the Silica Surface, 1995.

[9]   V. Sanchez Escribano, G. Garbarino, E. Finocchio, G. Busca, γ-Alumina and Amorphous Silica–Alumina: Structural Features, Acid Sites and the Role of Adsorbed Water, Top. Catal. 60 (2017) 1554–1564. https://doi.org/10.1007/s11244-017-0838-5.

[10]   J.H. de Boer, Constitution and properties of silica-alumina-catalysts, Discuss. Faraday Soc. 52 (1971) 109–112. https://doi.org/10.1039/DF9715200109.

[11]   G. Busca, Silica-alumina catalytic materials: A critical review, Catal. Today. 357 (2020) 621–629. https://doi.org/10.1016/j.cattod.2019.05.011.

[12]   A. Fihri, C. Len, R.S. Varma, A. Solhy, Hydroxyapatite: A review of syntheses, structure and applications in heterogeneous catalysis, Coord. Chem. Rev. 347

(2017) 48–76. https://doi.org/10.1016/j.ccr.2017.06.009.

[13] M.I. Kay, R.A. Young, A.S. Posner, Crystal Structure of Hydroxyapatite, Nature. 204 (1964) 1050–1052. https://doi.org/10.1038/2041050a0.

[14] L. Silvester, J.-F. Lamonier, R.-N. Vannier, C. Lamonier, M. Capron, A.-S. Mamede, F. Pourpoint, A. Gervasini, F. Dumeignil, Structural{,} textural and acid–base properties of carbonate-containing hydroxyapatites, J. Mater. Chem. A. 2 (2014) 11073–11090. https://doi.org/10.1039/C4TA01628A.

[15] R. Prins, On the structure of γ-Al2O3, J. Catal. 392 (2020) 336–346. https://doi.org/10.1016/j.jcat.2020.10.010.

[16] M. Trueba, S.P. Trasatti, γ-alumina as a support for catalysts: A review of fundamental aspects, Eur. J. Inorg. Chem. (2005) 3393–3403. https://doi.org/10.1002/ejic.200500348.

[17] Z. Vít, J. Vala, J. Málek, Acid-base properties of aluminium oxide, Appl. Catal. 7 (1983) 159–168.

[18] R.H. Nielsen, J.H. Schlewitz, H. Nielsen, Zirconium and Zirconium compounds, in: Kirk-Othmer Encycl. Chem. Technol., 2000: p. 621.

[19] T. Nakamura, H. Usami, H. Ohnishi, M. Takeuchi, H. Nishida, T. Sekino, H. Yatani, The effect of adding silica to zirconia to counteract zirconia's tendency todegrade at low temperatures, Dent. Mater. J. 30 (2011) 330–335. https://doi.org/10.4012/dmj.2010-142.

[20] Y. Zhao, W. Li, M. Zhang, K. Tao, A comparison of surface acidic features between tetragonal and monoclinic nanostructured zirconia, Catal. Commun. 3 (2002) 239–245. https://doi.org/10.1016/S1566-7367(02)00089-4.

[21] T. Viinikainen, H. Rönkkönen, H. Bradshaw, H. Stephenson, S. Airaksinen, M. Reinikainen, P. Simell, O. Krause, Acidic and basic surface sites of zirconia-based biomass gasification gas clean-up catalysts, Appl. Catal. A Gen. 362 (2009) 169–177. https://doi.org/10.1016/j.apcata.2009.04.037.

[22] S. Bagheri, N. Muhd Julkapli, S. Bee Abd Hamid, Titanium dioxide as a catalyst support in heterogeneous catalysis, Sci. World J. 2014 (2014). https://doi.org/10.1155/2014/727496.

[23] G.D. PARFITT, The Surface of Titanium Dioxide, ACADEMIC PRESS, INC., 1976. https://doi.org/10.1016/b978-0-12-571811-0.50009-1.

[24] L. Ferretto, A. Glisenti, Surface acidity and basicity of a rutile powder, Chem. Mater. 15 (2003) 1181–1188. https://doi.org/10.1021/cm021269f.

[25] F. Zaccheria, N. Scotti, M. Marelli, R. Psaro, N. Ravasio, Unravelling the properties of supported copper oxide: Can the particle size induce acidic behaviour?, Dalt. Trans. 42 (2013) 1319–1328. https://doi.org/10.1039/c2dt32454g.

[26] F. Boccuzzi, A. Chiorino, G. Martra, M. Gargano, N. Ravasio, B. Carrozzini, Preparation, characterization, and activity of Cu/TiO2 catalysts: I. Influence of the preparation method on the dispersion of copper in Cu/TiO2, J. Catal. 165 (1997) 129–139. https://doi.org/10.1006/jcat.1997.1475.

[27] N. Scotti, M. Dangate, A. Gervasini, C. Evangelisti, N. Ravasio, F. Zaccheria, Unraveling the role of low coordination sites in a cu metal nanoparticle: A step toward the selective synthesis of second generation biofuels, ACS Catal. 4 (2014) 2818–2826. https://doi.org/10.1021/cs500581a.

[28] F. Boccuzzi, A. Chiorino, M. Gargano, N. Ravasio, Preparation, Characterization and Activity of CuTiO2 Catalysts, J. Catal. 165 (1997) 140–149.

[29] F. Zaccheria, M. Mariani, N. Scotti, R. Psaro, N. Ravasio, Catalytic upgrading of lactose: A rest raw material from the dairy industry, Green Chem. 19 (2017) 1904–1910. https://doi.org/10.1039/c7gc00741h.

[30] D. Cavuoto, N. Ravasio, F. Zaccheria, M. Marelli, G. Cappelletti, S. Campisi, A. Gervasini, Tuning the Cu/Sio2 Wettability Features for Bio-Derived Platform Molecules Valorization, Mol. Catal. 528 (2022) 112462. https://doi.org/10.2139/ssrn.4103197.

[31] I. Langmuir, THE CONSTITUTION AND FUNDAMENTAL PROPERTIES OF SOLIDS AND LIQUIDS. PART I. SOLIDS., J. Am. Chem. Soc. 38 (1916) 2221–2295. https://doi.org/10.1021/ja02268a002.

[32] D. Cavuoto, N. Ravasio, N. Scotti, A. Gervasini, S. Campisi, M. Marelli, G. Cappelletti, F. Zaccheria, A green solvent diverts the hydrogenation of γ − valerolactone to 1 , 4 - pentanediol over Cu / SiO 2, Mol. Catal. 516 (2021) 111936. https://doi.org/10.1016/j.mcat.2021.111936.

7 RESEARCH ACHIEVEMENTS

Publications

- D. Cavuoto, F. Zaccheria, M. Marelli, C. Evangelisti, O. Piccolo, N. Ravasio, *The Role of Support Hydrophobicity in the Selective Hydrogenation of Enones and Unsaturated Sulfones over Cu/SiO₂,* Catalysts, 2020, 10, 515.

- V.M. Pappalardo, D. Cavuoto, S. Sangiorgio, G. Speranza, G. Cappelletti, N. Ravasio, F. Zaccheria, *Clays as Effective Solid Acid Catalysts for the Preparation of Sugar Esters with Surfactant Properties*, ChemistrySelect, 2020, 5, 8009–8014.

- D. Cavuoto, F. Zaccheria, N. Ravasio *Some Critical Insights into the Synthesis and Applications of Hydrophobic Solid Catalysts*, Catalyst, 2020, 10, 1337.

- D. Cavuoto, N. Ravasio, N. Scotti, A. Gervasini, S. Campisi, M. Marelli, G. Cappelletti, F. Zaccheria *A green solvent diverts the hydrogenation of γ-valerolactone to 1,4-pentandiol over Cu/SiO₂,* Molecular Catalysis, 516, 2021, 111936.

- D. Cavuoto, N. Ravasio, F. Zaccheria, M. Marelli, G. Cappelletti, S. Campisi and A. Gervasini, *Tuning the Cu/SiO₂ wettability features for bio-derived platform molecules valorization*, Mol. Catal., 2022, 528, 112462

- D. Cavuoto, A. Gervasini, F. Zaccheria, N. Scotti, M. Marelli, C. Bisio, F. Begni and N. Ravasio, *Synthesis of green solvents from bio-based lactones using copper catalysts,* Catalysis Today, 2023, 418, 114104

- D. Cavuoto, L. Ardemani, N. Ravasio, F. Zaccheria, N. Scotti, *Some insights into the use of heterogeneous copper catalysts in the hydroprocessing of levulinic acid,* Catalyst, submitted.

Communications (poster and oral)

- European Federation for the Science and Technologies of Lipids (20-23 October 2019) - **Oral comunication:** Pappalardo, V., Cavuoto, D., Zaccheria, F., Ravasio, N. Speranza G., Cappelletti G., *Synthesis of biosurfactants using solid acid catalysts*.

- Green Chemistry Post Graduated Summer School (4-10 July 2021) - **Poster presentation**: D.Cavuoto, A. Gervasini, F. Zaccheria, N.Ravasio, *Green amination strategies for the production of biobased building-blocks.*

- XXVII Congresso Nazionale della Società Chimica Italiana (14-23 September 2021) – **Oral presentation:** D. Cavuoto, N. Ravasio, N. Scotti, A. Gervasini, S. Campisi, M. Marelli, G. Cappelletti, F. Zaccheria, *The role of support wettability and acidity in the hydrogenation of γ- valerolactone over Cu/SiO$_2$ catalyst.*

- 5th EuChem Conference on Green and Sustainable Chemistry (26-29 September 2021) – **Mini-oral presentation:** D. Cavuoto, N. Ravasio, N. Scotti, A. Gervasini, S. Campisi, M. Marelli, G. Cappelletti, F. Zaccheria, *The role of support wettability and acidity in the hydrogenation of γ- valerolactone over Cu/SiO$_2$ catalyst.*

- European Federation for the Science and Technologies of Lipids (18-21 October 2021) - **Oral comunication:** D. Cavuoto, F. Bertini, A. Vignali, N. Ravasio and F. Zaccheria*, Styrene-free thermosetting resins from vegetable oils*

- International Winter School of Inorganic Materials (15-18 December 2021) – **Poster presentation:** D. Cavuoto, A. Gervasini, F. Zaccheria and N. Ravasio, *Green catalytic amination strategies for the production of biobased building-blocks.*

- IX Workshop Green Chemistry – Chimica Sostenibile (22-23 Giugno 2022) - **Oral presentation**: D. Cavuoto, N. Ravasio, F. Zaccheria, M. Marelli, G. Cappelletti, S. Campisi and A. Gervasini, *Tuning the Cu/SiO$_2$ wettability features for bio-derived platform molecules valorization*

- XXII National Congress of Catalysis 2022 (11-14 September 2022) - **Oral presentation**: D. Cavuoto, N. Ravasio, F. Zaccheria, M. Marelli, G. Cappelletti, S. Campisi and A. Gervasini, *Tuning the Cu/SiO$_2$ wettability features for bio-derived platform molecules valorization*

- XXII National Congress of Catalysis 2022 (11-14 September 2022) – **Poster presentation:** D. Cavuoto, N. Ravasio, F. Zaccheria, N. Scotti and A. Gervasini, *Synthesis of green solvents from biomass derived γ-valerolactone*

Attended Schools, Congresses and Seminars

- L'Industria Chimica Italiana Abbraccia la Chimica Verde (28 October 2020)
- SINCHEM Winter School (4-6 February 2020)
- Green Chemistry post graduated summer school (4-10 July 2021) (poster presentation)
- Contest CIG2021 Catalisi In Gioco (27-30 July 2021)
- XXVII Congresso Nazionale della Società Chimica Italiana (14-23 September 2021)
- 5th EuChem Conference on Green and Sustainable Chemistry (26-29 September 2021)
- International Winter School of Inorganic Materials (15-18 December 2021) (poster presentation)
- IX Workshop Green Chemistry – Chimica Sostenibile (22-23 Giugno 2022)
- XXII National Congress of Catalysis 2022 (11-14 September 2022)

Assistance, tutoring

- PLS Biocatalisi A (referente Dr. Carlo Morelli) – 24 h (2020)
- 993/P-Esercitazioni per: Chimica Organica (Prof. Maria Cristina Bellucci) (2021): 27h

8 Permissions

Figure S1 was taken by an article available under the Creative Commons CC-BY-NC-ND license and permits non-commercial use of the work as published, without adaptation or alteration provided the work is fully attributed.

Figure S2 from reference: Global Environmental Change 39 (2016) 305–315. See following attachment.

Figure S4 and S5 from reference: Dalton Trans., 2013, 42, 1319. See following attachment.

ELSEVIER LICENSE
TERMS AND CONDITIONS

Feb 02, 2023

This Agreement between Denise Cavuoto ("You") and Elsevier ("Elsevier") consists of your
license details and the terms and conditions provided by Elsevier and Copyright Clearance
Center.

License Number	5480851228715
License date	Feb 02, 2023
Licensed Content Publisher	Elsevier
Licensed Content Publication	Global Environmental Change
Licensed Content Title	Copper demand, supply, and associated energy use to 2050
Licensed Content Author	Ayman Elshkaki,T.E. Graedel,Luca Ciacci,Barbara K. Reck
Licensed Content Date	Jul 1, 2016
Licensed Content Volume	39
Licensed Content Issue	n/a
Licensed Content Pages	11
Start Page	305
End Page	315
Type of Use	reuse in a thesis/dissertation
Portion	figures/tables/illustrations

Number of figures/tables/illustrations	1
Format	both print and electronic
Are you the author of this Elsevier article?	No
Will you be translating?	No
Title	Green strategies for the synthesis of biobased building blocks
Institution name	Università degli Studi di Milano
Expected presentation date	Mar 2023
Portions	Figure 1 (d)
Requestor Location	Denise Cavuoto Via Golgi 19 Milano, Milano 20133 Italy Attn: Denise Cavuoto
Publisher Tax ID	GB 494 6272 12
Total	0.00 EUR

Terms and Conditions

INTRODUCTION

1. The publisher for this copyrighted material is Elsevier. By clicking "accept" in connection with completing this licensing transaction, you agree that the following terms and conditions apply to this transaction (along with the Billing and Payment terms and conditions established by Copyright Clearance Center, Inc. ("CCC"), at the time that you opened your Rightslink account and that are available at any time at http://myaccount.copyright.com).

GENERAL TERMS

2. Elsevier hereby grants you permission to reproduce the aforementioned material subject to the terms and conditions indicated.

178

CCC | Marketplace

Order Number: 1317824
Order Date: 31 Jan 2023

Payment Information

Denise Cavuoto
denise.cavuoto@unimi.it
Payment method: Invoice

Billing Address:
Denise Cavuoto
Via Golgi 19
Milano, Milano 20133
Italy

+39 3341505087
denise.cavuoto@unimi.it

Customer Location:
Denise Cavuoto
Via Golgi 19
Milano, Milano 20133
Italy

Order Details

1. Dalton transactions : an international journal of inorganic chemistry

Billing Status: Open

Article: Unravelling the properties of supported copper oxide: can the particle size induce acidic behaviour?

Order License ID	1317824-1	Type of use	Republish in a thesis/dissertation
Order detail status	Completed		
ISSN	1477-9226	Publisher	ROYAL SOCIETY OF CHEMISTRY
		Portion	Chart/graph/table/figure

0,00 EUR
Republication Permission

LICENSED CONTENT

Publication Title	Dalton transactions : an international journal of inorganic chemistry	Rightsholder	Royal Society of Chemistry
		Publication Type	Journal
Article Title	Unravelling the properties of supported copper oxide: can the particle size induce acidic behaviour?	Start Page	1319
		End Page	1328
		Issue	5
		Volume	42
Author/Editor	Royal Society of Chemistry (Great Britain)		
Date	01/01/2003		
Language	English		
Country	United Kingdom of Great Britain and Northern Ireland		

REQUEST DETAILS

Portion Type	Chart/graph/table/figure	Distribution	Worldwide
		Translation	Original language of publication
Number of Charts / Graphs / Tables / Figures Requested	2	Copies for the Disabled?	No
Format (select all that apply)	Print, Electronic	Minor Editing Privileges?	No
Who Will Republish the Content?	Academic institution	Incidental Promotional Use?	No
Duration of Use	Life of current edition	Currency	EUR
Lifetime Unit Quantity	Up to 499		
Rights Requested	Main product		

NEW WORK DETAILS

Title	Green strategies for the synthesis of biobased building blocks	Institution Name	Università degli Studi di Milano
		Expected Presentation Date	2023-03-31
Instructor Name	Denise Cavuoto		

ADDITIONAL DETAILS

The Requesting Person/Organization to Appear on the License	Denise Cavuoto

REUSE CONTENT DETAILS

Title, Description or Numeric Reference of the Portion(s)	Figure n. 2, Figure n. 4	Title of the Article/Chapter the Portion Is From	Unravelling the properties of supported copper oxide: can the particle size induce acidic behaviour?
Editor of Portion(s)	Zaccheria, Federica; Scotti, Nicola; Marelli, Marcello; Psaro, Rinaldo; Ravasio, Nicoletta	Author of Portion(s)	Zaccheria, Federica; Scotti, Nicola; Marelli, Marcello; Psaro, Rinaldo; Ravasio, Nicoletta
Volume of Serial or Monograph	42		
Page or Page Range of Portion	1319-1328	Issue, if Republishing an Article From a Serial	5
		Publication Date of Portion	2013-02-07

Total Items: 1

	Subtotal:	0,00 EUR
	Order Total:	**0,00 EUR**

Marketplace Order General Terms and Conditions

180